


REPORT DOCUMENTATION PAGE		1. REPORT NO. NCEER-92-0029	2.	3.  PB93-227528
4. Title and Subtitle Seismic Resistance of Reinforced Concrete Frame Structures Designed Only for Gravity Loads: Part III - Experimental Performance and Analytical Study of a Structural Model.			5. REPORT DATE December 1, 1992	
7. Author(s) J.M. Bracci, A.M. Reinhorn and J.B. Mander			6.	
9. Performing Organization Name and Address Department of Civil Engineering State University of New York at Buffalo Buffalo, New York 14260			8. Performing Organization Rept. No.	
12. Sponsoring Organization Name and Address National Center for Earthquake Engineering Research State University of New York at Buffalo Red Jacket Quadrangle Buffalo, New York 14260			10. Project/Task/Work Unit No.	
			11. Contract(G) or Grant(G) No. BCS 90-25010 NEC-91029	
			13. Type of Report & Period Covered Technical report	
			14.	
15. Supplementary Notes This research was conducted at the State University of New York at Buffalo and was partially supported by the National Science Foundation under Grant No. BCS 90-25010 and the New York State Science and Technology Foundation under Grant No. NEC-91029.				
16. Abstract (Limit: 200 words) This report is Part III of a three-part series prepared for a comprehensive evaluation of typical gravity load designed low-rise reinforced concrete frame buildings (lightly reinforced concrete structures) for seismic adequacy. The study was done at State University of New York at Buffalo - Earthquake Simulation Laboratory on a 1:3 scale building model designed for gravity loads only. The one-third scale three story model, one-bay by three-bay, of a typical office building was constructed to represent the critical interior bay of a prototype structure. A series of ground motion tests were performed on the one-third scale building model using scaled accelerograms on the shaking table to represent minor to severe earthquakes. The dynamic characteristics of the model after each seismic event were identified from white noise shaking table tests. Results of this experimental investigation are presented here. Analytical models were developed to predict and interpret seismic response of the building model based on identified member properties from engineering approximations, component tests, and an experimental response fit. It is shown in this report that the response predictions based on integrating the behavior from component tests (presented in Part II of this report series) provide adequate correlation of the seismic structural response behavior, emphasizing the importance of such component testing. A damage evaluation of the building model was performed analytically to assess structural integrity after the induced ground motion in terms of damage states. A modified damage model is proposed.				
17. Document Analysis				
a. Descriptors				
b. Identifiers/Open-Ended Terms				
Lightly reinforced concrete frames. Earthquake engineering.		Gravity load design. Scale models		Shaking table tests.
c. OOBATI Field/Group				
18. Availability Statement Release Unlimited		19. Security Class (This Report) Unclassified		20. No. of Pages 168
		20. Security Class (This Page) Unclassified		21. Price



PB93-121128

**NATIONAL CENTER FOR EARTHQUAKE
ENGINEERING RESEARCH**

State University of New York at Buffalo

**Seismic Resistance of Reinforced Concrete
Frame Structures Designed Only
for Gravity Loads:**

**Part III — Experimental Performance
and Analytical Study of a Structural Model**

by

J.M. Bracci, A.M. Reinhorn and J.B. Mander

State University of New York at Buffalo
Department of Civil Engineering
Buffalo, New York 14260

Technical Report NCEER-92-0029

December 1, 1992

Reproduced by
National Technical Information Service
U.S. Department of Commerce
Springfield, VA 22161

This research was conducted at the State University of New York at Buffalo and was partially supported by the National Science Foundation under Grant No. BCS 90-25010 and the New York State Science and Technology Foundation under Grant No. NEC-91029.

NOTICE

This report was prepared by the State University of New York at Buffalo as a result of research sponsored by the National Center for Earthquake Engineering Research (NCEER) through grants from the National Science Foundation, the New York State Science and Technology Foundation, and other sponsors. Neither NCEER, associates of NCEER, its sponsors, the State University of New York at Buffalo, nor any person acting on their behalf:

- a. makes any warranty, express or implied, with respect to the use of any information, apparatus, method, or process disclosed in this report or that such use may not infringe upon privately owned rights; or
- b. assumes any liabilities of whatsoever kind with respect to the use of, or the damage resulting from the use of, any information, apparatus, method or process disclosed in this report.

Any opinions, findings, and conclusions or recommendations expressed in this publication are those of the author(s) and do not necessarily reflect the views of the National Science Foundation, the New York State Science and Technology Foundation, or other sponsors.



**Seismic Resistance of Reinforced Concrete
Frame Structures Designed Only
for Gravity Loads:**

**Part III - Experimental Performance
and Analytical Study of a Structural Model**

by

J.M. Bracci¹, A.M. Reinhorn² and J.B. Mander³

December 1, 1992

Technical Report NCEER-92-0029

NCEER Project Numbers 89-1001A, 90-1001A and 91-3111B

NSF Master Contract Number BCS 90-25010

and

NYSSSTF Grant Number NEC-91029

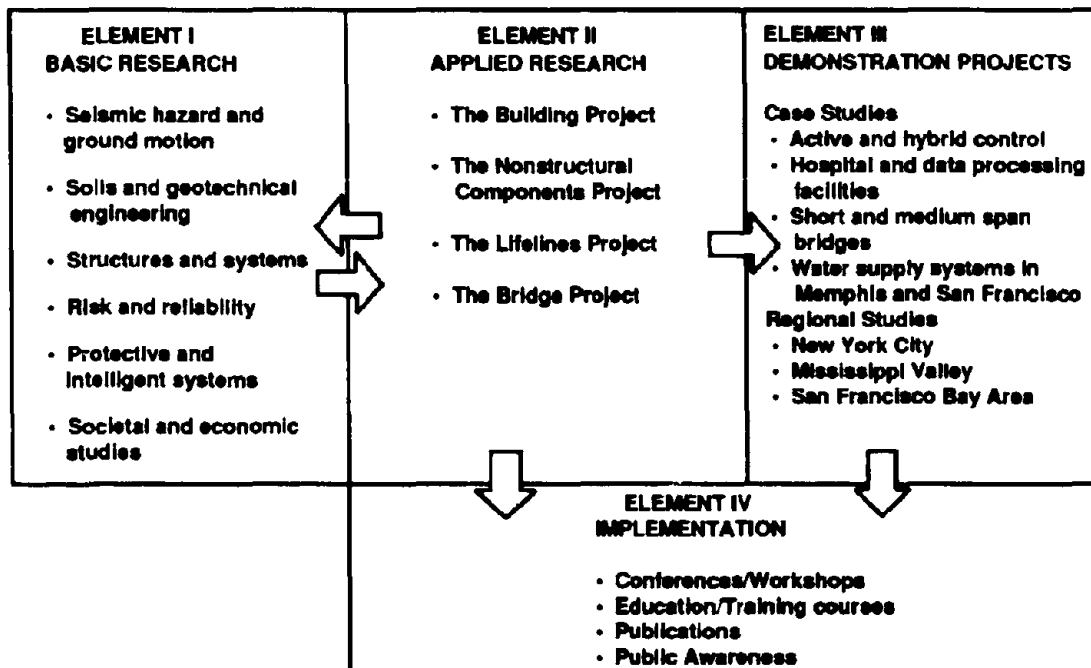
- 1 Research Associate, Department of Civil Engineering, State University of New York at Buffalo
- 2 Professor, Department of Civil Engineering, State University of New York at Buffalo
- 3 Assistant Professor, Department of Civil Engineering, State University of New York at Buffalo

NATIONAL CENTER FOR EARTHQUAKE ENGINEERING RESEARCH
State University of New York at Buffalo
Red Jacket Quadrangle, Buffalo, NY 14261

PREFACE

The National Center for Earthquake Engineering Research (NCEER) was established to expand and disseminate knowledge about earthquakes, improve earthquake-resistant design, and implement seismic hazard mitigation procedures to minimize loss of lives and property. The emphasis is on structures in the eastern and central United States and lifelines throughout the country that are found in zones of low, moderate, and high seismicity.

NCEER's research and implementation plan in years six through ten (1991-1996) comprises four interlocked elements, as shown in the figure below. Element I, Basic Research, is carried out to support projects in the Applied Research area. Element II, Applied Research, is the major focus of work for years six through ten. Element III, Demonstration Projects, have been planned to support Applied Research projects, and will be either case studies or regional studies. Element IV, Implementation, will result from activity in the four Applied Research projects, and from Demonstration Projects.



Research in the **Building Project** focuses on the evaluation and retrofit of buildings in regions of moderate seismicity. Emphasis is on lightly reinforced concrete buildings, steel semi-rigid frames, and masonry walls or infills. The research involves small- and medium-scale shake table tests and full-scale component tests at several institutions. In a parallel effort, analytical models and computer programs are being developed to aid in the prediction of the response of these buildings to various types of ground motion.

Two of the short-term products of the **Building Project** will be a monograph on the evaluation of lightly reinforced concrete buildings and a state-of-the-art report on unreinforced masonry.

The **structures and systems program** constitutes one of the important areas of research in the **Building Project**. Current tasks include the following:

1. Continued testing of lightly reinforced concrete external joints.
2. Continued development of analytical tools, such as system identification, idealization, and computer programs.
3. Perform parametric studies of building response.
4. Retrofit of lightly reinforced concrete frames, flat plates and unreinforced masonry.
5. Enhancement of the IDARC (inelastic damage analysis of reinforced concrete) computer program.
6. Research infilled frames, including the development of an experimental program, development of analytical models and response simulation.
7. Investigate the torsional response of symmetrical buildings.

One of the key accomplishments in the development of evaluation methods for existing buildings was the design and shake-table testing of three-story gravity-load designed buildings at the University at Buffalo and at Cornell University. These tests followed extensive preparatory full and reduced-scale component tests and the development of computer models.

This is the third in a series of three reports summarizing the test program at the University at Buffalo. The results of the shaking table tests of the building model and extensive analytical studies are reported. The behavior of the building model under a series of increasingly higher level ground motions is described. Particular attention is paid to the damage levels and the drift levels for a building not designed for lateral loads.

ABSTRACT

This report is Part III of a three-part series prepared for a comprehensive **Evaluation** of typical gravity load designed low-rise reinforced concrete frame buildings (lightly reinforced concrete structures) for seismic adequacy. The study was done at State University of New York at Buffalo - Earthquake Simulation Laboratory on a 1:3 scale building model designed for gravity loads only. No considerations were made for seismic resistance and the general non-seismic detailing provisions of ACI-318-89 were used for the design. The one-third scale three story model, one-bay by three-bay, of a typical office building was constructed to represent the critical interior bay of a prototype structure.

Part I of the Evaluation Series presented the design objectives, geometric dimensions, material strengths and initial dynamic properties of the model building, along with the simulated base motions, so that analytical models could be developed and used to predict the inelastic response of the model building during more severe earthquakes. The initial vibration tests and the response from a minor earthquake were presented to enable analytical structural modeling and verification of elastic response.

Components of structure, ie., structural subassemblages of columns, column-to- beam joints and column-beam-slabs models were constructed from the same materials as the structural model and at same scale. These components were tested with cyclic loading to failure to determine their structural parameters and ultimate limits. The results of components study were the subject of Part II of the Evaluation Series.

A series of varying intensity simulated ground motion tests were performed on the one-third scale building model using scaled accelerograms on the shaking table to represent minor, moderate, and severe earthquakes. The dynamic characteristics of the model after each seismic event were identified from white noise shaking table tests. The results of this experimental investigation are presented in this report (Part III of the Evaluation series).

Analytical models were developed to predict and interpret seismic response of the building model based on identified member properties from engineering approximations, component tests, and an experimental response fit. It is shown in this report that the response predictions based on integrating the behavior from component tests (presented in Part II of these report series) provide adequate correlation of the seismic structural response behavior, emphasizing the importance of such component testing. A damage evaluation of the building model was

performed analytically to assess structural integrity after the induced ground motions in terms of damage states. A modified damage model was proposed to incorporate the additional damage from P-delta effects in columns. The results of the analytical evaluations are presented in this report.

It is shown in this report series that gravity load designed structures have some inherent strength for resisting seismic forces. However a weak column - strong beam behavior was evident in the experimental response and large story drifts, beyond 2% of the story height (exceeding current code recommended limits), may develop during strong earthquakes.

TABLE OF CONTENTS

SECTION	TITLE	PAGE
1	INTRODUCTION	
1.1	Background.....	1-1
1.2	Overall Objectives of Research Program	1-4
1.3	Scope of this Report	1-7
1.4	Summary of Structural Behavior during Minor Base Motions	1-7
2	INELASTIC RESPONSE DURING MODERATE AND SEVERE SHAKING	
2.1	Introduction	2-1
2.2	Response to Moderate Earthquake	2-1
2.2.1	Global Response.....	2-1
2.2.2	Local Response	2-4
2.3	Dynamic Properties after Moderate Shaking	2-6
2.4	Response to Severe Earthquake.....	2-31
2.4.1	Global Response.....	2-31
2.4.2	Local Response	2-33
2.5	Dynamic Properties after Severe Shaking	2-35
2.6	Summary Discussions	2-59
2.6.1	Maximum Story Response from Shaking Table Tests.....	2-59
2.6.2	Summary of Dynamic Characteristics of Model.....	2-60
2.6.3	Concluding Remarks on Testing of LRC Model	2-61
3	ANALYTICAL DAMAGE EVALUATION OF MODEL	
3.1	Introduction	3-1
3.2	Analytical Modeling and Response Results	3-1
3.2.1	Modeling with Engineering Approximations.....	3-2
3.2.2	Modeling with Component Tests	3-5
3.2.3	Modeling with Properties Identified using Response Fit	3-6
3.2.3.1	Minor Shaking.....	3-6
3.2.3.2	Moderate and Severe Shaking.....	3-7
3.3	Damage Quantification.....	3-33
3.4	Identification of Final Collapse Mechanism and Critical Earthquake	3-38

TABLE OF CONTENTS (cont.)

SECTION	TITLE	PAGE
3.5	Modified Damage Index for P-Delta Effect	3-39
3.6	Elastic Analysis and Response Reduction Factors	3-51
3.7	Summary Discussions	3-56
4	SUMMARY, CONCLUSIONS, AND RECOMMENDATIONS FOR FUTURE WORK	
4.1	Summary of LRC Frame Model Testing.....	4-1
4.1.1	Design	4-1
4.1.2	Experimental Study	4-1
4.1.3	Analytical Studies	4-3
4.2	Conclusions on LRC Frame Structures during Earthquakes	4-5
4.3	Recommendations for Future Research on the Design and Evaluation of LRC Frame Structures	4-6
5	REFERENCES	5-1

LIST OF FIGURES

FIGURE	TITLE	PAGE
1-1	Current Research Program	1-2
2-1	Shaking Table Motion for the Taft N21E Base Motion, PGA 0.20 g.....	2-10
2-2	Story Displacement Time Histories for TFT_20	2-11
2-3	Story Shear Force Time Histories for TFT_20	2-12
2-4	Overlaid Global Response Time History Segments for TFT_20	2-13
2-5	Story Displacements and Shears at Maximum First Story Drift for TFT_20	2-14
2-6	Story Shear versus Inter-Story Drift Histories for TFT_20	2-15
2-7	Energy Time History for TFT_20.....	2-16
2-8	Member Designations	2-17
2-9	Base Column Shear Forces for TFT_20	2-18
2-10a	Interaction Histories for the South-East Columns from TFT_20	2-19
2-10b	Interaction Histories for the North-East Columns from TFT_20	2-20
2-11a	First Story Beam Bending Moment Time Histories for TFT_20 - South Side.....	2-21
2-11b	First Story Beam Bending Moment Time Histories for TFT_20 - North Side.....	2-22
2-12a	Moment versus Curvature for TFT_20 - Exterior Joint.....	2-23
2-12b	Moment versus Curvature for TFT_20 - Interior Joint	2-24
2-13	Moment Diagram at Maximum Story Drift from TFT_20	2-25
2-14	Observed Structural Damage from TFT_20	2-26
2-15	Measured Damage State of the Model after TFT_20	2-27
2-16	Transfer Functions of the Story Level Accelerations from WHN_E.....	2-28
2-17	Smoothed Transfer Functions of the Story Level Accelerations from WHN_E.....	2-29
2-18	Story Shear versus Inter-Story Drift Histories for WHN_E	2-30
2-19	Shaking Table Motion for the Taft N21E Base Motion, PGA 0.30 g.....	2-39
2-20	Story Displacement Time Histories for TFT_30	2-40
2-21	Story Shear Force Time Histories for TFT_30	2-41
2-22	Overlaid Global Response Time History Segments for TFT_30	2-42
2-23	Story Displacements and Shear Forces at Maximum First Story Drift for TFT_30.....	2-43
2-24	Story Shear versus Inter-Story Drift Histories for TFT_30	2-44

LIST OF FIGURES (cont.)

FIGURE	TITLE	PAGE
2-25	Energy Time History for TFT_30.....	2-45
2-26	Base Column Shear Forces for TFT_30	2-46
2-27a	Interaction Diagram for the South-East Columns from TFT_30.....	2-47
2-27b	Interaction Diagram for the North-East Columns from TFT_30.....	2-48
2-28a	First Story Beam Bending Moment Time Histories for TFT_30 - South Side.....	2-49
2-28b	First Story Beam Bending Moment Time Histories for TFT_30 - North Side.....	2-50
2-29a	Moment versus Curvature for TFT_30 - Exterior Joint.....	2-51
2-29b	Moment versus Curvature for TFT_30 - Interior Joint.....	2-52
2-30	Moment Diagram at Maximum Story Drift from TFT_30	2-53
2-31	Observed Structural Damage from TFT_30	2-54
2-32	Measured Damage State of the Model after TFT_30	2-55
2-33	Transfer Functions of the Story Level Accelerations from WHN_F.....	2-56
2-34	Smoothed Transfer Functions of the Story Level Accelerations from WHN_F.....	2-57
2-35	Story Shear versus Inter-Story Drift Histories for WHN_F	2-58
2-36	Response Spectra Acceleration Amplification for Taft N21E.....	2-65
3-1	Hysteretic Parameters in IDARC.....	3-9
3-2a	Displacement Comparisons for Minor Shaking - Engineering Approximations.....	3-11
3-2b	Shear Force Comparisons for Minor Shaking - Engineering Approximations.....	3-12
3-3a	Displacement Comparisons for Moderate Shaking - Engineering Approximations.....	3-13
3-3b	Shear Force Comparisons for Moderate Shaking - Engineering Approximations.....	3-14
3-4a	Displacement Comparisons for Severe Shaking - Engineering Approximations.....	3-15
3-4b	Shear Force Comparisons for Severe Shaking - Engineering Approximations.....	3-16
3-5a	Displacement Comparisons for Minor Shaking - Component Tests	3-17
3-5b	Shear Force Comparisons for Minor Shaking - Component Tests	3-18
3-6a	Displacement Comparisons for Moderate Shaking - Component Tests	3-19

LIST OF FIGURES (cont.)

FIGURE	TITLE	PAGE
3-6b	Shear Force Comparisons for Moderate Shaking - Component Tests.....	3-20
3-7a	Displacement Comparisons for Severe Shaking - Component Tests	3-21
3-7b	Shear Force Comparisons for Severe Shaking - Component Tests	3-22
3-8	Collapse Mode (Shakedown) Analysis	3-23
3-9a	Displacement Comparisons for Minor Shaking - Analytical Fit	3-24
3-9b	Shear Force Comparisons for Minor Shaking - Analytical Fit	3-25
3-10a	Displacement Comparisons for Moderate Shaking - Analytical Fit	3-26
3-10b	Shear Force Comparisons for Moderate Shaking - Analytical Fit	3-27
3-11a	Displacement Comparisons for Severe Shaking - Analytical Fit	3-28
3-11b	Shear Force Comparisons for Severe Shaking - Analytical Fit	3-29
3-12a	Comparison of Damage State after Minor Shaking	3-30
3-12b	Comparison of Damage State after Moderate Shaking	3-31
3-12c	Comparison of Damage State after Severe Shaking	3-32
3-13	Damage Quantifications of the Model	3-37
3-14	Resulting Member Damage Indices for the Various PGAs	3-41
3-15	Conceptual Model of Damage with P-delta Effect	3-43
3-16	First Story Interior Columns Monotonic Strength Deformation.....	3-44
3-17	First Story Interior Column Damage Index for 0.20 g with (w) and without (w/o) P- Δ Effect.....	3-46
3-18	First Story Interior Column Damage Index for 0.25 g with (w) and without (w/o) P- Δ Effect.....	3-47
3-19	First Story Interior Column Damage Index for 0.30 g with (w) and without (w/o) P- Δ Effect.....	3-48
3-20	First Story Interior Column Damage Index for 0.35 g with (w) and without (w/o) P- Δ Effect.....	3-49
3-21	First Story Interior Column Damage Index for 0.40 g with (w) and without (w/o) P- Δ Effect.....	3-50
3-22	Typical Structural Response	3-54
3-23	Elastic Base Shear Response.....	3-55

LIST OF TABLES

TABLE	TITLE	PAGE
1-1	NCEER Publications Summarizing Current Study.....	1-6
2-1	Maximum Response for Moderate Earthquake TFT_20	2-3
2-2	Dynamic Properties and Stiffness Matrix before and after Moderate Shaking.....	2-8
2-3	Low Amplitude Initial Stiffnesses from the Shear versus Inter-Story Drift Histories	2-9
2-4	Analytical and Experimental Comparisons of the Dynamic Properties.....	2-9
2-5	Maximum Response for Severe Earthquake TFT_30.....	2-32
2-6	Dynamic Properties and Stiffness Matrix before and after Severe Shaking	2-37
2-7	Low Amplitude Initial Stiffnesses from the Shear versus Inter-Story Drift Histories	2-38
2-8	Analytical and Experimental Comparison of the Dynamic Properties	2-38
2-9	Maximum Response from Shaking Table Testing.....	2-59
2-10	Dynamic Characteristic History of the Model	2-60
3-1	Summary of Member Parameters for Analytical Modeling.....	3-10
3-2	Maximum Response and Damage Index Comparisons	3-40
3-3	Strength Reduction Comparisons.....	3-53

SECTION 1

INTRODUCTION

1.1 Background

The study presented herein is part of a comprehensive research program sponsored by the National Center for Earthquake Engineering Research (NCEER) on the seismic damage assessment and performance evaluation of buildings in zones of low seismicity, such as in the Eastern and Central United States. Buildings in such zones are typically designed only for gravity loads ($U = 1.4D + 1.7L$, herein referred to as GLD) according to the non-seismic detailing provisions of the code. These buildings are also termed lightly reinforced concrete (LRC) structures throughout this study. Although such structures are designed without consideration of lateral loads, they still possess an inherent lateral strength which may be capable of resisting some minor and moderate earthquakes. However the deficient detailing of members can lead to inadequate structural performance during seismic activity.

Two main parts from the current study (i) a seismic performance **Evaluation** of gravity load designed R/C Frame Buildings and (ii) an evaluation of seismic **Retrofit** of R/C frame structures. The first part will be mentioned as **Evaluation** and the second as **Retrofit**.

A research program on the **Evaluation of the seismic performance of gravity load designed R/C frame buildings** was developed and carried out according to the plan outlined in Fig. 1-1.

Based on a survey of typical building construction practices in the Eastern and Central United States (Lao, 1990 and El-Attar et al., 1991a and 1991b), a one-third scale model was constructed and tested on the shaking table in the State University of New York (SUNY) at Buffalo Earthquake Simulation Laboratory. The prototype design, model construction and similitude, initial dynamic characteristics, shaking table testing program along with the simulated ground motions, and the elastic response of the model from minor base motions are presented in Part I of the Evaluation Report Series (Bracci et al 1992a). Based on this report, analytical models can be developed and used to predict the inelastic response of the model building during more severe earthquakes.

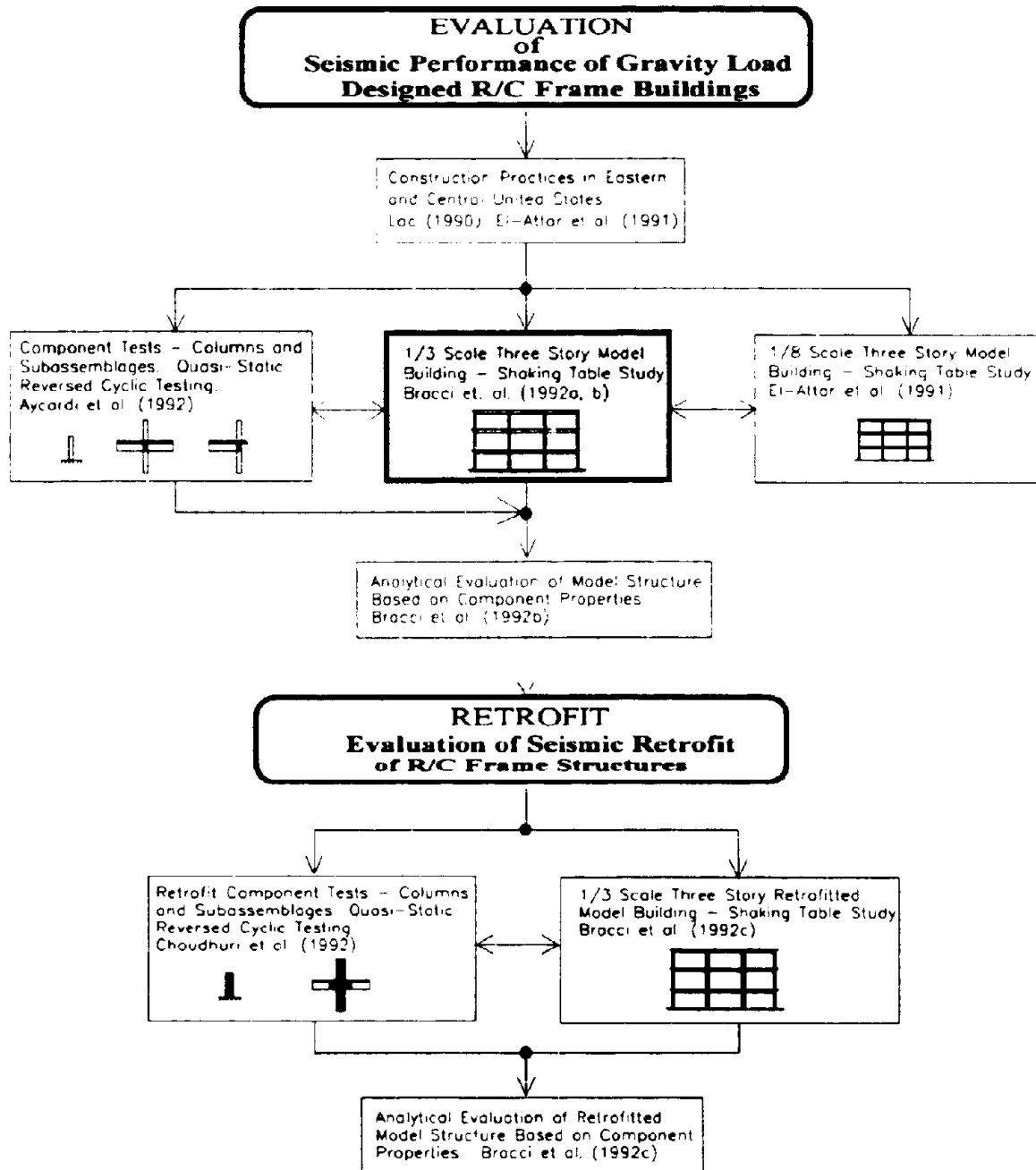


FIG. 1-1 Research Context - Seismic Performance of Gravity Load Designed Reinforced Concrete Frame Buildings

Companion reduced scale slab-beam-column subassemblages were also constructed with the same materials in conjunction with the construction of the one-third scale model building are presented in Part II of the Evaluation Report Series (Aycardi et al., 1992). The components were tested under quasi-static reversed cyclic loading and conducted prior to the testing of the model building. The results of the component tests were used to identify the behavior of localized members and subassemblages of the structure and the member properties for predicting the overall response of the model building with analytical tools.

The experimental and analytical performance of the model building during moderate and severe shaking is presented in Part III of the Evaluation Report Series (this report). The analytical predictions of the model building during these earthquakes are presented based on member behavior developed from engineering approximations and component tests. Some of the conclusions of the evaluation study are that the response of the model is governed by weak column - strong beam behavior and large story drifts develop under moderate and severe earthquakes. A one-eighth scale model of the same prototype building was also constructed and tested at Cornell University by El-Attar et al. (1991b) as part of a collaborative study with SUNY/Buffalo. A comparison of the response behavior between the two scale models is also presented.

A second part of this research program was conducted to evaluate various **seismic retrofit techniques for R/C frame structures** typically constructed in low seismicity zones (see Fig. 1-1). Based on the seismic behavior of the one-third scale model from the previous study, a series of retrofit schemes were proposed for improved seismic resistance and presented in Part II of the Retrofit Report Series (Bracci et al, 1992b).

In Part I of the Retrofit Report Series (Choudhuri et al., 1992) of this research program, a capacity analysis and redesign method for seismic retrofitting of R/C structures is developed and tested. Retrofit using an improved concrete jacketing technique was selected and first performed on companion components. The retrofitted components were then tested under quasi-static reversed cyclic loading and used to identify the behavior of the individual members. Retrofit of the components was also performed to verify the constructability of the retrofit technique for the model building.

The work done in Part I of the Retrofit Report Series is used as base to evaluate and model the member properties of the beam column components with the concrete jacketing technique and is used further for predicting the response of the overall retrofitted model building with analyses

presented in Part II of the Retrofit Report Series (Bracci et al, 1992b). Based on analytical estimates, a global seismic retrofit for the one-third scale model building was proposed and constructed. An experimental and analytical shaking table study of the retrofitted model building was then conducted and the response behavior is presented. The main conclusions from this study are that seismic retrofit of gravity load designed R/C frame buildings: (i) can be designed to successfully enforce a strong column - weak beam behavior; and (ii) is a viable economic and structural alternative as compared to demolition and reconstruction of another.

1.2 Overall Objectives of Research Program

The objectives of the overall research program are summarized below along with the corresponding NCEER publications from Table 1-1:

1. Investigate the performance and principal deficiencies of typical LRC frame buildings during earthquakes through shaking table testing of a one-third scale model under minor, moderate, and severe earthquakes. (*Seismic Resistance of R/C Frame Structures Designed only for Gravity Loads: Parts I and III*, Evaluation report series, by J.M. Bracci, A.M. Reinhorn, and J.B. Mander)
2. Identify the potential collapse mechanisms for typical LRC frame buildings. (*Seismic Resistance of R/C Frame Structures Designed only for Gravity Loads: Part III*, Evaluation report series, by J.M. Bracci, A.M. Reinhorn, and J.B. Mander)
3. Determine the behavior and material properties of individual members and sub-assemblages of the structure. (*Seismic Resistance of R/C Frame Structures Designed only for Gravity Loads: Part II*, Evaluation report series, by L.E. Aycardi, J.B. Mander, and A.M. Reinhorn)
4. Determine the contribution of components in the overall response of the structure near collapse. (*Seismic Resistance of R/C Frame Structures Designed only for Gravity Loads: Parts II and III*, Evaluation report series, by J.M. Bracci, L.E. Aycardi, A.M. Reinhorn, and J.B. Mander)
5. Compare the measured response of the model building with that predicted by analytical models developed from engineering approximations or from component

tests using a non-linear time history dynamic analysis. (*Seismic Resistance of R/C Frame Structures Designed only for Gravity Loads: Part III*, Evaluation report series, by J.M. Bracci, A.M. Reinhorn, and J.B. Mander)

6. Investigate appropriate local and global retrofit techniques for improving the seismic performance of LRC buildings. (*Evaluation of Seismic Retrofit of R/C Frame Structures: Part II*, Retrofit report series, by J.M. Bracci, A.M. Reinhorn, and J.B. Mander)
7. Investigate the seismic performance of the retrofitted model building and compare the measured response with the response of the original (unretrofitted) model from the same earthquakes. (*Evaluation of Seismic Retrofit of R/C Frame Structures: Part II*, Retrofit report series, by J.M. Bracci, A.M. Reinhorn, and J.B. Mander)
8. Determine the behavior and material properties of the retrofitted members and subassemblages of the structure. (*Evaluation of Seismic Retrofit of R/C Frame Structures: Part I*, Retrofit report series, by D. Choudhuri, J.B. Mander, and A.M. Reinhorn)
9. Determine the contribution of retrofitted and unretrofitted components in the overall response of the structure near collapse. (*Evaluation of Seismic Retrofit of R/C Frame Structures: Part I*, Retrofit report series, by D. Choudhuri, J.B. Mander, and A.M. Reinhorn)
10. Compare the measured response of the retrofitted model building with that predicted by analytical models developed from engineering approximations or from component tests using a non-linear time history dynamic analysis. (*Evaluation of Seismic Retrofit of R/C Frame Structures: Part II*, Retrofit report series, by J.M. Bracci, A.M. Reinhorn, and J.B. Mander)

TABLE 1-1 NCEER Publications Summarizing Current Study

EVALUATION SERIES:
Seismic Resistance of R/C Frame Structures Designed only for Gravity Loads
Part I: Design and Properties of a One-Third Scale Model Structure (by J.M. Bracci, A.M. Reinhorn, and J.B. Mander), NCEER-92-0027
<ul style="list-style-type: none"> (i) Identification of deficiencies of current engineering practice. (ii) Scale modeling. (iii) Experimental identification of structural characteristics. (iv) Ground motions for structural evaluation and experimental program. <p>Note: This report serves as bare material for evaluation of analytical tools.</p>
Part II: Experimental Performance of Subassemblages (by L.E. Aycardi, J.B. Mander, and A.M. Reinhorn), NCEER-92-0028
<ul style="list-style-type: none"> (i) Identify behavior and deficiencies of various components in structures. (ii) Identify member characteristics for developing analytical models to predict the seismic response of the one-third scale model structure. <p>Note: This report serves as evaluation of structural characteristics to be incorporated in the evaluation of the entire structural system.</p>
Part III: Experimental Performance and Analytical Study of Structural Model (by J.M. Bracci, A.M. Reinhorn, and J.B. Mander), NCEER-92-0029
<ul style="list-style-type: none"> (i) Investigate the performance and principal deficiencies of typical gravity load designed frame buildings during earthquakes through shaking table testing of a one-third scale model under minor, moderate and severe earthquakes. (ii) Identify the potential collapse mechanisms for such typical frame buildings. (iii) Compare the measured response of the model building with that predicted by analytical models developed from (1) engineering approximations, (2) component tests, and (3) an experimental fit using a non-linear time history dynamic analysis. <p>Note: This report emphasizes the structural behavior, collapse margins via damage, and efficiency of predictions using component properties evaluated from tests.</p>

RETROFIT SERIES:
Evaluation of Seismic Retrofit of R/C Frame Structures
Part I: Experimental Performance of Retrofitted Subassemblages (by D. Choudhuri, J.B. Mander, and A.M. Reinhorn), NCEER-92-0030
<ul style="list-style-type: none"> (i) Presentation of retrofit techniques. (ii) Identify constructability and behavior of retrofitted components. (iii) Identify retrofitted member characteristics for developing analytical models to predict seismic response of the retrofitted model building.
Part II: Experimental Performance and Analytical Study of Retrofitted Structural Model (by J.M. Bracci, A.M. Reinhorn, and J.B. Mander), NCEER-92-0031
<ul style="list-style-type: none"> (i) An analytical seismic evaluation of retrofitted gravity load designed frame buildings using various local and global retrofit techniques. (ii) Shaking table testing of one of the proposed retrofit techniques on the 1/3 scale model under minor, moderate, and severe earthquakes. (iii) Verify a change in formation of the potential collapse mechanism under ultimate load from an undesirable column-sidesway/soft-story mechanism to a more desirable beam-sidesway mechanism. (iv) Compare the measured response of the retrofitted model building with that predicted by analytical models developed from engineering approximations and component tests using a non-linear time history dynamic analysis.

1.3 Scope of this Report

The intentions of this report are to identify: (i) the structural behavior during seismic activity; (ii) the safety margin before collapse based on damage evaluation and (iii) the adequacy of predictions of response using component properties evaluated from tests.

Section 2 details the response of the model from tests with moderate and severe earthquake motions. A corresponding damage evaluation and identification of the ensuing dynamic characteristics of the model is provided. The maximum story response and dynamic characteristic history of the model from the minor, moderate, and severe earthquakes is summarized. Finally, the concluding remarks on the seismic excitation of typical LRC buildings are outlined.

Section 3 presents the analytical models developed for predicting the seismic response of the model and the comparison with the experimentally measured response. The member and overall structural damage from the earthquakes is analytically quantified in terms of damage indices. Identification of the critical earthquake and collapse patterns for the model are also made analytically. A modified damage index is proposed to incorporate the additional damage from the P-delta effect in columns. Finally, an elastic analysis is used to help identify the response reduction factors of the inelastic response.

Section 4 presents a summary and conclusions of the third and final phase of the evaluation study.

1.4 Summary of Structural Behavior During Minor Base Motions

The global and local response of the model building during the minor earthquake (Taft N21E, PGA 0.05g) was presented in Part I of the Evaluation report series (Bracci et al, 1992a). It was shown that the response of the model was primarily governed by elastic deformations. However some slight cracking was observed in some of the columns. The white noise identification test showed that only slight changes of natural frequencies and story stiffnesses resulted from the minor base motion. Therefore, it was concluded that although the gravity load designed buildings are not designed for lateral forces, the inherent lateral strength and flexibility of such buildings are sufficient to resist the forces of very minor earthquakes.

SECTION 2

INELASTIC RESPONSE DURING MODERATE AND SEVERE SHAKING

2.1 Introduction

The structural response for the one-third scale three story model tested on the shaking table for dynamic characteristic identifications and under a minor (low level earthquake) base excitation (TFT_05) was presented by Bracci et al. (1992a). It was shown that the response was primarily governed by elastic deformations with little energy dissipated by each story.

In this section, a moderate base motion, the Taft N21E accelerogram with the peak ground acceleration (PGA) scaled to 0.20 g, is first used for expected large story drifts and inelastic deformations in the model. The structural response, the damage evaluation, and the identification of the ensuing dynamic characteristics of the model are presented.

A more severe shaking is subsequently used (Taft N21E accelerogram with the PGA scaled to 0.30 g) to create further inelastic structural behavior and to identify the potential dynamic collapse mechanism for the model. Likewise, the response results, damage evaluation, and ensuing dynamic characteristics of the model are presented.

2.2 Response to Moderate Earthquake

Following the identification tests for determining the current dynamic properties and stiffness matrix of the model (WHN_C and WHN_D), a moderate table motion, the Taft N21E accelerogram component normalized for a PGA of 0.20 g, was used to excite the model (herein referred to as TFT_20). Figs. 2-1a and 2-1b show the desired and achieved shaking table acceleration motions for TFT_20. Fig. 2-1c shows a short segment of the desired and achieved shaking table motions, from which a high degree of similarity exists.

2.2.1 Global Response

Fig. 2-2 shows the story displacement time histories of the model for shaking table test TFT_20. Figs. 2-3c and 2-3b show the shear force time histories identified from the load cells in the first and second story columns. Since load cells are not installed in the third story columns, the third

maximum response magnitudes exist between the tests. Some explanations are due to: (i) the different inertial mass and natural frequencies; (ii) the different Taft component of base motion; and (iii) the different material properties.

TABLE 2-1 Maximum Response for Moderate Earthquake TFT_20

Story	Max. Story Displacement (in.)	Max. Inter-Story Drift (%)	Max. Story Shear (kips)	Max. Story Load (kips)	Peak Story Acceleration (g)
Third	1.32	0.54	5.6	5.6	0.20
Second	1.14	1.07	9.3	5.7	0.20
First	0.64	1.33	12.3 (15.2%W)	7.8	0.25

Fig. 2-6 shows the story shear force versus inter-story drift histories for each floor of the model for TFT_20, along with the low amplitude initial stiffnesses from the previous white noise excitation (WHN_D). The post-cracking/-yielding story stiffness (herein referred to as the secondary stiffness) is also identified for TFT_20 as 16.5 kip/in and 15.6 kip/in for first and second floors, respectively. Since the third story remains primarily elastic, the third story secondary stiffness can not be identified from this intensity motion. A comparison of the resulting secondary stiffnesses from the severe ground motion will be pursued to detect any changes due to continued inelastic deformation and strength deterioration in the members of that story. It can be observed from Fig. 2-6 that considerable inelastic behavior and corresponding stiffness reductions has primarily occurred to the first and second stories from TFT_20. It should be noted that story shear force versus inter-story drift histories corresponds to the response of the story as a whole. Therefore, although inelastic deformations can be observed, the location of such damage can not be distinguished, but will be identified later through the local response.

Fig. 2-7 shows the energy time histories for TFT_20. The total input energy to the structural system is 24.0 kip-in, which is about 14 times greater than the input energy from TFT_05 (1.7 kip-in). The percentage ratio of the dissipated hysteretic and viscous damped energies by each floor with respect to the total structural energy dissipation is 53.2% : 33.2% : 13.6%, respectively for the first, second, and third stories. It should be noted that although the hysteretic and viscous damped energies can not be identified separately since damping is included in the experimental

recordings of the story shears, a majority of the dissipated energies occurs due to inelastic deformations or hysteresis in the stories. This is speculated based on the small equivalent viscous damping present and the large quantity of dissipated energies.

2.2.2 Local Response

The internal forces in the column and beams, member sections designated in Fig 2-8, were measured during the moderate shaking and are presented in the following discussions.

Fig. 2-9 shows the induced shear forces on the exterior and interior first story columns (base shear) for table motion TFT_20. It can be observed that the shear force demands in the interior columns are similar and are larger than the exterior columns. Also note that the exterior columns attract higher shear forces when the axial force increases. Thus the resulting shear force demands in the exterior columns with greater axial force are about 75% of interior column shear force demands, while the exterior columns with less axial force are about 50%.

Fig. 2-10 shows the bending moment versus axial load interaction histories for the columns of the first and second stories. The cracking, nominal ultimate, and projected dynamic ultimate surfaces were presented in Part I of the Evaluation series (Bracci et al, 1992a). It can be observed that the bending moment versus axial load interaction histories in the columns extend well beyond the cracking surface and in some cases beyond the nominal ultimate bounds. For columns #3 and #4 (first floor south-east columns), the moment-axial load interaction extends to the projected dynamic ultimate surface. This extension occurs on the "large pulse" and then remains within the nominal ultimate bounds. Therefore, it is concluded that large inelastic deformations and yielding of first and second story column members has occurred for TFT_20, especially during the "large pulse". Also axial loads variations exist in the exterior columns (observed by the slope in the interaction history) with very little fluctuation occurring in the interior columns.

Figs. 2-11a and 2-11b show the first story beam bending moment time histories in the south and north sides of the model at the column face along with the ultimate moment surfaces. The ultimate surfaces for the beams were presented in Part I of the Evaluation series (Bracci et al, (1992a) and considered strength contributions from the slab reinforcement within the flange width from the ACI Code (18 in.) and also within the full slab width (60 in.). It can be observed that the positive moment demand (plotted negative) in exterior beam section Exbm151 exceeds the nominal ultimate bounds which considers the pull-out effect of the positive longitudinal reinforcement, while the others remain within this surface. Note that the positive nominal

ultimate surfaces without pull-out considerations are shown for representation but can be discarded since the required development lengths of the bottom rebars are not provided for full strength. Also the negative moment demands (plotted positive) in several of the beams exceed the nominal ultimate surface which considers the slab steel within the ACI flange width. But since larger contributions of slab steel remain throughout the slab, the members are well within the ultimate bounds.

Fig. 2-12 shows the bending moment versus corrected curvatures for the instrumented members of the first floor north-east exterior and interior joints at the column and beam faces along with the member moment capacities. Yielding and inelastic behavior can be observed in the columns and in exterior beam section Exbm151 (positive pull-out moment direction). The full positive moment capacity, considering the pull-out effect, is achieved and yielding has occurred. However, pull-out of the bottom beam reinforcement is not evident since the bending moment strength has not deteriorated and large curvatures do not develop. Note that the inelastic behavior in the columns would be more appreciable on the south-east side of the model. This can be observed in Fig. 2-10a where the interaction histories for columns #3 and #4 extend to the projected dynamic ultimate surface, whereas the interaction histories for columns #1 and #2 remain within the projected dynamic ultimate surface. The interior beam sections, Exbm152 and Exbm153, remain primarily elastic. Therefore as expected, the slab steel from the full slab width has significant contribution to the beam moment capacity. In conclusion, yielding has occurred in the columns and in section Exbm151.

The bending moment diagrams for the model when the first story drift was maximum in each direction, along with the corresponding story displacements and nominal moment capacities, are shown in Fig. 2-13. It can be observed that most of the column moments in the first and second stories have reached the nominal ultimate capacities. Only the exterior columns away from the direction in which the structure was moving (at that instant in time) remain below nominal capacity. Thus a complete column-sidesway or soft-story failure mechanism did not develop at this instant in time.

The observed visual structural damage to the scaled model due to the TFT_20 shaking table test is shown in Fig. 2-14. The following points highlight the observed structural damage which are typical for the east and west frames of the model:

- (a) flexural cracks appeared in the splice zone of the first and second story, interior and exterior columns near the location of the transverse hoop reinforcement;

- (b) flexural cracks appeared in the columns at the underside of the first and second story longitudinal beams and above the first story slab;
- (c) vertical flexural cracks appeared in the web of the exterior longitudinal beams (sections Exbm151 and Exbm481 of the first and second stories) near the location of the transverse beam reinforcement;
- (d) exterior columns cracked at the construction joint fully around the columns and at the beam-column joint intersections.

Fig. 2-15 shows the damage state (potential dynamic collapse mechanism) of the model after TFT_20. It can be observed that yielding has occurred in the first and second story columns. Some yielding in the beams also occurs during the "large pulse", especially in the pull-out moment direction for beam section Exbm151. Therefore, the development of a column-sidesway or soft-story collapse mechanism is expected to occur under ultimate loading.

2.3 Dynamic Properties after Moderate Shaking

The identification of the ensuing dynamic properties after TFT_20 are determined from the white noise excitation label as WHN_E. Fig. 2-16 shows the story transfer functions for each floor of the model. Inelastic response from a stick-slip type condition can be observed by the excitation of many frequencies near the modes of vibration. To filter these high frequencies, the signal of the story transfer functions are smoothed using a moving average of three digital points and are shown in Fig. 2-17. Since small damping and well separated modes can be observed, the average natural frequencies after TFT_20 are identified as follows and tabulated in Table 2-2:

$$\mathbf{f}_i = \begin{pmatrix} 1.42 \\ 4.37 \\ 6.18 \end{pmatrix} \text{ Hz.} \quad (2.1)$$

It can be observed from Table 2-2 that the modal natural frequency reductions of 17.0%, 16.3%, and 15.6%, respectively occurred due to the TFT_20 test. These reductions correspond to inelastic deterioration and are considerably larger than that after TFT_05.

The modal shapes and participation factors after test TFT_20 are also identified from the story transfer functions of test WHN_E and tabulated in Table 2-2. Slightly varying modal shapes and participation factors can be observed before (WHN_D) and after (WHN_E) test TFT_20. This can be attributed to the inelastic behavior of the model from the moderate excitation.

The equivalent viscous damping factors are determined from the transfer functions (see Part I, Bracci et al., 1992a) as 6.6%, 5.6%, and 2.8%, respectively. A large variation can be observed in comparing the damping factors before and after TFT_20 from Table 2-2. Again since the model experienced inelastic deformations from test TFT_20, large equivalent viscous damping has occurred due to the contributions from hysteretic damping. Therefore, non-linear damping characteristics occur from the inelastic deformations.

The updated stiffness matrix of the model is developed using the dynamic characteristics of white noise excitation WHN_E (see Part I, Bracci et al., 1992a) and shown in Table 2-2. It can be observed that the sum of the diagonal terms of the stiffness matrix is reduced by an additional 29.2% after the TFT_20 test or 36.7% of the undamaged model (WHN_B). Story stiffness reductions of 41.7%, 30.5%, and 20.7%, respectively for the first, second, and third stories, have resulted from TFT_20.

Fig. 2-18 shows the story shear versus inter-story drift histories for WHN_E. The low amplitude initial stiffnesses after TFT_20 (WHN_E) are tabulated in Table 2-3 along with the results of WHN_B and WHN_D. It can be observed that the stiffnesses are reduced by an additional 30.6%, 33.2%, and 29.0% or 33.6%, 38.0%, and 40.0% of the original stiffnesses from WHN_B, respectively for the first, second, and third floors. Note that the average of these reductions is similar to the reductions found in the stiffness matrix in Table 2-2.

To obtain the first mode natural frequency identified from WHN_E after the TFT_20 base motion (1.42 Hz.), by analysis, the member stiffness properties used in STAAD™ were:

$$(EI)_{\text{member}} = 0.358 (EI)_g \quad (2.2)$$

where $(EI)_{\text{member}}$ is the reduced beam or column member stiffness based on the respective gross member area.

Note these reduced member stiffnesses are 31.2% less than the stiffnesses used after TFT_05 and 37.6% less than the undamaged state. The analytical prediction of the natural frequencies, modal shapes, and stiffness matrix of the model after TFT_20 based on input member properties in STAAD [Eq. (2.2)] are shown in Table 2-4 along with the results from WHN_E. It can be observed that the first mode natural frequency and modal shape matrices are comparable with the identified results from WHN_E. But note that slight deviations occur in the second and third mode natural frequencies. Also a 0.3% deviation is observed in the sum of the diagonal terms of the identified stiffness matrix and comparable story stiffnesses are observed. Therefore an accurate prediction of the stiffness matrix is achieved when the first mode natural frequency is duplicated in STAAD.

TABLE 2-2 Dynamic Properties and Stiffness Matrix before and after Moderate Shaking

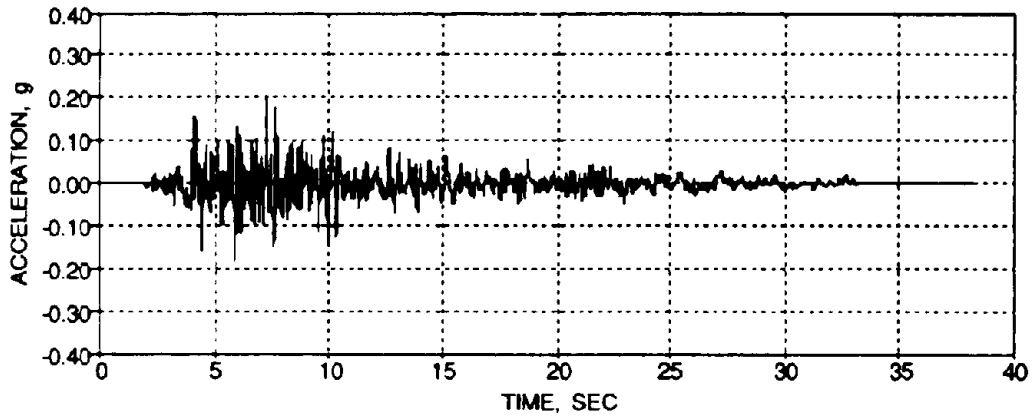
	WHN_D (before)	WHN_E (after)
Natural Frequencies (Hz.)	$f_i = \begin{pmatrix} 1.71 \\ 5.22 \\ 7.32 \end{pmatrix}$	$f_i = \begin{pmatrix} 1.42 \\ 4.37 \\ 6.18 \end{pmatrix}$
Modal Shapes	$\Phi_y = \begin{pmatrix} 1.00 & -0.88 & -0.40 \\ 0.79 & 0.58 & 1.00 \\ 0.41 & 1.00 & -0.86 \end{pmatrix}$	$\Phi_y = \begin{pmatrix} 1.00 & -0.95 & -0.45 \\ 0.83 & 0.55 & 1.00 \\ 0.43 & 1.00 & -0.78 \end{pmatrix}$
Modal Participation Factors	$\Gamma_i = \begin{pmatrix} 0.43 \\ 0.13 \\ -0.05 \end{pmatrix}$	$\Gamma_i = \begin{pmatrix} 0.44 \\ 0.11 \\ -0.05 \end{pmatrix}$
Damping Ratios (%)	$\xi_i = \begin{pmatrix} 4.0 \\ 2.9 \\ 1.3 \end{pmatrix}$	$\xi_i = \begin{pmatrix} 6.6 \\ 5.6 \\ 2.8 \end{pmatrix}$
Stiffness Matrix (kip/in)	$\mathbf{K}_y = \begin{pmatrix} 44.6 & -45.8 & -2.7 \\ -45.8 & 92.8 & -44.9 \\ -2.7 & -44.9 & 94.1 \end{pmatrix}$	$\mathbf{K}_y = \begin{pmatrix} 36.4 & -36.3 & -1.0 \\ -36.3 & 67.6 & -31.2 \\ -1.0 & -31.2 & 59.9 \end{pmatrix}$
Story Stiffnesses (kip/in)	$\mathbf{k}_i = \begin{pmatrix} 45.8 \\ 44.9 \\ 49.2 \end{pmatrix}$	$\mathbf{k}_i = \begin{pmatrix} 36.3 \\ 31.2 \\ 28.7 \end{pmatrix}$

TABLE 2-3 Low Amplitude Initial Stiffnesses from the Shear versus Inter-Story Drift Histories

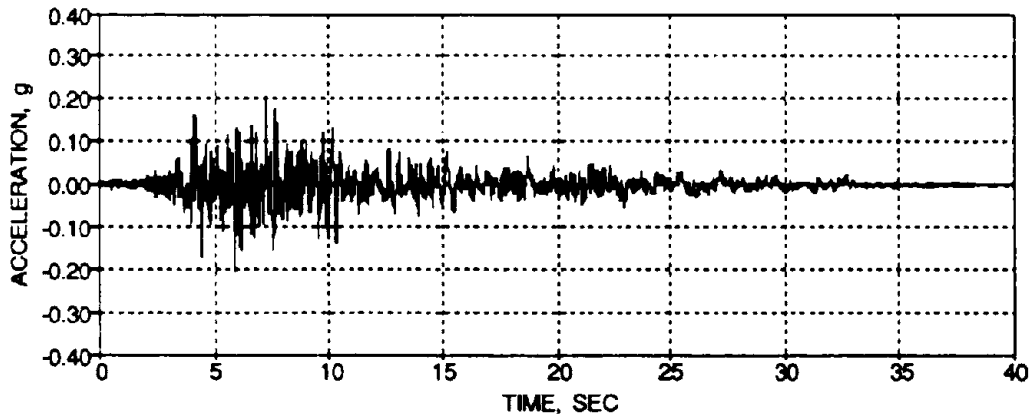
Story	WHN_B (kip/in)	WHN_D (kip/in)	WHN_E (kip/in)
Third	40.0	33.8	24.0
Second	42.4	39.4	26.3
First	51.2	49.0	34.0

TABLE 2-4 Analytical and Experimental Comparison of the Dynamic Properties

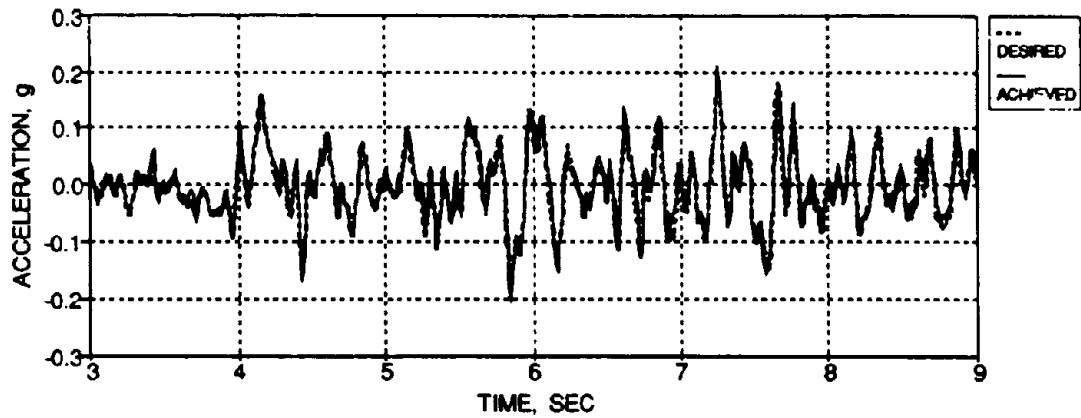
	Experimental (WHN_E)	Analytical [STAAD (0.358 (EI) _g)]
Natural Frequencies (Hz.)	$f_i = \begin{pmatrix} 1.42 \\ 4.37 \\ 6.18 \end{pmatrix}$	$f_i = \begin{pmatrix} 1.42 \\ 4.14 \\ 6.32 \end{pmatrix}$
Modal Shapes	$\Phi_{ij} = \begin{pmatrix} 1.00 & -0.95 & -0.45 \\ 0.83 & 0.55 & 1.00 \\ 0.43 & 1.00 & -0.78 \end{pmatrix}$	$\Phi_{ij} = \begin{pmatrix} 1.00 & -0.81 & -0.43 \\ 0.78 & 0.53 & 1.00 \\ 0.40 & 1.00 & -0.88 \end{pmatrix}$
Stiffness Matrix (kip/in)	$K_{ij} = \begin{pmatrix} 36.4 & -36.3 & -1.0 \\ -36.3 & 67.6 & -31.3 \\ -1.0 & -31.3 & 59.9 \end{pmatrix}$	$K_{ij} = \begin{pmatrix} 29.6 & -32.3 & 2.8 \\ -32.3 & 65.1 & -35.6 \\ 2.8 & -35.6 & 68.6 \end{pmatrix}$
Story Stiffnesses (kip/in)	$k_i = \begin{pmatrix} 36.3 \\ 31.2 \\ 28.7 \end{pmatrix}$	$k_i = \begin{pmatrix} 32.3 \\ 35.6 \\ 33.0 \end{pmatrix}$



(a) Desired Base Motion

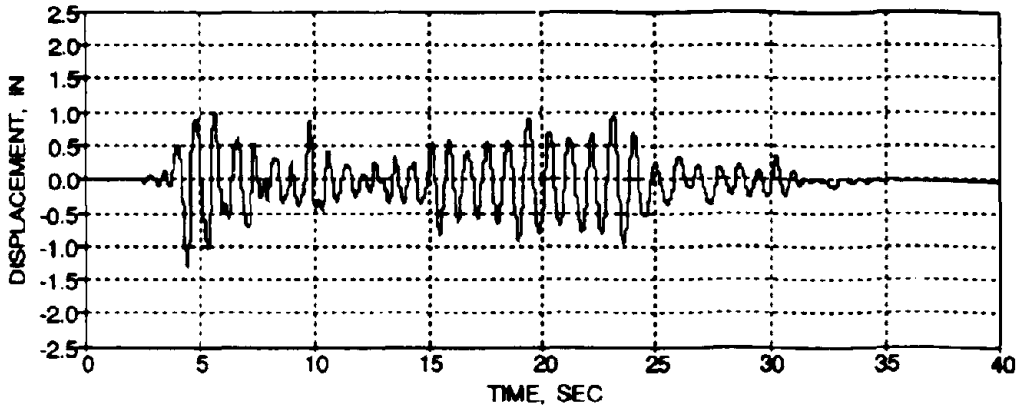


(b) Achieved Base Motion

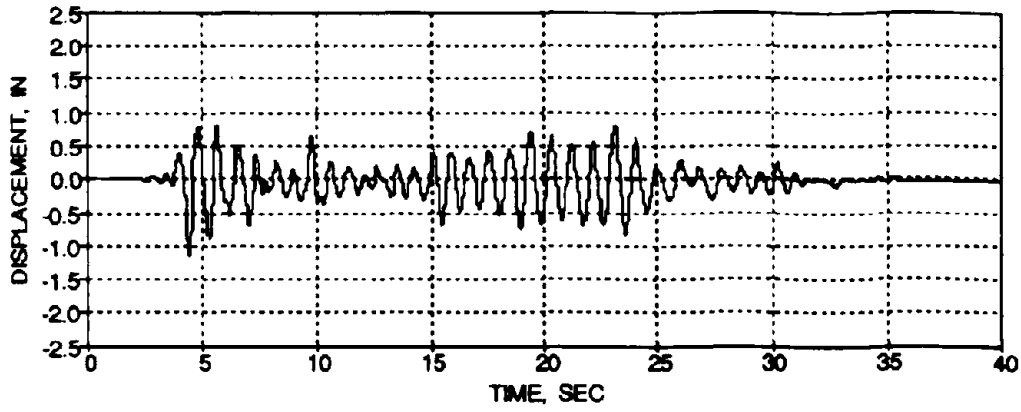


(c) Short Segment Comparison of the Desired and Achieved Base Motions

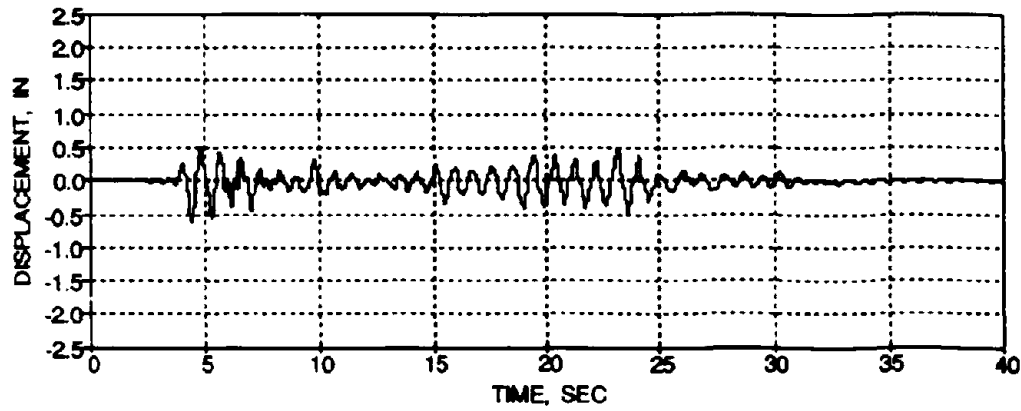
FIG. 2-1 Shaking Table Motion for the Taft N21E Base Motion, PGA 0.20 g



(a) Third Floor

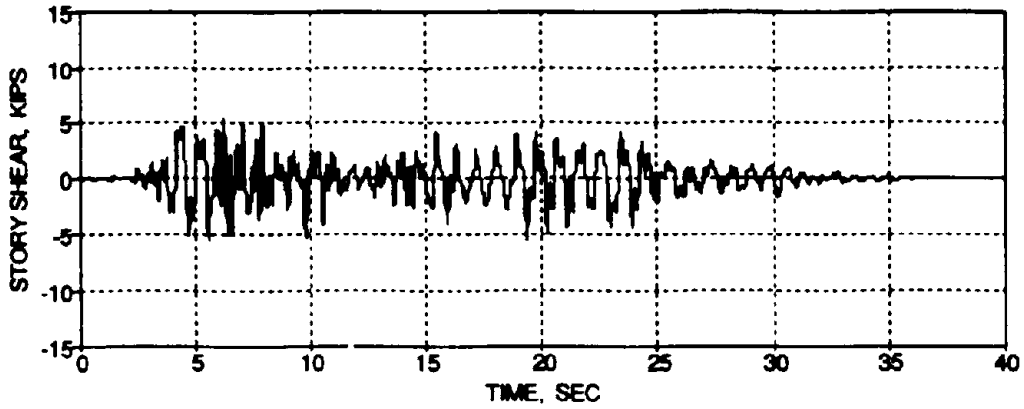


(b) Second Floor

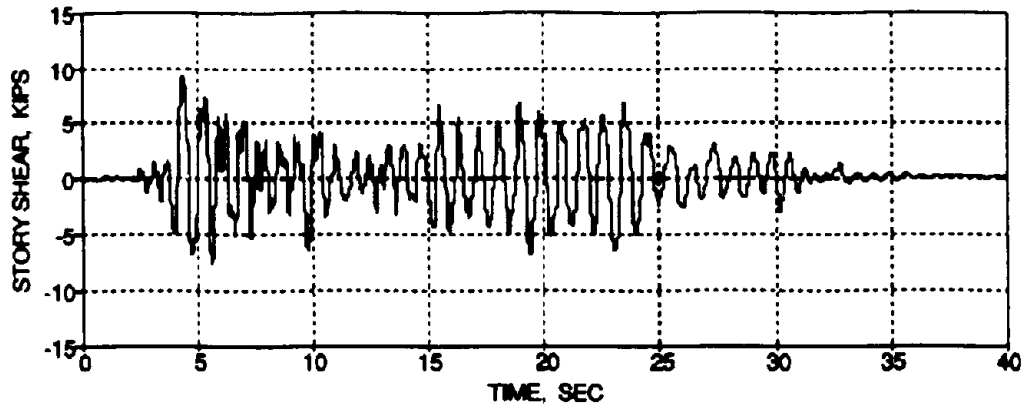


(c) First Floor

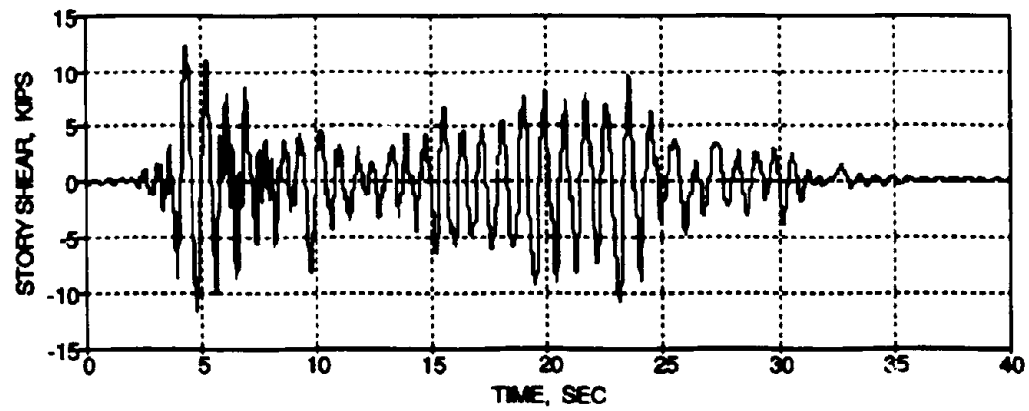
FIG. 2-2 Story Displacement Time Histories for TFT_20



(a) Third Floor

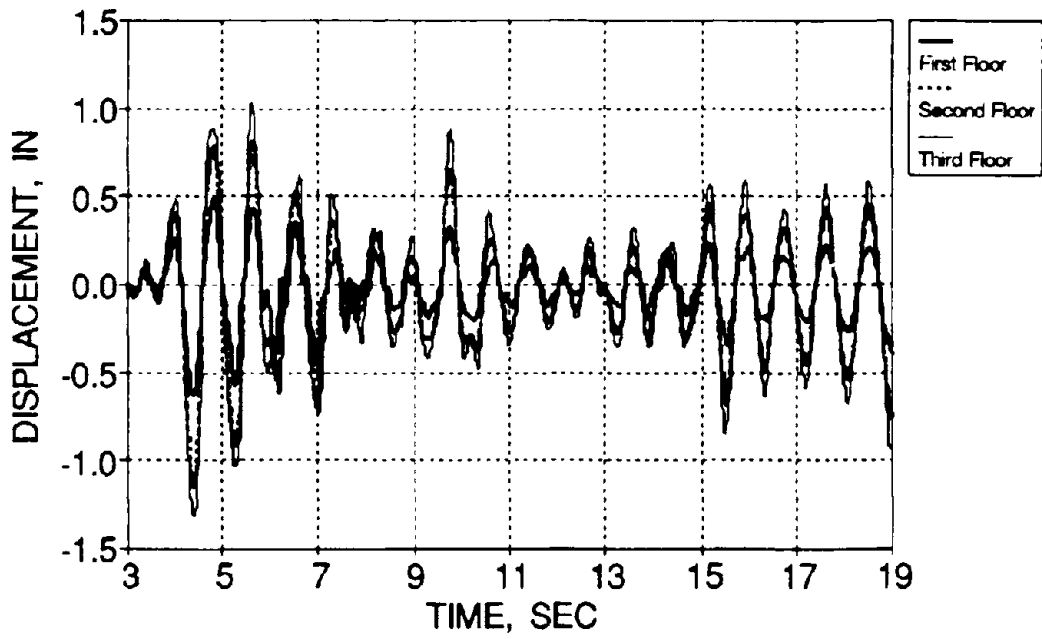


(b) Second Floor

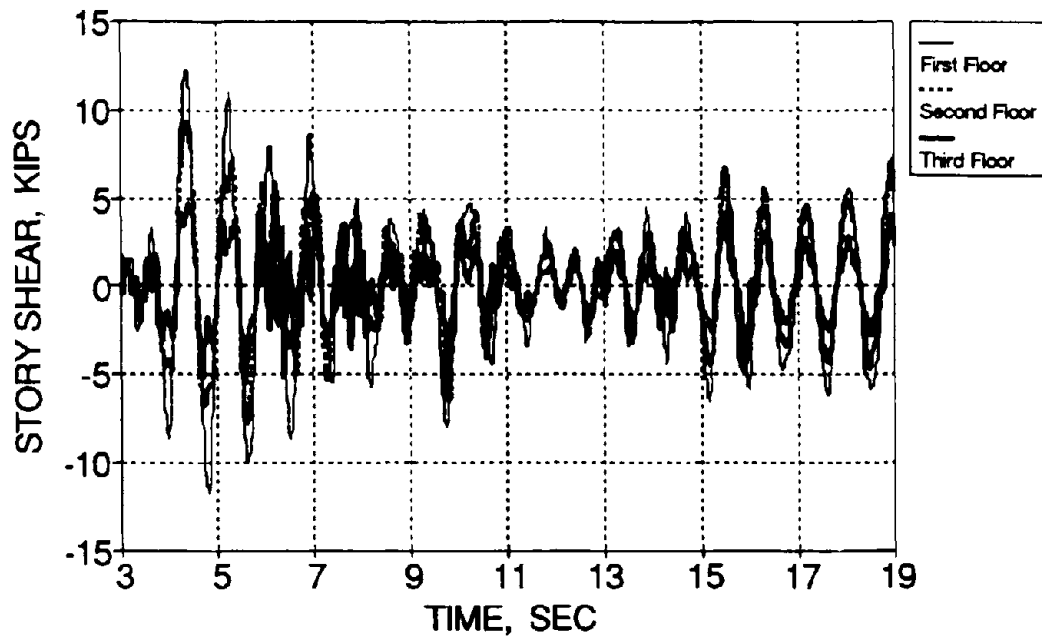


(c) First Floor

FIG. 2-3 Story Shear Force Time Histories for TFT_20

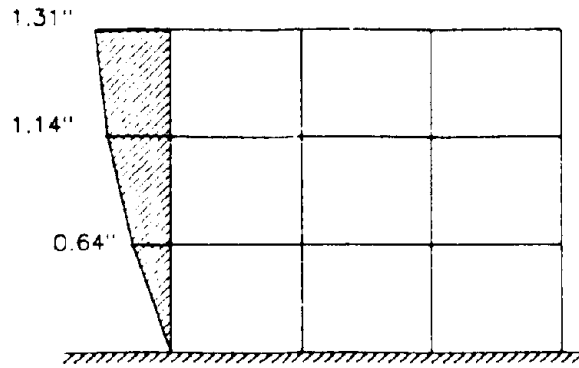


(a) Story Displacements

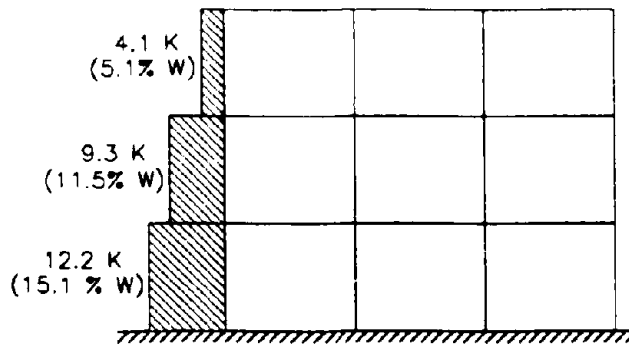


(b) Story Shear Forces

FIG. 2-4 Overlaid Global Response Time History Segments for TFT_20

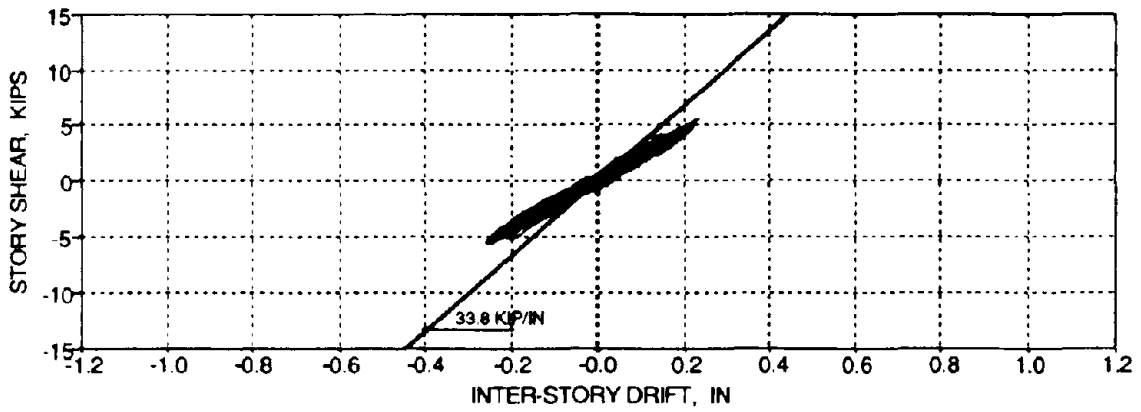


(a) Story Displacements (Time= 4.36 sec)

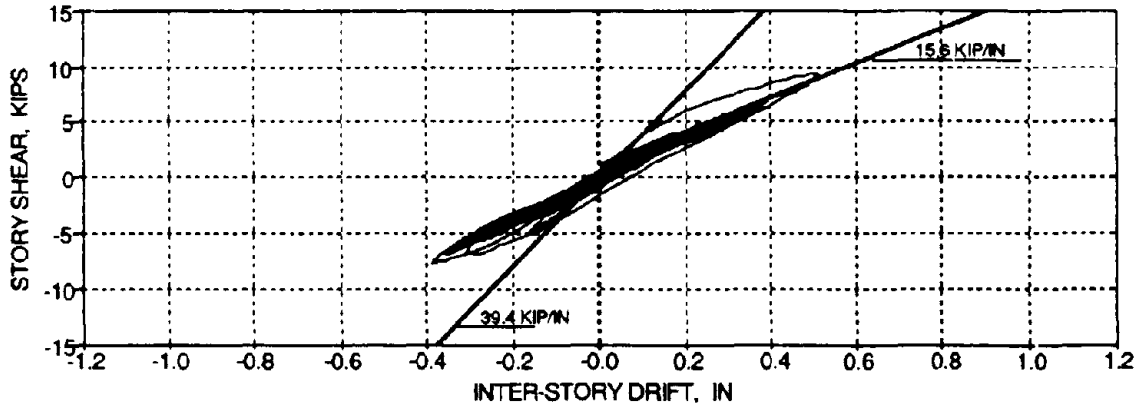


(b) Story Shear Forces (Time = 4.36 sec)

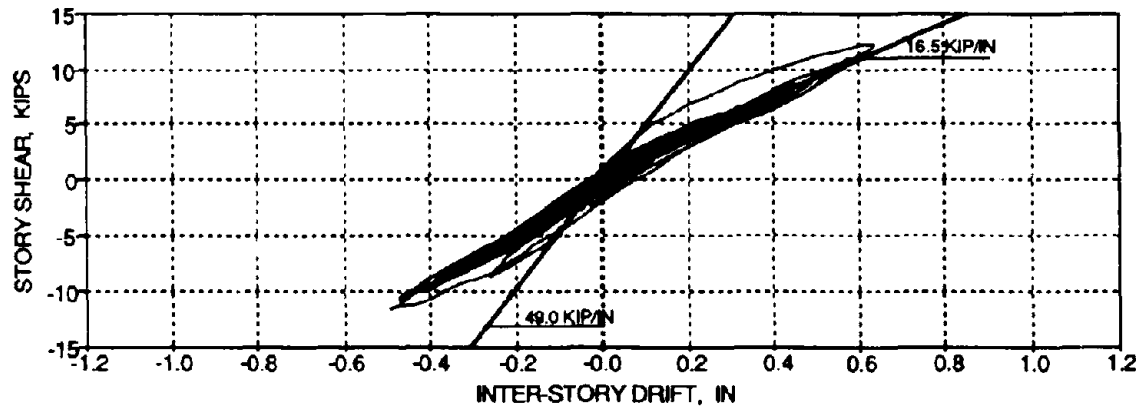
FIG. 2-5 Story Displacements and Shears at Maximum First Story Drift for TFT_20



(a) Third Floor

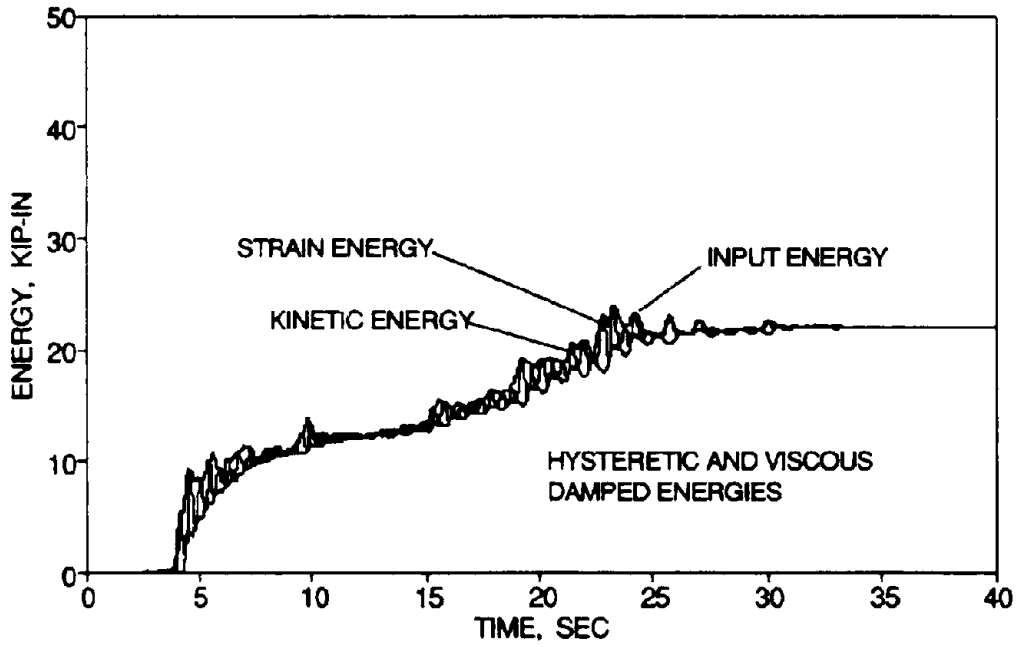


(b) Second Floor

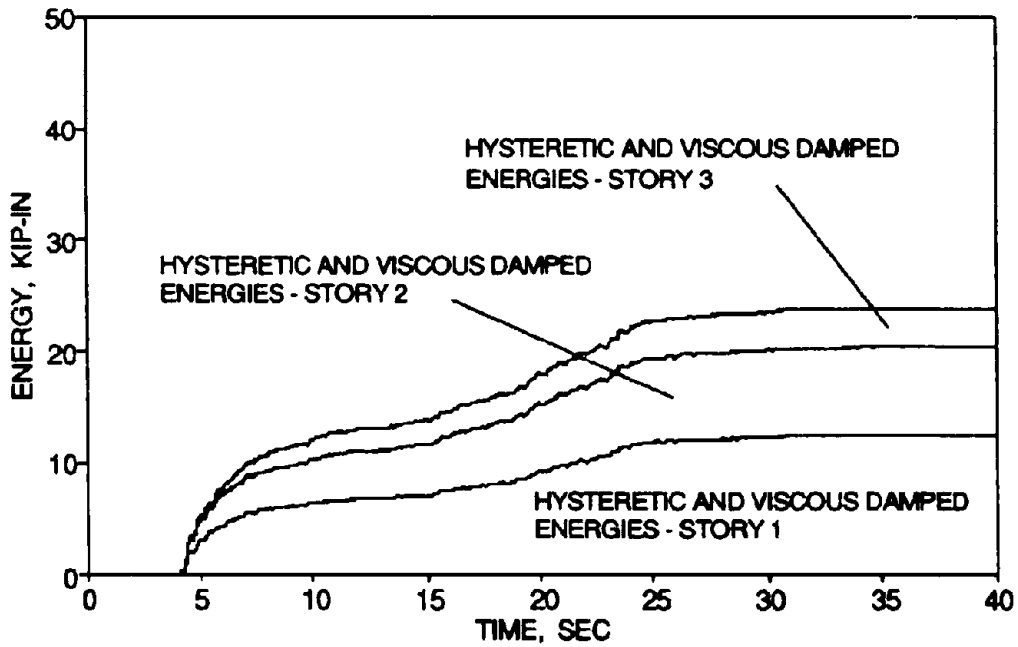


(c) First Floor

FIG. 2-6 Story Shear versus Inter-Story Drift Histories for TFT_20



(a) Energy Balance



(b) Story Dissipated Energies

FIG. 2-7 Energy Time History for TFT_20

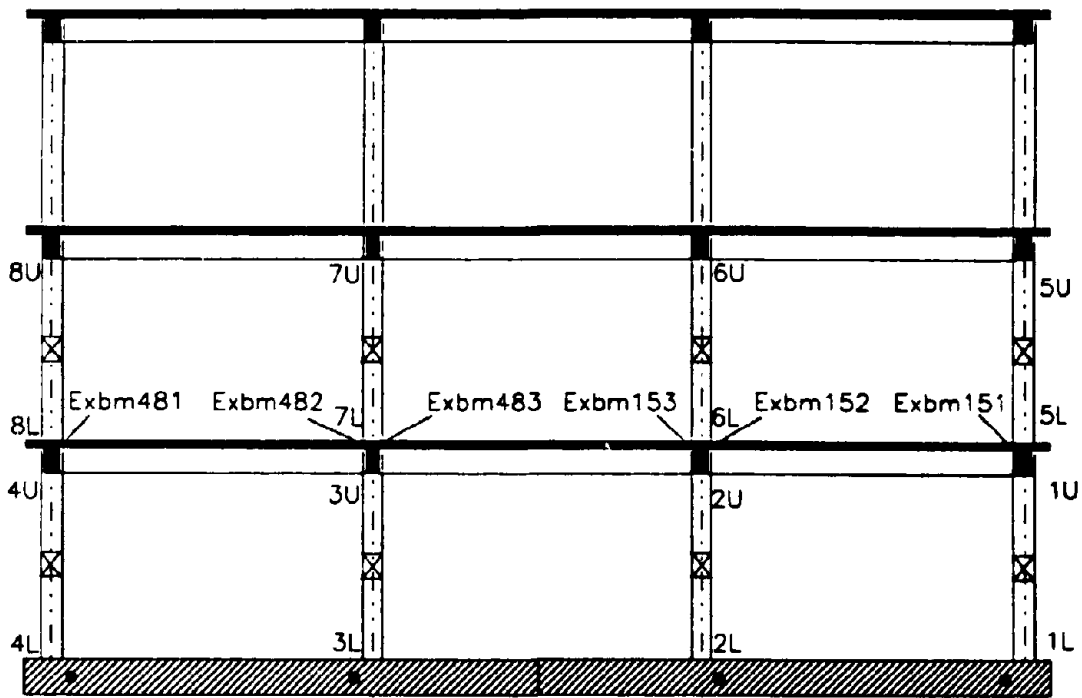
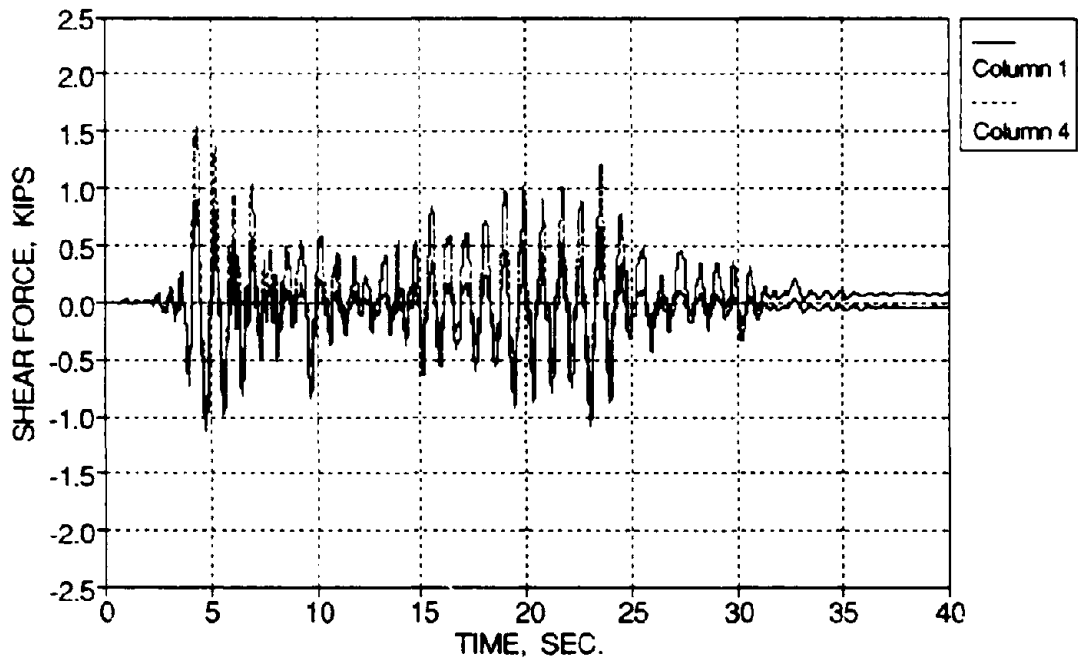
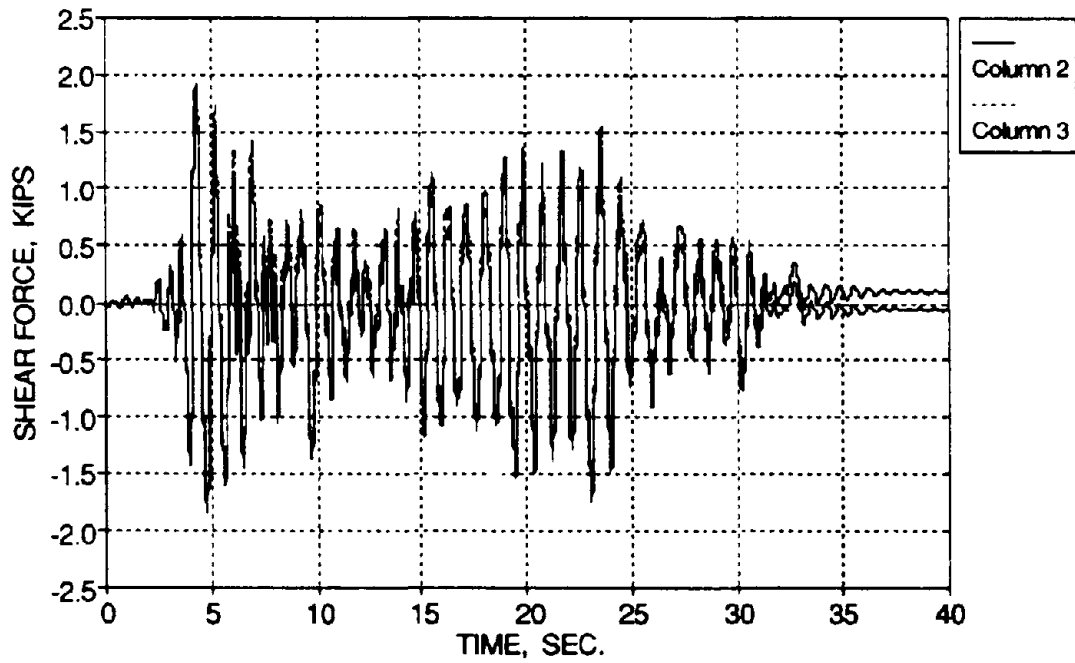


FIG. 2-8 Member Designations

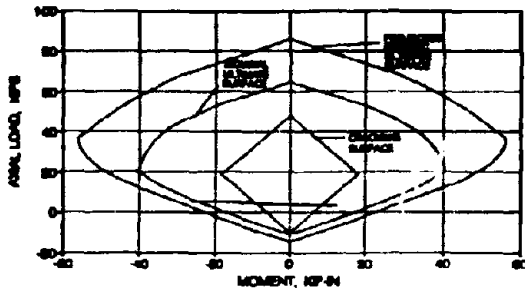


(a) Exterior Columns

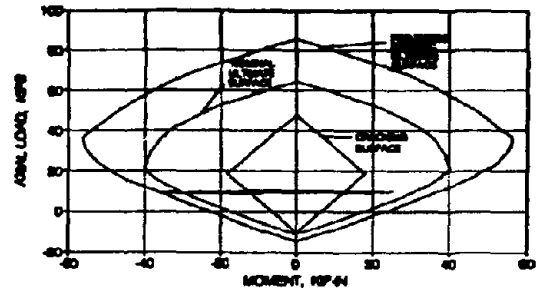


(b) Interior Columns

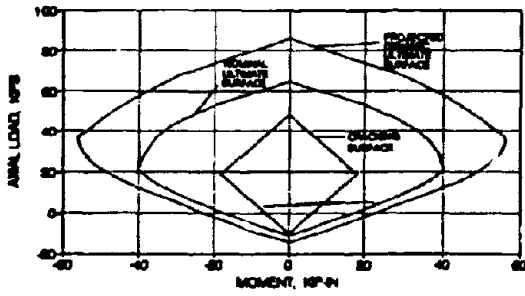
FIG. 2-9 Base Column Shear Forces for TFT_20



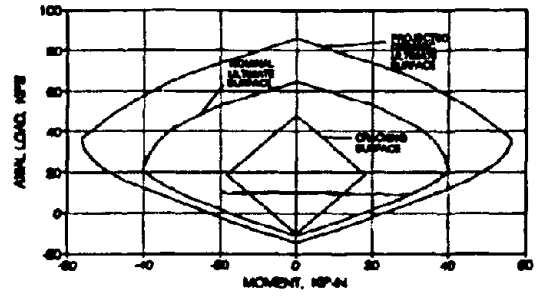
Column 8U



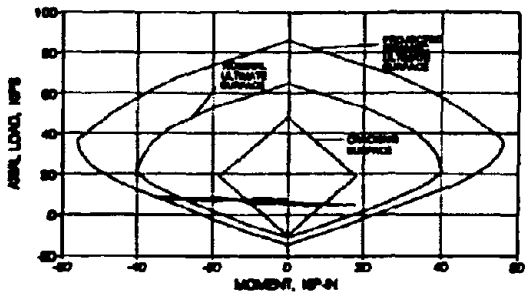
Column 7U



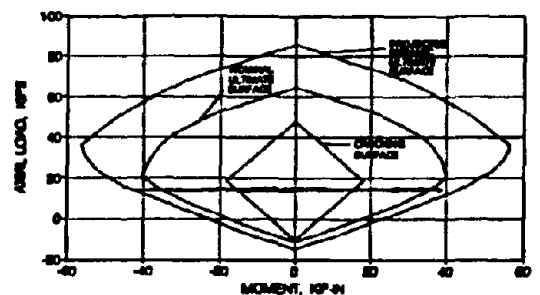
Column 8L



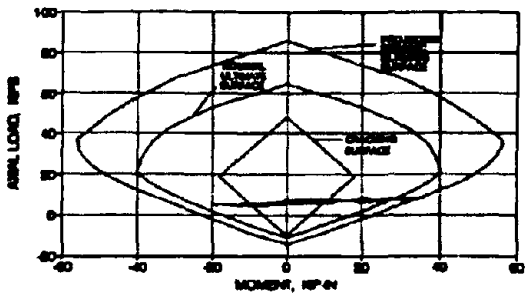
Column 7L



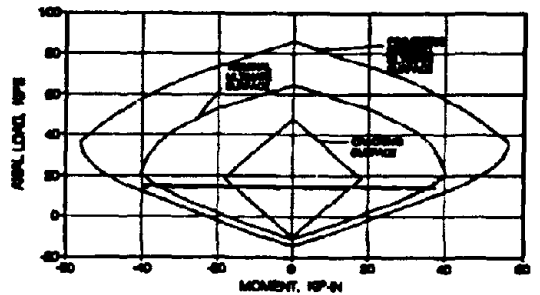
Column 4U



Column 3U

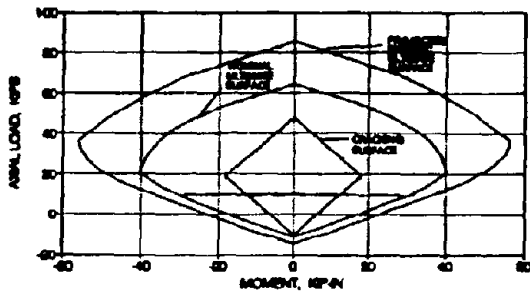


Column 4L

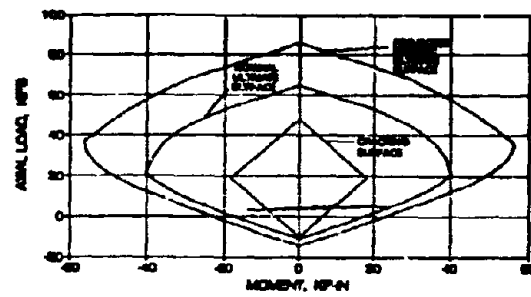


Column 3L

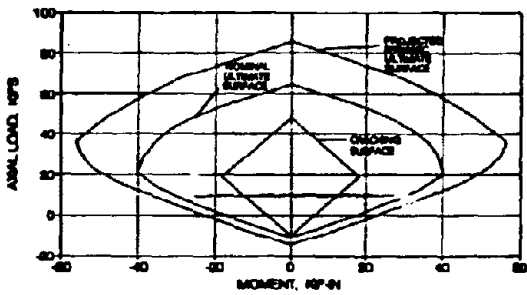
FIG. 2-10a Interaction Histories for the South-East Columns from TFT_20



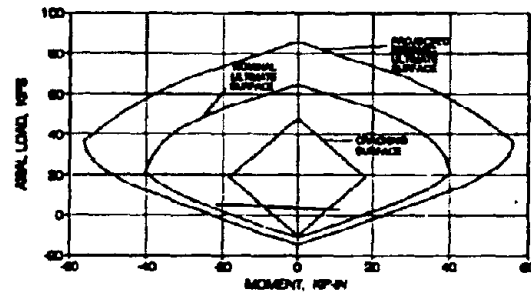
Column 6U



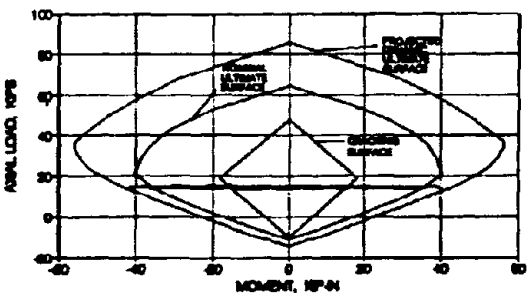
Column 5U



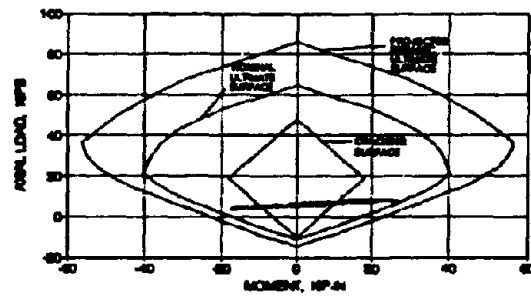
Column 6L



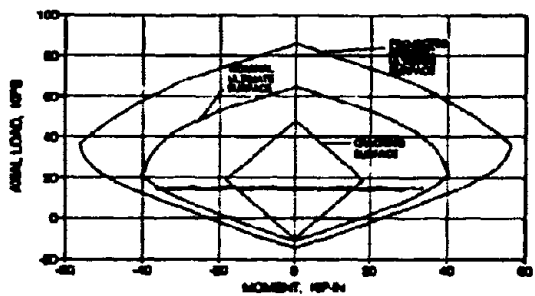
Column 5L



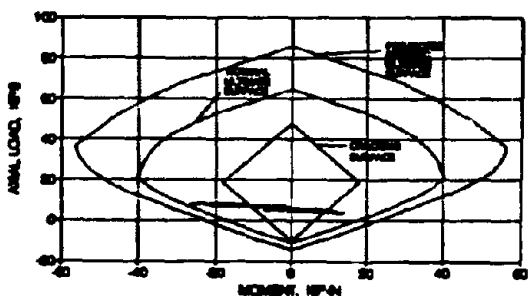
Column 2U



Column 1U

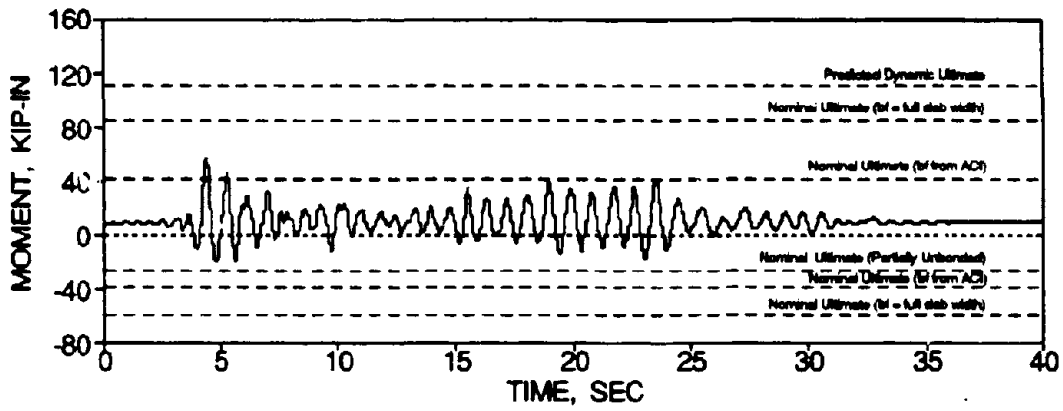


Column 2L

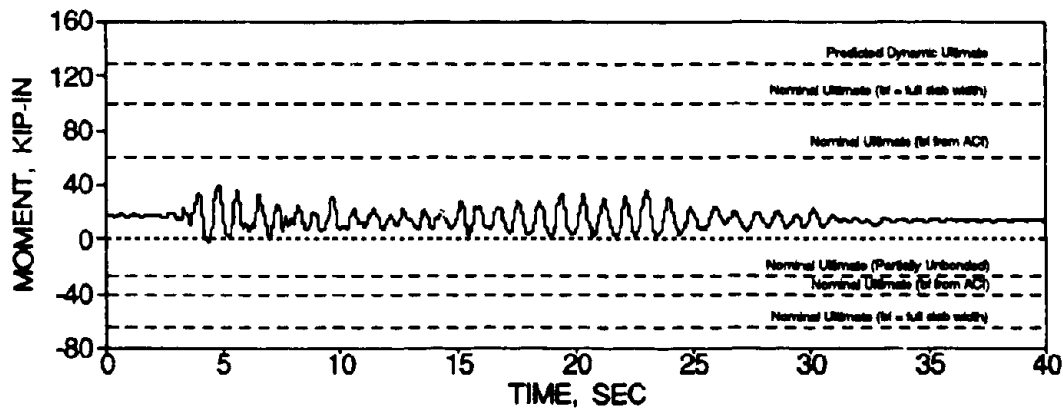


Column 1L

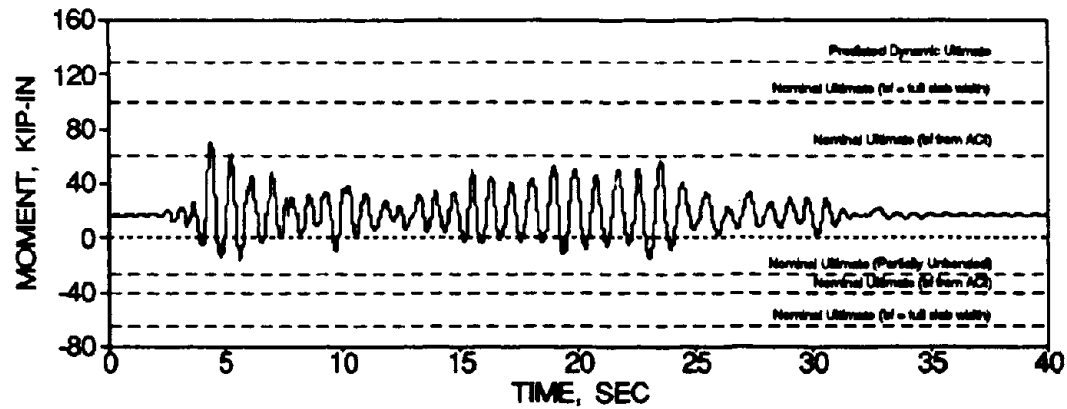
FIG. 2-10b Interaction Histories for the North-East Columns from TFT_20



(a) Exbm481

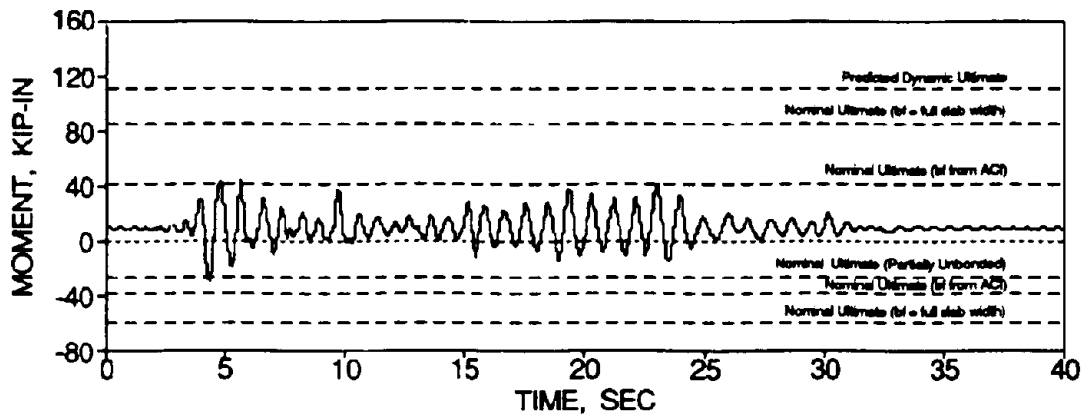


(b) Exbm482

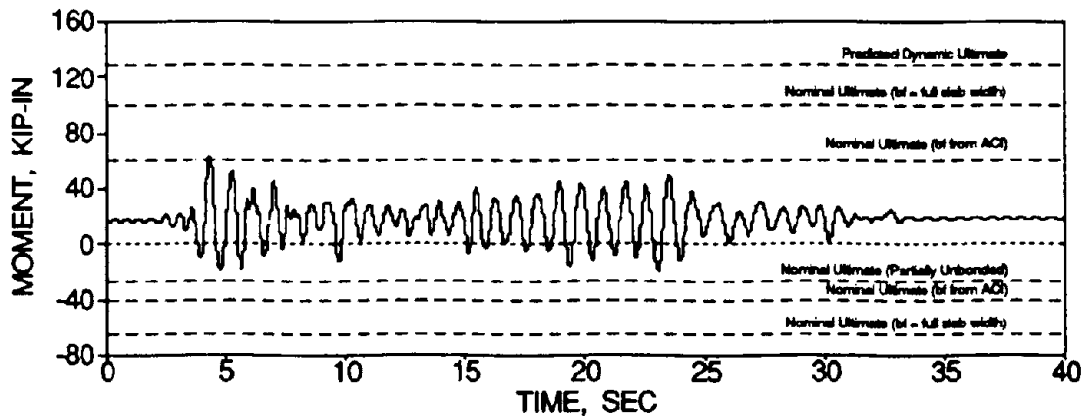


(a) Exbm483

FIG. 2-11a First Story Beam Bending Moment Time Histories for TFT_20 - South Side



(a) Exbm151



(b) Exbm152

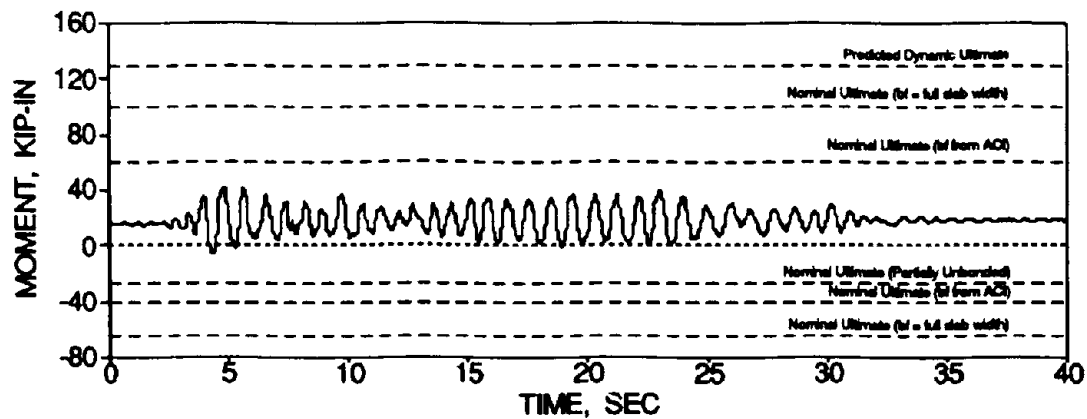
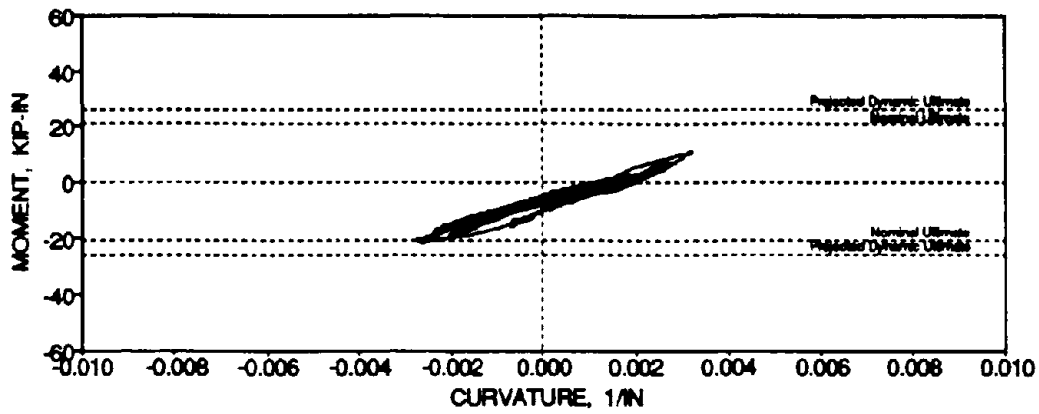
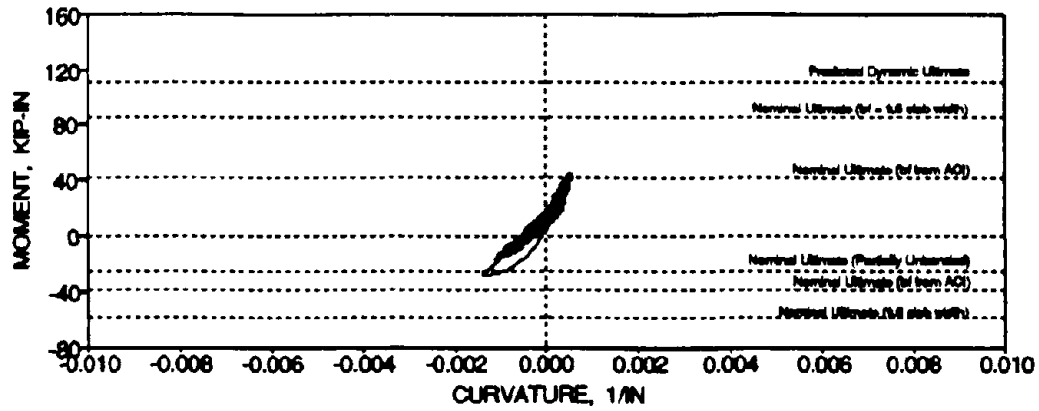


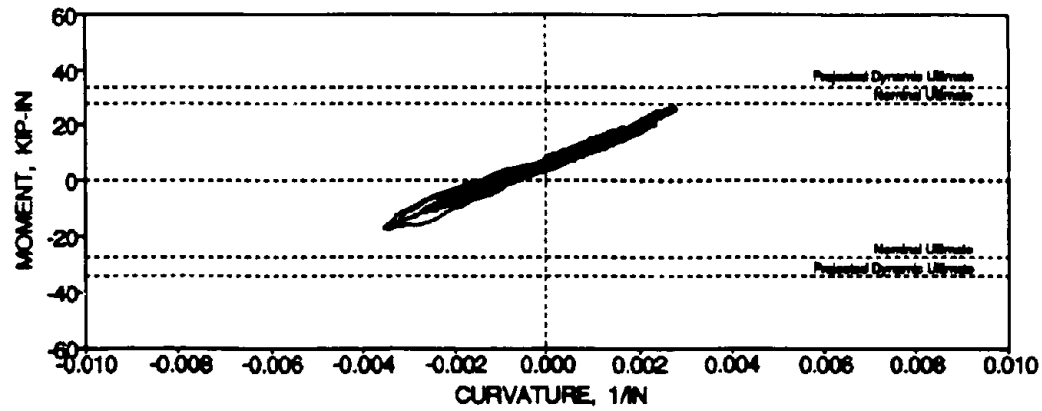
FIG. 2-11b First Story Beam Bending Moment Time Histories for TFT_20 - North Side



Column 5L

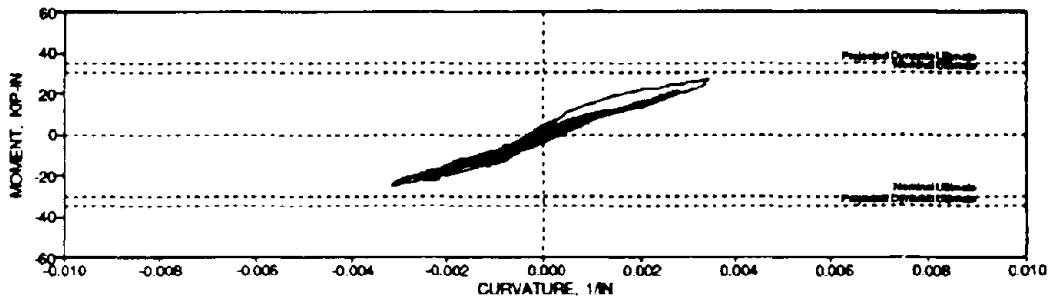


Beam Exbn151

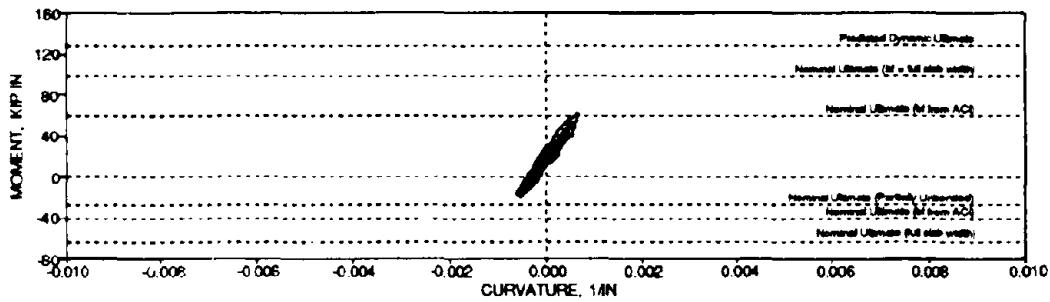


Column 1U

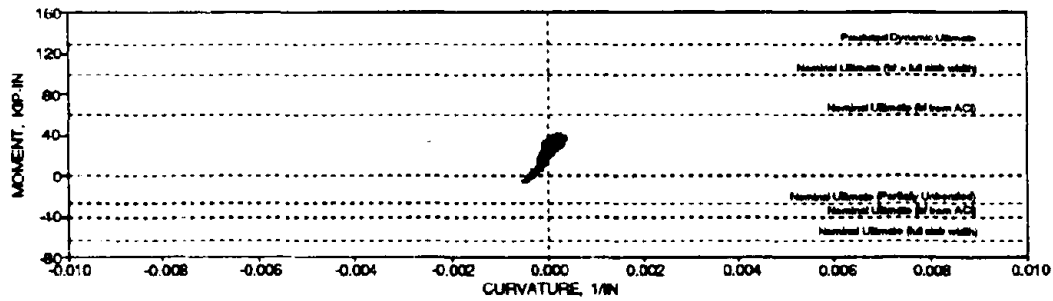
FIG. 2-12a Moment versus Curvature from TFT_20 - Exterior Joint



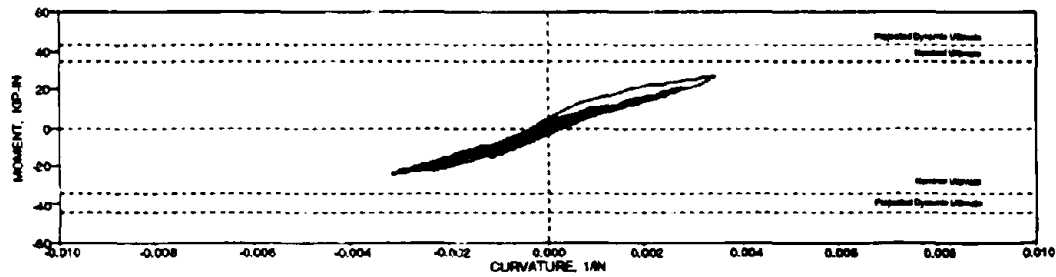
Column 6L



Beam Exbm152

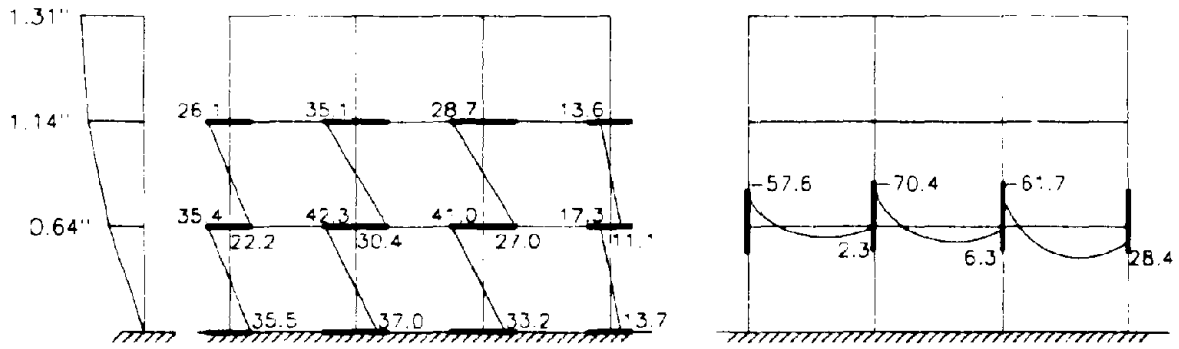


Beam Exbm153



Column 2U

FIG. 2-12b Moment versus Curvature from TFT_20 - Interior Joint

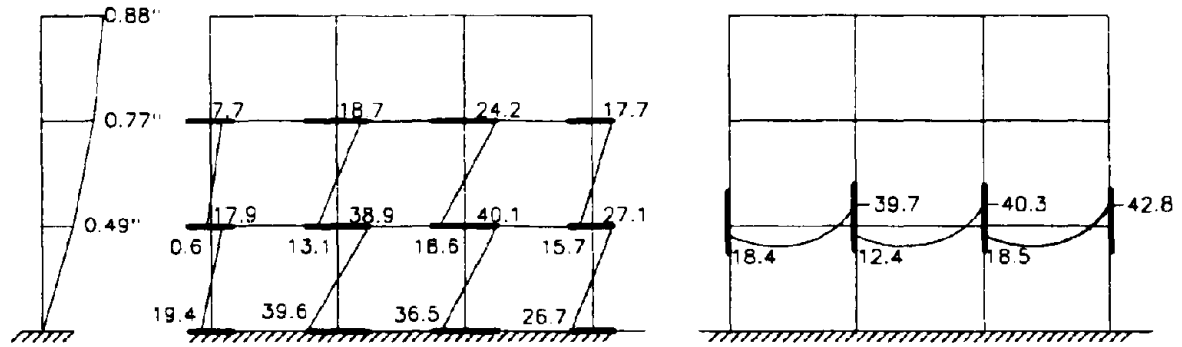
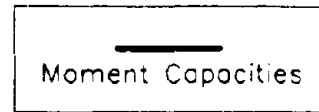


Displacements

Column Moments

Beam Moments

(a) Time = 4.36 sec.



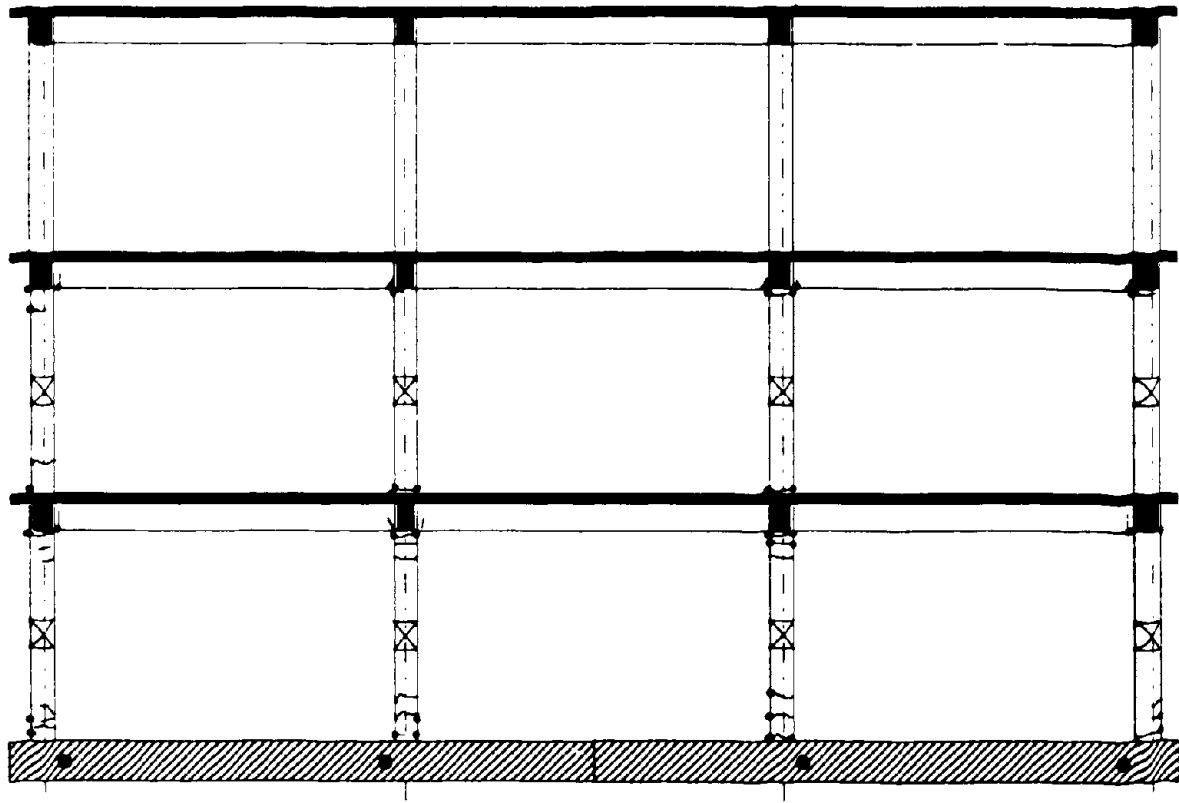
Displacements

Column Moments

Beam Moments

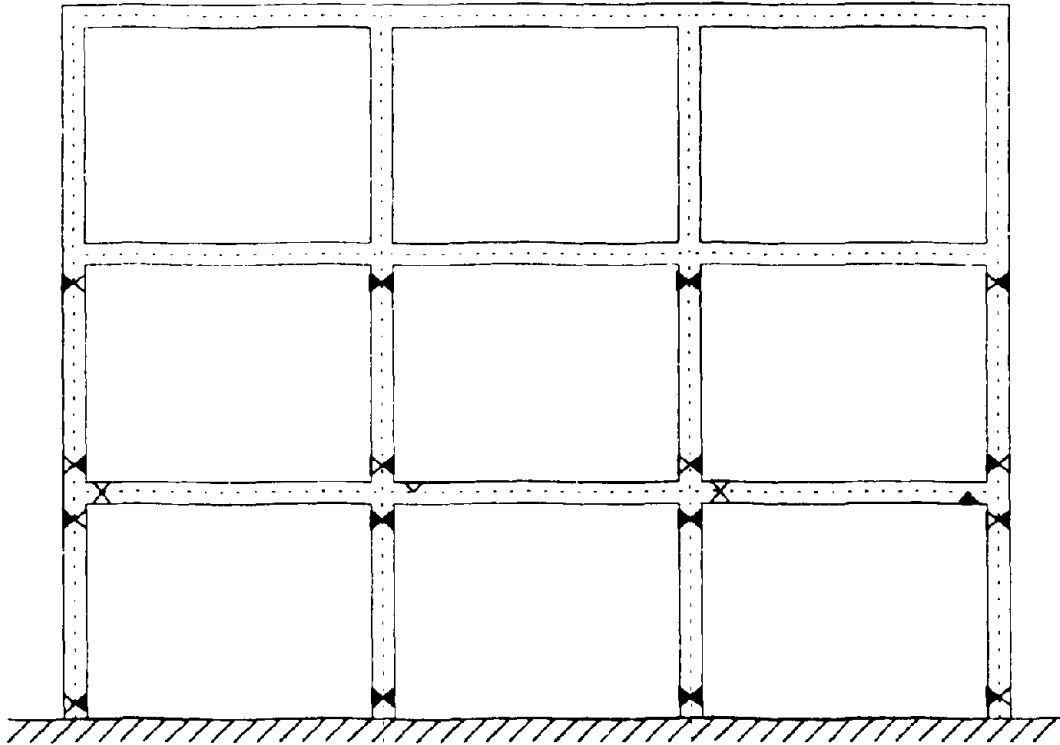
(b) Time = 4.82 sec

FIG. 2-13 Moment Diagram at Maximum Story Drift from TFI_20



• Crack
~ Crack

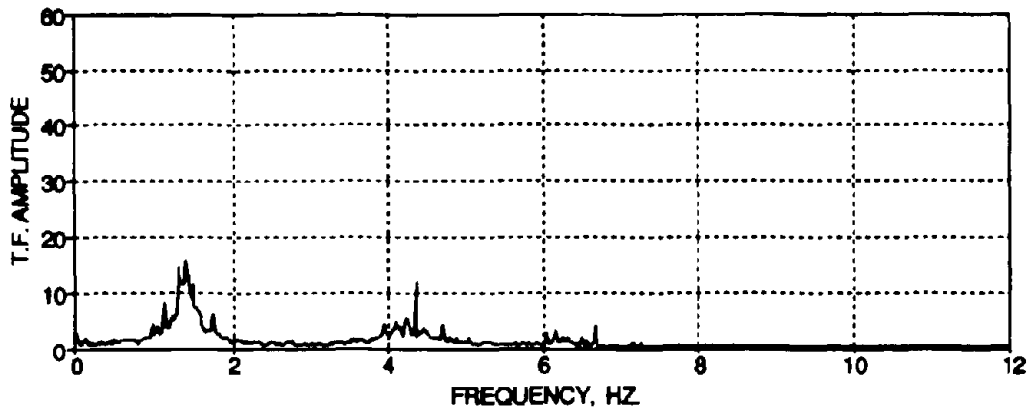
FIG. 2-14 Observed Structural Damage from TFT_20



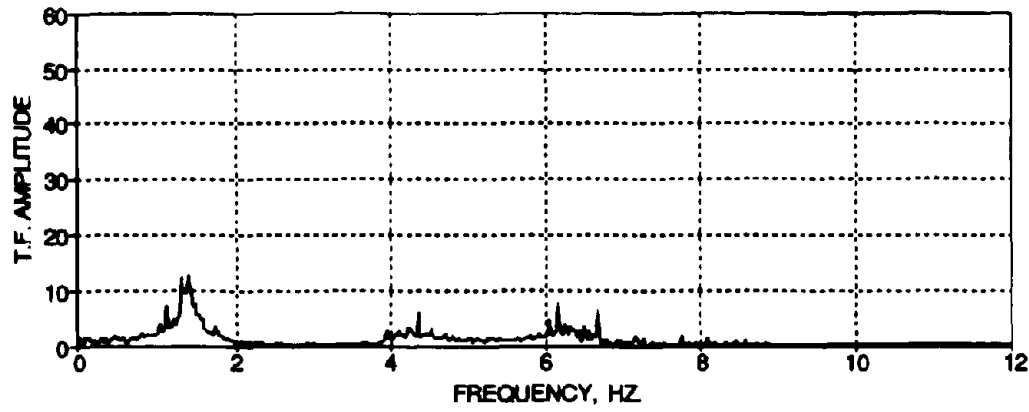
▷ Cracked
▶ Yielded

NOTE: 2nd story beams and above
were not quantitatively observed

FIG. 2-15 Measured Damage State of the Model after TFT_20



(a) Third Floor



(b) Second Floor

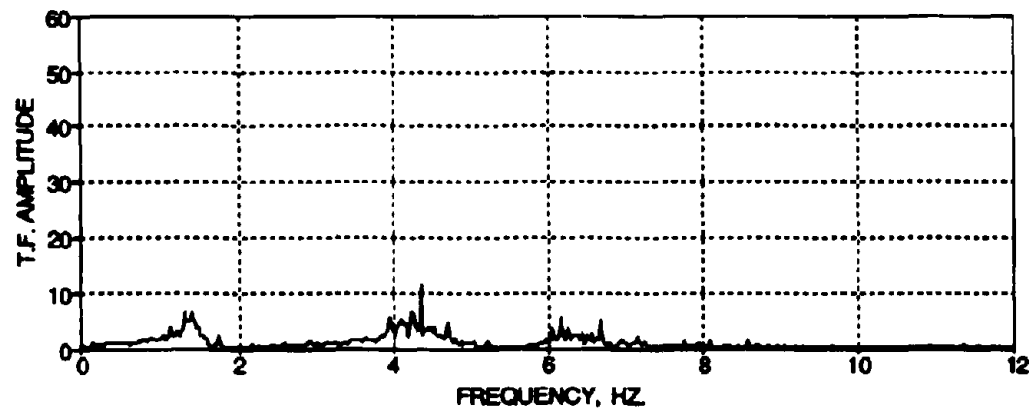
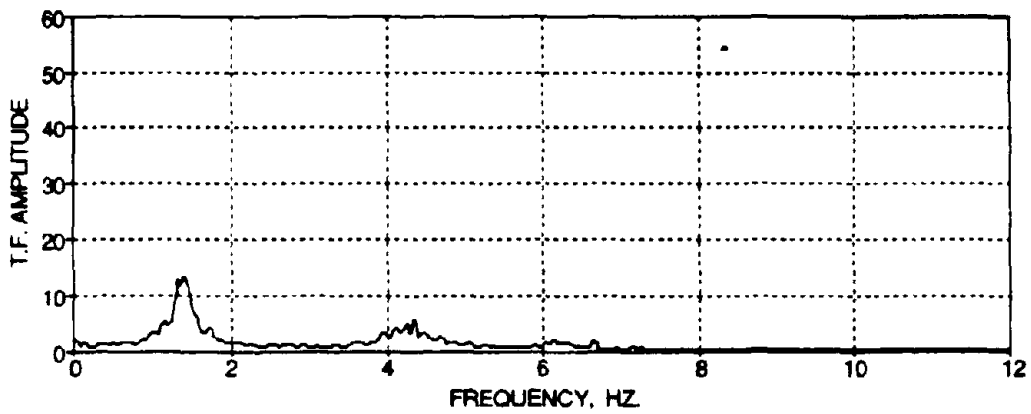
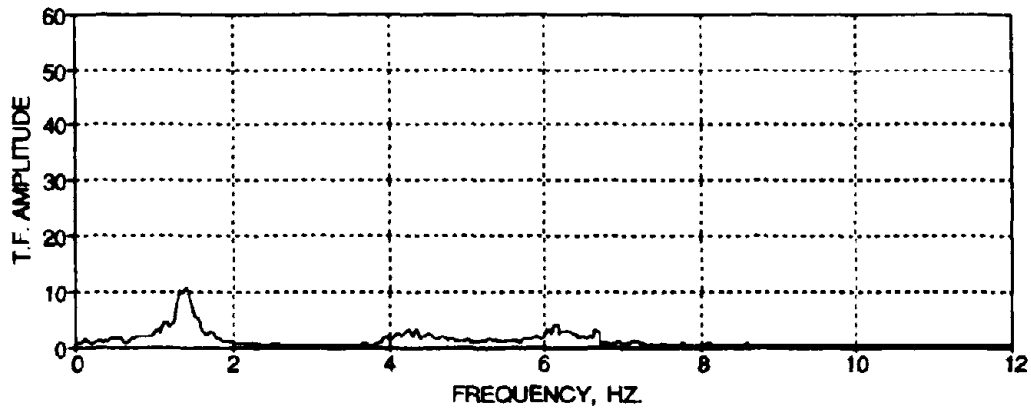


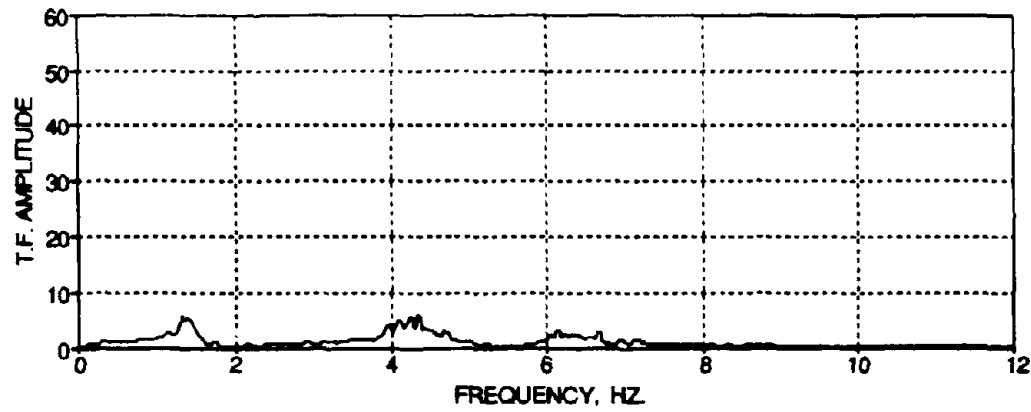
FIG. 2-16 Transfer Functions of the Story Level Accelerations from WHN_E



(a) Third Floor

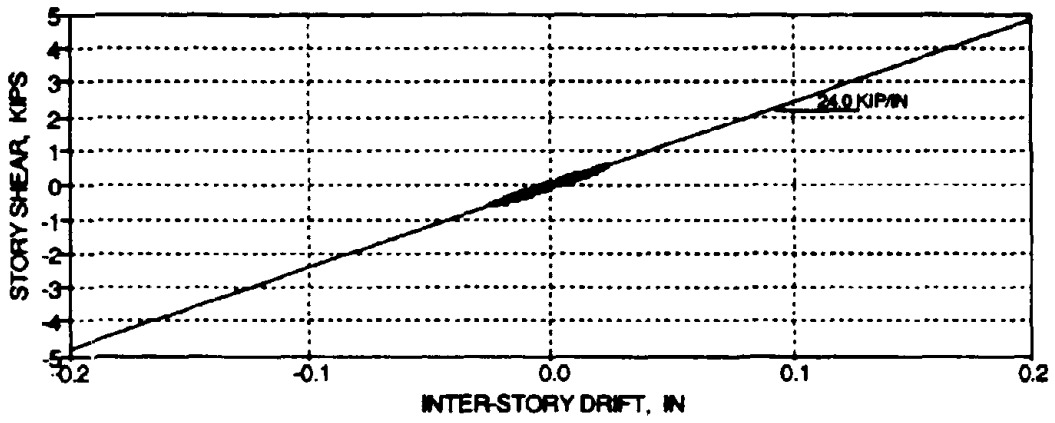


(b) Second Floor

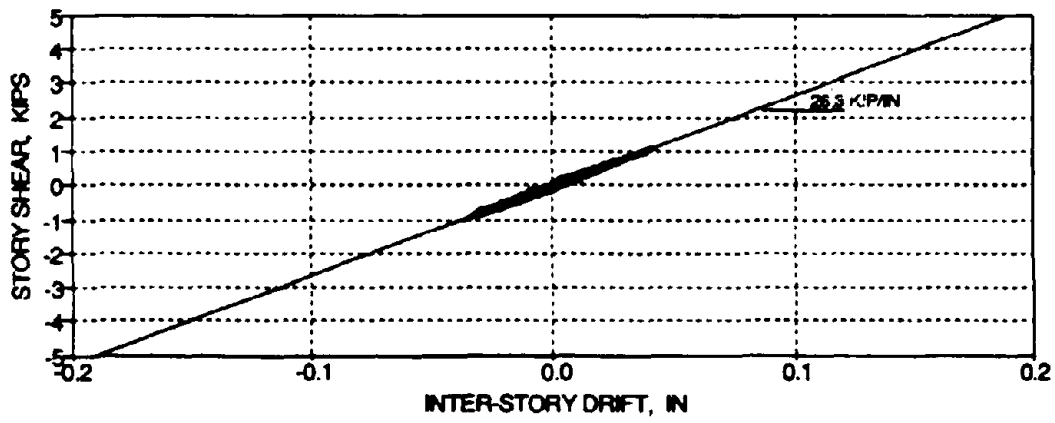


(c) First Floor

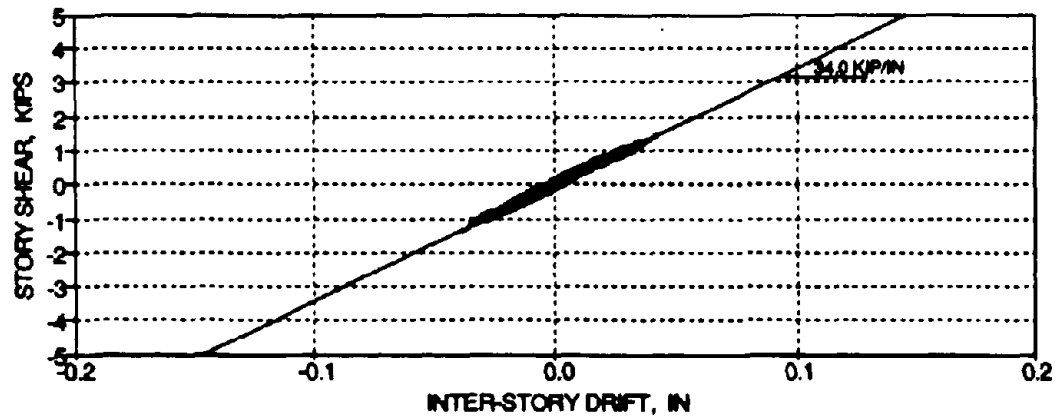
FIG. 2-17 Smoothed Transfer Functions of the Story Level Accelerations from WHN_E



(a) Third Floor



(b) Second Floor



(c) First Floor

FIG. 2-18 Story Shear versus Inter-Story Drift Histories for WHN_E

2.4 Response to Severe Earthquake

A severe table motion, the Taft N21E accelerogram scaled for a peak ground acceleration PGA of 0.30 g, was used subsequently to excite the model (herein referred to as TFT_30). Figs. 2-19a and 2-19b show the desired and achieved shaking table acceleration motions for TFT_30. Fig. 2-19c shows a short segment of the desired and achieved shaking table motions, which indicate good reproduction of the original earthquake.

2.4.1 Global Response

Fig. 2-20 shows the story displacement time histories of the model for test 'TFT_20. Fig. 2-21 shows the story shear force time histories identified from the load cells and the third story level accelerometers. Figs. 2-22a and 2-22b show a magnified overlaid portion of the story displacements and shear forces, respectively. Initially, both the story displacements and shear forces are observed to be moving primarily in phase, including the "large pulse". Then out-of-phase actions, resembling the second mode of vibration, can be observed. Figs. 2-23a and 2-23b show the story displacements and shear forces when the maximum first story drift occurred. The shape of the magnitudes of the story displacements at this point in time resembles the shape caused by the first mode of vibration of the model. However, the magnitude of the second story shear force is comparable with the first story shear at this instant of time. Therefore, it is concluded that the structural response is initially governed by the first mode of vibration for the TFT_30 test, followed by contributions from the higher modes (mostly the second mode).

From Fig. 2-20, it can also be observed that a slight permanent second story displacement has occurred due to the TFT_30 test. The displacement of the third story is an offset caused by the permanent displacement of the second floor.

Table 2-5 summarizes the maximum story displacements, inter-story drifts, story shear forces, story loads, and peak story accelerations for each floor of the model for TFT_30. It can be observed that the maximum inter-story drifts for the first and second stories are 2.03% and 2.24%, with the larger drift occurring at the second floor. The base shear force demand (12.4 kips) is 15.3% of the total structural weight and is only increased slightly as compared to TFT_20 (12.3 kips). Therefore a response reduction occurred due to inelastic behavior (quantified in Section 3). Also the maximum story shear force for the second floor is comparable with that of the first floor and is increased by about 25% as compared to TFT_20 (9.3 kips). Therefore,

from larger inter-story drifts and shear force demands, severe damage is expected on the second floor for this base motion. Also note from Table 2-5 that there are little story level acceleration reductions. This is due to the inelastic behavior of the model under such table motions.

El-Attar et al. (1991), for the Taft S69E motion at a PGA of 0.35 g, observed maximum first and second story drifts of 2.63% and 1.94% of the story height and a base shear demand of 9.4% of the total structural weight [or 12.11% based on the weight proportions with this study (see Section 2.2.1)]. Some deviations in the response magnitudes can be observed and also note that the first story was critical in his test.

TABLE 2-5 Maximum Response for Severe Earthquake TFT_30

Story	Max. Story Displacement (in.)	Max. Inter-Story Drift (%)	Max. Story Shear (kips)	Max. Story Load (kips)	Peak Story Acceleration (g)
Third	2.35	0.89	7.1	7.1	0.25
Second	2.05	2.24	11.6	7.4	0.22
First	0.97	2.03	12.4 (15.3%W)	9.4	0.29

Fig. 2-24 shows the story shear force versus the inter-story drift histories for each floor of the model for test TFT_30. It can be observed that a considerable amount of inelastic deformations occurs in all stories from the severe table motion TFT_30, especially on the first and second stories during the "large pulse". The secondary stiffnesses are identified on the first and second stories as 11.3 kip/in and 10.2 kip/in, respectively. This corresponds to secondary stiffness degradations of 31.5% and 34.6%, respectively for the first and second stories as compared to TFT_20. Therefore, the inelastic properties of the R/C members degrade as a result of continued inelastic deformations (history dependent), as expected.

Fig. 2-25 shows the energy time histories for TFT_30. The total input energy to the model is 34.4 kip-in, which is about 20 times and 1.4 times greater than the input energy from TFT_05 and TFT_20, respectively. The percentage ratio of the dissipated energies by each floor with respect to the total structural energy dissipation is 41.5% : 42.6% : 15.9%, respectively for the

first, second, and third stories. In comparison with TFT_20, the percentage ratio was 53.2% : 33.2% : 13.6%, respectively. Therefore, a larger amount of dissipated energy is absorbed by the second floor from TFT_30.

2.4.2 Local Response

Fig. 2-26 shows the induced shear forces on the exterior and interior first story columns (base shear) for table motion TFT_30. It can be observed that the shears in the interior columns are larger than the exterior columns. However, at the "large pulse", the shear force demand in the exterior column in the direction of motion (column #4 with greater axial force) is comparable with the interior columns. This implies that the interior columns have reached capacity and the additional shear is absorbed by the exterior columns. However the shear in the exterior columns with less axial force are about 50% of the interior column shears. Note that the exterior columns also attract higher shear forces throughout the time history when the axial force increases.

Fig. 2-27 shows the bending moment versus axial load interaction diagrams for the columns of the first and second stories. It can be observed that the actual interaction histories in the columns during the test extend beyond the nominal ultimate bounds. For columns #3, #4, #7, and #8 (first and second floor south-east columns), the moment-axial interactions extend beyond the projected dynamic ultimate surface. This extension occurs on the first "large pulse" and then remains within the projected dynamic ultimate bounds. Therefore large damage develops in the columns of the first and second floors. Since this extension is beyond the projected dynamic ultimate surface and the model did not collapse, it can be also assumed that the material strengths considering strain rate effects and hardening were slightly underestimated.

Figs. 2-28a and 2-28b show the first story beam bending moment time histories at the column face. The ultimate moment surfaces are also specified for comparison. It can be observed that the positive moment demand (plotted negative) in exterior beam Exbm151 exceeds the nominal ultimate bounds which considers the pull-out effect of the positive longitudinal reinforcement. Therefore, a 50% reduction in rebar area (based on the ratio of the provided and required prototype embedments lengths) for calculating beam moment capacity with insufficient anchorage was overconservative. Also, this surface was developed with slab steel contributions only within the ACI-318 flange width. Therefore, slab steel contributions within the full slab width may have influenced the additional positive beam moment capacities. The negative moment demands (plotted positive), in general, exceed the nominal ultimate surface which considers the slab steel

within the ACI flange width (18"). However, the demand is well within the ultimate bounds when the slab steel within the full slab width is considered. Therefore, it is concluded that the beams remain primarily undamaged (with exception of the exterior beams) and that the capacity of the beams are influenced by the full slab reinforcement (not only within ACI-318 specified width), which diverts damage from the beams.

Fig. 2-29 shows the moment versus curvature for the instrumented members of a first floor (north-east exterior and interior joints). Strong inelastic behavior can be observed in the columns with moment demands near capacities. Inelastic behavior also occurs in beam section Exbm151 with full positive moment capacity based on partial unbonded reinforcement being achieved. Some pull-out of the positive beam reinforcement, associated with reinforcement slip, develops at this section as observed by the pinching in Fig. 2-29a. The interior beams sections suffer only slight inelastic deformations and are well within their ultimate strengths (full slab steel contributions to beam moment capacity are attributed). Reinforcement slip has not occurred in the interior beam-column joints (Fig. 2-29b). Note that the inelastic behavior is more appreciable in the columns of the south-east side of the model. This can be observed in Fig. 2-27a for columns #3, #4, #7, and #8, in which the actual moments extend beyond the projected dynamic ultimate surface.

The bending moment diagrams for the model when the first story drift was maximum in each direction, along with the corresponding story displacements and nominal moment capacities, are shown in Fig. 2-30. It can be observed that most of the moment demands in the first and second stories column have reached the nominal ultimate capacities. Only the exterior columns away from the direction in which the structure was moving (at that instant in time) remain below nominal capacity (a similar observation was previously made with the column base shears). Thus, a complete failure mechanism did not develop at this instant in time, but the structure is very close to failure on the second floor.

The observed visual structural damage to the model due to the TFT_30 shaking table test is shown in Fig. 2-31. The following points highlight the observed structural damage:

- (a) cracking in the splice zone near the location of the transverse hoop reinforcement in the lower interior and exterior columns;

- (b) cracking in the upper columns at the underside of the first and second story longitudinal beams and near the transverse hoop reinforcement;
- (c) columns cracked at construction joints fully around the columns and in the beam-column joints;
- (d) vertical cracks in the web of the exterior longitudinal beams near the location of the transverse beam reinforcement;
- (e) large vertical cracks at the column face in the second story exterior beams. Since large response were observed on the second story, pull-out of the discontinuous rebars probably occurred;
- (f) some slab cracks were observed along the transverse beams.

Fig. 2-32 shows the damage state of the model after TFT_30. It can be observed that yielding has occurred in the first and second story columns. Some yielding in the beams also occurred during the "large pulse", especially in the exterior beams. It is evident that a column-sidesway or soft-story collapse mechanism is in development. El-Attar et al. (1991) also observed the same incipient collapse mechanisms.

2.5 Dynamic Properties after Severe Shaking

The identification of the ensuing dynamic properties after TFT_30 are determined from the white noise excitation label as WHN_F. Figs. 2-33 and 2-34 show the transfer functions and smoothed transfer functions for each floor of the model, respectively. Many frequencies are excited in the vicinity of the modes of vibration due to the stick-slip type conditions caused by member cracking, which actually signifies inelastic response in the structure. Since small damping and well separated modes can be observed, the average natural frequencies are obtained as follows (see also Table 2-6):

$$f_i = \begin{pmatrix} 1.20 \\ 3.76 \\ 5.27 \end{pmatrix} \text{ Hz.} \quad (2.3)$$

It can be observed that the three natural frequencies (see Table 2-6) are reduced by an additional 15.5%, 14.0%, and 14.7%, respectively. The modal shapes and modal participation factors are also calculated from the story transfer functions and are shown in Table 2-6. Deviations can be observed among the various tests, especially note the variation in the first mode.

The equivalent viscous damping factors are determined from the smoothed transfer functions as 7.0%, 2.3%, and 1.8%, respectively. Since the model experiences inelastic deformations during test TFT_30, a larger first mode damping factor is observed due to contributions from hysteretic damping. Also note that the second and third mode damping factors have decreased, inevitably due to smoothing of the transfer functions.

The updated stiffness matrix of the model, developed from the smoothed transfer functions, is shown in Table 2-6. It can be observed that the sum of the diagonal terms of the stiffness matrix after the TFT_30 test is reduced by an additional 26.9% as compared to WHN_E or 53.7% of the undamaged model (WHN_B). Additional story stiffness reductions of 28.2% and 31.7% have resulted on second and third stories, respectively from TFT_30. This is evident from the response from TFT_30 where large demands occur in the second floor. The first story suffers only slight deterioration. Therefore, large stiffness deteriorations occur in the second and third floors from TFT_30. Total story stiffness reductions from the shaking table motions are 43.3%, 58.8%, and 53.6%, respectively as compared to WHN_B.

Fig. 2-35 shows the story shear versus inter-story drift histories for WHN_F. The low amplitude initial stiffnesses after TFT_30 (WHN_F) are tabulated in Table 2-7 along with the results of WHN_B and WHN_E. It can be observed that the story stiffnesses are reduced by an additional 18.2%, 45.6%, and 40.4% from WHN_E (after strong shaking) or 45.7%, 66.3%, and 64.3% of the original stiffnesses from WHN_B. Note the large reductions of the upper floors. Also, the averages of these reductions are similar to the reductions found in the stiffness matrix in Table 2-6.

The analysis using STAAD is used to verify the calculation of the first natural frequency from WHN_F after the TFT_30 base motion (1.20 Hz.). The analytical model is used with reduced member stiffnesses of $0.255 EI_p$. The analytical results for the natural frequencies, modal shapes, and stiffness matrix of the model are shown in Table 2-8 along with the results from WHN_F. It can be observed that the natural frequencies, modal shapes, and stiffness matrix (2.9% error) are comparable with the identified results from WHN_F. Therefore, by using a reduced stiffness

that fits the first natural frequency, the analytical model used in STAAD can produce accurate values for all dynamic properties. For comparison, the original "undamaged" analytical model (WHN_B) used reduced member stiffnesses of $0.565 EI_g$ (total reduction of 54.9%).

TABLE 2-6 Dynamic Properties and Stiffness Matrix before and after Severe Shaking

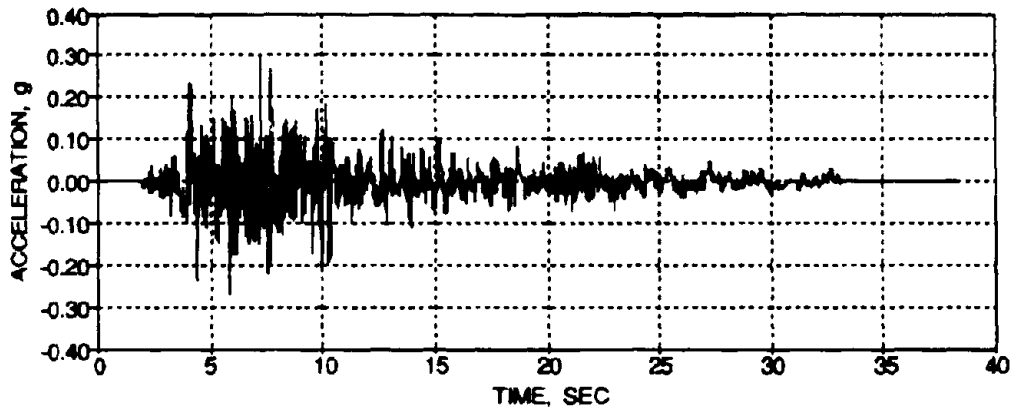
	WHN_E (before)	WHN_F (after)
Natural Frequencies (Hz.)	$\mathbf{f}_i = \begin{pmatrix} 1.42 \\ 4.37 \\ 6.18 \end{pmatrix}$	$\mathbf{f}_i = \begin{pmatrix} 1.20 \\ 3.76 \\ 5.27 \end{pmatrix}$
Modal Shapes	$\Phi_y = \begin{pmatrix} 1.00 & -0.95 & -0.45 \\ 0.83 & 0.55 & 1.00 \\ 0.43 & 1.00 & -0.78 \end{pmatrix}$	$\Phi_y = \begin{pmatrix} 1.00 & -0.86 & -0.46 \\ 0.75 & 0.64 & 1.00 \\ 0.33 & 1.00 & -0.94 \end{pmatrix}$
Modal Participation Factors	$\Gamma_i = \begin{Bmatrix} 0.44 \\ 0.11 \\ -0.05 \end{Bmatrix}$	$\Gamma_i = \begin{Bmatrix} 0.43 \\ 0.14 \\ -0.07 \end{Bmatrix}$
Damping Ratios (%)	$\xi_i = \begin{Bmatrix} 6.6 \\ 5.6 \\ 2.8 \end{Bmatrix}$	$\xi_i = \begin{Bmatrix} 7.0 \\ 2.3 \\ 1.8 \end{Bmatrix}$
Stiffness Matrix (kip/in)	$\mathbf{K}_y = \begin{pmatrix} 36.4 & -36.3 & -1.0 \\ -36.3 & 67.6 & -31.2 \\ -1.0 & -31.2 & 59.9 \end{pmatrix}$	$\mathbf{K}_y = \begin{pmatrix} 23.3 & -24.8 & 0.7 \\ -24.8 & 45.6 & -22.4 \\ 0.7 & -22.4 & 50.9 \end{pmatrix}$
Story Stiffnesses (kip/in)	$\mathbf{k}_i = \begin{pmatrix} 36.3 \\ 31.2 \\ 28.7 \end{pmatrix}$	$\mathbf{k}_i = \begin{pmatrix} 24.8 \\ 22.4 \\ 28.5 \end{pmatrix}$

TABLE 2-7 Low Amplitude Initial Stiffnesses from the Shear versus Inter-Story Drift Histories

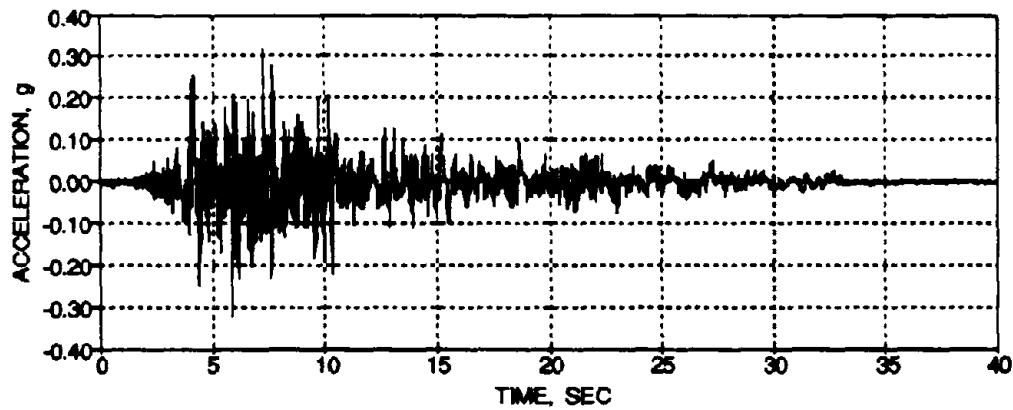
Story	WHN_B (kip/in)	WHN_E (kip/in)	WHN_F (kip/in)
Third	40.0	24.0	14.3
Second	42.4	26.3	14.3
First	51.2	34.0	27.8

TABLE 2-8 Analytical and Experimental Comparison of the Dynamic Properties

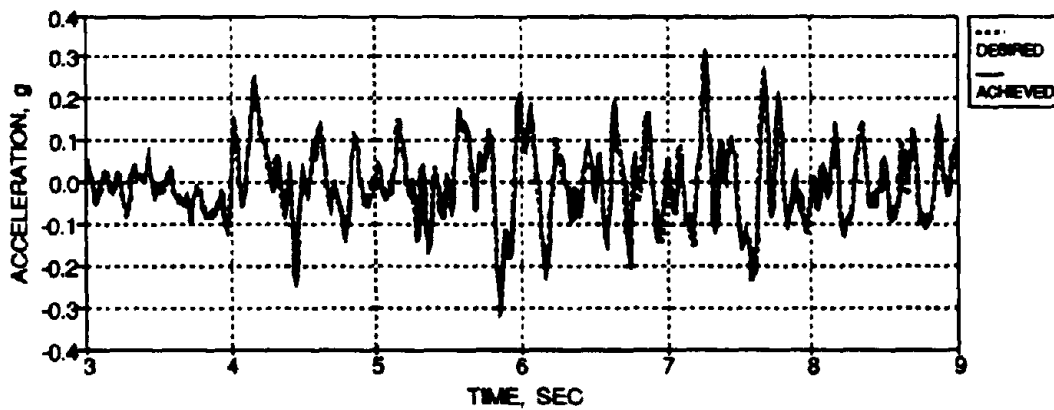
	Experimental (WHN_F)	Analytical [STAAD (0.255 (EI) _y)]
Natural Frequencies (Hz.)	$f_i = \begin{pmatrix} 1.20 \\ 3.76 \\ 5.27 \end{pmatrix}$	$f_i = \begin{pmatrix} 1.20 \\ 3.50 \\ 5.33 \end{pmatrix}$
Modal Shapes	$\Phi_y = \begin{pmatrix} 1.00 & -0.86 & -0.46 \\ 0.75 & 0.64 & 1.00 \\ 0.33 & 1.00 & -0.94 \end{pmatrix}$	$\Phi_y = \begin{pmatrix} 1.00 & -0.81 & -0.43 \\ 0.78 & 0.53 & 1.00 \\ 0.40 & 1.00 & -0.88 \end{pmatrix}$
Stiffness Matrix (kip/in)	$K_y = \begin{pmatrix} 23.3 & -24.8 & 0.7 \\ -24.8 & 45.6 & -22.4 \\ 0.7 & -22.4 & 50.9 \end{pmatrix}$	$K_y = \begin{pmatrix} 21.1 & -23.0 & 1.9 \\ -23.0 & 46.4 & -25.3 \\ 1.9 & -25.3 & 48.9 \end{pmatrix}$



(a) Desired Base Motion

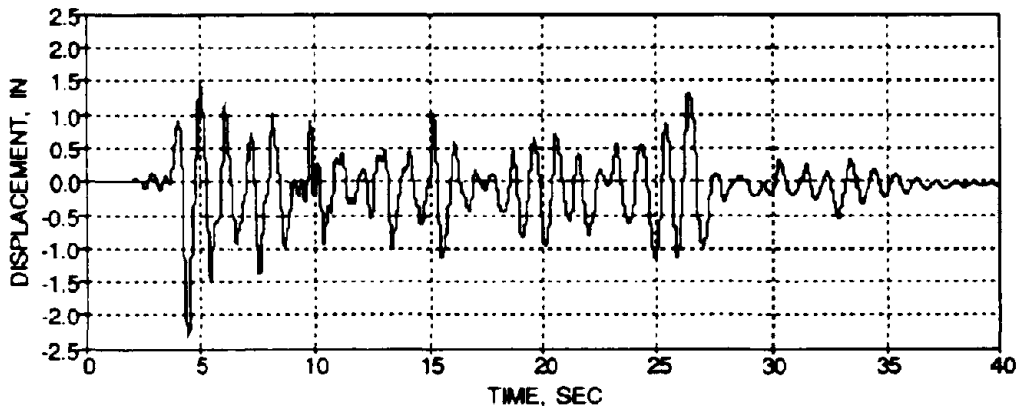


(b) Achieved Base Motion

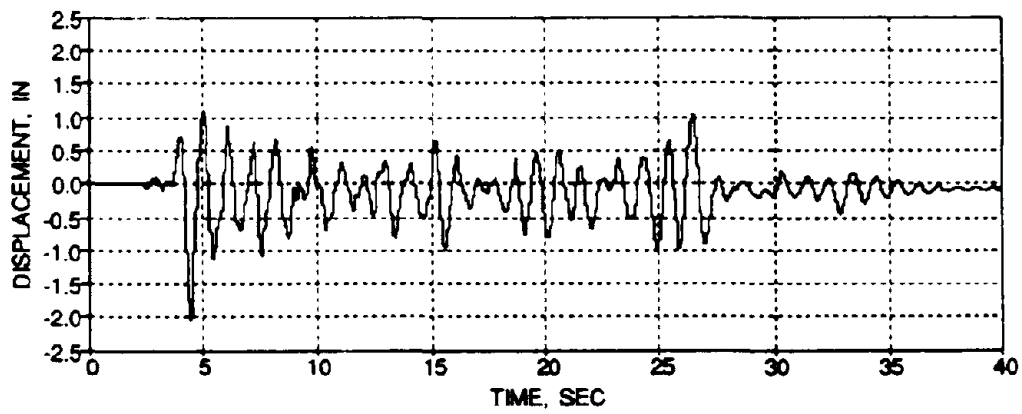


(c) Short Segment Comparison of the Desired and Achieved Base Motions

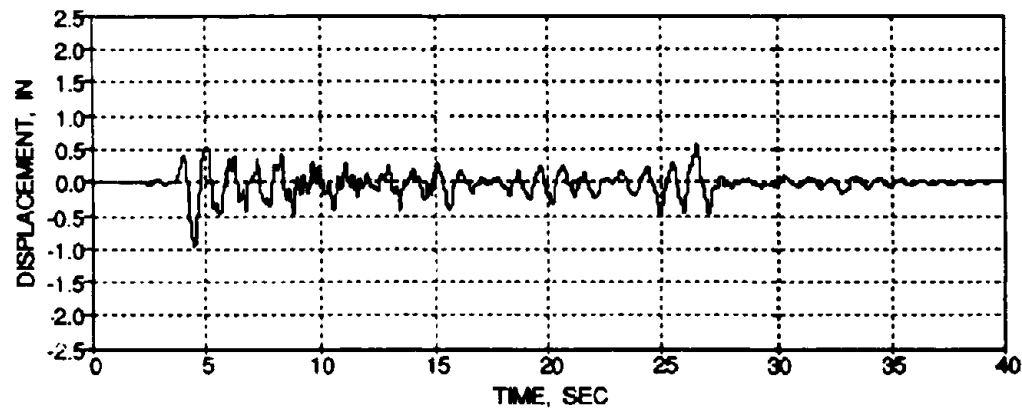
FIG. 2-19 Shaking Table Motion for the Taft N21E Base Motion, PGA 0.30 g



(a) Third Floor

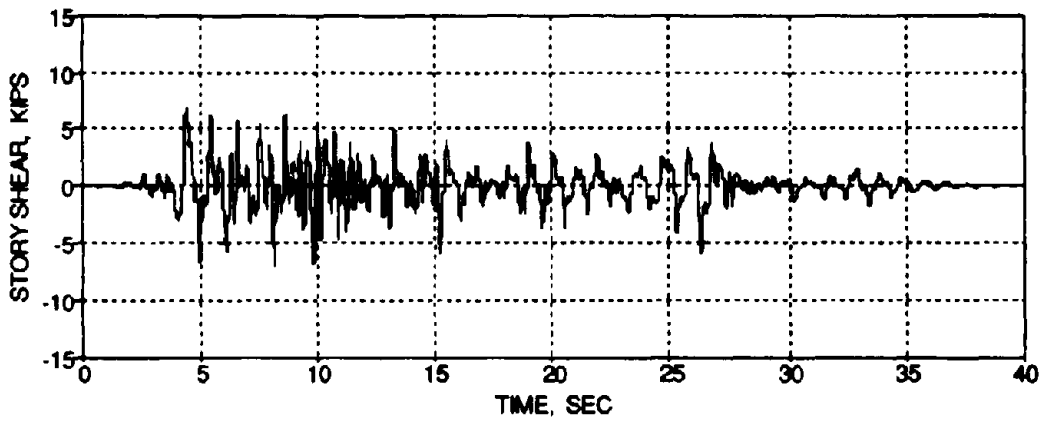


(b) Second Floor

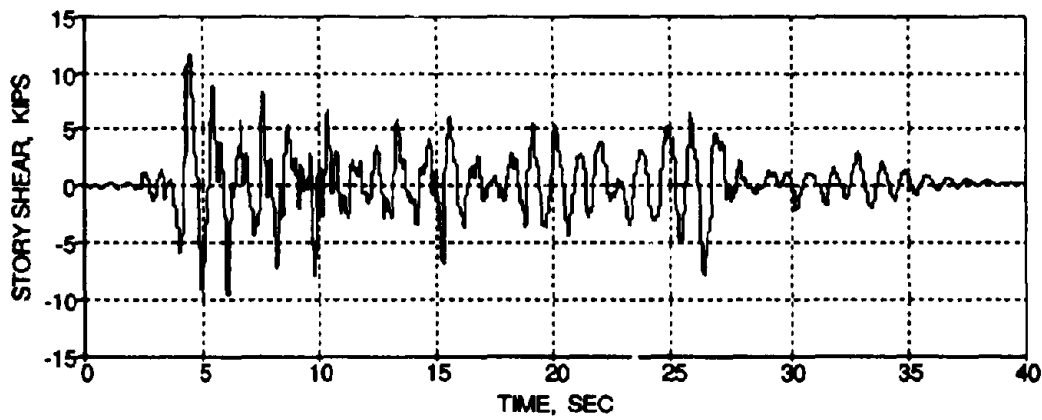


(c) First Floor

FIG. 2-20 Story Displacement Time Histories for TFT_30



(a) Third Floor



(b) Second Floor

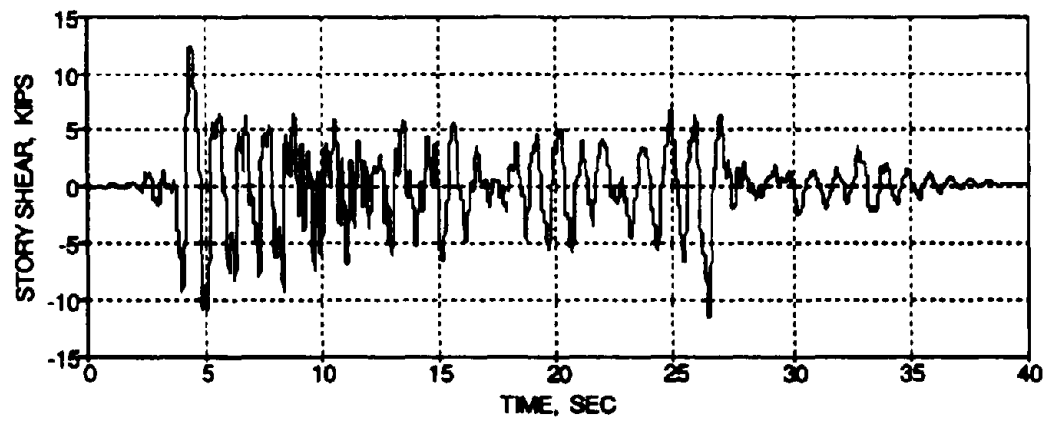
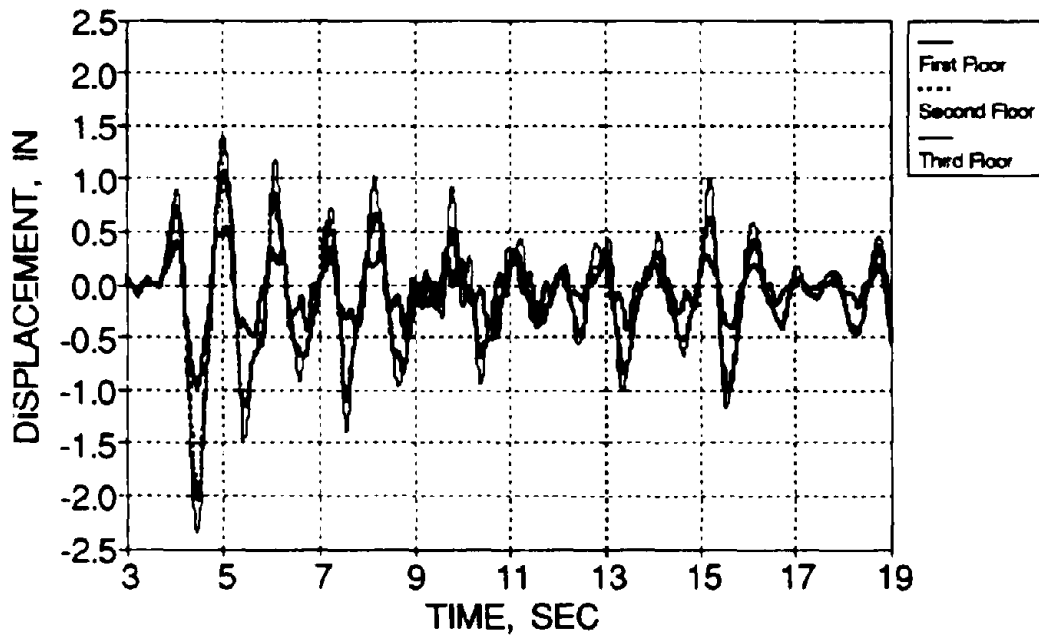
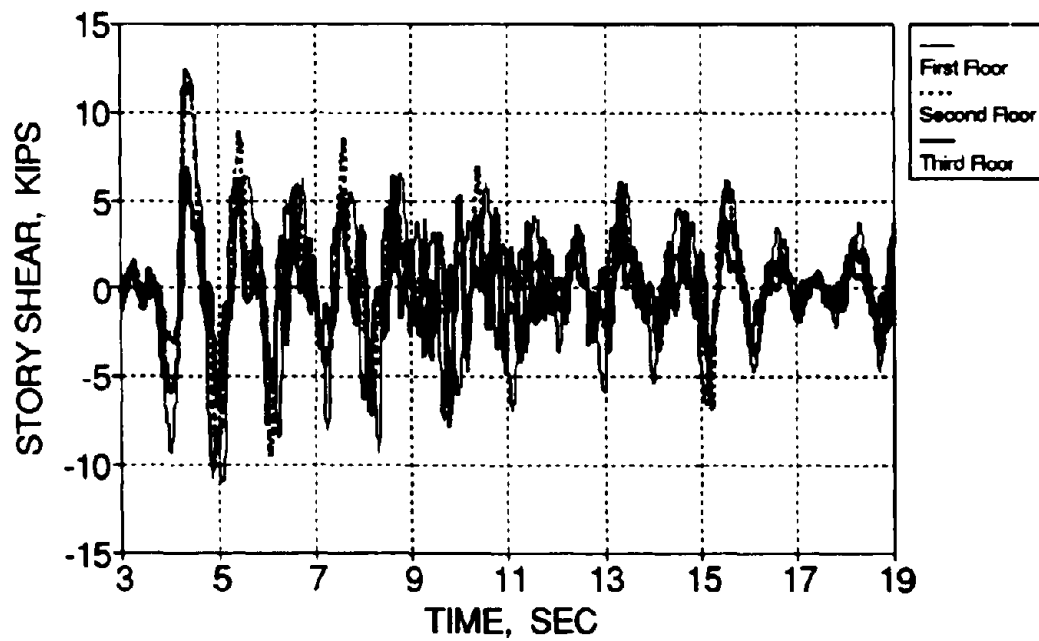


FIG. 2-21 Story Shear Time Histories for TFT_30

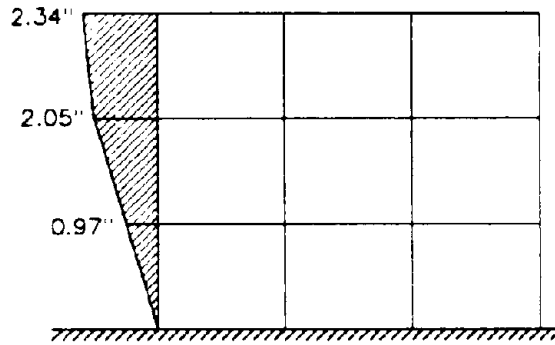


(a) Story Displacements

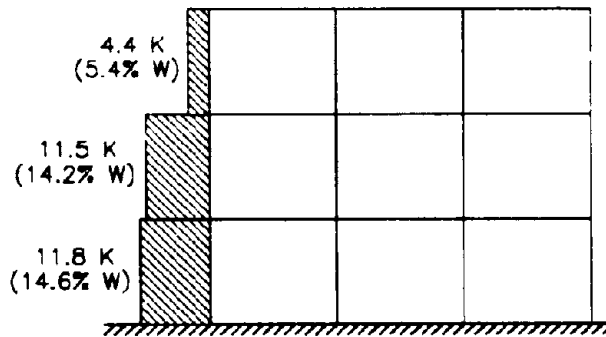


(b) Story Shear Forces

FIG. 2-22 Overlaid Global Response Time History Segments for TFT_30



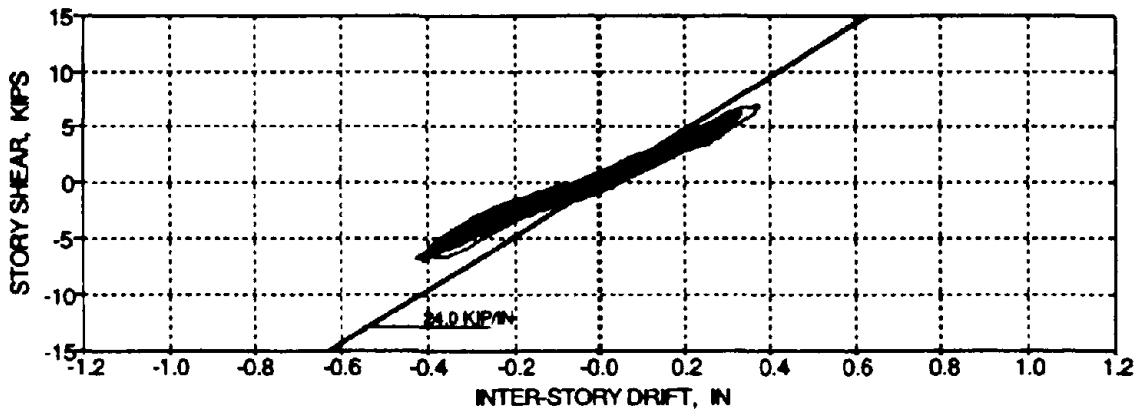
(a) Story Displacements (Time= 4.45 sec)



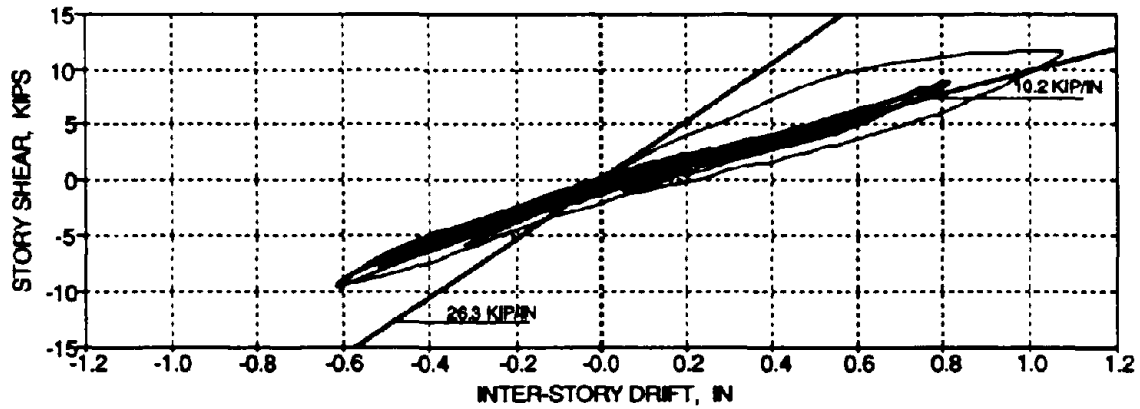
(b) Story Shear Forces (Time = 4.45 sec)

(b) Story Shears (Time = 4.45 sec)

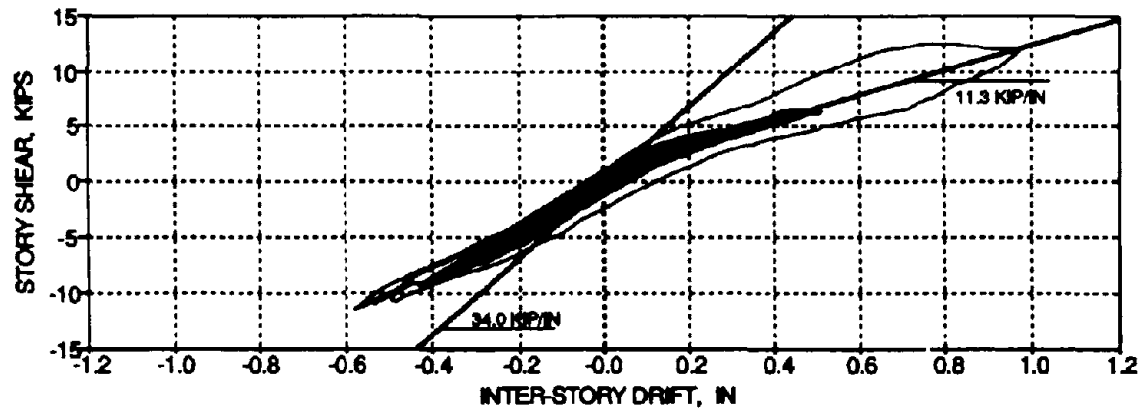
FIG. 2-23 Story Displacements and Shear Forces at Maximum First Story Drift for TFT_30



(a) Third Floor

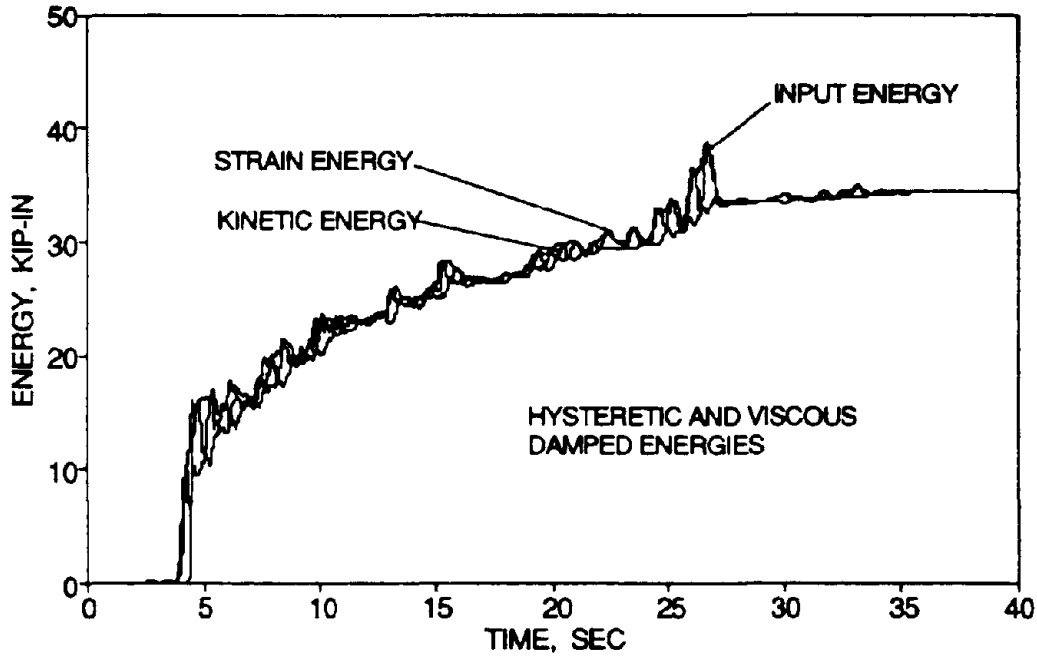


(b) Second Floor

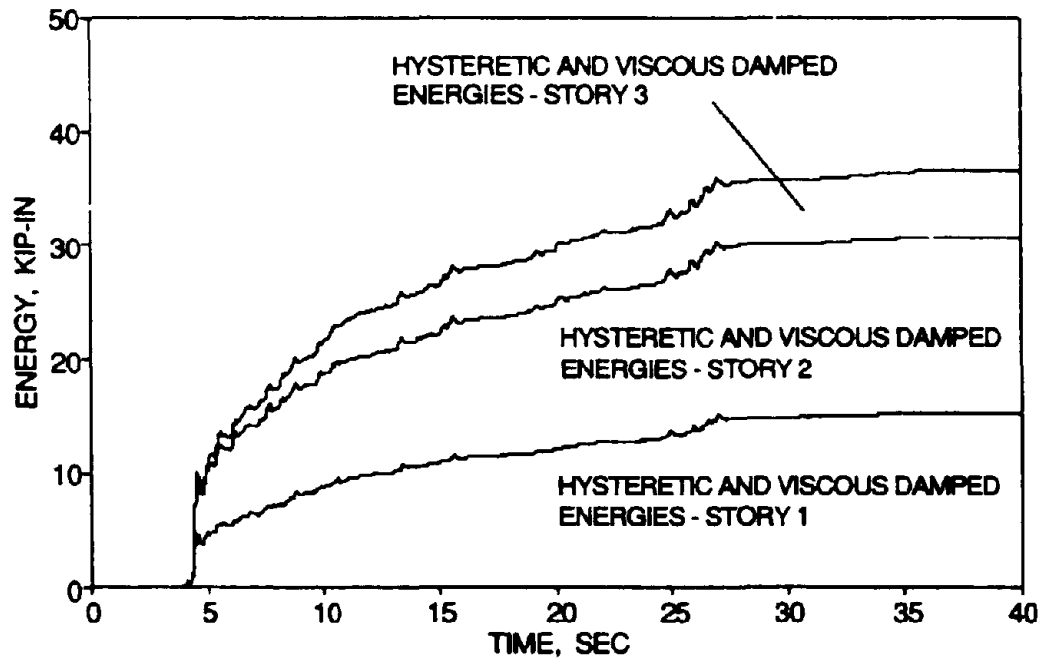


(c) First Floor

FIG. 2-24 Story Shear versus Inter-Story Drift Histories for TFT_30

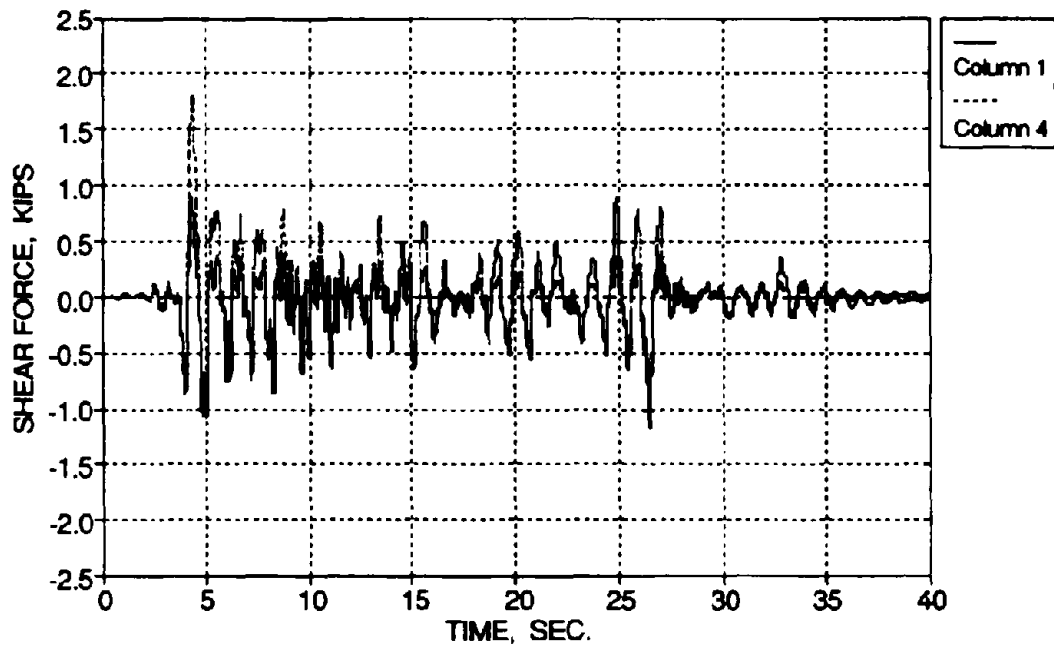


(a) Energy Balance



(b) Story Dissipated Energies

FIG. 2-25 Energy Time History for TFT_30



(a) Exterior Columns

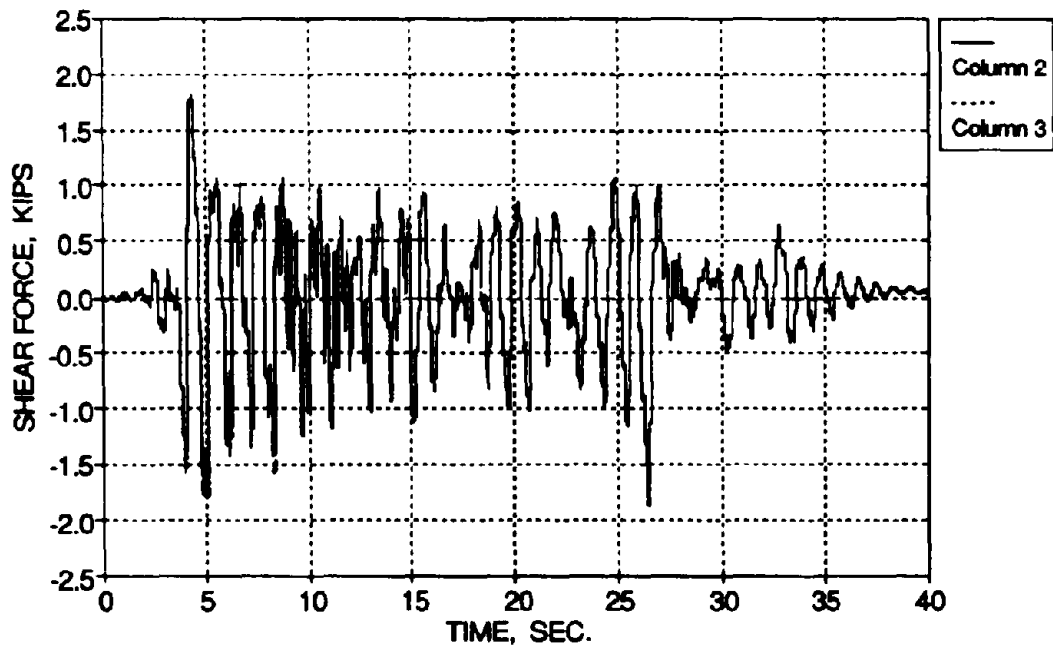
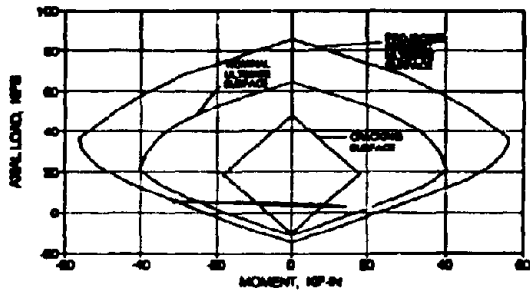
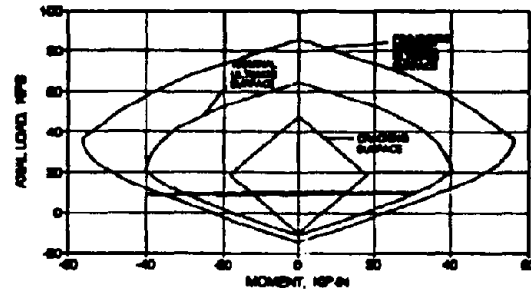


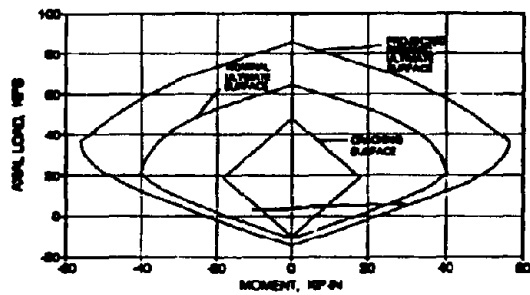
FIG. 2-26 Base Column Shear Forces for TFT_30



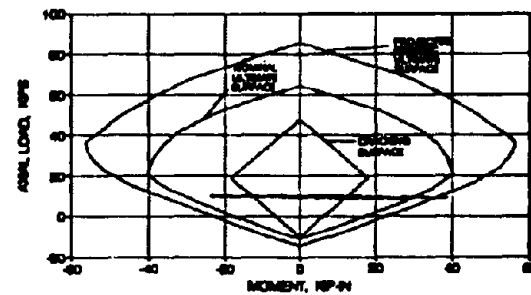
Column 8U



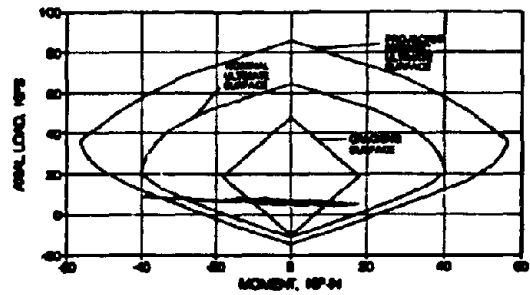
Column 7U



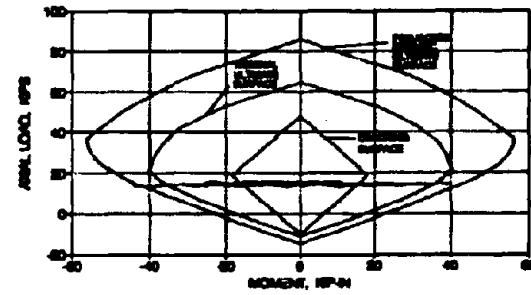
Column 8L



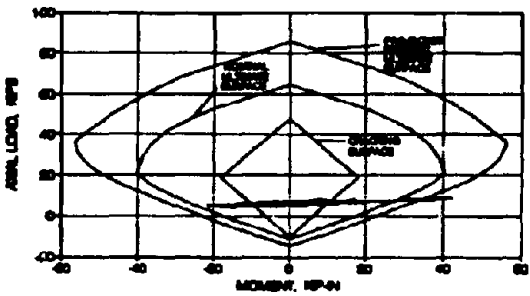
Column 7L



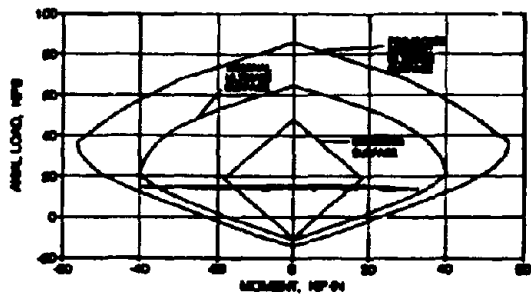
Column 4U



Column 3U

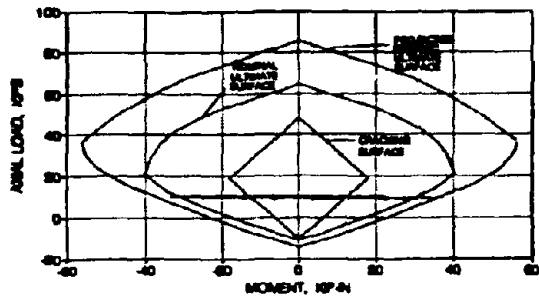


Column 4L

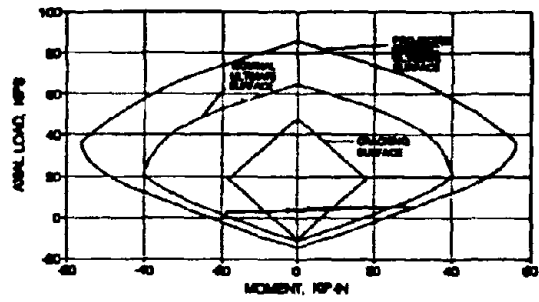


Column 3L

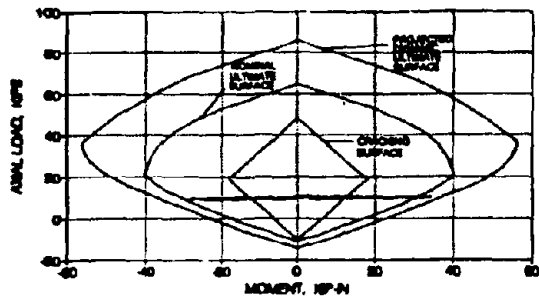
FIG. 2-27a Interaction Diagram for the South-East Columns from TFT_30



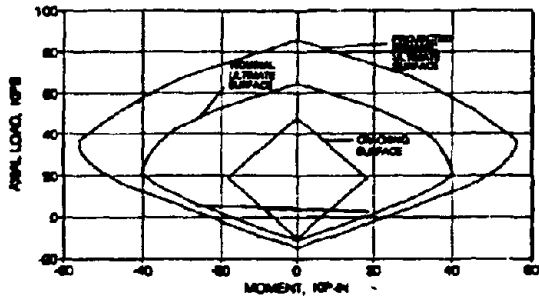
Column 6U



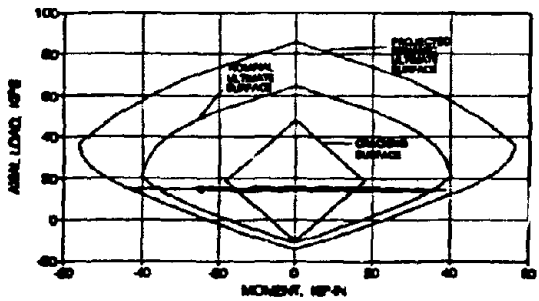
Column 5U



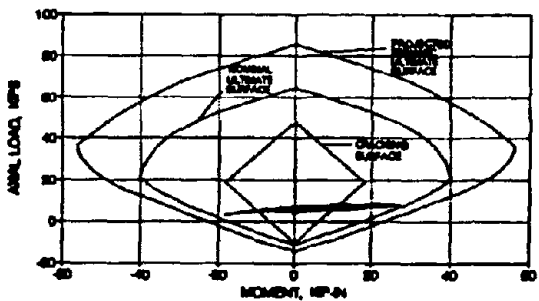
Column 6L



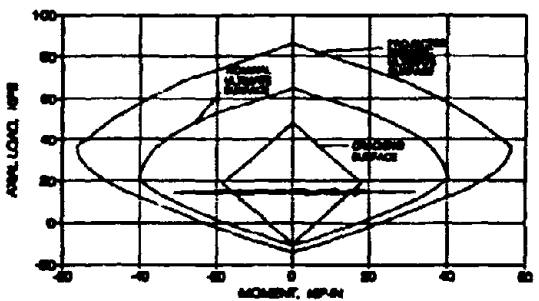
Column 5L



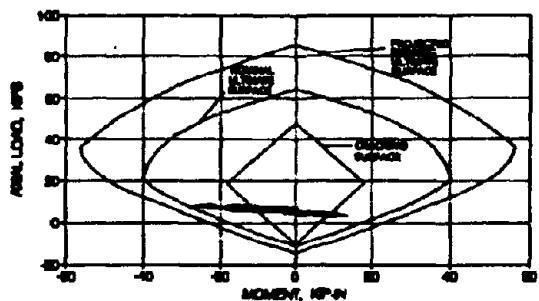
Column 2U



Column 1U

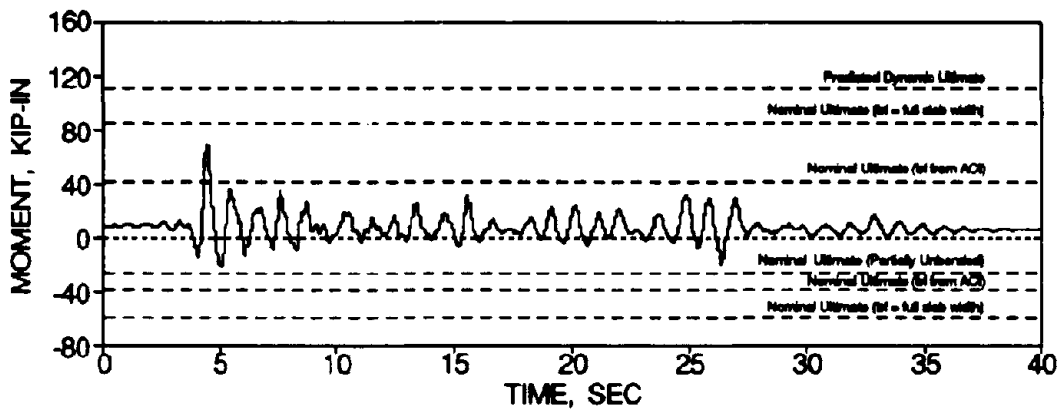


Column 2I

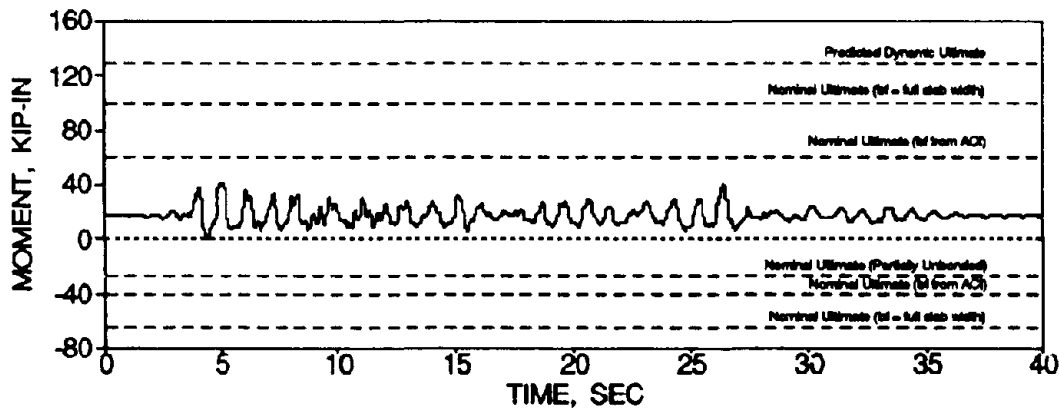


Column 1L

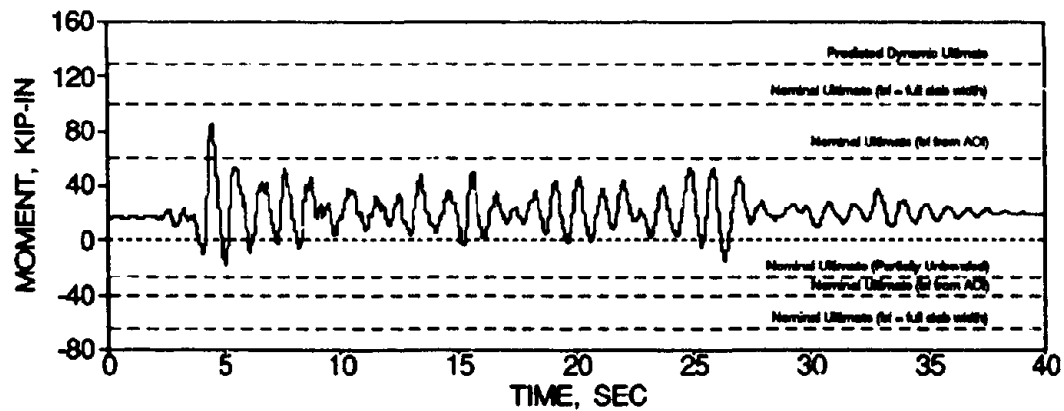
FIG. 2-27b Interaction Diagram for the North-East Columns from TFT_30



(a) Exbm481

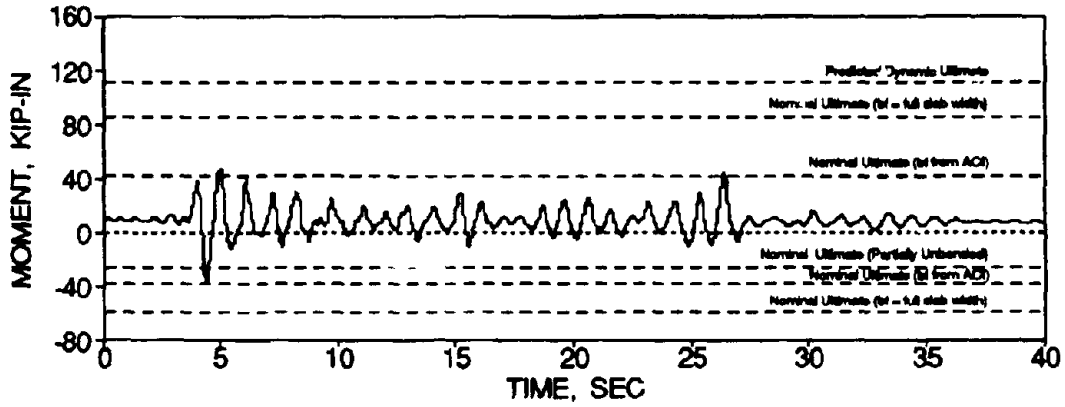


(b) Exbm482

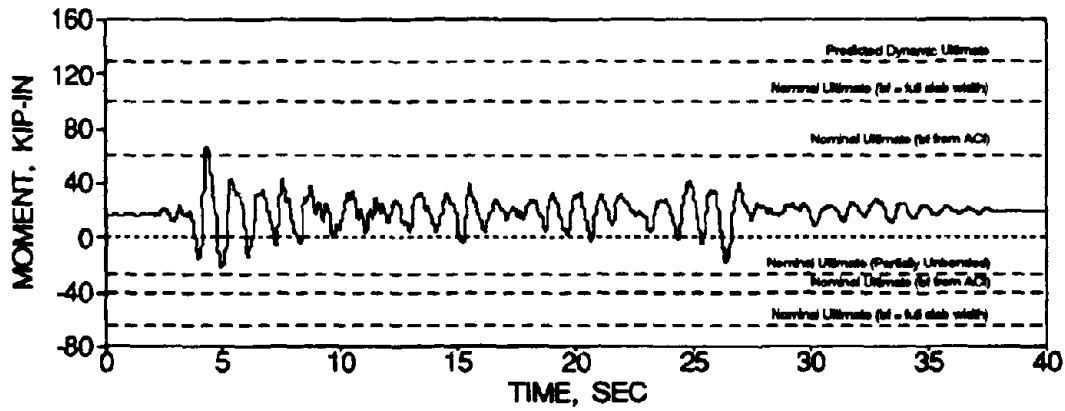


(c) Exbm483

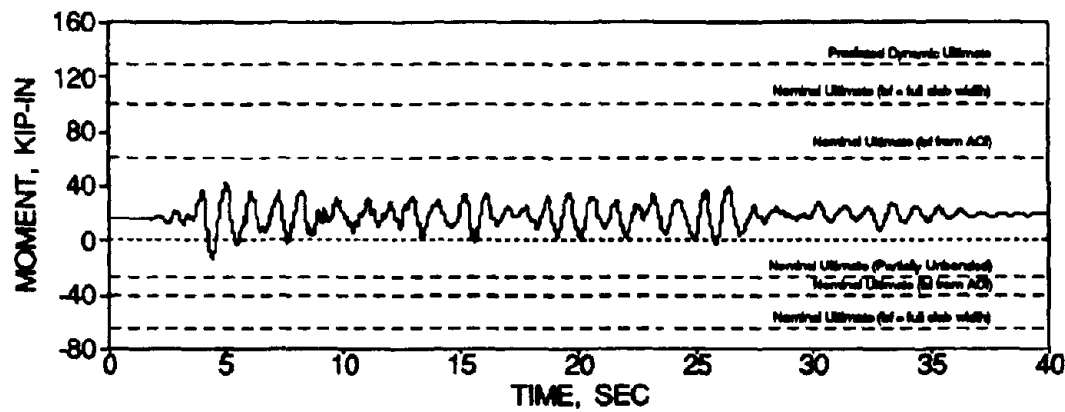
FIG. 2-28a First Story Beam Bending Moment Time Histories for TFT_30 - South Side



(a) Exbm151

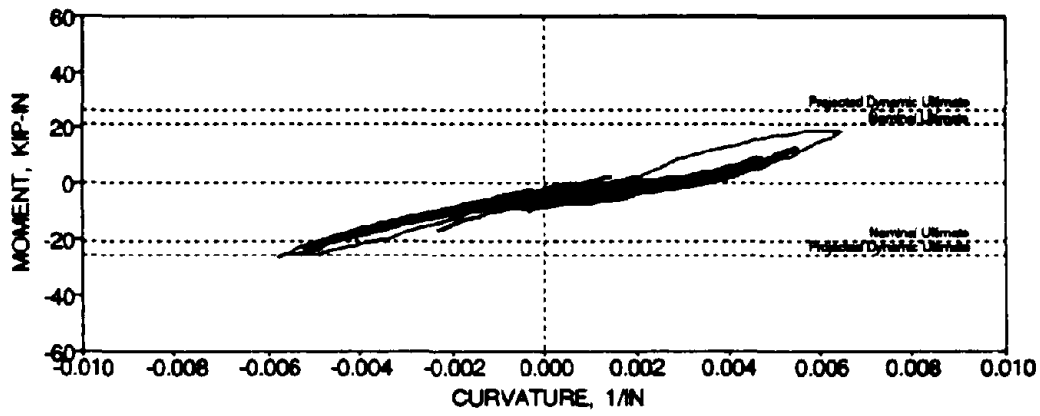


(b) Exbm152

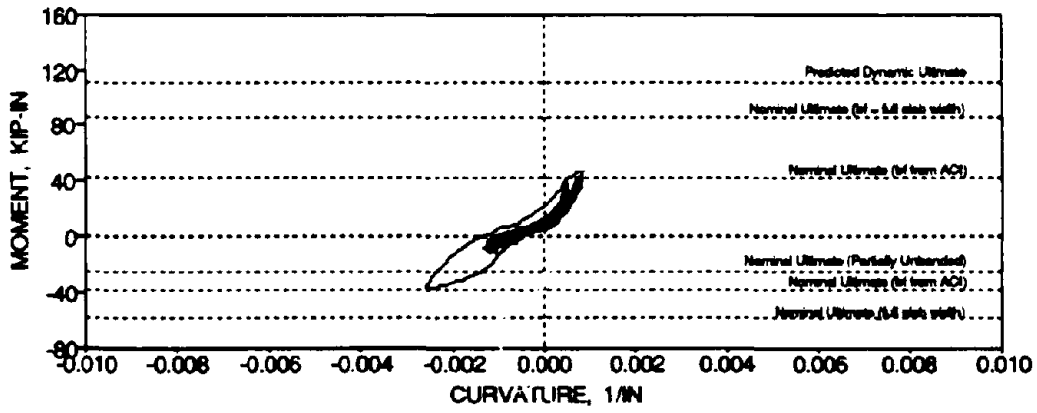


(a) Exbm153

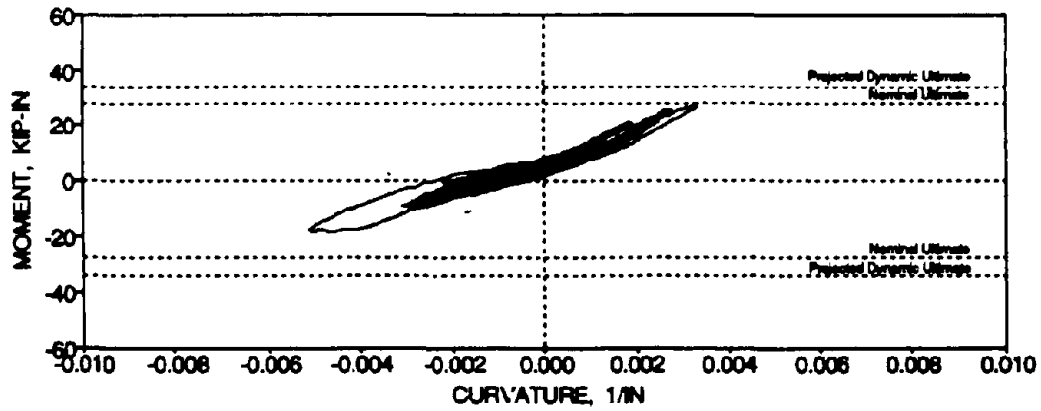
FIG. 2-28b First Story Beam Bending Moment Time Histories for TFT_30 - North Side



Column 5L

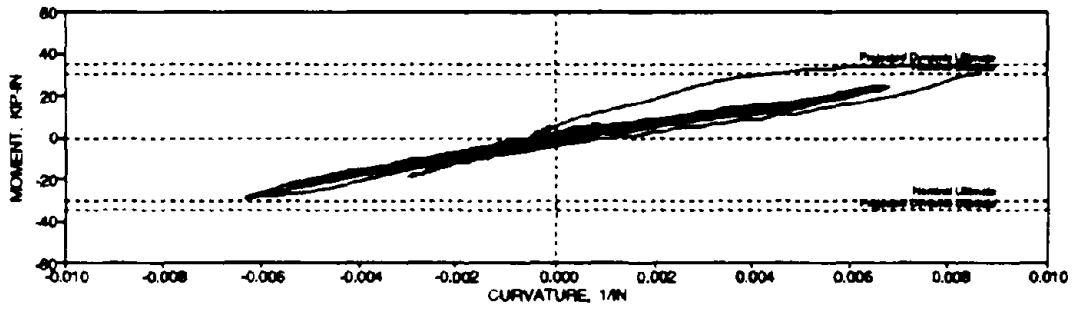


Beam Exbm151

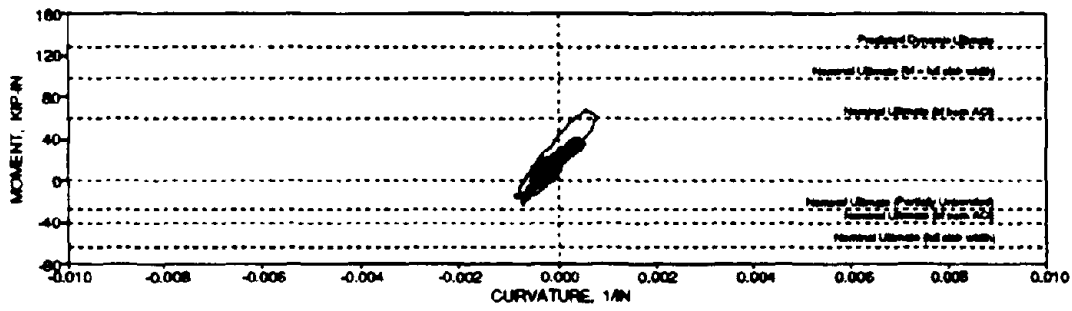


Column 1U

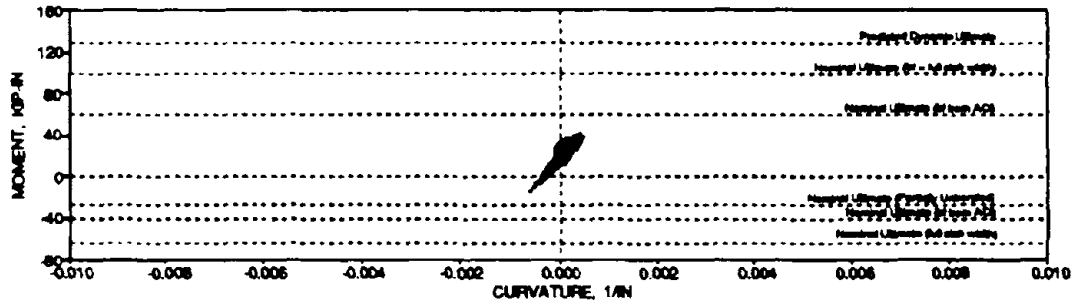
FIG. 2-29a Moment versus Curvature for TFT_30 - Exterior Joint



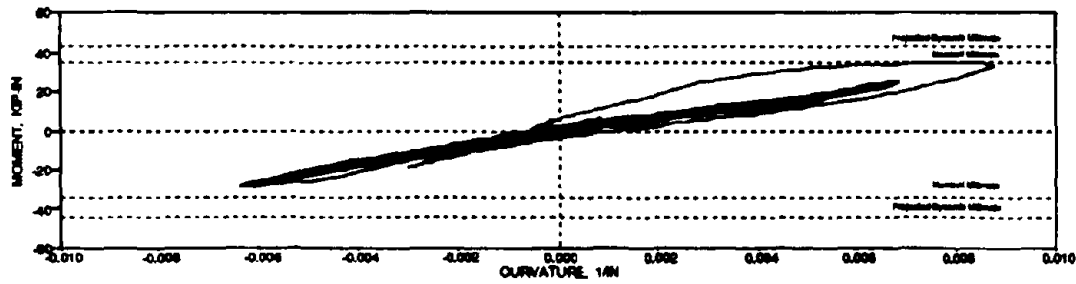
Column 6L



Beam Exbm152

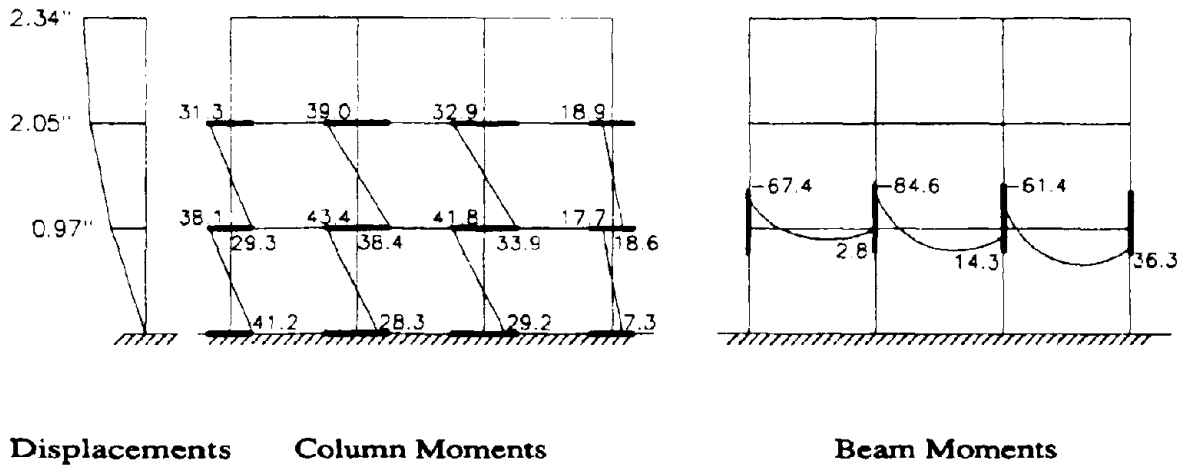


Beam Exbm153

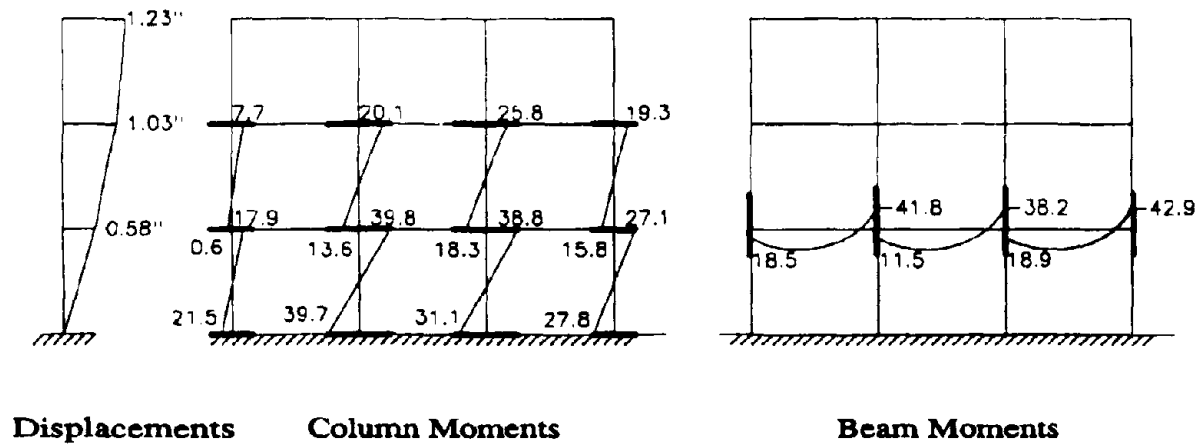
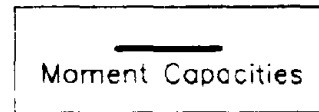


Column 2U

FIG. 2-29b Moment versus Curvature for TFT_30 - Interior Joint



(a) Time = 4.45 sec.



(b) Time = 26.43 sec

FIG. 2-30 Moment Diagram at Maximum Story Drift from TFT_30

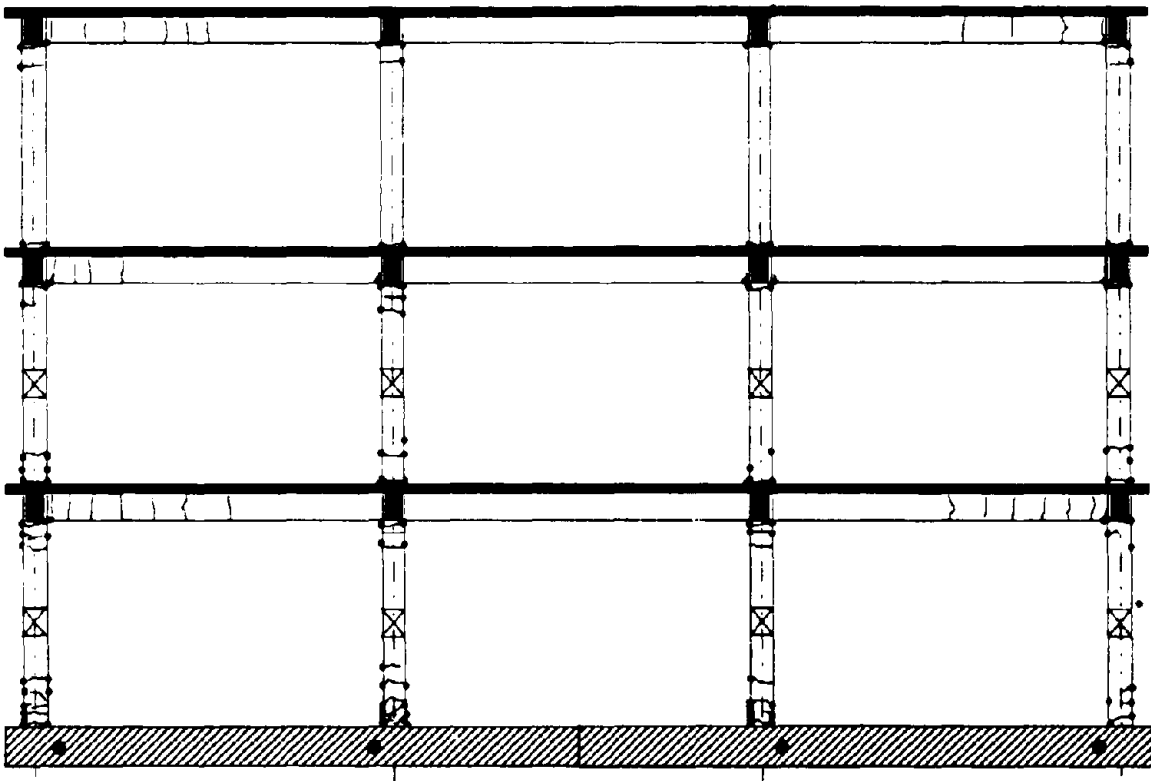
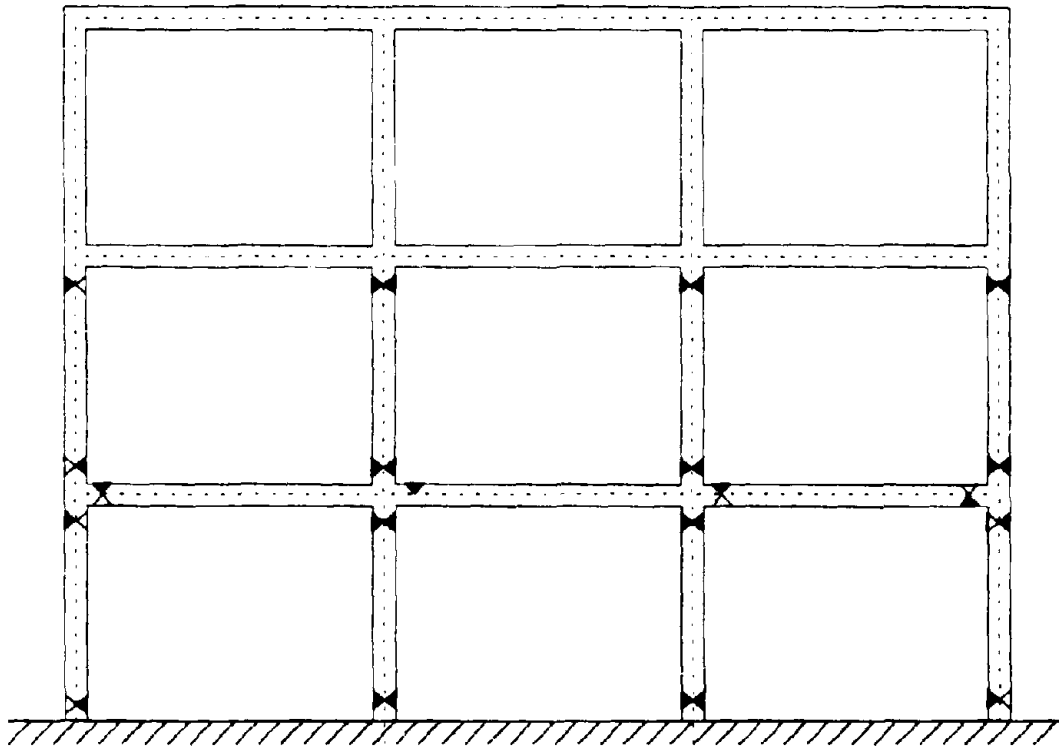


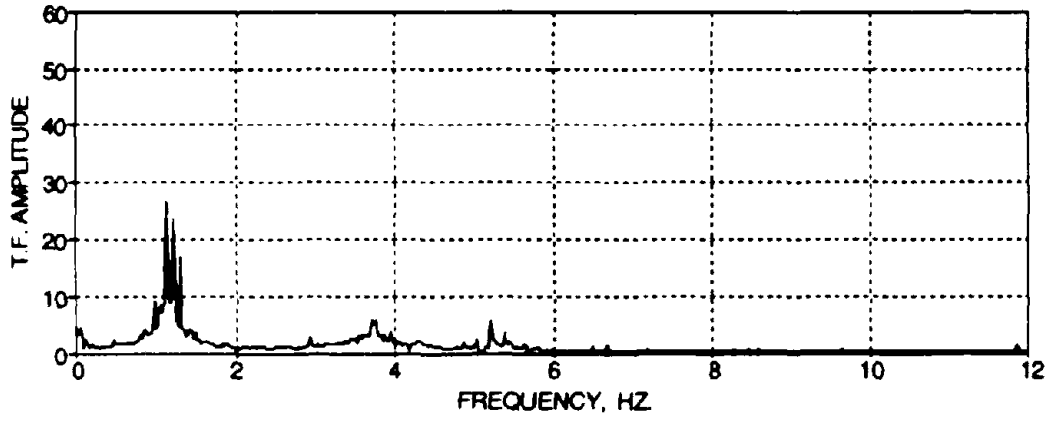
FIG. 2-31 Observed Structural Damage from TFT_30



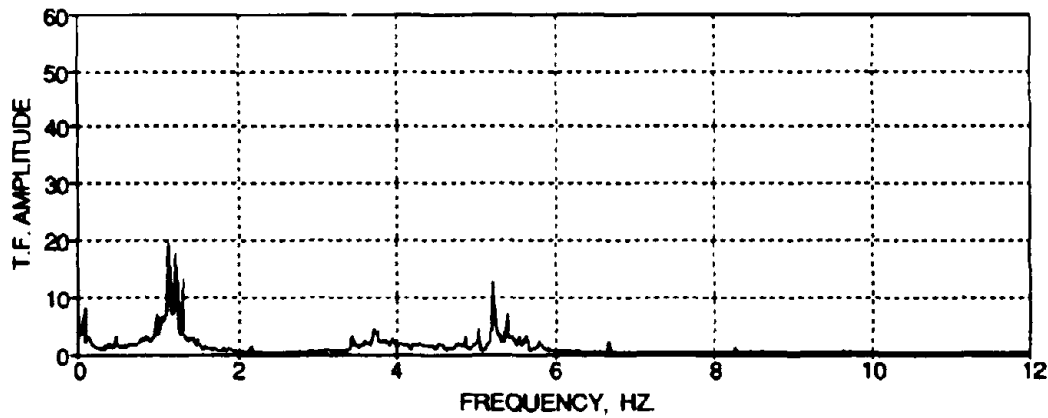
▷ Cracked
▶ Yielded

NOTE: 2nd story beams and above
were not quantitatively observed

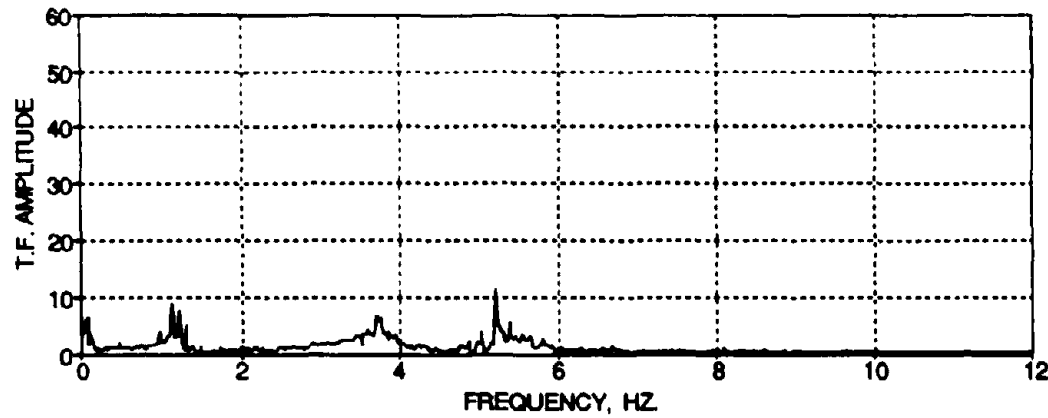
FIG. 2-32 Measured Damage State of the Model after TFT_30



(a) Third Floor

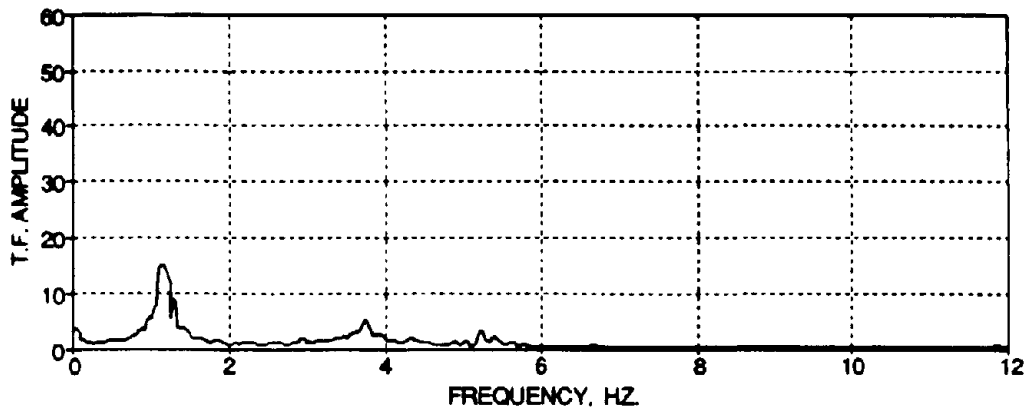


(b) Second Floor

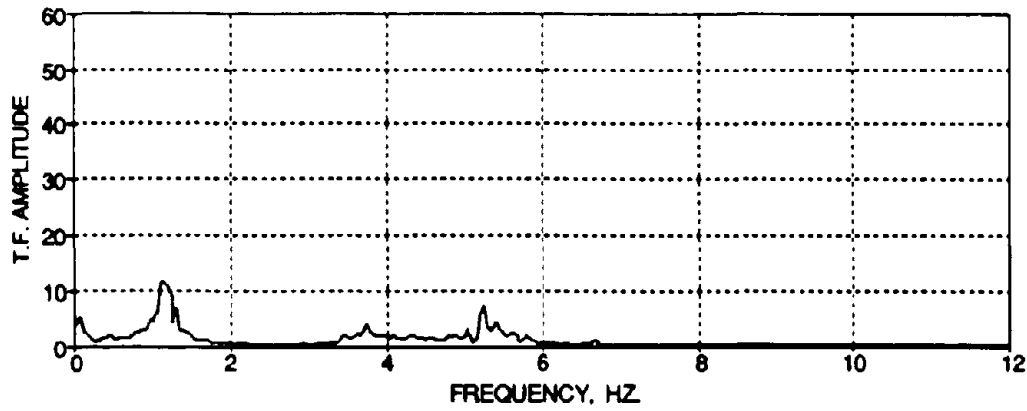


(c) First Floor

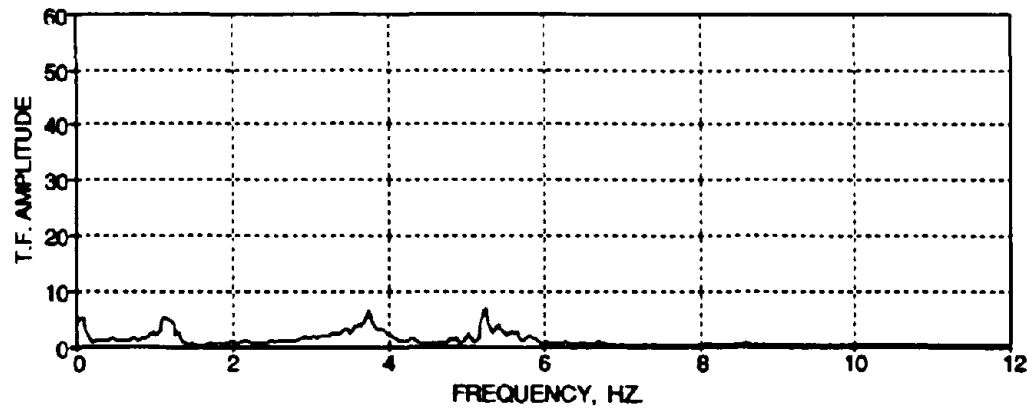
FIG. 2-33 Transfer Functions of the Story Level Accelerations from WHN_F



(a) Third Floor

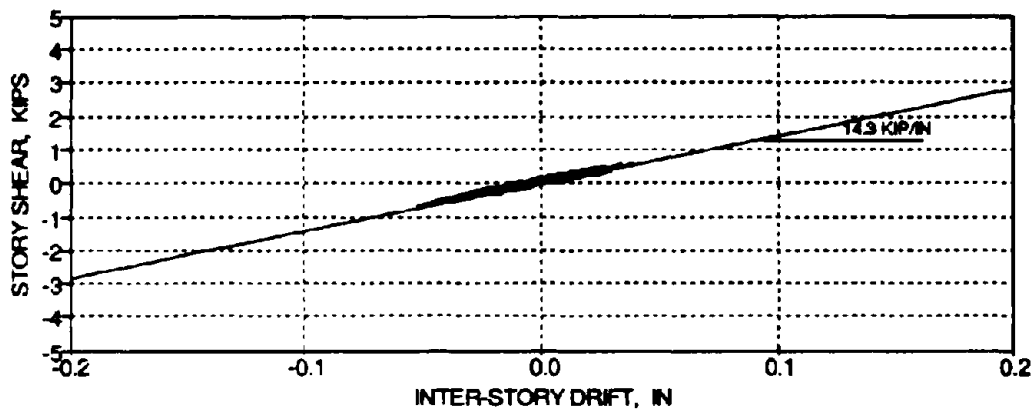


(b) Second Floor

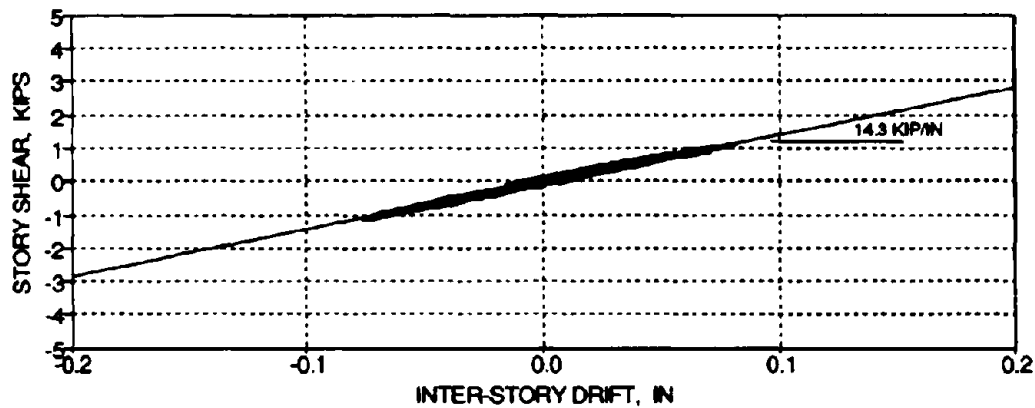


(c) First Floor

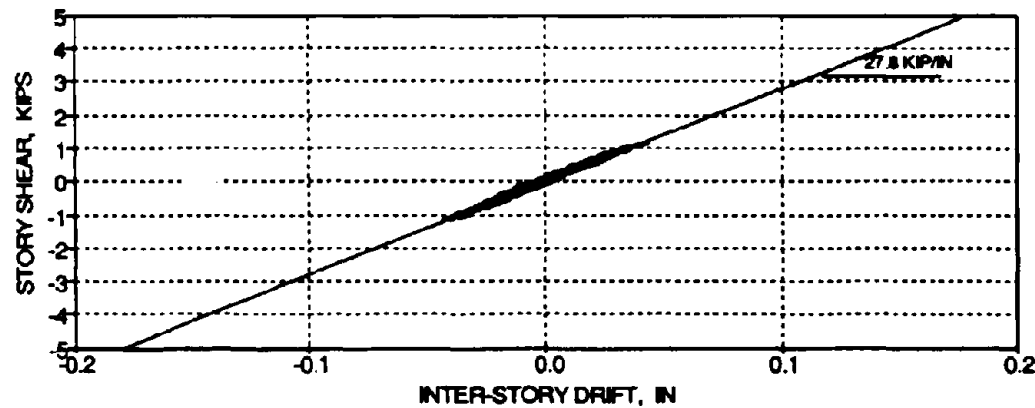
FIG. 2-34 Smoothed Transfer Functions of the Story Level Accelerations from WHN_F



(a) Third Floor



(b) Second Floor



(c) First Floor

FIG. 2-35 Story Shear versus Inter-Story Drift Histories for WHN_F

2.6 Summary Discussions

The local and global response of the model from the moderate and severe shaking table motions (Taft N21E, PGA 0.20 g and 0.30 g, respectively) are presented in this section. The following summarize the maximum response of the model from the earthquake tests, the dynamic characteristic history throughout the testing, and the resulting conclusions.

2.6.1 Maximum Story Response from Shaking Table Tests

The maximum global story response of the one-third scale LRC framed model for the minor, moderate, and severe shaking table motions are presented in a Table 2-9 for comparison.

TABLE 2-9 Maximum Response from Shaking Table Testing

Test	Story	Max. Story Displacement (in.)	Max. Inter-Story Drift (%)	Max. Story Shear (kips)	Peak Story Acceleration (g)
Minor Shaking Taft N21E PGA 0.05 g	Third	0.30	0.23	3.4	0.12
	Second	0.22	0.24	4.2	0.09
	First	0.14	0.28	5.3 (6.5%)	0.09
Moderate Shaking Taft N21E PGA 0.20 g	Third	1.32	0.54	5.6	0.20
	Second	1.14	1.07	9.3	0.20
	First	0.64	1.33	12.3 (15.2%)	0.25
Severe Shaking Taft N21E PGA 0.30 g	Third	2.35	0.89	7.1	0.25
	Second	2.05	2.24	11.6	0.22
	First	0.97	2.03	12.4 (15.3%)	0.29

It can be observed that: (i) the large story drifts occur on the first and second stories (2.03% and 2.24% of the story height, respectively for the severe shaking). The increase in drift is almost proportional to the level of excitation, except for the second floor during the severe shaking; (ii) the top story displacement for the severe shaking is 2.35 in., which corresponds to 7.05 in. in the prototype building; (iii) the base shear is 6.5% of the total weight for the minor ("elastic") shaking (PGA 0.05 g) and increases to 15.2% for the moderate shaking (PGA 0.20 g). However, for the severe shaking (PGA 0.30 g), the base shear remains almost the same

(15.3%). Therefore, a relative reduction in base shear demand occurs in the moderate and severe shaking as a result of inelastic behavior (quantified in Section 3); (iv) the peak story accelerations show amplifications for the minor shaking, no amplification for the moderate shaking, and some reductions for the severe shaking.

2.6.2 Summary of Dynamic Characteristics of Model

The natural frequencies, modal shapes, stiffness matrix, and damping characteristics of the model throughout the shaking testing program are summarized in Table 2-10.

Table 2-10 Dynamic Characteristic History of the Model

Test	Frequency	Modal Shapes	Stiffness Matrix	Story StiffnessEs	Equivalent Viscous Damping
	f_i (Hz.)	Φ_v	K_v (kip/in)	k_s (kip/in)	ξ (%)
WHN_B	$\begin{pmatrix} 1.78 \\ 5.32 \\ 7.89 \end{pmatrix}$	$\begin{pmatrix} 1.00 & -0.82 & -0.46 \\ 0.80 & 0.46 & 1.00 \\ 0.42 & 1.00 & -0.83 \end{pmatrix}$	$\begin{pmatrix} 51.9 & -53.4 & 2.5 \\ -53.4 & 102.4 & -54.4 \\ 2.5 & -54.4 & 104.7 \end{pmatrix}$	$\begin{pmatrix} 53.4 \\ 54.4 \\ 50.3 \end{pmatrix}$	$\begin{pmatrix} 2.0 \\ 2.4 \\ 2.0 \end{pmatrix}$
		Taft N21E		PGA 0.05 g	
WHN_C	$\begin{pmatrix} 1.71 \\ 5.08 \\ 7.42 \end{pmatrix}$	$\begin{pmatrix} 1.00 & -0.84 & -0.42 \\ 0.79 & 0.52 & 1.00 \\ 0.40 & 1.00 & -0.82 \end{pmatrix}$	$\begin{pmatrix} 44.5 & -46.8 & -0.2 \\ -46.8 & 94.9 & -47.3 \\ -0.2 & -47.3 & 92.2 \end{pmatrix}$	$\begin{pmatrix} 46.8 \\ 47.3 \\ 44.9 \end{pmatrix}$	$\begin{pmatrix} 4.3 \\ 4.2 \\ 3.0 \end{pmatrix}$
WHN_D	$\begin{pmatrix} 1.71 \\ 5.22 \\ 7.32 \end{pmatrix}$	$\begin{pmatrix} 1.00 & -0.88 & -0.40 \\ 0.79 & 0.58 & 1.00 \\ 0.41 & 1.00 & -0.86 \end{pmatrix}$	$\begin{pmatrix} 44.6 & -45.8 & -2.7 \\ -45.8 & 92.8 & -44.9 \\ -2.7 & -44.9 & 94.1 \end{pmatrix}$	$\begin{pmatrix} 45.8 \\ 44.9 \\ 49.2 \end{pmatrix}$	$\begin{pmatrix} 4.0 \\ 2.9 \\ 1.3 \end{pmatrix}$
		Taft N21E		PGA 0.20 g	
WHN_E	$\begin{pmatrix} 1.42 \\ 4.37 \\ 6.18 \end{pmatrix}$	$\begin{pmatrix} 1.00 & -0.95 & -0.45 \\ 0.83 & 0.55 & 1.00 \\ 0.43 & 1.00 & -0.78 \end{pmatrix}$	$\begin{pmatrix} 36.4 & -36.3 & -1.0 \\ -36.3 & 67.6 & -31.2 \\ -1.0 & -31.2 & 59.9 \end{pmatrix}$	$\begin{pmatrix} 36.3 \\ 31.2 \\ 28.7 \end{pmatrix}$	$\begin{pmatrix} 6.6 \\ 5.6 \\ 2.8 \end{pmatrix}$
		Taft N21E		PGA 0.30 g	
WHN_F	$\begin{pmatrix} 1.20 \\ 3.76 \\ 5.27 \end{pmatrix}$	$\begin{pmatrix} 1.00 & -0.86 & -0.46 \\ 0.75 & 0.64 & 1.00 \\ 0.33 & 1.00 & -0.94 \end{pmatrix}$	$\begin{pmatrix} 23.3 & -24.8 & 0.7 \\ -24.8 & 45.6 & -22.4 \\ 0.7 & -22.4 & 50.9 \end{pmatrix}$	$\begin{pmatrix} 24.8 \\ 22.4 \\ 28.5 \end{pmatrix}$	$\begin{pmatrix} 7.0 \\ 2.3 \\ 1.8 \end{pmatrix}$

It can be observed that: (i) large natural frequency and story stiffness reductions result after the moderate and severe shaking. The proportion of story stiffness reductions are similar for the minor and moderate shaking. However for the severe shaking, a large stiffness reduction occurs on the second floor. The total reduction of story stiffnesses from the "undamaged" state (WHN_B) are 43.3%, 58.8%, and 53.6%, respectively; (ii) the change in first mode natural frequency is proportional to the root of the ratio of first story stiffnesses. However for the severe shaking, this relationship is no longer valid since a large stiffness reduction occurs in the second floor; (iii) the mode shapes remain the same after the minor shaking, vary slightly in the higher modes for the moderate shaking, and vary in all modes for the severe shaking, especially the first mode; (iv) the equivalent viscous damping approximately doubles after the minor shaking and more than triples for the moderate and severe shaking. This increased equivalent damping is due to contributions from hysteretic damping.

2.6.3 Concluding Remarks on Testing of LRC Model

In the following, the results specified in the previous sections are summarized and discussed.

(a) Inter-Story Drifts

It can be observed from Table 2-9 that the maximum first and second story drifts of the LRC model for the Taft N21E earthquake motions are 1.33% and 1.07% of the story heights for the moderate shaking (PGA 0.20 g) and 2.03% and 2.24% for the severe shaking (PGA 0.30 g), respectively. The recommended provisions of National Earthquake Hazard Reduction Program, NEHRP (1991), suggest inter-story drift limitations for this classification of buildings of 1.50% of the story height. The Commentary for same provisions NEHRP (1991) states that the reasons for a drift limit are to control inelastic strains in members, for stability considerations and P-delta effect, and to restrict damage to non-structural elements. The Uniform Building Code, UBC (1991), recommends elastic inter-story drifts limits of either $0.04/R_w$ [for the structure studied here, R_w (the strength reduction factor) = 5, therefore the limit is equivalent to 0.8%] or 0.5% of the story height. UBC (1991) states that the drift limit may be exceeded if it is demonstrated that greater drifts can be tolerated by both structural and non-structural elements that affect life safety. It can be observed that the story drifts for the minor shaking are within the elastic limit. UBC (1991) also suggests that the inelastic drift limit can be estimated by multiplying the calculated elastic drift by an additional factor of $3/8 R_w$ related to the (inelastic) ductility. This results in a limit of (0.94% of the story height for the model building in this study). The above

limit is derived from service loads without load factors. Considering the load factors, this limit might be somewhat larger approaching this recommended by NEHRP. The inter-story drift maxima observed in this study for the severe shaking exceeds the recommended limits of both NEHRP (1991) and UBC (1991), while the moderate shaking exceeds limits of UBC (1991). However the observed story damage is not as large as expected with so large inter-story drifts. The damage to non-structural elements is expected to be much larger, however this evaluation was not the subject of this study. El-Attar et al. (1991) also observed large inter-story drifts for the 1/8 scale model replica. However the maximum displacement response were slightly varied from the study presented herein. Therefore it is concluded that large inter-story drifts develop in LRC frame structures from strong ground motions that might affect nonstructural components but minimally affect the structural ones.

(b) Damage to Beam-Column Joints

It was observed that there was no resulting damage or slip of the discontinuous beam reinforcement in the first story interior beam-column joints from the shaking table excitations. However some deformations were observed in the first story exterior beam-column joints possibly due to reinforcement slip or pull out (the resulting damage is quantified in Section 3). Large positive moments were also recorded in the exterior beams along with visually observed cracks, especially on the second floor. Therefore it can be concluded that complete pull-out cannot occur since less critically loaded members in the frame restrain its lateral motion and limit deformations. However, reinforcement slip does occur while the discontinuous bar still carries appreciable force.

There were also no signs of cover concrete spalling in the exterior beam-column joints.

(c) Slab Contributions to the Moment Capacity of the Beams

It was observed that the interior beams suffered only minor damage with very little cracking or yielding. This can be attributed to slab steel contributions from the full slab width, which has a dramatic effect on the flexural strength of the beams. For a typical first story beam-slab-column component, the moment capacity of the beams exceeds the capacity of the columns by about 50%, which under large lateral loads can lead to undesirable failure mechanisms. Thus a weak column - strong beam structural behavior exists. According to the seismic provision of ACI 318-89 for special frames, the flexural strengths of the columns must be greater than 1.2 times

the sum of the overstrength beam capacities. Therefore LRC structures would not satisfy the design strength provisions for special frames. Since the damage to the beams was determined to be relatively minor, it can be concluded that the story slabs contribute substantially to the strength of beams that remain primarily elastic.

(d) Apparent Collapse Mechanism

The base motions of the model introduced hinging in the columns at the first and second stories and only some hinging in the positive pull-out direction of the exterior beams. Thus an undesirable column-sidesway collapse mechanism for the model was apparently in development. Also, from the observations of the story response and story stiffness comparisons, the second story of the model was in a more severe damage state after the severe shaking and the possibility of soft-story collapse mechanism actually develops. El-Attar et al. (1991) tested one-eighth scale replica model to collapse using the Taft S69E component base motion with a large peak ground acceleration (0.8 g). The resulting mechanism that occurred was due to failure of the first story interior columns from the P-delta effect, which resulted in a sudden collapse of the structure. The corresponding mode of failure was a column-sidesway or soft-story collapse mechanism of the first floor. This global failure mechanism is also a well documented failure in lightly R/C structures experiencing large lateral forces [Moehle and Mahin (1991)]. Good correlation of the developing failure mechanism and the actual collapse mechanism, El-Attar et al. (1991), can be noted. Therefore, it can be concluded that the weak column - strong beam behavior can result in the undesirable column-sidesway or soft-story collapse mechanism in LRC frame structures under strong ground motions.

(e) "Second Mode" Effect

Higher mode effects are negligible during the minor and moderate base motions. However the "second mode" effect was evident in the story displacements and shear forces of the model during the severe shaking, TFT_30. This effect may have developed due to the softening of the model from the moderate shaking and may explain the more severe damage to the second story of the model in the severe test. El-Attar et al. (1991) observed only first mode contributions in the response of the 1/8 scale model. The different response observations among tests may have resulted from slightly different concrete and rebar strengths and also a different component of the ground motion (El-Attar et al. (1991) used the S69E component of the Taft earthquake).

(f) Deterioration of Story Stiffnesses and Natural Frequencies

Due to the resulting damage in the columns of the first and second stories, large deterioration of story stiffnesses and natural frequencies occur (see Table 2-10). The elastic response spectrum for 2% damping is shown in Fig. 2-36 along with the range of first mode period changes in the model during the shaking table tests (from 0.562 sec. in the "undamaged" state to 0.833 sec. in the final state). It can be observed that the structural softening results in a decreased acceleration amplification. However, the reduced story stiffness contributes to the large inter-story drifts and total displacements.

From Table 2-10, the observed first mode (elastic) period of the model is 0.562 sec. The approximation recommended by UBC (1991) for calculating the elastic first mode natural period of a building is:

$$T = C_t(h_n)^{3/4} \quad (2.4)$$

where T = first mode period, sec
 C_t = 0.030 for R/C moment resisting frames
 h_n = building height, ft

From Eq. (2.4), the calculated period for the prototype building according to UBC (1991) is 0.441 sec. Using a period scale factor of $1/\sqrt{3}$ (see Appendix A, in Part I of the Evaluation series (Bracci et al, 1992a), the calculated period for the model is 0.255 sec. It can be observed that a large discrepancy exists in predicting the elastic first mode period. Since LRC structures are designed without considering lateral loads, the flexibility of these structures is not accounted in the above formulation. A different value for the factor, C_t , may be necessary to describe these buildings. More parametric and field studies should be made to determine an appropriate quantity.

(g) Story Shear Force Demands

It can be observed from Table 2-9 that the base shear demands are similar during the moderate and severe base motions (with base shear coefficients of 15.2% and 15.3%, respectively). This slight increase in demand implies that the base shear capacity is attained during these motions. However, this does not imply total collapse of the model, since additional strain hardening of the reinforcement takes place and the total failure mechanism does not develop. Also note that

a large shear forces develop in the second floor during the severe earthquake. El-Attar et al. (1991) reported base shear demands of 9.4% and 9.7% of the total structural weight for severe motions with PGA's of 0.35 g and 0.80 g, respectively (or 12.11% and 12.50% for comparison with this study due to different prototype weight considerations). This variation can be attributed to: (i) the different inertial story mass and natural frequencies; (ii) the different Taft component of base motion; and (iii) the varying material properties among the different model tests. An analytical evaluation is used in Section 3 to characterize the base shear reduction factor for inelastic behavior (similar to R_w in UBC) during the moderate and severe shaking.

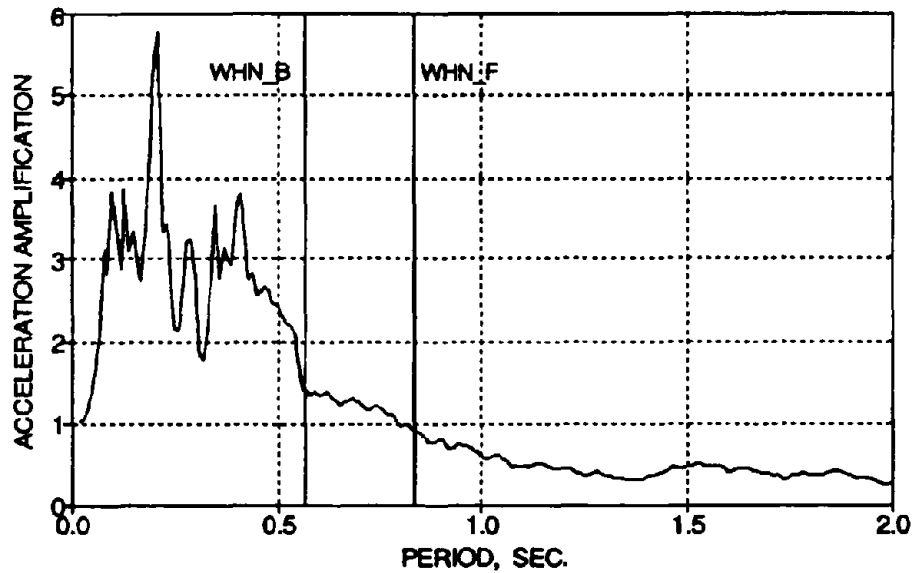


FIG. 2-36 Response Spectra Acceleration Amplification for Taft N21E

SECTION 3

ANALYTICAL DAMAGE EVALUATION OF MODEL

3.1 Introduction

The experimental response of the three story model from the minor (0.05 g), moderate (0.20 g), and severe (0.30 g) shaking table motions were summarized in the previous section. In this section, three inelastic analysis models are presented and used to predict the story response from induced base motions. The damage to the individual members, story levels, and overall structure from the induced earthquakes is evaluated analytically in terms of damage indicators defined as *damage indices*. The damage indices are used to evaluate the extent of damage on a scale representing minor, moderate, or severe damage and the damage potential or reserve capacity of the structure.

An incremental intensity analysis was performed using the identified structural parameters and the scaled Taft N21E acceleration motion. The input peak ground acceleration was analytically varied to identify the critical peak acceleration motion and collapse patterns of the model. A modified damage index is further proposed to incorporate the P-delta effect in column members and is also used for determining the critical peak ground acceleration (PGA) that produces actual collapse.

Also, an elastic analysis was presented to identify the corresponding responses reduction factors due to inelastic behavior and are compared with the recommended values of strength reduction factors from UBC (1991).

3.2 Analytical Modeling and Response Results

Analytical modeling of the structural model was performed using the nonlinear analysis platform IDARC: Inelastic Dynamic Analysis of Reinforced Concrete Frame-Wall Structures, Kunnath et al. (1990), with the structural parameters identified from: (i) engineering approximations; (ii) component tests; and (iii) an experimental response fit. IDARC uses a trilinear moment-curvature skeleton (backbone) curve. Since concrete has some tensile capacity, the concrete has an influence on member behavior until cracks develop. Also, members under large bending moments can develop cracks without yielding of the reinforcement. These effects, which were observed in tests, can be captured with the trilinear skeleton curve. IDARC also employs a

hysteretic rule using three parameters for simulating stiffness degradation, strength deterioration, and pinching behaviors. The pinching behavior is composed of a target slip factor, which determines the target point after the zero crossing as a factor of the yield point, and a slip reduction factor, which determines the slip length as a factor of the distance to the target point. Fig. 3-1 illustrates the effect of the parameters. The Newmark-Beta algorithm is utilized for determining a step-by-step solution of the dynamic equation of motion. More details and additional features of IDARC are described by Kunnath et al. (1990).

The structural parameters for each analytical model that need to be identified are: (i) the initial, post-cracking, and post-yielding stiffnesses; (ii) the cracking and yielding moments; (iii) the equivalent viscous damping characteristics; and (iv) the hysteretic properties. The equivalent viscous damping characteristics in R/C systems during elastic deformations results due to micro-cracking, friction, etc. in members. Hysteretic energy dissipation due to inelastic deformations is represented by the hysteretic model and not by equivalent viscous damping. A summary of the model parameters determined from component testing (see Part II, Aycardi et al, 1990) and from engineering models are presented in Table 3-1.

3.2.1 Modeling with Engineering Approximations

In lieu of more precise way to determine of the structural parameters, an engineer must make approximations of the member properties for proper analytical representation to predict the seismic response of structures. Firstly, the initial column and beam stiffnesses (EI_{col} and EI_{bm}) of the model are assumed to be:

$$EI_{col} = 0.55(EI_{col})_g \quad (3.1a)$$

$$EI_{bm} = 0.45(EI_{bm})_g \quad (3.1b)$$

where $(EI_{col})_g$ = stiffness based on the gross column section dimensions

$(EI_{bm})_g$ = stiffness based on the gross beam section dimensions with full slab contributions

Since micro-cracking is present in R/C members, a reduction factor was applied to the gross member properties. It can be observed that a smaller reduction was used for the columns to account for the compressive pressure of the axial loads in closing some of the micro-cracks. The initial member stiffnesses that can predict the first natural frequency of the model was 56.5% of the gross section stiffness (see Part I, Bracci et al., 1992a). Note that the "fully cracked"

stiffness properties are 23% and 13% of the gross section properties for the column and beams, respectively. Paulay and Priestley (1992) suggest the effective range for moment of inertia of rectangular beams, T-beams, L-beams, and columns of varying axial loads as follows: or columns with axial loads of about $0.2 f_c A_g$, the suggested range for effective moments of inertia is between $0.5 I_g$ and $0.7 I_g$. For columns with axial load greater than $0.5 f_c A_g$, the suggested range is between $0.7 I_g$ and $0.9 I_g$. For T-beam members, the suggested range is between $0.25 I_g$ and $0.45 I_g$. However, the effective flange (slab) width is based on 1/2 the flange width from strength provisions of ACI-318 and not on the full slab width as calculated above. Therefore, the assumed stiffnesses for the analysis are within the suggested range according to Paulay and Priestley (1992), for the columns and are about two times stiffer for the beams.

Shahrooz and Moehle (1987) developed an analytical model based on one-half (0.5) the uncracked member stiffness (gross section properties) to predict the response of an R/C set-back model building excited on the shaking table. They reported that acceptable estimates of maximum response and natural periods were achieved.

For development of the hysteretic rule, a post-cracking stiffness of $EI/2$ is assumed. The yield strengths of the beams and columns are computed from basic principles. Note that the beam moments consider slab steel contributions from the full slab width. Also note that the beam yielding moment in the positive direction considers the effect of pull-out of the discontinuous bottom beam reinforcement (50% reduction in rebar area based on the prototype ratio of provided and required embedment lengths).

The hysteretic properties of the analytical model (see Fig. 3-1) for the beams and columns cannot be determined from engineering principles since they are dependent on the hysteretic model. Therefore these parameters were determined from component tests reported in Part II of these Evaluation series (Aycardi et al, 1992). Their values are described in the following: (i) $\alpha = 0.50$ for the stiffness degradation factor; (ii) $B = 0.04$ for the strength degradation factor; (iii) $\gamma = 0.70$ for the target slip factor; (iv) 1.00 for the slip reduction factor; (v) 1.5% for the post-yielding stiffness ratio; and (vi) 2% for the equivalent viscous damping ratio. It should be noted that these properties are selected based on results and observations from previously conducted component tests, since no other sources are available. The equivalent viscous damping ratio was found experimentally during a white noise shaking table excitation to be about 2%.

The platform program IDARC is used to carry out the analysis based on the analytical model proposed from engineering approximations. From static computations, the first natural frequency is determined to be 1.72 Hz. Note from the experimental white noise excitation before earthquake shaking that the first natural frequency was determined to be 1.76 Hz. (see Table 2-10). From a shakedown analysis based on a 2% story drift limit, a base shear capacity of 12.2 kips (15.0% of the total structural weight W) is computed. Note that a shakedown (collapse mode) analysis is an inverted triangular static loading on the structure that continuously increases until the drift limit is achieved. From Table 2-9, the observed base shear maxima during minor, moderate, and severe shaking were 5.3 kips (6.5% W), 12.3 kips (15.2% W), and 12.4 kips (15.3% W), respectively. Therefore, according to this model, the base shear capacity from a shakedown analysis has been reached and exceeded during the moderate and severe shaking. However, collapse did not occur due to strain hardening of the rebars and increased material strengths from strain rate effects. Also note from Section 2 that the full collapse mechanism had not developed during the shaking.

Figs. 3-2a and 3-2b show the analytical versus experimental response comparisons for the minor shaking (Taft N21E, PGA 0.05 g). It can be observed that some deviations in the response magnitudes develop in the history, but the period of vibration remains primarily in-phase. The story displacements and shear forces are slightly overpredicted in the initial part of the history.

Since the minor shaking was shown to be governed by elastic deformations (Part I, Bracci et al., 1992a), the same analytical model for member properties is carried out with IDARC for the moderate and severe shaking. However, the subsequent white noise excitation after the minor shaking showed a slight decay in the first natural frequency (1.66 Hz. from Table 2-10). The moderate and severe motions are applied in a sequential history (back-to-back) to capture the degradation due to continued inelastic cycling. The corresponding response comparisons are shown in Figs. 3-3 and 3-4, respectively. Initially for the moderate shaking, the story displacement and shear force predictions are closely related to the experiment. However, the response magnitudes are slightly underpredicted in the latter part of the history. For the severe shaking, the analytical response is closely related to the experiment in the beginning of the history, where the peak magnitudes are captured. However, deviations in magnitude occur in the latter part of the history, but the period of vibration remains in-phase.

It can be concluded that the analytical response with the proposed approximations is not totally in correlation with the experiment. However, the peak story displacements and shear forces are captured and the response trends are similar for the earthquake motions. Therefore, adequate correlation of the analytical response is achieved based on structural parameter approximations.

3.2.2 Modeling with Component Tests

Aycardi et al. (1992) (see Part II of this Evaluation series) tested quasi-statically column and subassemblage components of the three story model. Components were constructed with the same materials during each phase in the construction of the model. The initial member stiffness were identified as follows:

$$EI_{int.col} = 0.49(EI_{col})_g \quad (3.2a)$$

$$EI_{ext.col} = 0.33(EI_{col})_g \quad (3.2b)$$

$$EI_{bm} = 0.32(EI_{bm})_g \quad (3.2c)$$

where $EI_{int.col}$, $EI_{ext.col}$ = interior and exterior column stiffnesses, respectively

It can be observed that a reduction in stiffness from the gross member dimensions develops from micro-cracking. Note that the extent of the reduction was less severe in the axially loaded interior columns. A post-cracking stiffness of about $EI/2$ was also identified initially. The member yield strengths were identified from the inelastic reversed cycling tests and were similar to calculations from basic principles. The hysteretic member properties used for this analytical model are the same as in the engineering approximations, which are based on the component tests.

The first natural frequency is calculated to be 1.50 Hz., which is slightly soft (flexible) as compared to the experimental identifications (1.76 Hz. and 1.66 Hz. before and after the minor shaking, respectively). From a shakedown analysis based on a 2% story drift limit, the base shear capacity is obtained to be 12.2 kips (15.0% W), which is the same as in engineering approximations.

Figs. 3-5, 3-6, and 3-7 show the response comparisons from the minor, moderate, and severe shaking, respectively. Note that the same analytical model of structural parameters is used for the sequential run of the moderate and severe shaking. It can be observed from the minor shaking that the predicted period of vibration is slightly different than the experiment. This discrepancy

occurs as a result of the soft first natural frequency in the proposed analytical model. However the peak story displacements and shear forces are similar. For the moderate and severe shaking, the response period of vibration is slightly out-of-phase with the experiment. It can be observed during the moderate shaking that the initial story displacements and shear forces are accurately predicted. However, the response magnitudes in the latter part of the history are underpredicted. For the severe shaking, the predicted maximum story displacements and shear forces are in agreement with the experimental response. Also, the response trends are similar throughout the history, with only slight deviations in magnitude in the latter part of the history.

Therefore, satisfactory predictions of the story displacements and shear forces are achieved by using the structural parameters from component tests for the moderate and severe shaking. The analytical model produced only slight discrepancies for predicting the period of vibration during the minor (primarily elastic response) and moderate shaking due to the inaccurate first natural frequency prediction. However, the maximum story displacements and shear forces were correlated.

3.2.3 Modeling with Properties Identified using Response Fit

3.2.3.1 Minor Shaking

A series of analytical models with different structural parameters for each group of members were developed to properly correlate the response calculations with the experimental response. For a good response fit during the minor shaking (0.05 g), the initial column stiffnesses were 0.588 ($EI_{col,g}$), 0.598 ($EI_{col,g}$), and 0.591 ($EI_{col,g}$), respectively for the first, second, and third story columns. The initial stiffness of the beams were 0.252 ($EI_{bm,g}$). This corresponds to slightly stiffer columns and softer beams in comparison with the previously assumed analytical models. However, note that roundoff of the initial stiffnesses will not significantly affect the calculated response. The post-cracking stiffness in the columns and beams was about $EI/2$ (similar to the previous models). The moment strengths are also similar to the previous models. However some slight deviations exist in the hysteretic properties: (i) the stiffness degradation factor was 0.5 for the first and second story columns and 0.9 for the third story columns and beams (0.5 in previous models); (ii) the strength degradation factor was 0.05 for all members (0.04 in previous models); (iii) the target slip factor was 0.5, 0.6 and 0.8 for the first, second, and third story columns, respectively, and 0.7 for the beams (0.7 in previous models); (iv) the slip reduction

factor was 1.0 for all members (same as in previous models); (v) the post-yielding stiffness ratio was 2% for the first and second story columns and 1% for the third story columns and beams (1.5% in previous models); and (vi) the damping ratio was 2% (same as in previous models).

The first natural frequency was determined to be 1.63 Hz., which is comparable with the experimental values (1.76 Hz. and 1.66 Hz. before and after the minor shaking, respectively).

The sequence of hinge formation in the model from a shakedown analysis, is shown in Fig. 3-8. It can be observed that yielding first occurs in the lower first story beams in the pull-out direction. Yielding then propagates to the columns of the first and second floor. At a drift limit of 2% of the building height, the base shear capacity of the model was 12.2 kips (15.0% of the total structural weight W). From Table 2-9, the maximum measured base shear during the moderate and severe earthquakes were 12.3 kips (15.2% W) and 12.4 kips (15.3% W). Therefore, according to this model, the base shear capacity has been achieved in the moderate and severe shaking. However, collapse does not occur due to additional reserve strength from strain hardening of the reinforcement and dynamic strain rate effects. Also note from Section 2 that the full collapse mechanism had not developed during the shaking.

Figs. 3-9a and 3-9b show the analytical versus experimental response comparisons for the minor shaking. It can be observed that the predicted story displacements are very similar with the experiment throughout the shaking history with only slight over-predictions of the shear forces.

3.2.3.2 Moderate and Severe Shaking

It was shown in Section 2 that some slight stiffness deterioration occurs and slight cracking develops in some columns from the minor shaking. Therefore, the column stiffnesses are varied to account for this decay for the moderate (0.20 g) and severe (0.30 g) shaking. The initial column stiffnesses used in the analysis were $0.391 EI_c$, $0.326 EI_c$, and $0.443 EI_c$, respectively for the first, second, and third stories. Note that the column stiffnesses are more varied between floors with the second floor being the most flexible. There are various explanations for this occurrence: (1) varying concrete strengths between floors, which was observed in representative cylinder tests (see Part I, Bracci et al., 1992a); and (2) slight irregularities of column placement. Note that since only elastic deformations develop in the beams during the minor shaking, the stiffnesses in the beams for the moderate and severe shaking are identical to the values for the minor shaking ($0.252 EI_b$).

The previous analytical models, based on engineering approximations and component tests, provide adequate, but not total, agreement with experimental response in the latter part of the shaking (underpredicted). To account for this, the post-cracking stiffness used in this analysis was modified to $EI/1.25$ (in comparison to $EI/2$ previously) to model stiffer behavior after cracking. Note that this model is very similar to a bilinear model. A trilinear backbone curve was used to represent reinforced concrete behavior in which a larger initial stiffness results from the contributions of the concrete in tension. However, in a cracked state, the influence of the concrete in tension is negligible and the tensile behavior is primarily governed by the rebar strengths. The hysteretic properties used were identical to the minor shaking.

Figs. 3-10 and 3-11 show the response comparisons for the moderate and severe earthquakes. Excellent correlation of the story displacements and shear forces can be observed in the moderate shaking with only slight disparities in the severe shaking. The peak response magnitudes and response trends are similar.

It was also important to compare the analytically predicted damage states of the model from the earthquakes with the experimentally measured. Analytically, the damage states are defined in accordance with the cracking and yielding moments from the analytical model. The descriptions of damage states includes two parts: (i) visual; and (ii) calculated. Some of the visual descriptions are classified from flexural and shear cracking, concrete spalling, concrete crushing, exposed reinforcement, buckled reinforcement, and fractured hoops. However, cracking and yielding is also observed experimentally through measured internal stresses of the model.

Figs. 3-12a, 3-12b, and 3-12c show the resulting damage states of the model predicted from the response fit analytical models in comparison with the experimentally measured damage states after each earthquake test. It can be observed that cracking results in some of the columns from the minor shaking (Taft 0.05 g) both analytically and experimentally. However, for the moderate and severe shaking (Taft 0.20 g and 0.30 g), yielding occurs in the columns of the first and second story and a plastic hinge develops in the first story exterior beam in the pull-out direction both analytically and experimentally. Also analytically, additional incipient beam yielding occurs for the severe shaking. It was observed that the apparent incipient collapse mechanism for the model under ultimate load is a column-sidesway or soft-story failure mechanism.

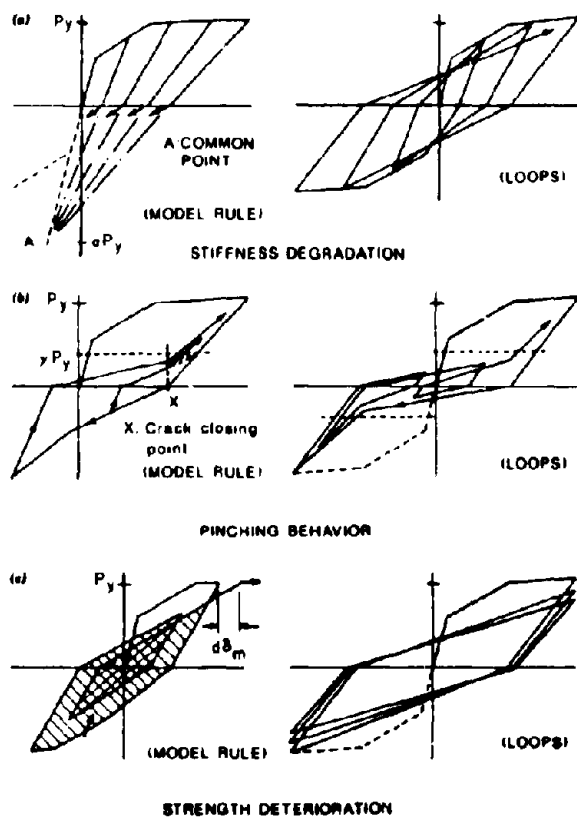


FIG. 3-1 Hysteretic Parameters in IDARC

TABLE 3-1 Member Parameters for Analytical Modeling

Modeling Type	Initial Stiffness			Post-Cracking Stiffness			Hysteretic Properties [E]				
	Interior Column (%EI _g) (2)	Exterior Column (%EI _g) (3)	Beams (%EI _g) (A) (4)	Column (%EI) (5)	Beam (%EI) (6)	Stiffness Deter. Factor (α) (7)	Strength Deter. Factor (β) (8)	Target Slip Factor (γ) (9)	Crack Closing Factor (X) (10)	Post-Yield Stiffness (%) (11)	Damping Ratio (%) (12)
1. Engineering Approximations	55 [B]	55 [B]	45 [C]	50	50	0.5	0.04	0.7	1.0	1.5	2.0
2. Component Tests [D]	49	33	32	50	50	0.5	0.04	0.7	1.0	1.5	2.0
3. Response Fit Minor Shaking	~60 [B]	~60 [B]	25 [B]	50	50	0.5 - 0.9	0.05	0.5 - 0.8	1.0	1.0 - 2.0	2.0
Moderate and Severe Shaking	33 - 44	33 - 44	25	80	25	0.5 - 0.9	0.05	0.5 - 0.8	1.0	1.0 - 2.0	2.0

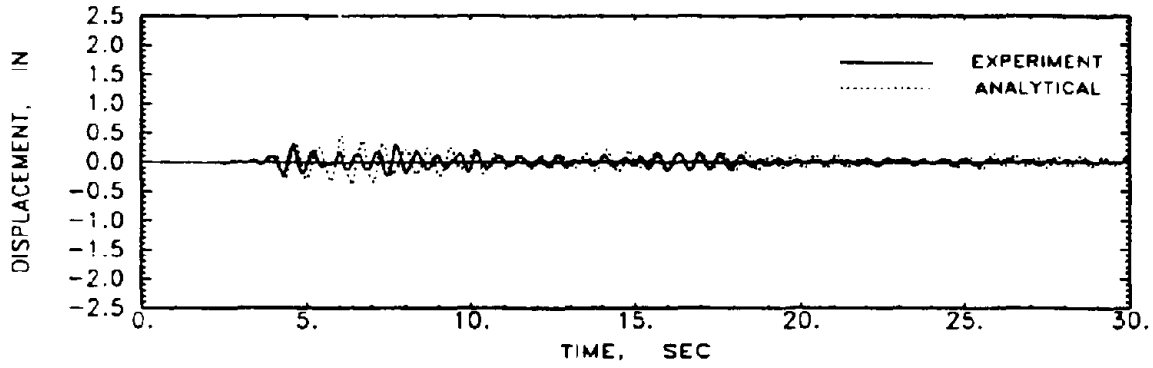
[A] Based on gross section properties with full slab width contributions.

[B] Suggested by Paulay and Priestley (1992).

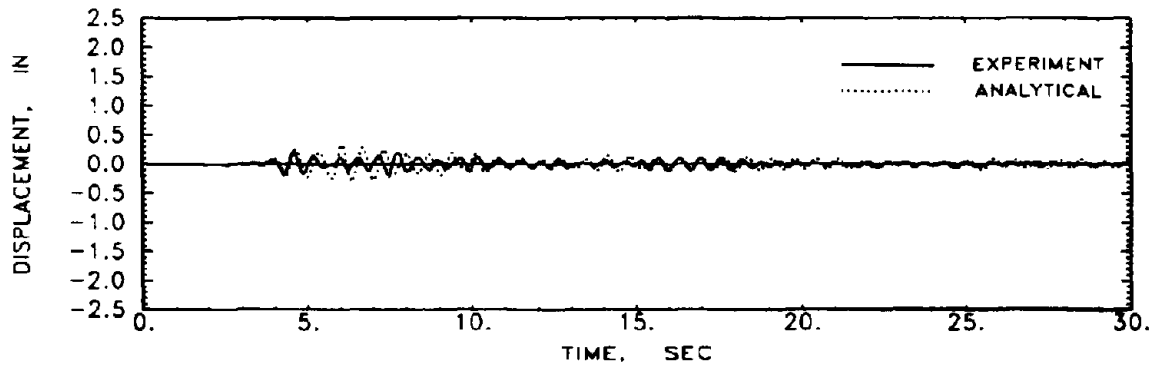
[C] Approximately 50% greater than suggested by Paulay and Priestley (1992).

[D] Based on subassembly tests by Aycardi et al. (1992).

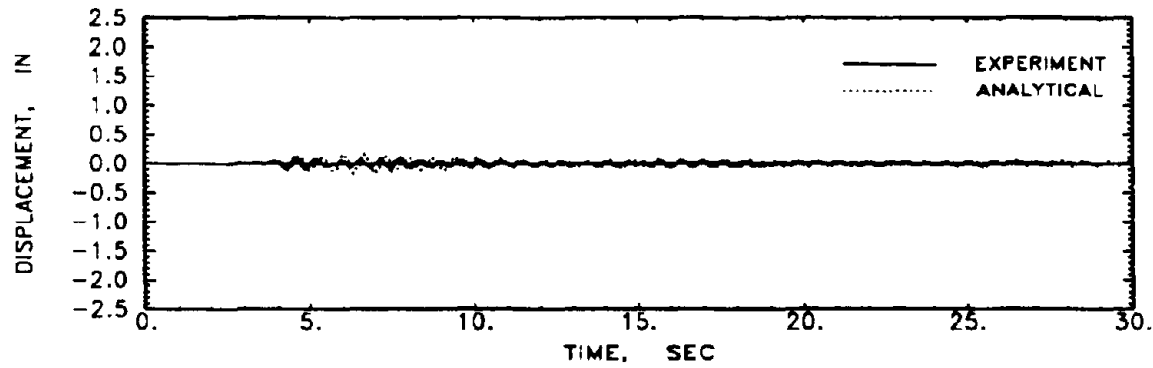
[E] Refer to Fig. 3-1 for notation.



(a) Third Story

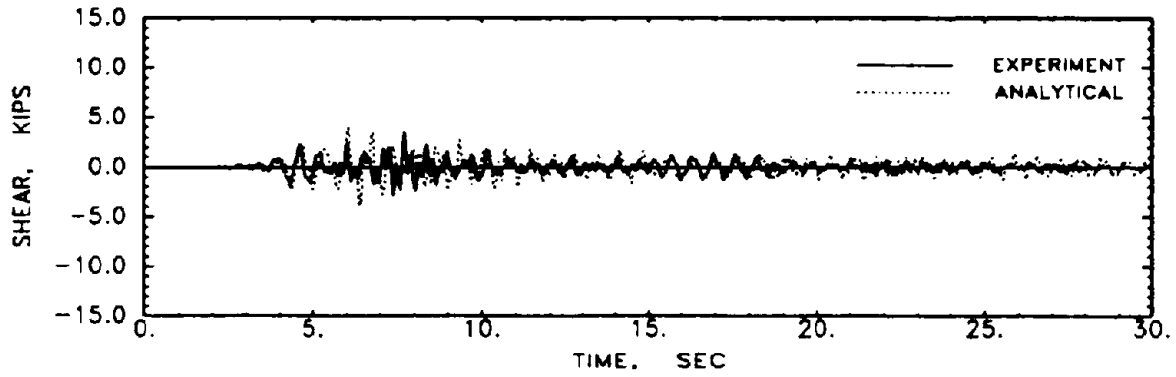


(b) Second Story

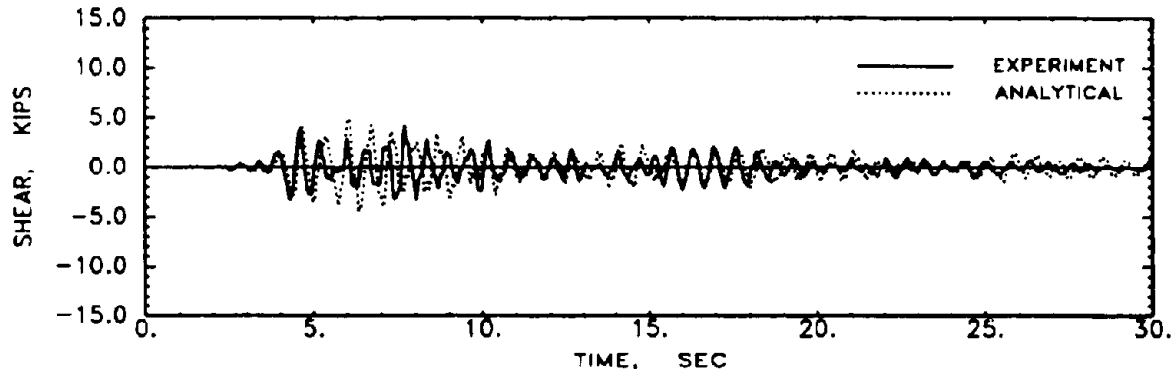


(c) First Story

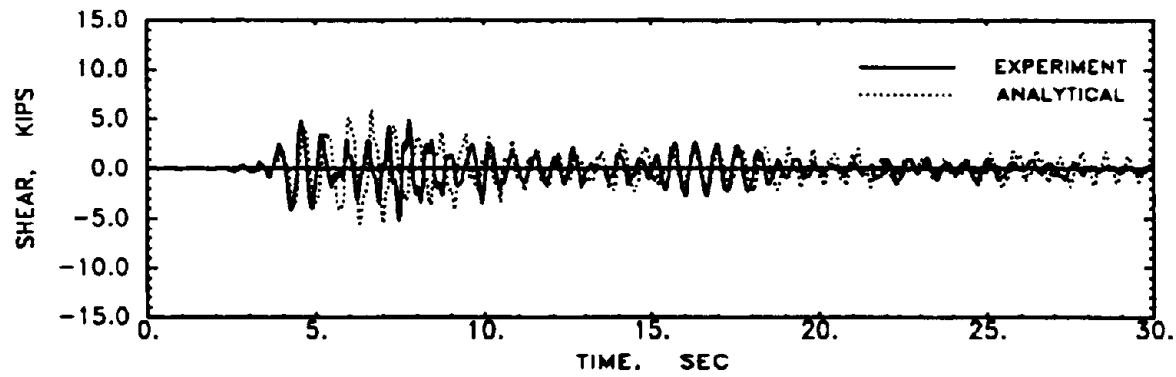
FIG. 3-2a Displacement Comparisons for Minor Shaking - Engineering Approximations



(a) Third Story

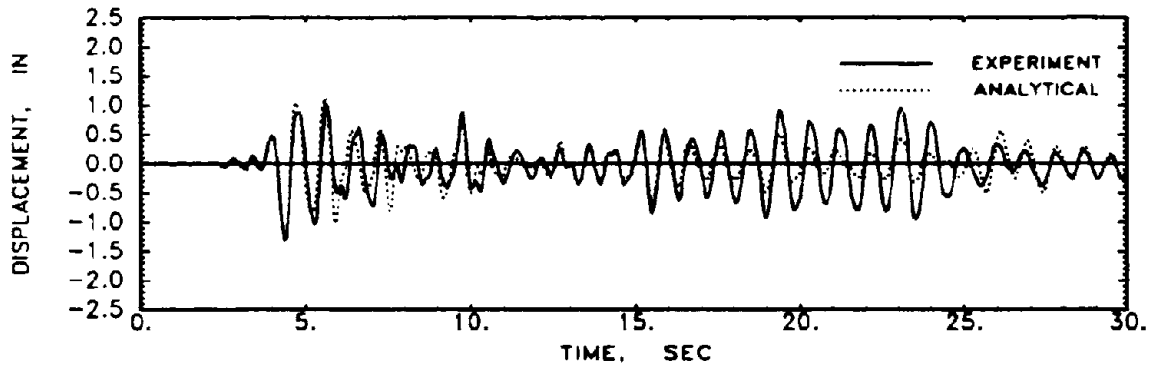


(b) Second Story

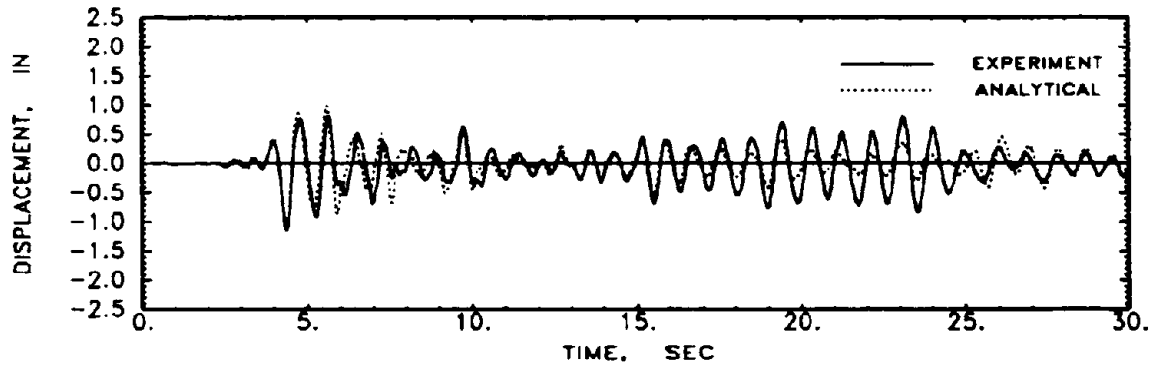


(c) First Story

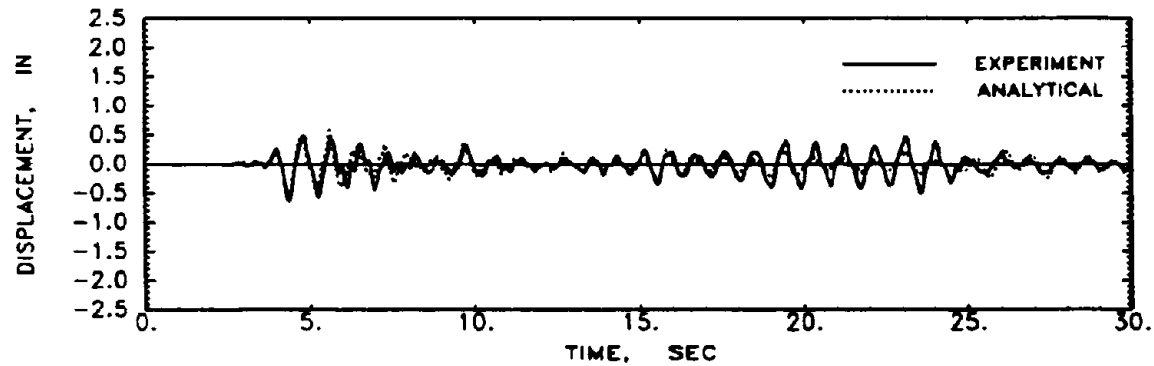
FIG. 3-2b Shear Force Comparisons for Minor Shaking - Engineering Approximations



(a) Third Story

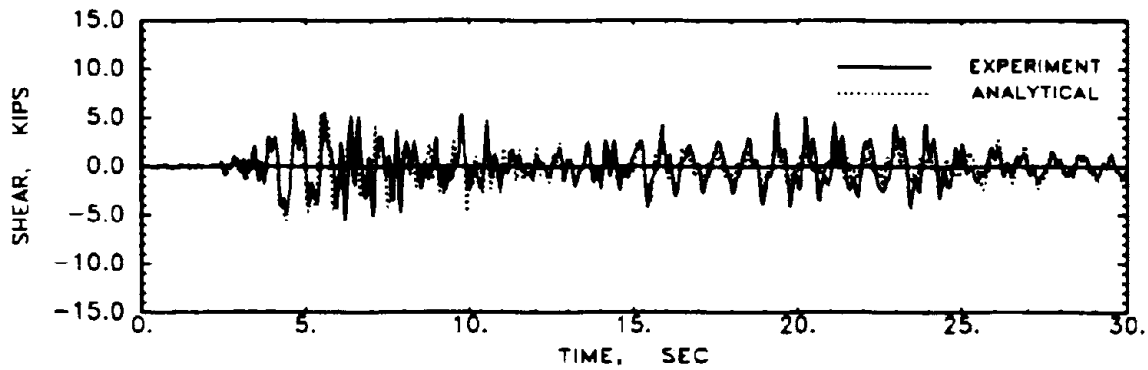


(b) Second Story

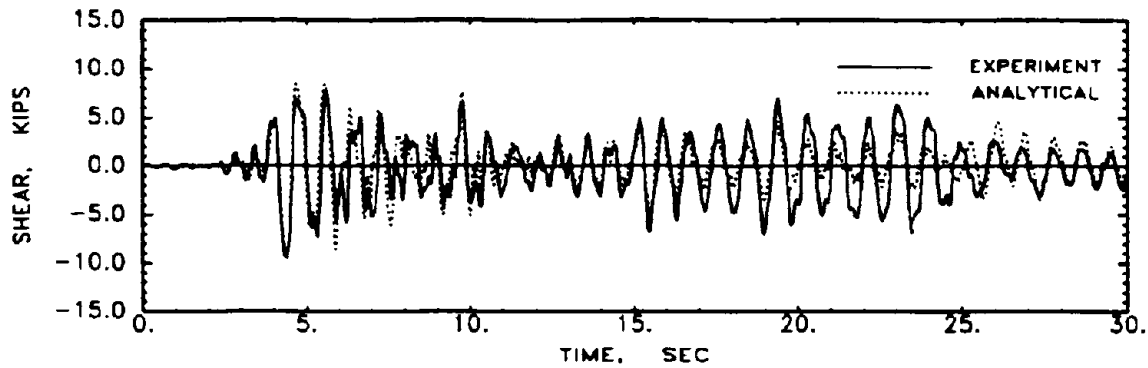


(c) First Story

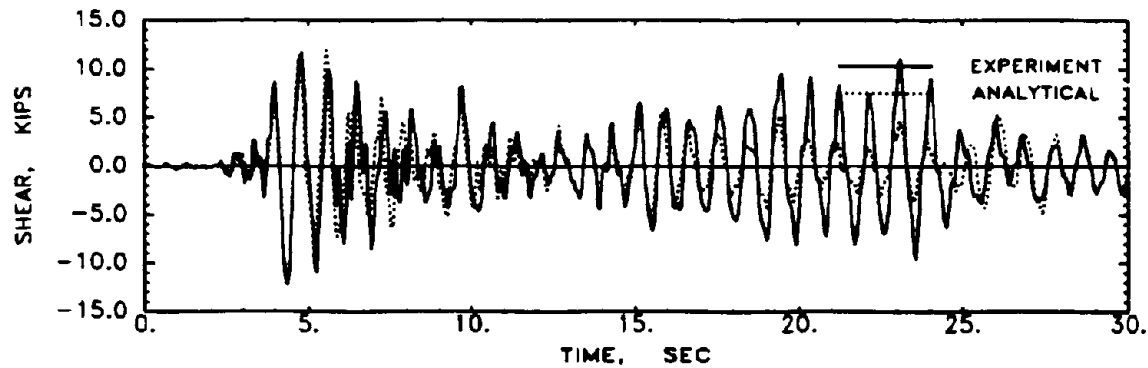
FIG. 3-3a Displacement Comparisons for Moderate Shaking - Engineering Approximations



(a) Third Story

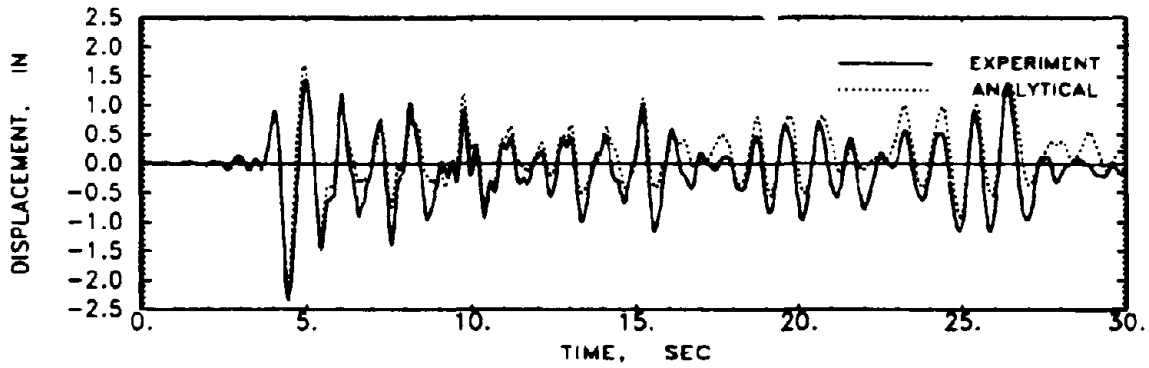


(b) Second Story

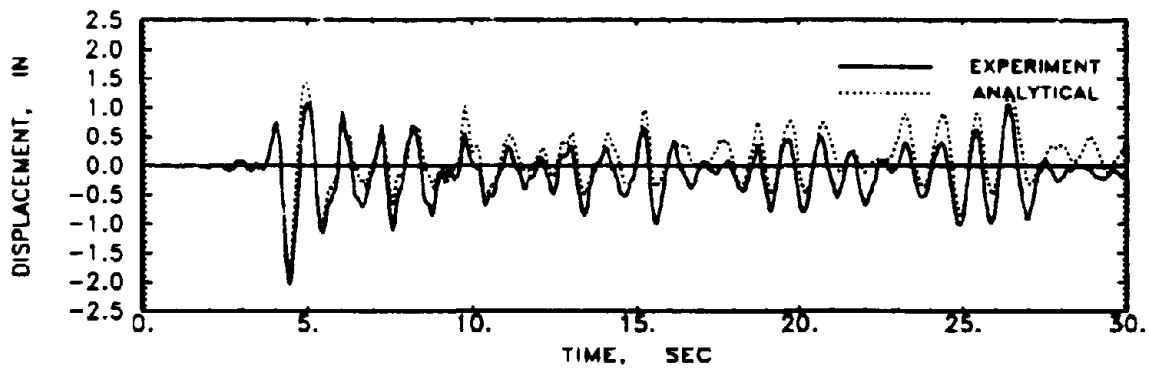


(c) First Story

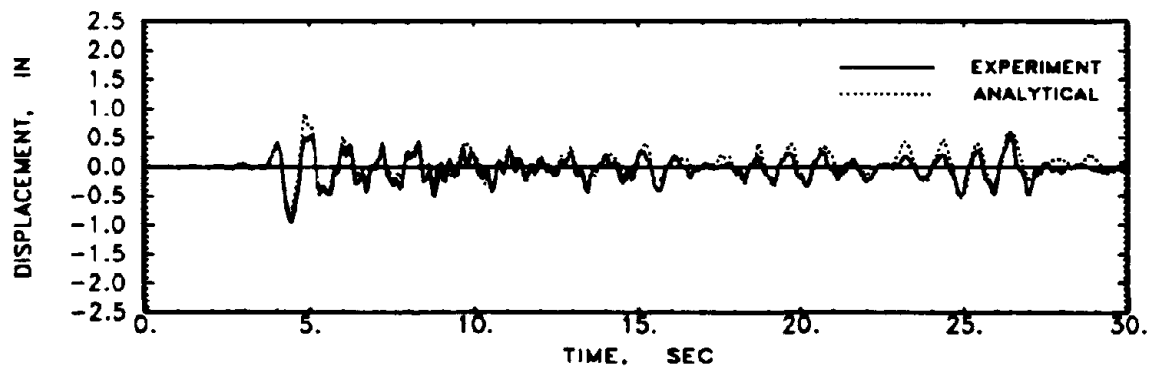
FIG. 3-3b Shear Force Comparisons for Moderate Shaking - Engineering Approximations



(a) Third Story

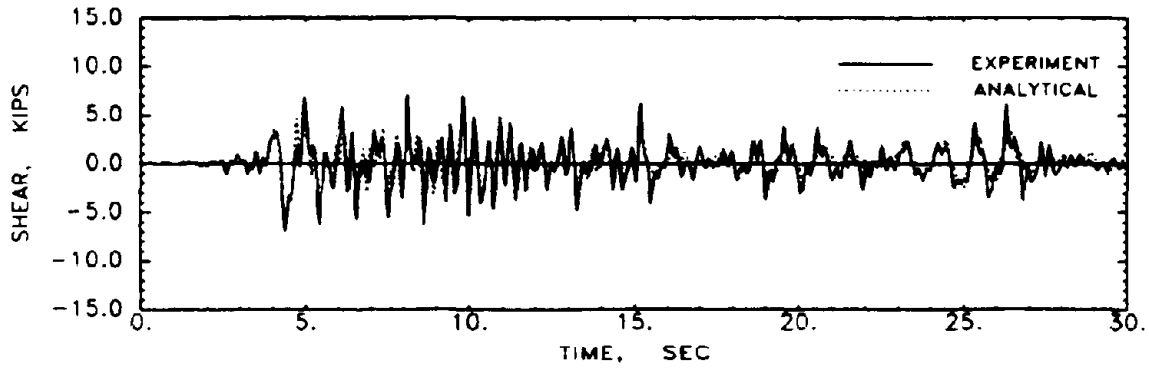


(b) Second Story

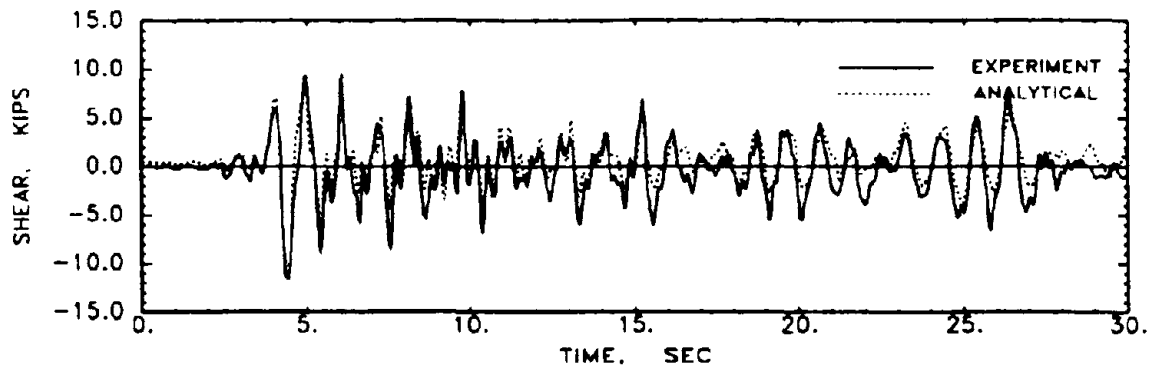


(c) First Story

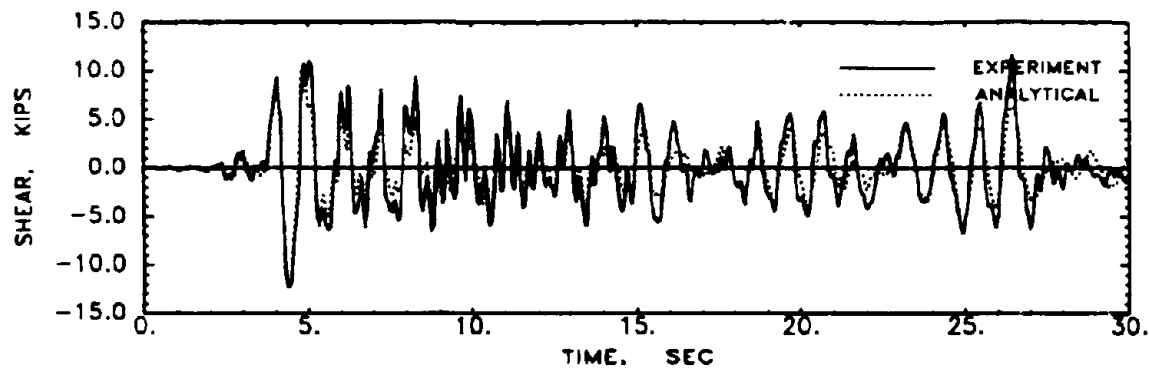
FIG. 3-4a Displacement Comparisons for Severe Shaking - Engineering Approximations



(a) Third Story

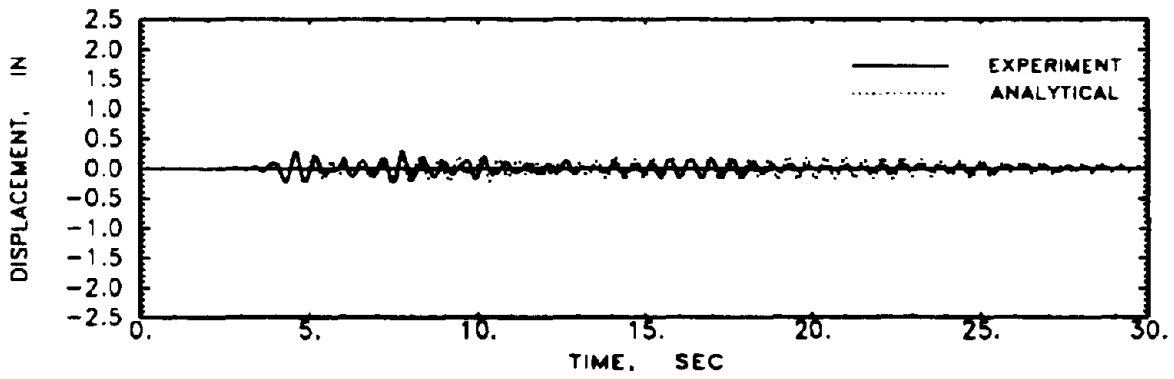


(b) Second Story

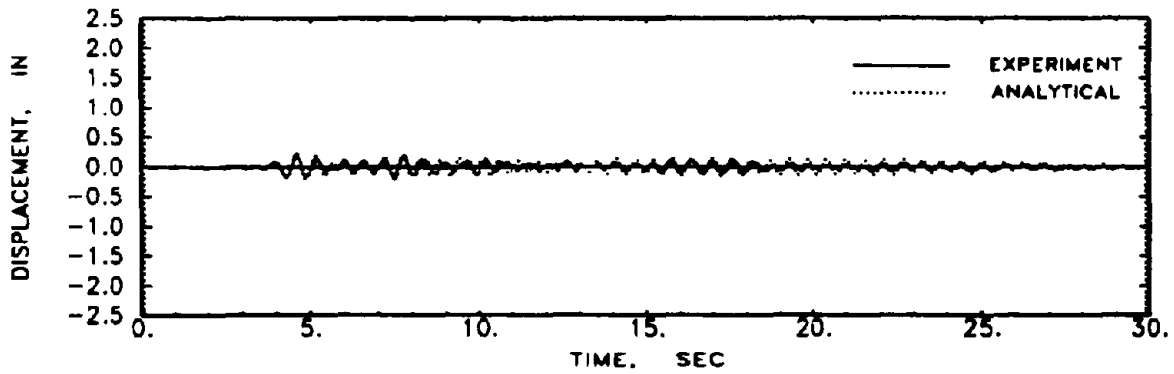


(c) First Story

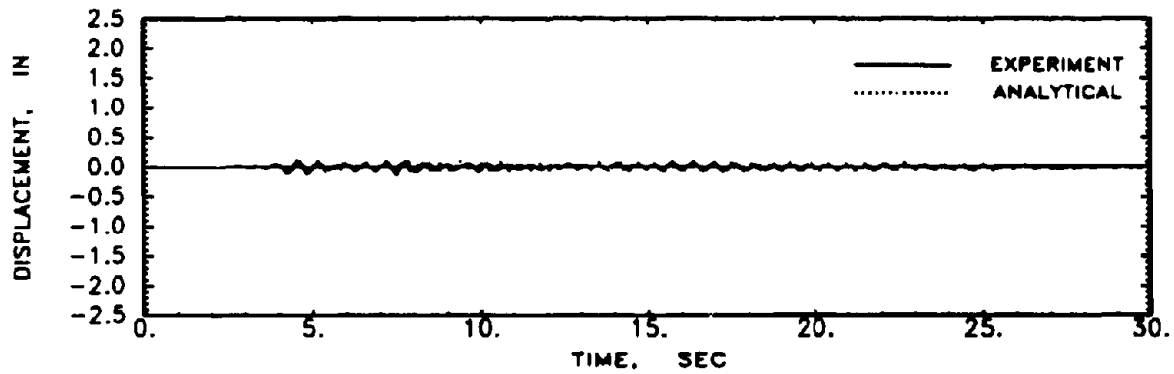
FIG. 3-4b Shear Force Comparisons for Severe Shaking - Engineering Approximations



(a) Third Story

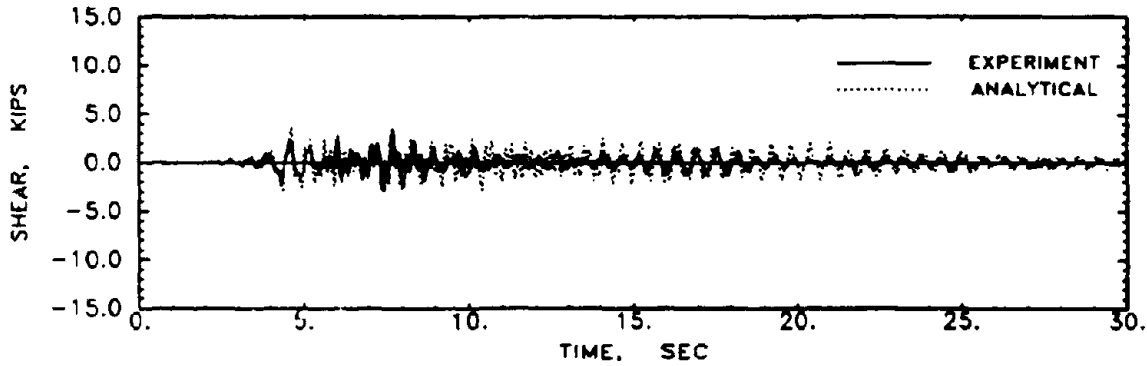


(b) Second Story

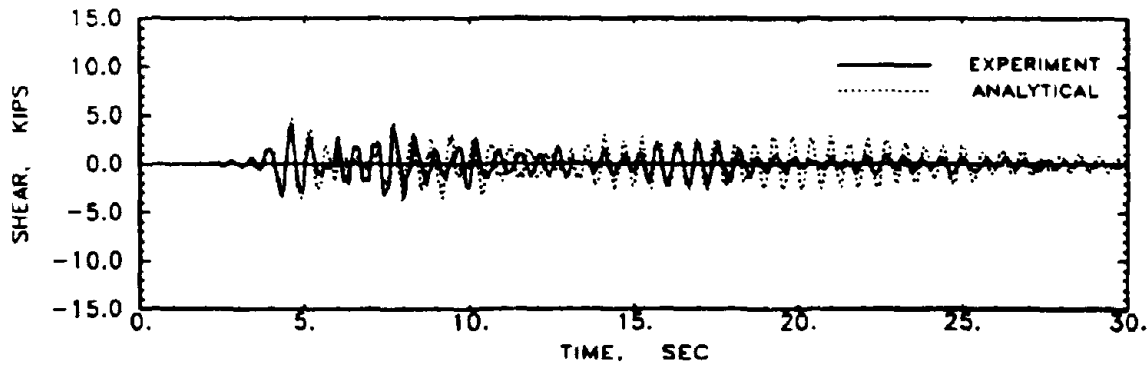


(c) First Story

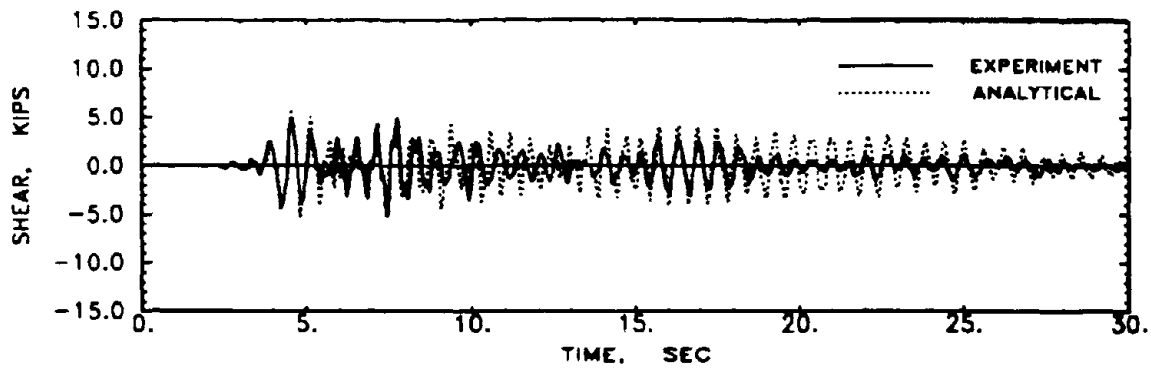
FIG. 3-5a Displacement Comparisons for Minor Shaking - Component Tests



(a) Third Story

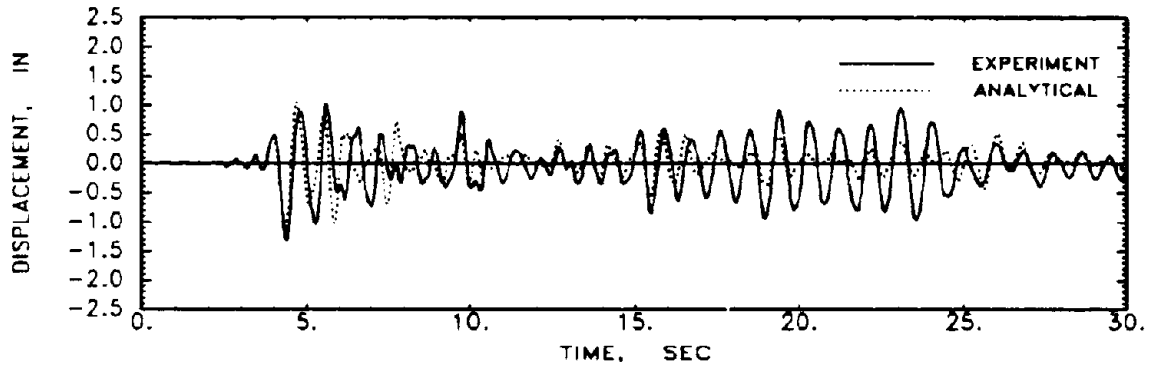


(b) Second Story

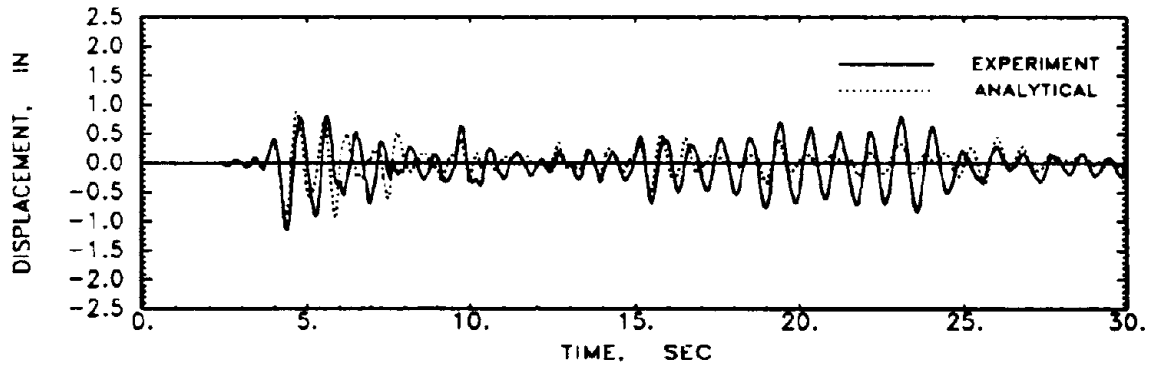


(c) First Story

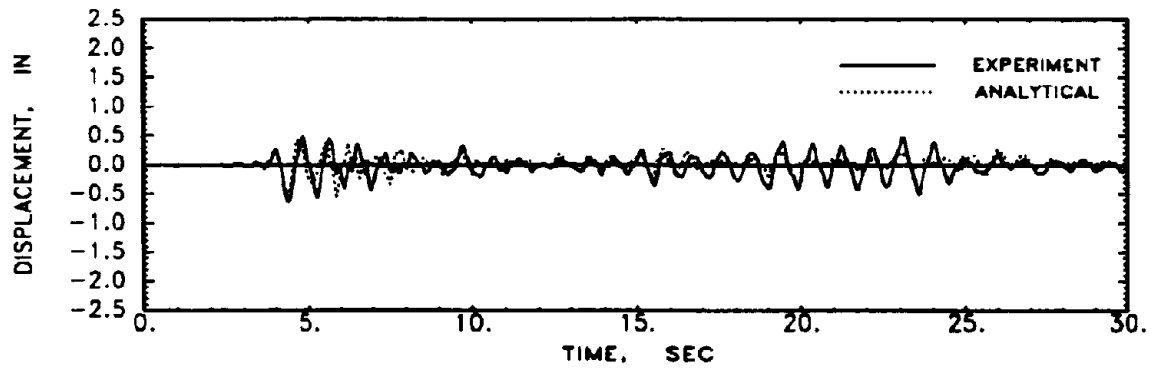
FIG. 3-5b Shear Force Comparisons for Minor Shaking - Component Tests



(a) Third Story

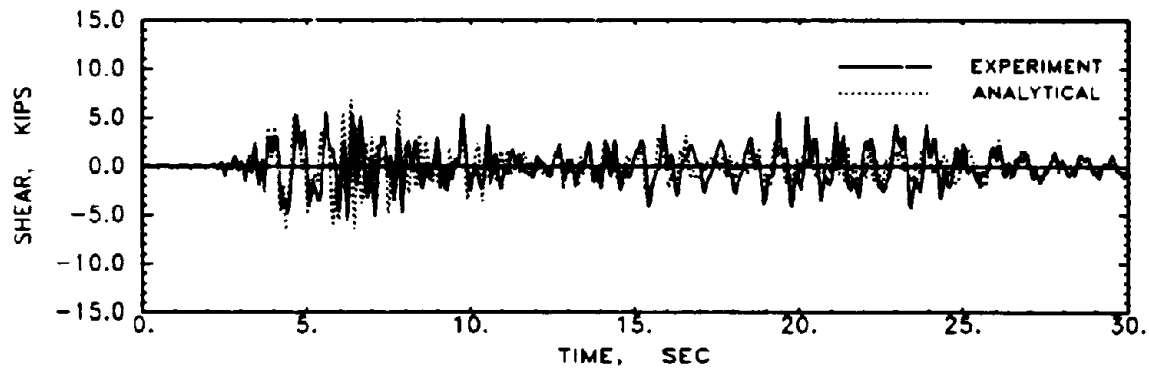


(b) Second Story

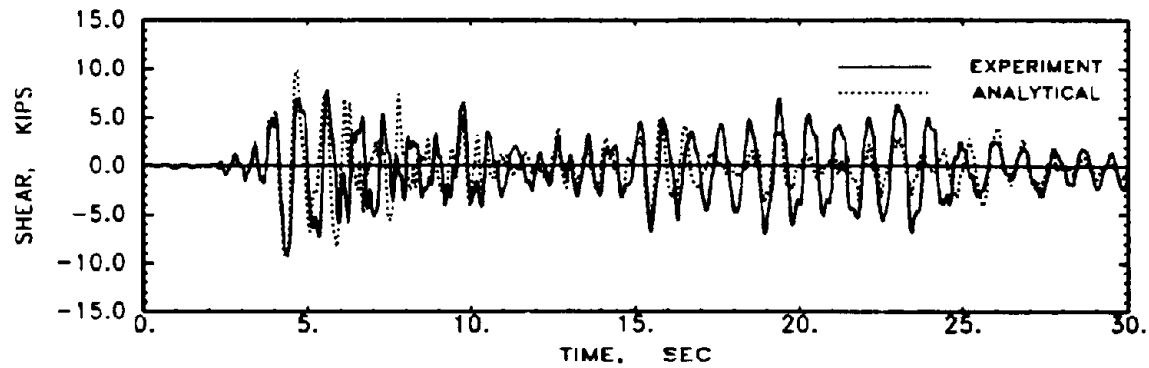


(c) First Story

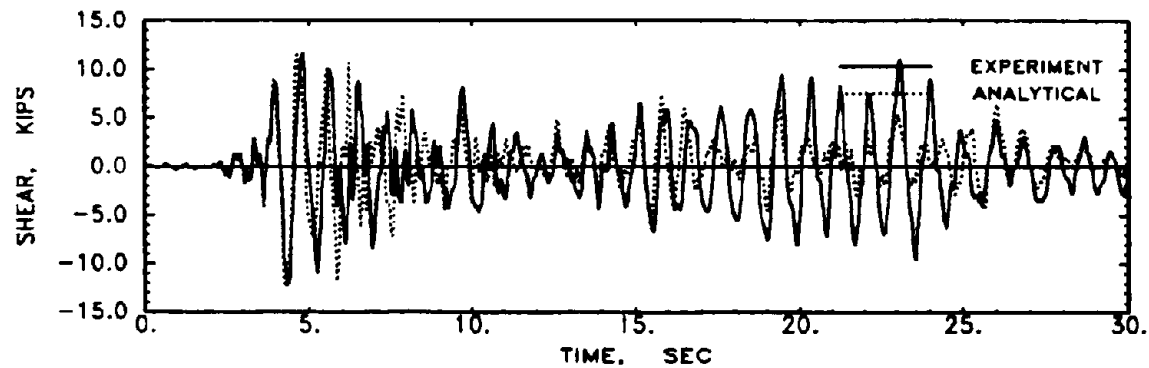
FIG. 3-6a Displacement Comparisons for Moderate Shaking - Component Tests



(a) Third Story

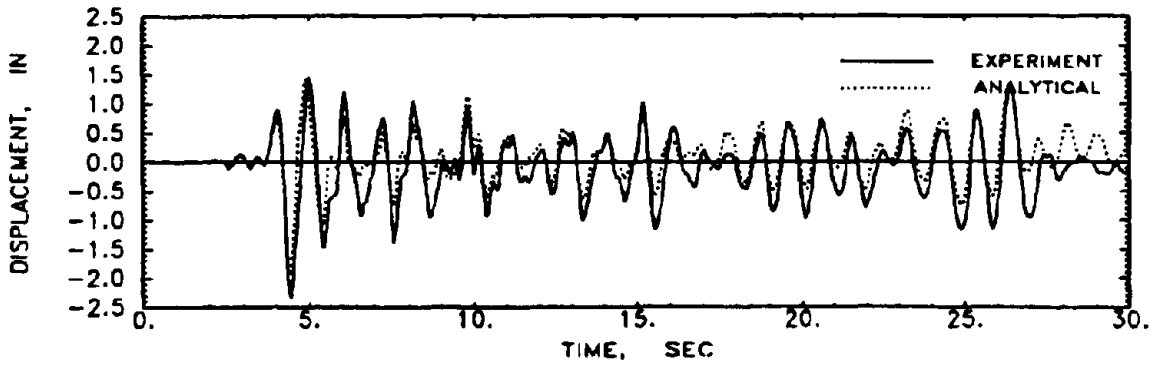


(b) Second Story

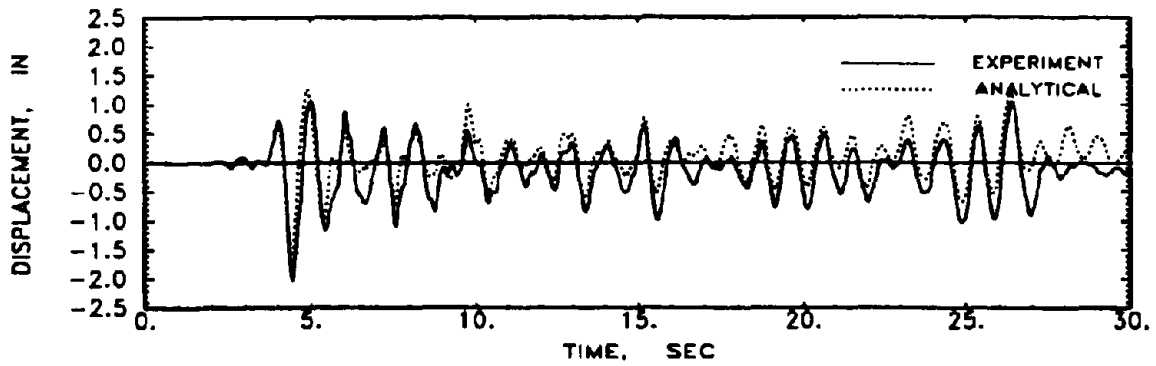


(c) First Story

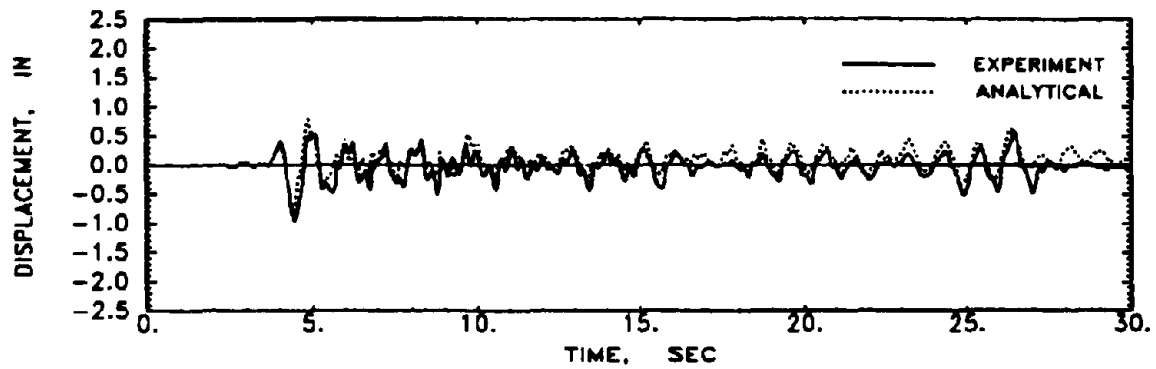
FIG. 3-6b Shear Force Comparisons for Moderate Shaking - Component Tests



(a) Third Story

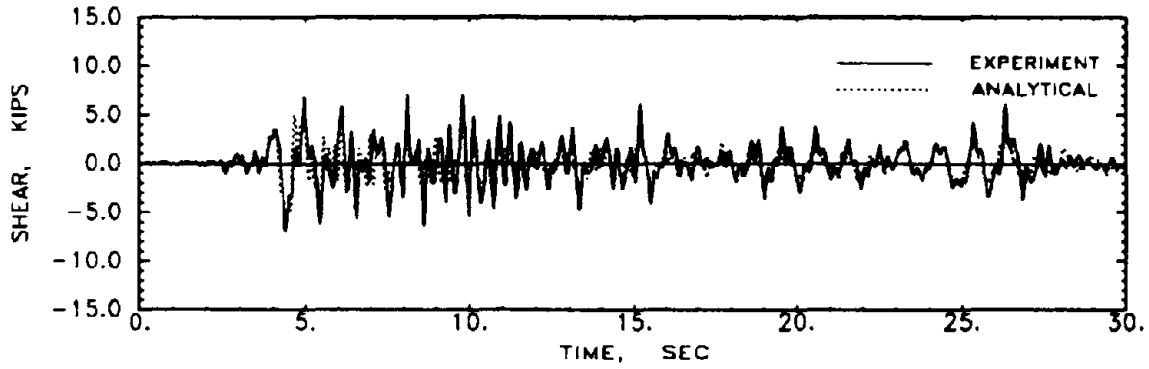


(b) Second Story

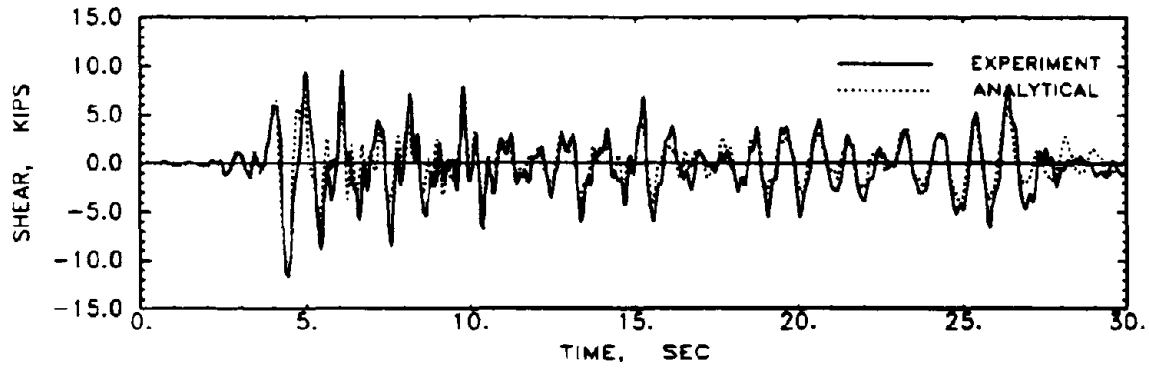


(c) First Story

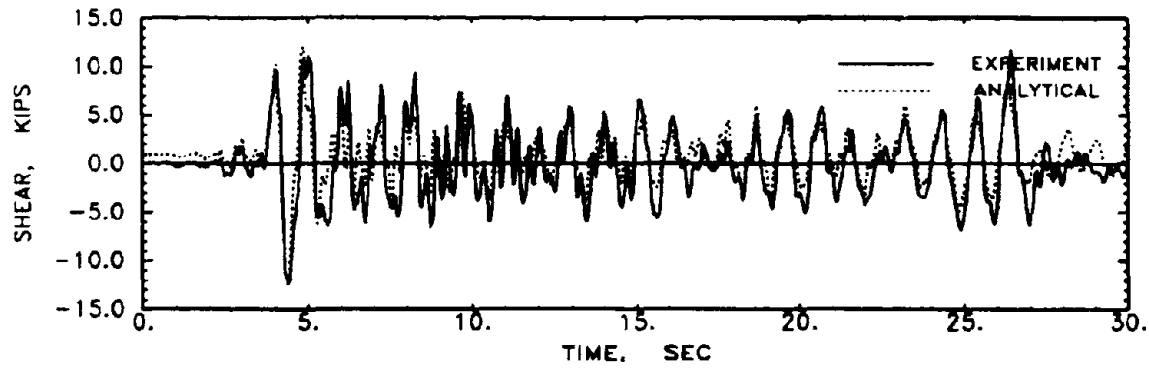
FIG. 3-7a Displacement Comparisons for Severe Shaking - Component Tests



(a) Third Story

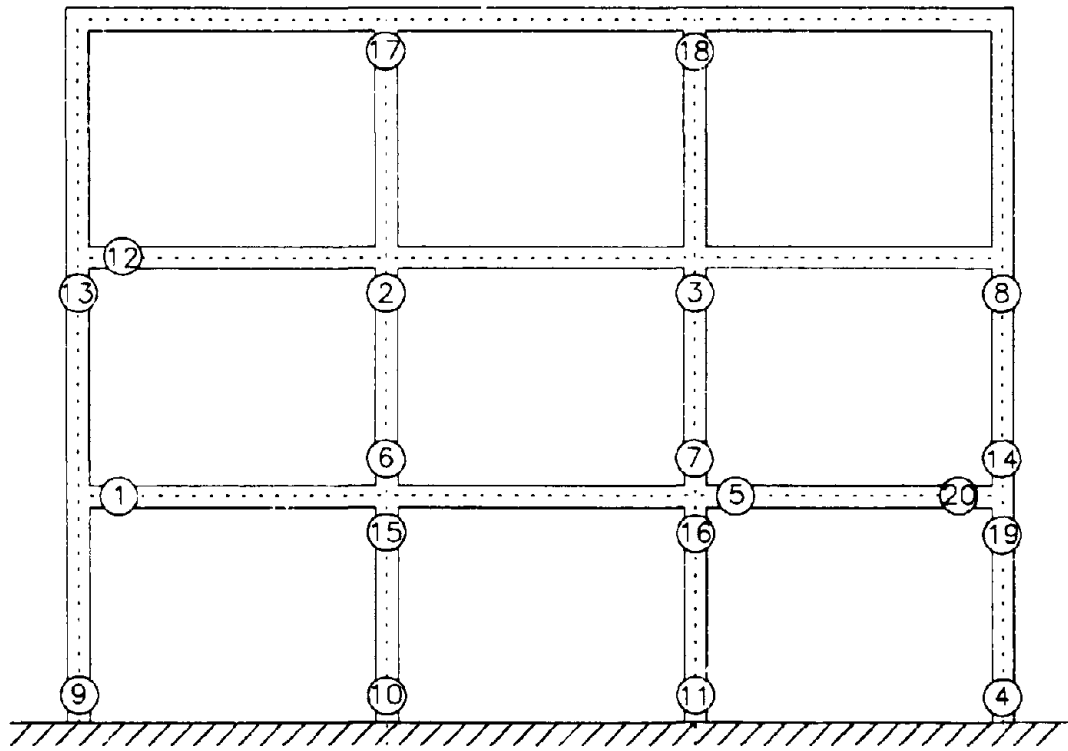


(b) Second Story



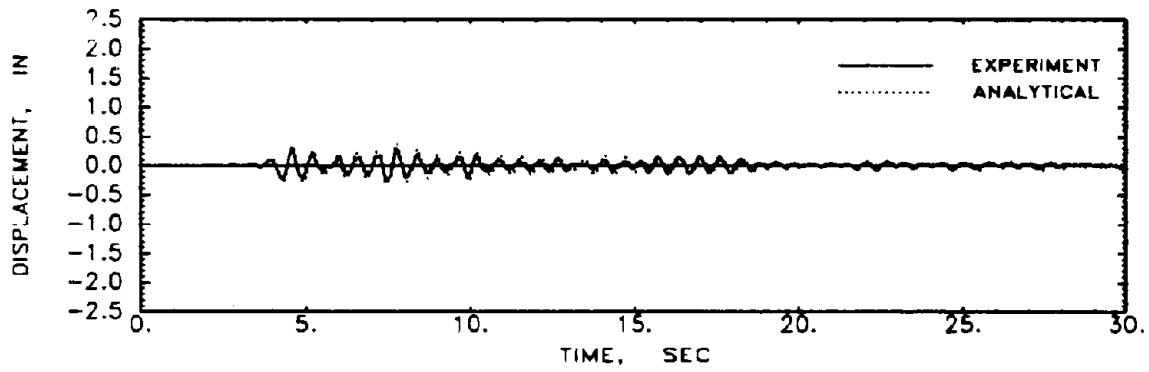
(c) First Story

FIG. 3-7b Shear Force Comparisons for Severe Shaking - Component Tests

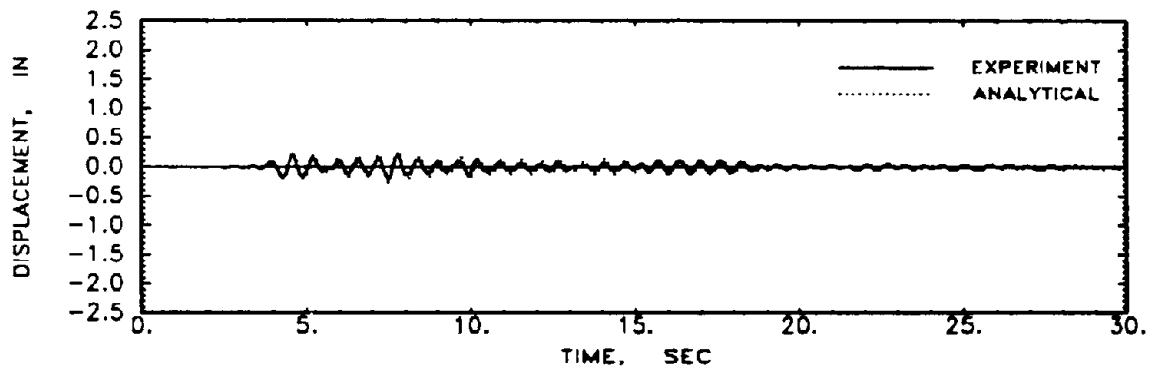


- Signifies sequence of yielding

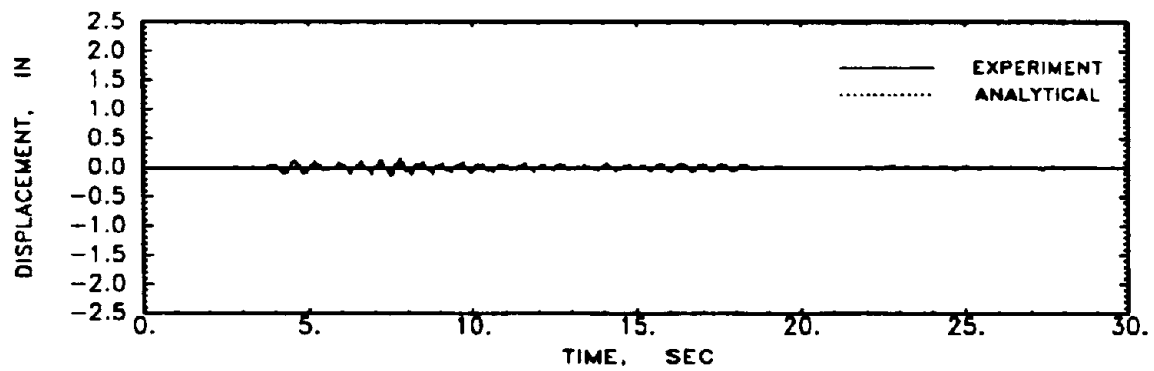
FIG. 3-8 Collapse Mode (Shakedown) Analysis



(a) Third Story

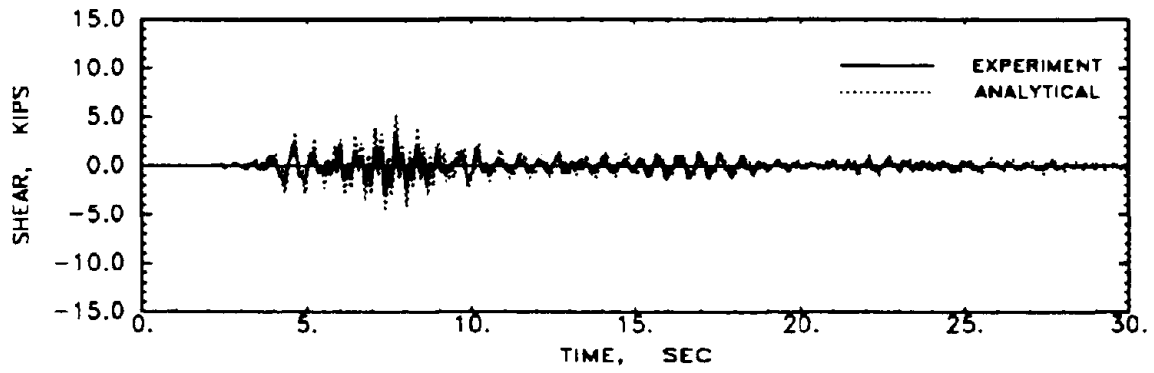


(b) Second Story

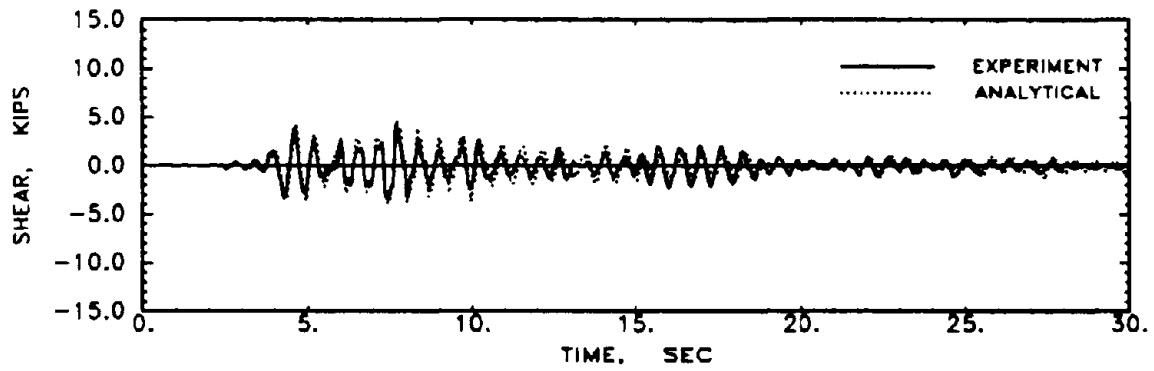


(c) First Story

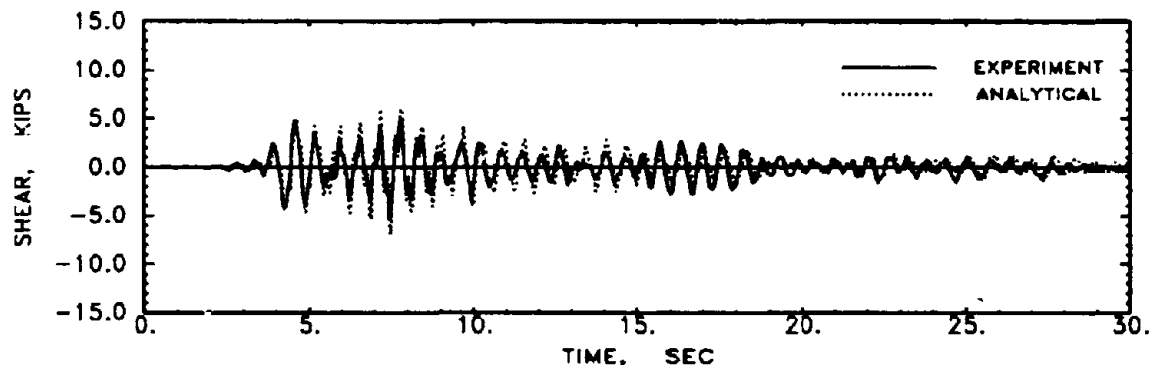
FIG. 3-9a Displacement Comparisons for Minor Shaking - Analytical Fit



(a) Third Story

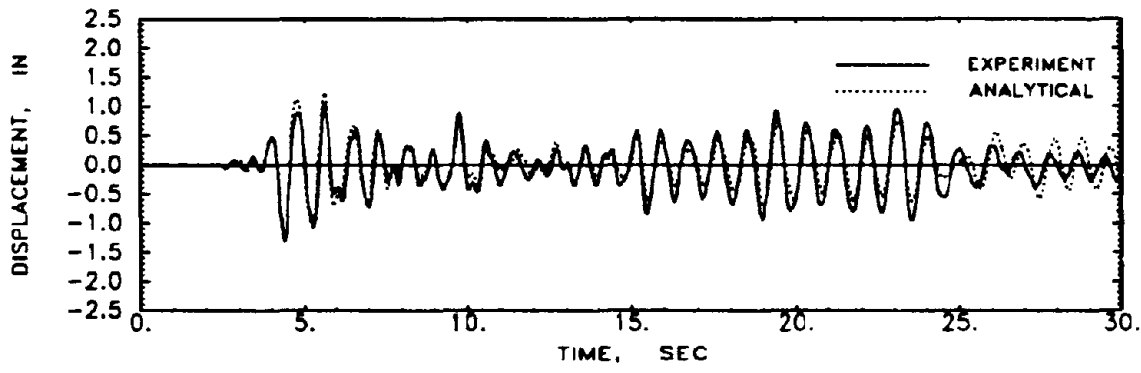


(b) Second Story

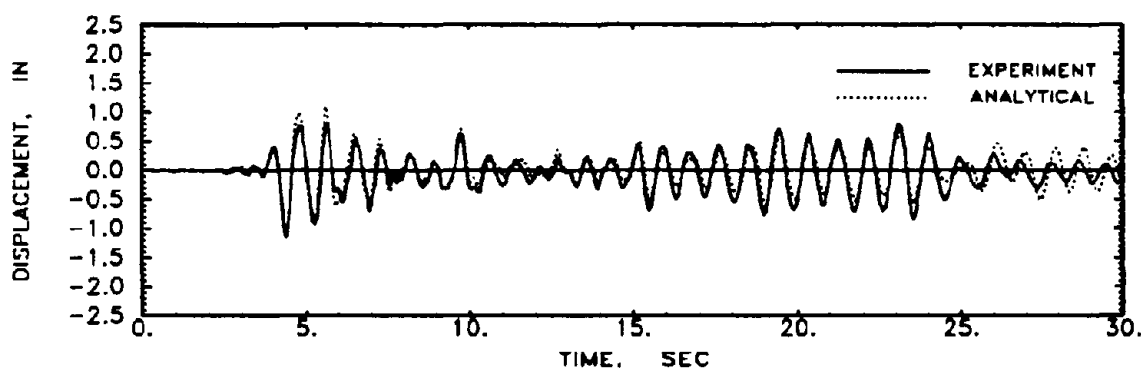


(c) First Story

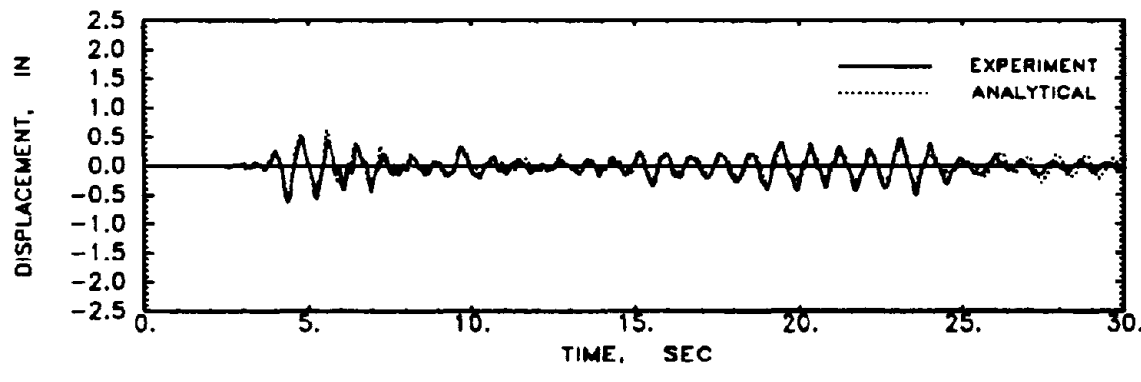
FIG. 3-9b Shear Force Comparisons for Minor Shaking - Analytical Fit



(a) Third Story

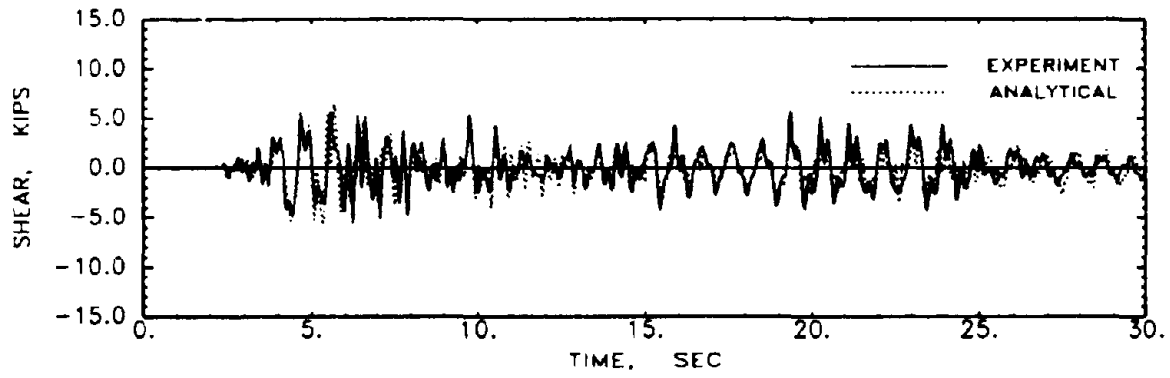


(b) Second Story

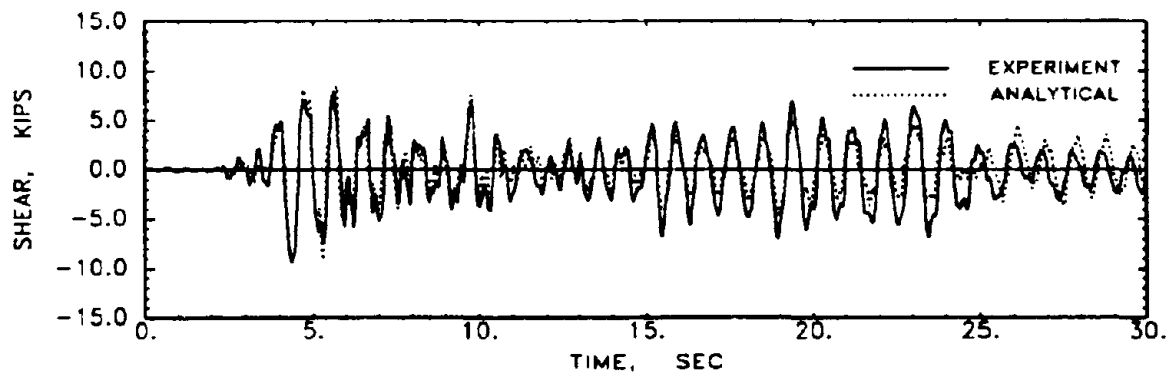


(c) First Story

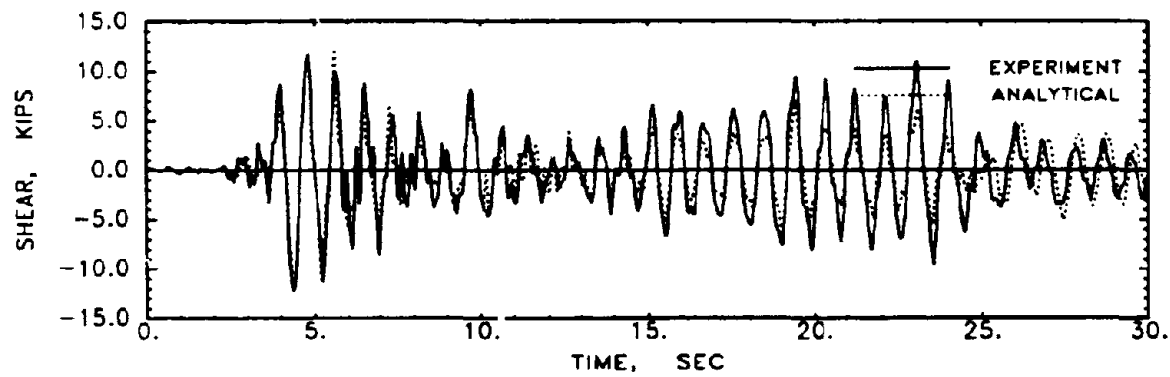
FIG. 3-10a Displacement Comparisons for Moderate Shaking - Analytical Fit



(a) Third Story

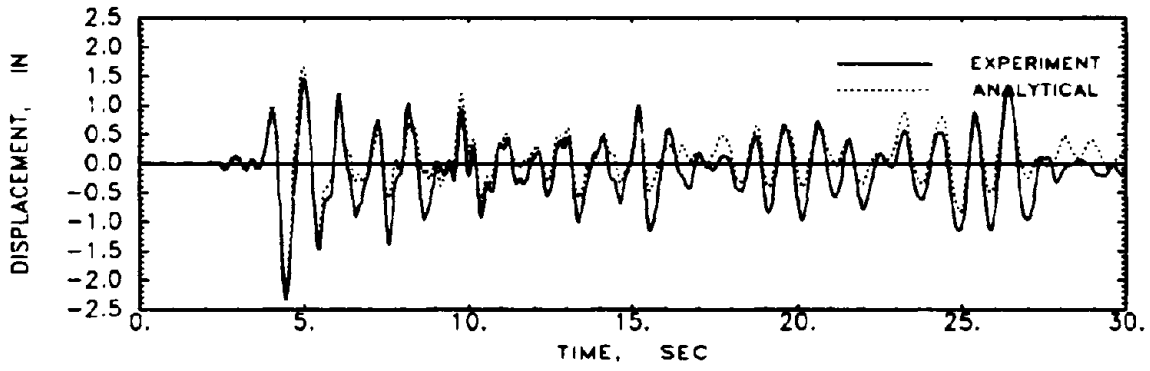


(b) Second Story

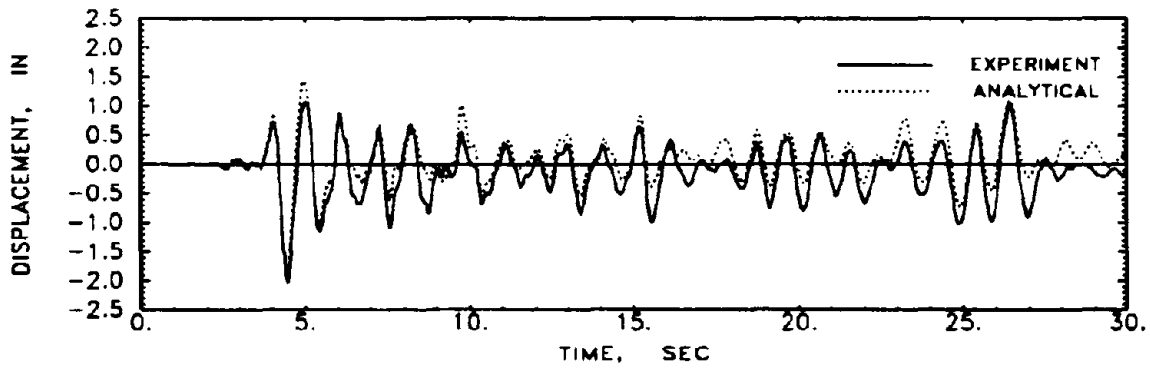


(c) First Story

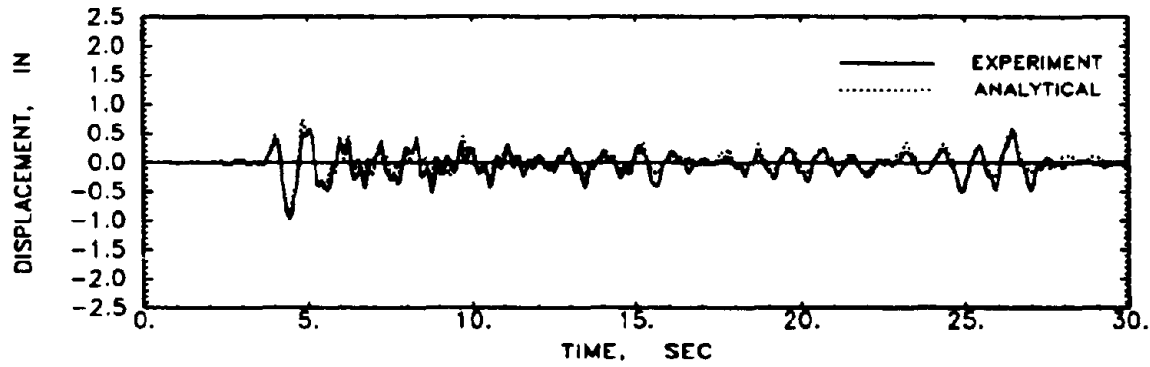
FIG. 3-10b Shear Force Comparisons for Moderate Shaking - Analytical Fit



(a) Third Story

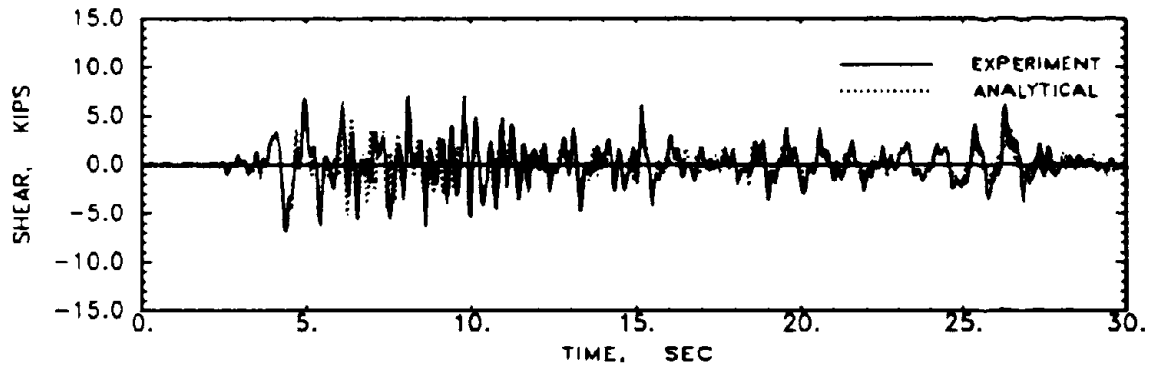


(b) Second Story

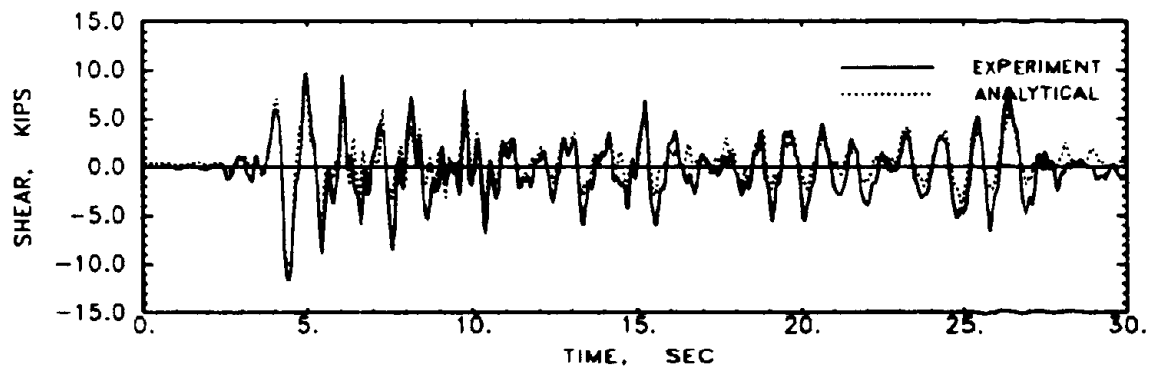


(c) First Story

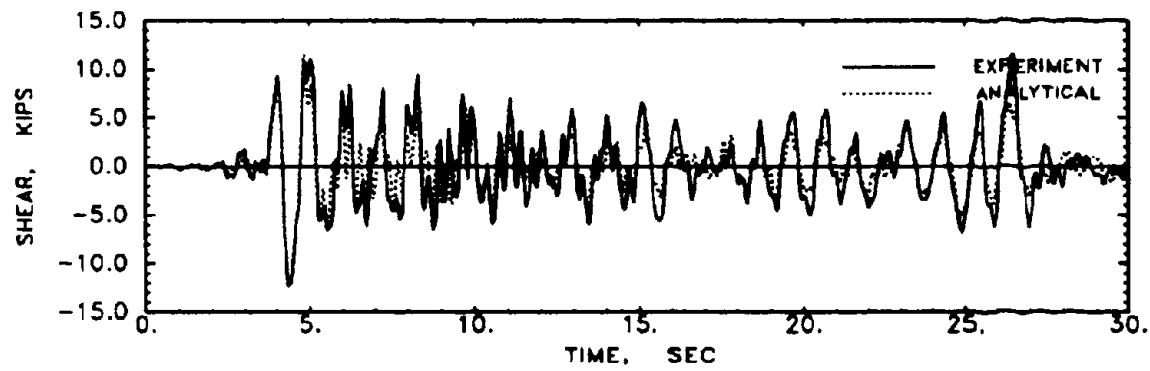
FIG. 3-11a Displacement Comparisons for Severe Shaking - Analytical Fit



(a) Third Story

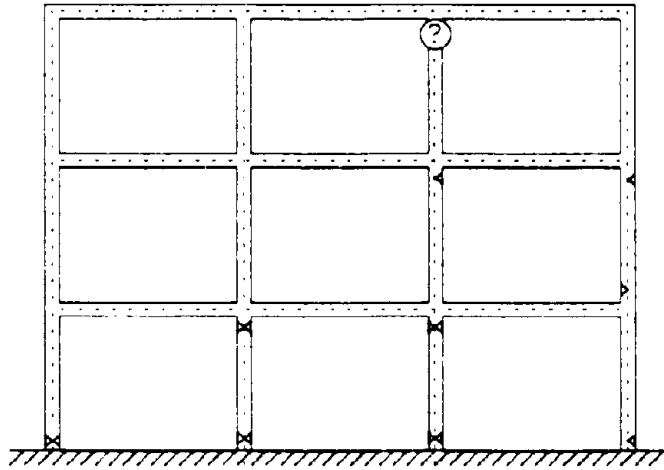


(b) Second Story

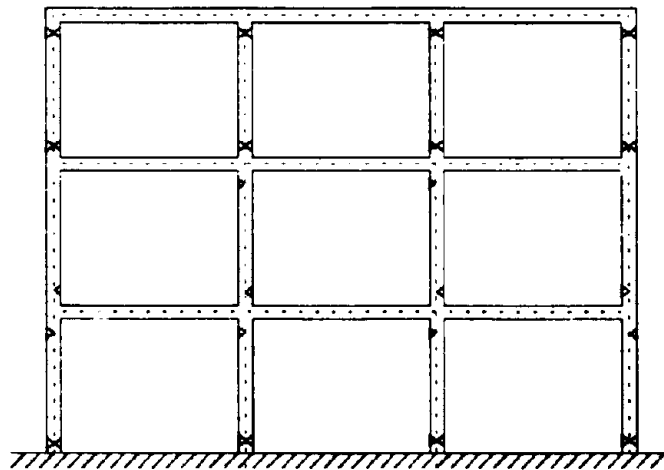


(c) First Story

FIG. 3-11b Shear Force Comparisons for Severe Shaking - Analytical Fit



(a) Experimental

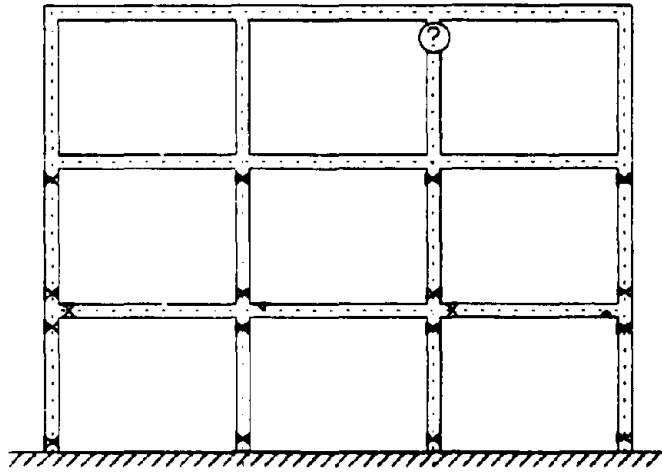


(b) Analytical

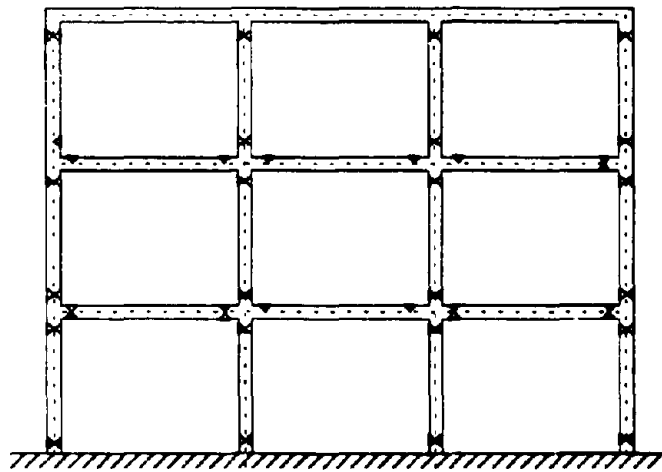
▷ Cracked
▶ Yielded

? NOTE: 2nd story beams and above were not quantitatively observed

FIG. 3-12a Comparison of Damage State after Minor Shaking



(a) Experimental

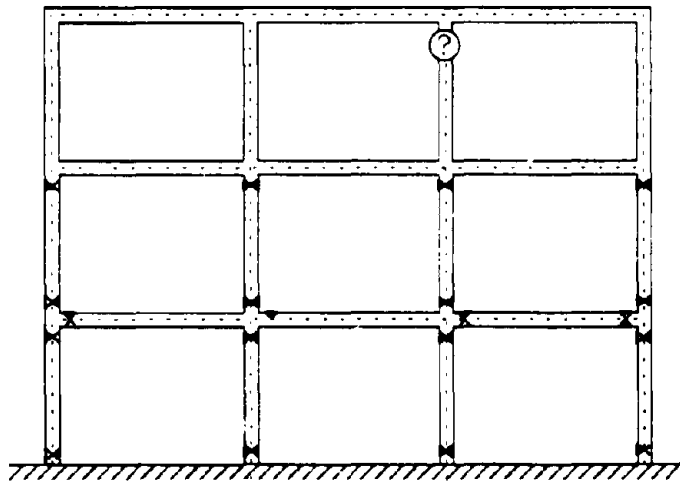


(b) Analytical

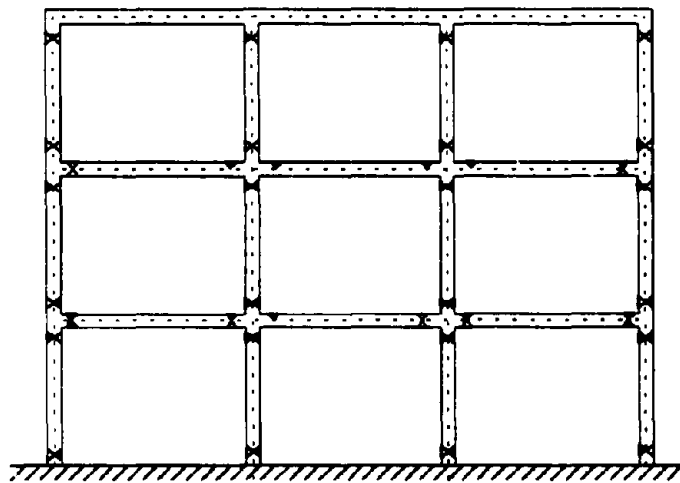
▷ Cracked
▶ Yielded

? NOTE: 2nd story beams and above were not quantitatively observed

FIG. 3-12b Comparison of Damage State after Moderate Shaking



(a) Experimental



(b) Analytical

▷ Cracked
▶ Yielded

? NOTE: 2nd story beams and above were not quantitatively observed

FIG. 3-12c Comparison of Damage States after Severe Shaking

3.3 Damage Quantification

The response results and observed damage states of the model after the shaking table tests were presented in previous sections. However, the extent of damage and reserve member strengths were not identified. To quantify the observed damage and the reserve margins before collapse of each member of the model, it was necessary to use some specific model of damage. The quantification obtained using such model would thereby permit an assessment of structural integrity in terms of damage states, such as *serviceability*, *repairability*, *irrepairability*, or *collapse*.

The amount of damage to the individual members, story levels, and overall structure from seismic excitations can be described analytically in terms of damage indicators defined as *damage indices*. These damage indices are used to evaluate the extent of damage on a scale representing minor, moderate, or severe damage. The damage potential or reserve strength of members can also be determined. Normally, the damage index of a member is defined to vary between 0.0 and 1.0, with the later implying failure. Many damage index models and modified models have been developed to incorporate effects of ductility demand and low cycle fatigue or strength deterioration: Park et al. (1985); Chung et al. (1987); Powell et al. (1988); and Bracci et al. (1989). It has been shown that the combination of deformation and strength deterioration damages provide an accurate assessment of the member damage and reserve capacity.

According to the original Park model (1985), a member damage index, DI, is defined as follows:

$$DI = \frac{\delta_m}{\delta_u} + \frac{\beta \int dE}{\delta_u P_y} \quad (3.3)$$

where δ_m = maximum observed deformation
 δ_u = ultimate deformation
 β = strength deterioration factor
 $\int dE$ = absorbed hysteretic energy
 P_y = yield force

Since IDARC computes the moments and curvatures at a section, a modified Park's Model was developed to use moment - curvature relations (instead of force - displacement relations) so that a damage index can be easily computed at each time step of the analysis as follows:

$$DI = \frac{\phi_m}{\phi_u} + \frac{\beta \int dE}{\phi_u M_y} \quad (3.4)$$

where ϕ_m = maximum observed curvature
 ϕ_u = ultimate curvature
 β = strength deterioration factor
 $\int dE$ = absorbed hysteretic energy
 M_y = yield moment

A procedure for determining the ultimate curvature in both columns and beams was proposed by Bracci et al. (1989) and was used for all analyses in this study.

With the damage index formulated to vary between 0.0 and 1.0, the damage states for members are defined below (see Bracci et al., 1989):

$DI = 1.00$	<i>Collapse</i>	(3.5)
$0.66 \leq DI < 1.00$	<i>Severe - "Irreparable" Damage</i>	
$0.33 \leq DI < 0.66$	<i>Moderate - "Repairable" Damage</i>	
$0.00 < DI < 0.33$	<i>Minor - "Serviceable" Damage</i>	

Story level damage indices are computed from the corresponding damage indices of the story components and separated into beam-slab (horizontal) and column-wall (vertical) damages. To combine damage indices, the component damage indices were themselves used as weighting factors. The overall structural damage index, $DI_{structure}$, is computed as a combination of the story damage indices in which a weighting factor is applied based on the amount of gravity load supported by that story. Therefore, the lower stories will have a greater weighting factor than

the upper stories and therefore would be more important. The overall damage index was recalibrated with respect to observed structural damage in several R/C buildings, Park et al. (1985), such that damage states were defined as shown below:

$$\begin{array}{ll}
 DI_{\text{structure}} = 1.00 & \text{Collapse} \\
 0.40 \leq DI_{\text{structure}} < 1.00 & \text{Moderate/Severe Damage} \\
 DI_{\text{structure}} < 0.40 & \text{Minor/Moderate Damage}
 \end{array} \tag{3.6}$$

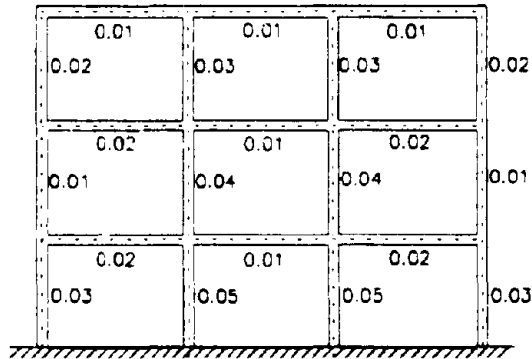
However, it should be noted that the overall structural damage index is not sufficient by itself to describe the extent of damage to a building. An example would be if an interior column in a building had failed ($DI = 1.00$). This column failure would probably initiate progressive collapse of the building. However, the overall structural damage index would not necessarily be 1.00 after combining the damage indices of all the structural elements ($DI_{\text{structure}} < 1.00$). Therefore, it is suggested that experimentally observed results in connection with Eq. (3.4) for the individual members, story levels, and the overall damage index be used to properly evaluate the induced damage to a structure.

Fig. 3-13 shows the quantified member damages in the model building computed from the modified Park's model in IDARC for the minor, moderate, and severe shaking from the experimental fit response results. It can be observed that small member damage indices (*minor* - "serviceable" damage) develop from the minor shaking (0.05 g), which is expected since the model is primarily governed by elastic deformations. However, for the moderate shaking (0.20 g), the damage indices in the first and second story interior columns reach values of 0.36 and 0.25, respectively. Therefore, according to Eq. (3.5), damage to the first story columns slightly extends to the *moderate* - "repairable" damage state while the second story columns remain within the *minor* - "serviceable" damage state. It can be observed from the story level damage indices that most of the resulting damage occurs in the columns. The overall structural damage index is 0.23, which implies a *minor/moderate* damage state according to Eq. (3.6). The only significant damage to the beams is the first story exterior beams with bottom reinforcement pulling out ($DI = 0.18$). Refer to Fig. 3-12b and Section 2 which describe the yielding that was observed in the bottom reinforcement for this beam section.

For the severe shaking (0.30 g), *severe* damage results to the interior columns of the first and second stories, damage indices of 0.72 and 0.67. It can be observed that there is little reserve strength remaining in these members. The damage indices of the exterior columns in these stories reach the *moderate* - "*repairable*" damage state. This correlates with the observed experimental response in Section 2 where large inter-story drifts, shear forces, and hysteretic energy occur on the first and second stories. Also, the column moment-axial load interaction diagrams of the first and second stories extend to the projected dynamic ultimate surface (see Fig. 2-27). The damage indices of the first and second story exterior beams are 0.49 and 0.05, respectively. For the first story beams, correlation exists since yielding is observed analytically and experimentally (Fig. 3-12c). However recall from the visual description of damage in Section 2 that large flexural cracks appeared in the exterior second story beams. This is not captured in the damage index analysis. The overall structural damage index obtained in analysis is 0.49, which implies *moderate/severe* damage as observed in the tests.

It is also interesting to compare the damage indices computed from the experimentally measured response with the damage indices obtained from the analytical simulations (shown in Fig. 3-13). For this evaluation, the damage index for a critical interior first story column was computed based on the experimental force-displacement response from the minor, moderate, and severe shaking. The ultimate story displacement was considered as 3% of the story height based on the component tests presented in part II of Evaluation series (Aycardi et al. 1992), where a decrease in strength had occurred. However this might be somewhat conservative estimate, since some resistance still exists at larger drifts. El-Attar et al. (1991) observed severe damage at a recorded first story drift of 2.63% for the Taft S69E motion with a PGA of 0.35 g. The yield force was determined from a static analysis with the analytical model of the experimental response fit (shown in Fig. 3-16). Damage indices of 0.01, 0.33, and 0.64 were calculated from the experimental response and compare with analytically determined damage indices of 0.05, 0.36, and 0.72, respectively for the minor, moderate, and severe shaking.

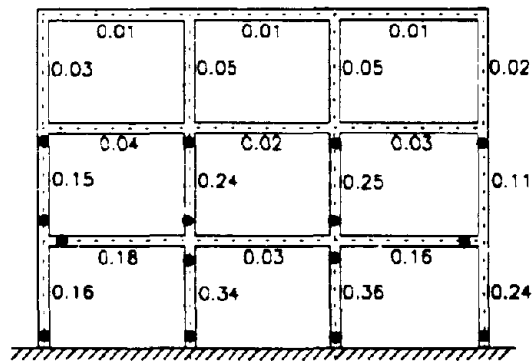
In conclusion to this damage evaluation building, it can be noted that: (i) *severe* damage was induced to the interior columns and *moderate* damage to the exterior columns both in the first and second floors; (ii) little reserve capacity remained in the first and second story columns to resist any future lateral loads; (iii) only slight damage developed in the first story beams with exception to the exterior beams in positive bending and (iv) the building was classified as *moderately/severely* damaged and in need of repairs to restore a serviceable condition.



STORY LEVEL DAMAGE INDICES

Story	Beam-Slab Damage	Col/Wall Damage
3	0.01	0.03
2	0.02	0.03
1	0.01	0.05
Overall Structural Damage		0.04

(a) TFT_05

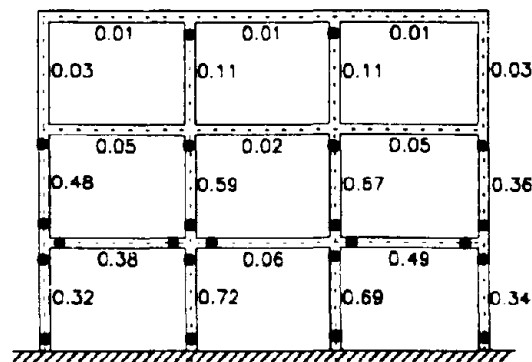


STORY LEVEL DAMAGE INDICES

Story	Beam-Slab Damage	Col/Wall Damage
3	0.01	0.04
2	0.03	0.21
1	0.12	0.30
Overall Building Damage		0.23

● Signifies Yielding

(b) TFT_20



STORY LEVEL DAMAGE INDICES

Story	Beam-Slab Damage	Col/Wall Damage
3	0.01	0.09
2	0.04	0.55
1	0.31	0.59
Overall Structural Damage		0.49

(c) TFT_30

FIG. 3-13 Damage Quantifications of the Model

A retrofit scheme for this structure to resist any future lateral loads was studied in another research phase of this program presented in the Retrofit Report Series which consists of two parts [Part I, Choudhuri, et al, (1992) and Part II, Bracci et al, (1992b)].

3.4 Identification of Final Collapse Mechanism and Critical Earthquake

IDARC was used to estimate the critical peak ground acceleration to scale the Taft N21E ground motion to induce collapse on the original undamaged model. Such analysis was done before and after the shaking table tests. Before the tests, analyses were done to estimate the maximum PGA for which the model will be near collapse, but will not collapse. After the tests, analyses were done using improved estimates of structural parameters and the results are presented herein. The criteria used to determine the critical peak ground motion are related to the following variables: (i) the maximum inter-story drifts; (ii) the base shear demand and capacity; and (iii) the damage index of the critical first story columns and of the overall structure. For this analytical evaluation, repetitive analyses were done using Taft N21E with the PGA varied from 0.20 g to 0.40 g.

Table 3-2 shows the comparisons of the maximum story response and damage indices for the various motions. It can be observed that the inter-story drifts for the first floor are within reasonable limits up to the 0.35 g motion (2.73% of the story height). Thereafter, the inter-story drift for the first floor exceeds 3%, which would exceed the ductility capacity in lightly R/C members. In Part II of the Evaluation series (Aycardi et al, 1992) it was shown that the maximum lateral capacity of the components was reached at drift levels between 2% and 3% and thereafter, with increasing drifts, began to degrade. This did not necessarily imply collapse, however, the critical displacement of the story model were near. The inter-story drift maxima for the second floor remains within tolerable limits and the third story displacements range from 1.11 in. to 2.60 in. for the various motions. The base shear force demands approach capacity very rapidly. For the 0.20 g motion, the base shear demand is about 91% of capacity. For the 0.40 g motion, the base shear demand reaches capacity. Therefore collapse is inevitable from this base motion. But also collapse is very probable for the 0.35 g PGA since the base shear demand is 98.3% of capacity.

Probably the most compelling variables for: determination of the critical PGA for collapse of the model are the member damage indices. Fig. 3-14 shows the resulting damage indices of the model for each PGA. It can be observed that most of the damage occurred to the columns

of the first and second floors. Thus the resulting failure mechanism is that of a column-sidesway or soft-story collapse mechanism. Since the columns are vital in carrying gravity loads in these failure mechanisms, the damage index for a critical first story interior columns (shown to be more critical than the second story columns) was monitored and is shown in Table 3-2. It can be observed that the damage index for this column remains within the *moderate* - "*repairable*" damage state ($0.33 \leq DI < 0.66$) for the 0.20 g and 0.25 g motions. However, the damage index reaches the *severe* - "*irreparable*" damage state ($0.66 \leq DI < 1.00$) for the 0.30 g motion. Finally at 0.35 g and 0.40 g, the damage index is 0.98 and 1.00, respectively. Therefore, a collapse of the first story interior column is likely from the Taft N21E with a PGA of 0.35 g and definite with 0.40 g. Also the overall structural damage index for the 0.35 g motion is 0.56, which indicates *moderate/severe* damage according to Eq. (3.6). Note that the damage index used for this analysis does not consider any damage due to P-delta effect. However a modified damage model is presented in Section 3.5 to capture this effect.

Therefore, from the response results for the various critical members and the overall structural damage indices from IDARC, it was determined that the Taft N21E component with a PGA of 0.35 g would have probably induced collapse of the critical first story interior column, thereby initiating progressive collapse of the model structure. El-Attar et al. (1991) observed this resulting failure mechanism for the 1/8 scale three story replica which collapsed progressively according to the soft-story mechanism initiated by the failure of the interior columns.

3.5 Modified Damage Index for P-Delta Effect

Bracci et al. (1989) proposed a damage index based on damage demand and potential, which is essentially similar to the Park, Ang, and Wen model but includes the correlation effect of displacement ductility and strength deterioration. The damage index, DI , is a combination of the deformation (ductility) and strength deterioration (strength loss) damages as follows:

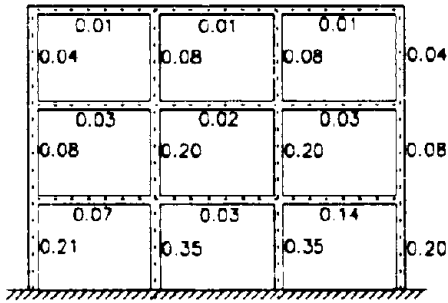
$$DI = D_2 + D_1(1 - D_2) \quad (3.7)$$

$$D_1 = \frac{\delta_m - \delta_y}{\delta_u - \delta_y}$$

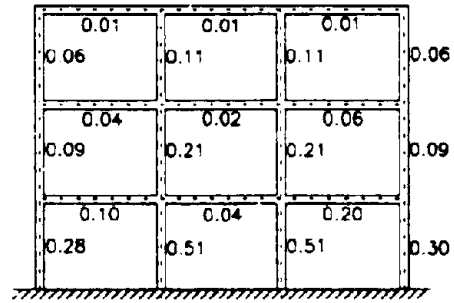
$$D_2 = \frac{S_{sd} \int dE}{\delta_y P_y}$$

Table 3-2 Maximum Response and Damage Index Comparison

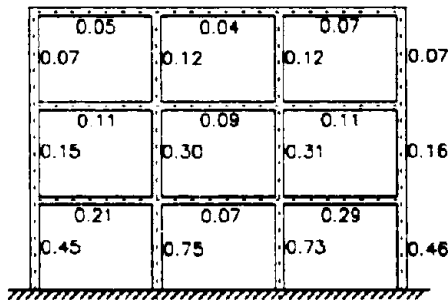
PGA		Inter-Story Drifts		Displacement	Base	Damage Index	
		First (%)	Second (%)	Third (in)	Shear (% W)	First Story Interior Col.	Structure
0.20 g	Demand Capacity	1.15	0.82	1.11	13.6 (15.0)	0.35	0.21
0.25 g	Demand Capacity	1.58	0.87	1.43	14.1 (15.0)	0.51	0.29
0.30 g	Demand Capacity	2.17	1.07	1.78	14.4 (15.0)	0.75	0.42
0.35 g	Demand Capacity	2.73	1.39	2.19	14.8 (15.0)	0.98	0.56
0.40 g	Demand Capacity	3.18	1.68	2.60	15.0 (15.0)	1.00	0.61



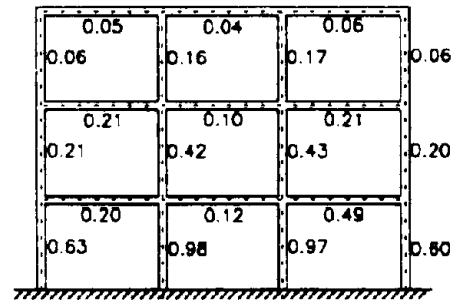
(a) 0.20 g



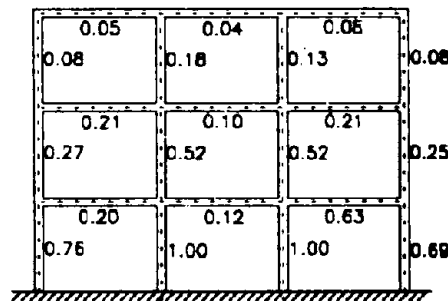
(b) 0.25 g



(c) 0.30 g



(d) 0.35 g



(e) 0.40 g

FIG. 3-14 Resulting Member Damage Indices for the Various PGAs

where D_1 = deformation damage
 D_2 = strength deterioration damage
 δ_m = maximum observed deformation
 δ_u = ultimate deformation
 δ_y = yield deformation
 P_y = yield force
 S_{sd} = strength deterioration factor
 $\int dE$ = absorbed hysteretic energy

In addition to the loss in strength due to strength deterioration from inelastic cycling, a strength demand occurs as a result of the P-delta effect in columns at large story displacements from the vertical axial loads. Fig. 3-15 shows a conceptual model of damage, which incorporates the P-delta effect. A bilinear-trapezoidal damage capacity loading diagram is hypothesized with the demand damages identified. The deformation damage (D_1) represents the associated damage due to demand ductility. The strength deterioration damage (D_2) represents the associated damage due to the loss in strength from repeated inelastic cycling. A third damage demand ($D_{P-\Delta}$) develops in the columns due the additional moments from the P-delta effect. This additional moment provides an additional strength damage demand for a bilinear representation as follows:

$$D_{P-\Delta} = \frac{N(\delta_u/h)}{P_y} \quad (3.8)$$

where $D_{P-\Delta}$ = strength damage from the P-delta effect
 N = applied axial loads
 δ_u = current story displacement
 P_y = yield force
 h = story height

Therefore, incorporating Eq. (3.8) into the strength damage index (D_2), a modified strength deterioration index, D_2^* , to include the associated damage from P-delta effect is proposed below:

$$D_2^* = \frac{S_{sd} \int dE}{\delta_s P_s} + \frac{N(\delta_d/h)}{P_s} \quad (3.9)$$

This strength damage index, incorporated in Eq. (3.7) by replacing D_2 , enables evaluation with a more appropriate strength damage index.

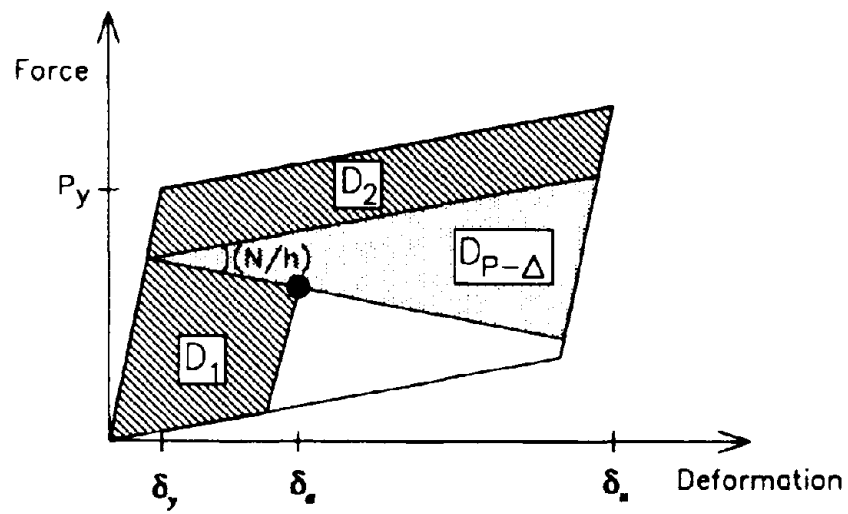


FIG. 3-15 Conceptual Model of Damage with P-delta Effect

The modified damage index with the P-delta effect was used to evaluate the damage to the critical first story interior columns in predicting the critical PGA for the model. Firstly, the column yield displacement, yield force, and ultimate displacement were found in IDARC by statically loading each story of the model with forces proportional to the inverted triangular loading. Fig. 3-16 shows the first story interior column shear force versus inter-story drift under increasing static loads. It was observed that cracking occurred at a displacement of 0.14 in. (0.30% of the story height) and yielding occurred at 0.55 in. (1.15% of the story height). The yielding shear force for the column was about 1.51 kips. The post-yielding shear force continually increases with displacement from the input strain hardening without a loss in strength. However, the ultimate monotonic displacement was assumed to be 3% of the story height (refer discussions in previous section).

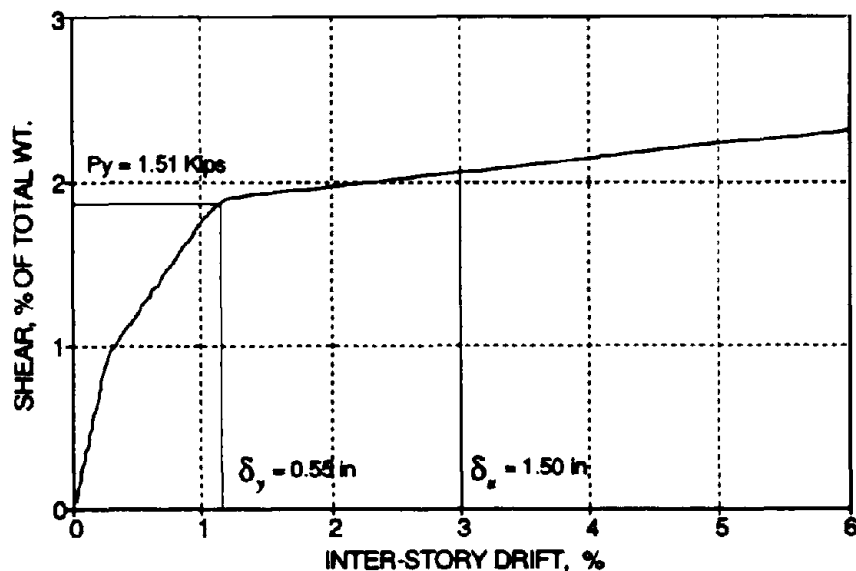


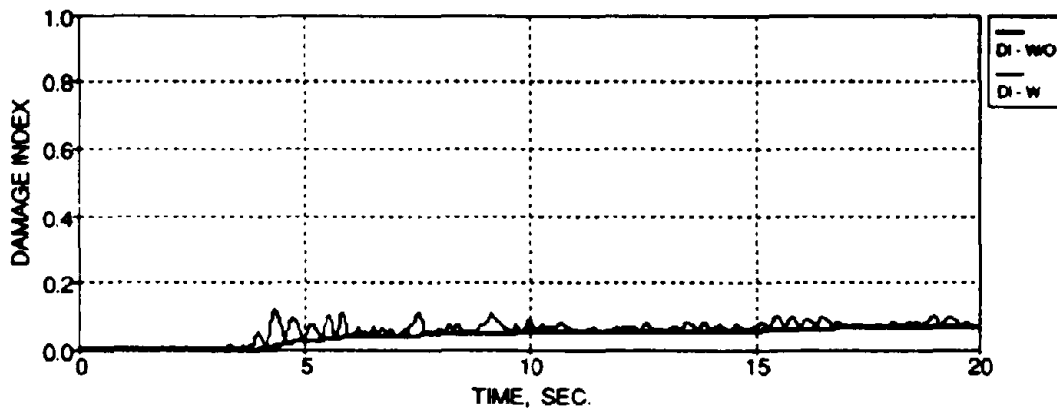
FIG. 3-16 First Story Interior Column Monotonic Strength-Deformation

Figs. 3-17 through 3-21 show the column damage index as a function of time, displacement ductility (δ_u/δ_y), and deformation damage ($(\delta_m - \delta_y)/(\delta_u - \delta_y)$). It was observed that the resulting damage index is relatively small for the 0.20 g motion. Since the observed story displacements do not exceed the corresponding yield displacement, the amount of deformation damage according to the proposed model is nil (see Fig. 3-17c). However, inelastic behavior (permanent deformations) occurs in R/C members after cracking takes place. Therefore, some discrepancies in the proposed damage index may develop for extremely minor member damage by assuming the bilinear-trapezoidal capacity loading. The damage for the 0.20 g motion was only a function of the strength deterioration and P-delta effect. The additional damage (strength deterioration demand) caused by the P-delta effect can be noticed in Fig. 3-17b when the observed displacement approaches yield (DI from about 0.02 to 0.12). The P-delta effect creates an amplification of the damage index with story displacement, thereby creating fluctuations in the damage index.

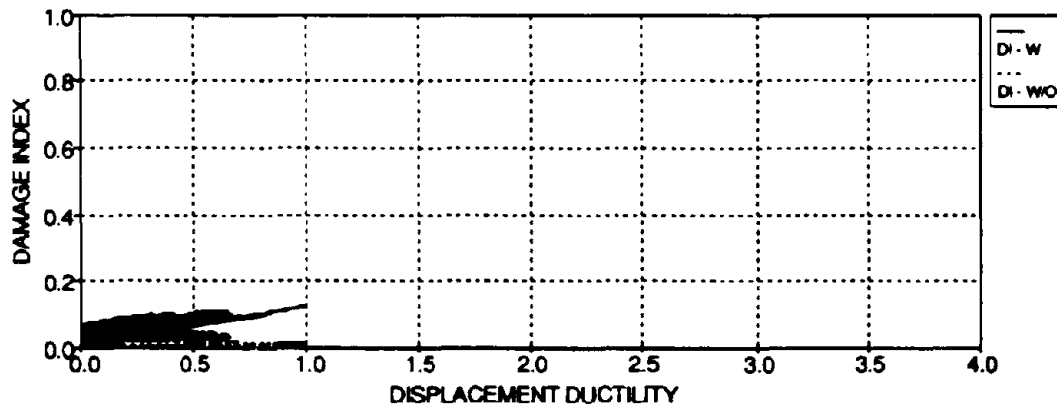
From Fig. 3-18, it can be observed that the story displacement exceeds the yield displacement for the 0.25 g motions. The corresponding deformation damage was about 0.22. The damage index associated with and without P-delta at the maximum observed displacement was observed as about 0.40 to 0.24, respectively (66% increase in damage). From Fig. 3-18b, note the slope in the damage index with the P-delta effect after the peak displacement occurs, whereas without the P-delta effect the slope is flat. This is obviously a result of the P-delta effect being proportional to the story displacement. The same observations were made for the 0.30 g base motions at peak displacement with the resulting damage index approaching 0.78 with the P-delta effect and only 0.58 without (about a 35% increase in damage).

For the 0.35 g motion, it was observed that the damage index without the P-delta effect was 0.98 at the end of the base motions with corresponding deformation damage of about 0.80. However, when the P-delta effect is considered, the damage index reaches 1.00 at about 4 seconds through the run which implies failure of the column and subsequently the structure. For the 0.40 g motion, the damage index with and without the P-delta effect was 1.0 (collapse) at about 4 sec. into the run.

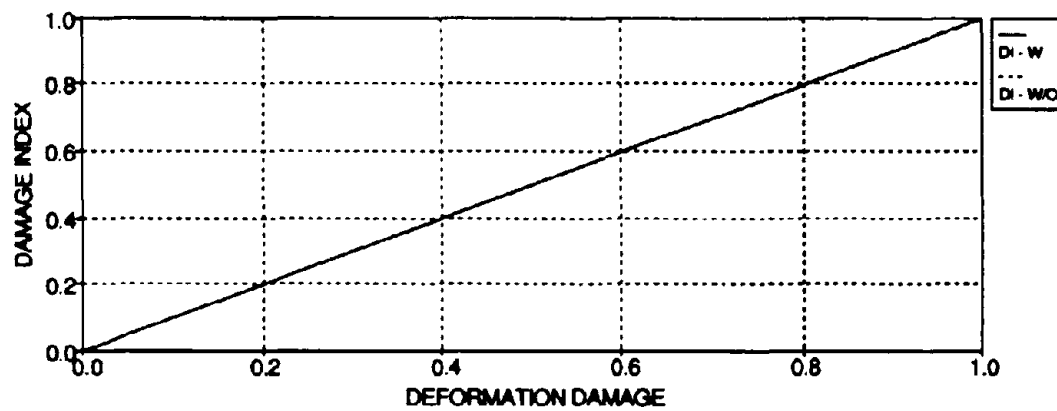
Therefore, with consideration of the P-delta effect in the modified damage index, the corresponding PGA of the Taft N21E component to cause collapse of the model was between 0.30g and 0.35 g. However, without consideration of the P-delta effect, the critical PGA was slightly above 0.35 g.



(a) Time History

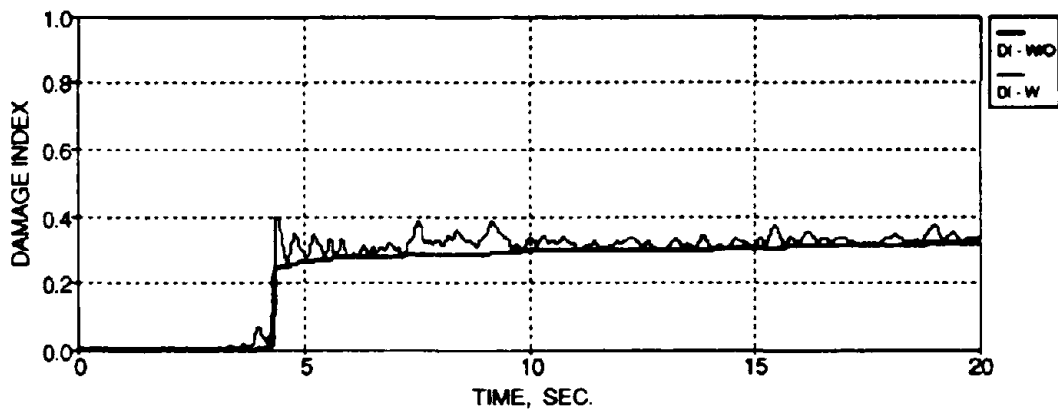


(b) Displacement Ductility History

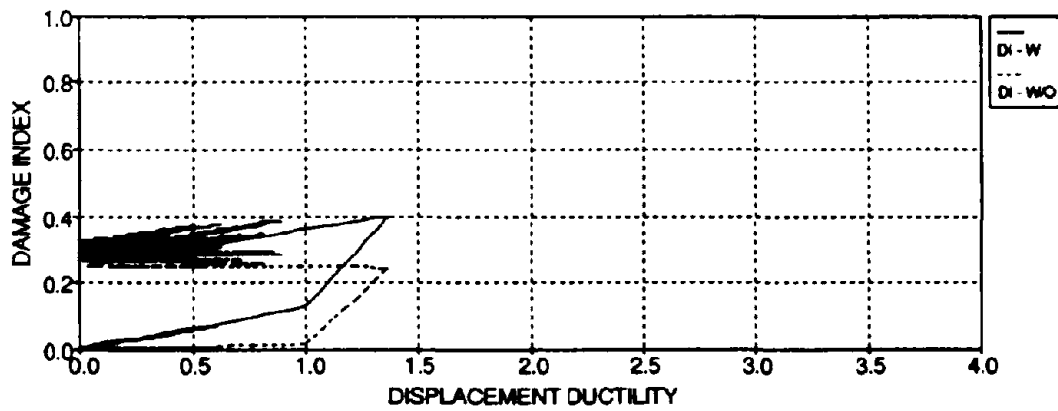


(c) Deformation Damage History

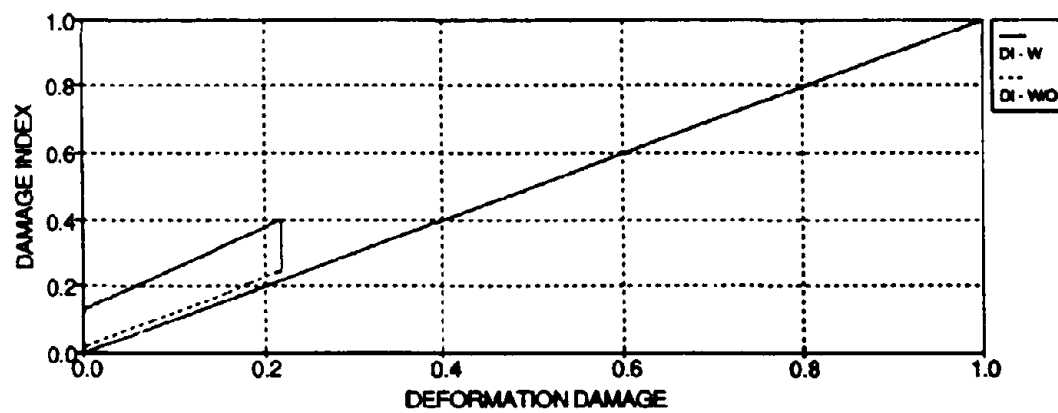
FIG. 3-17 First Story Interior Column Damage Index for 0.20 g with (w) and without (w/o) P- Δ Effect



(a) Time History

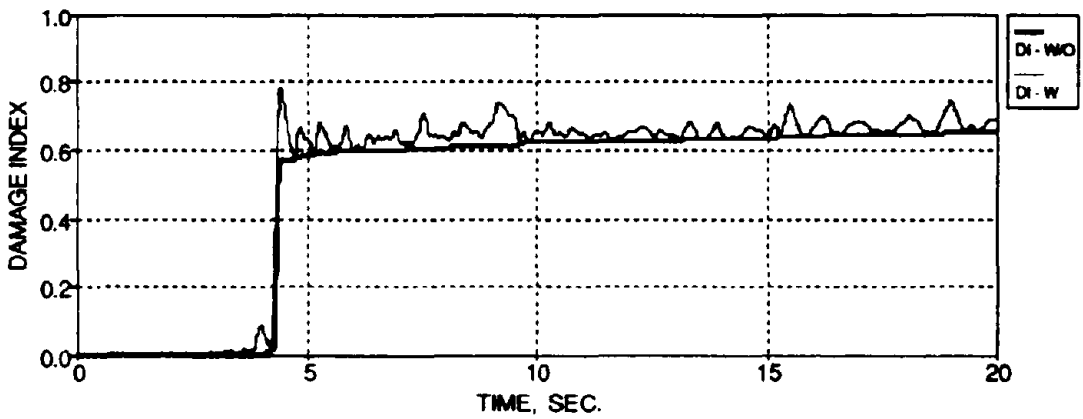


(b) Displacement Ductility History

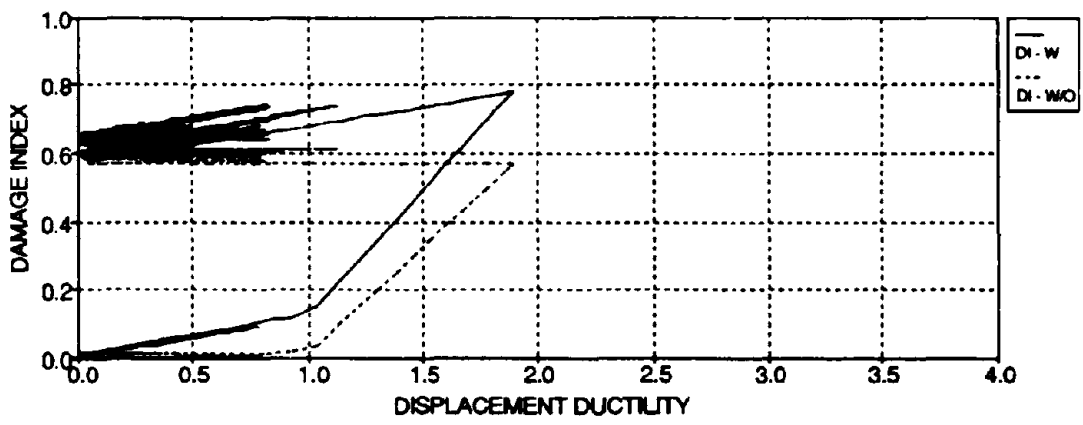


(c) Deformation Damage History

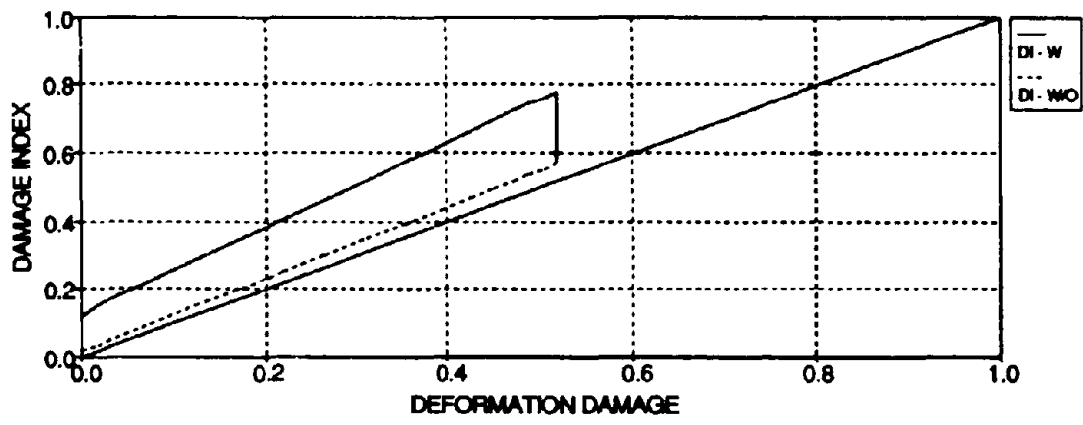
FIG. 3-18 First Story Interior Column Damage Index for 0.25 g with (w) and without (w/o) P- Δ Effect



(a) Time History

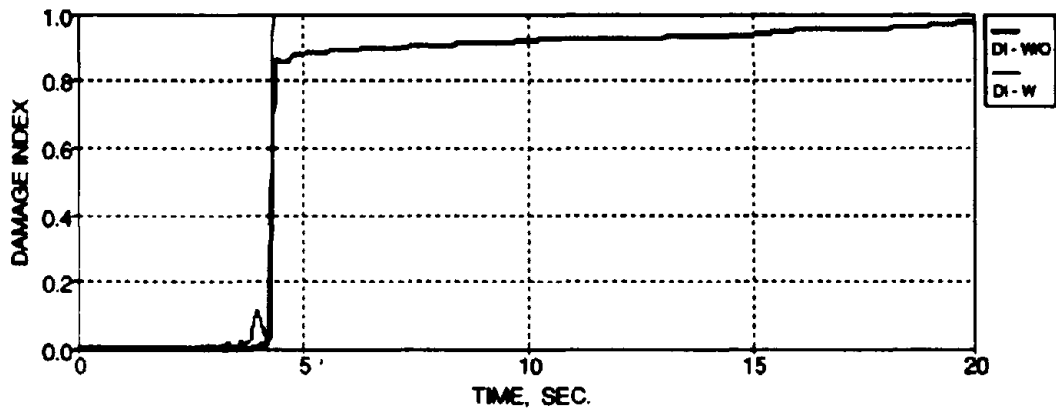


(b) Displacement Ductility History

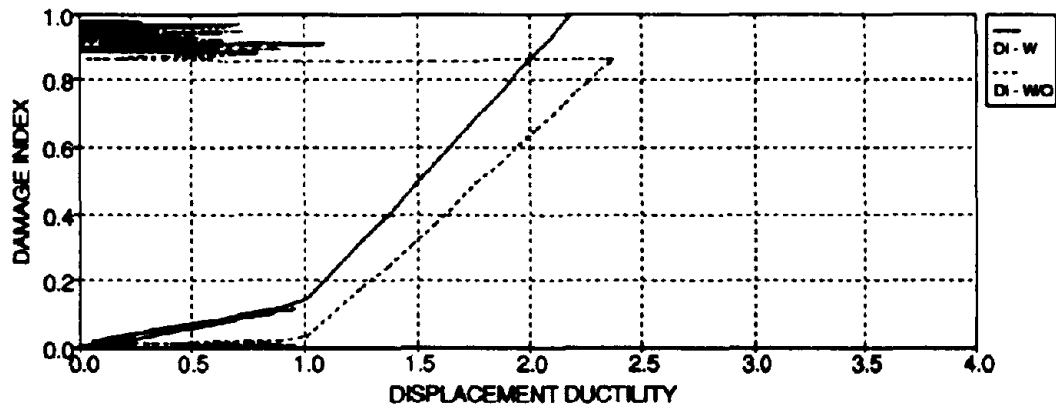


(c) Deformation Damage History

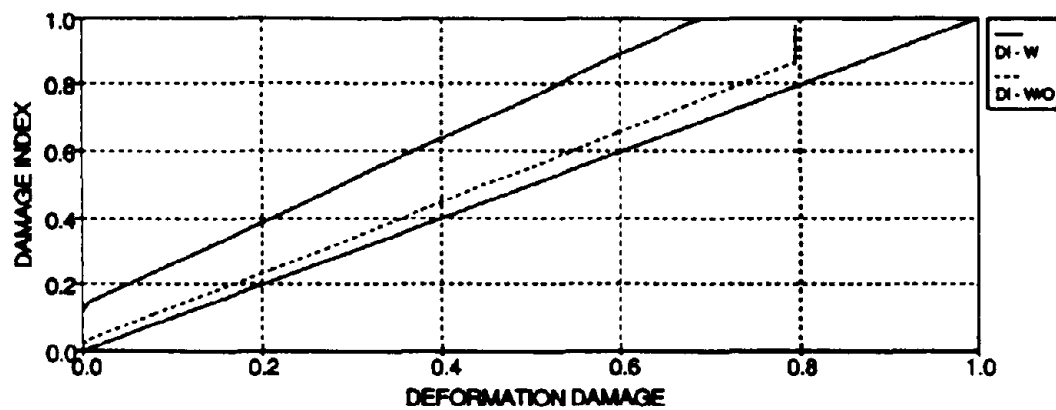
FIG. 3-19 First Story Interior Column Damage Index for 0.30 g with (w) and without (w/o) P-Δ Effect



(a) Time History

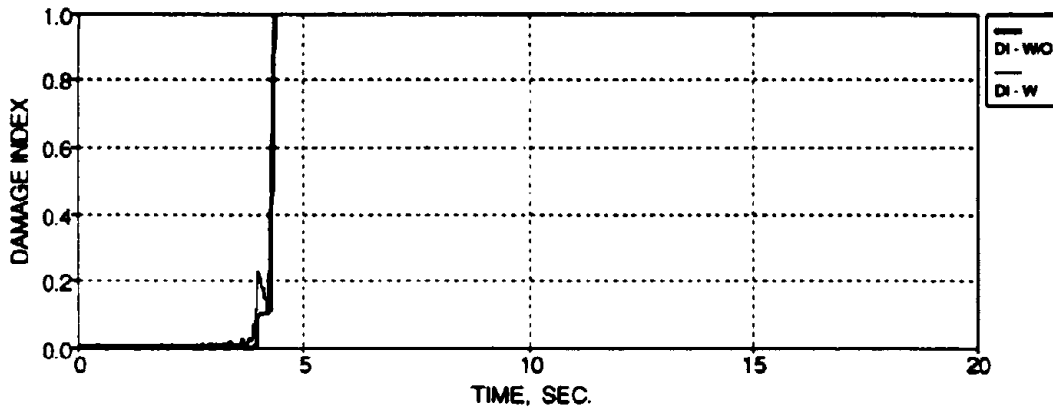


(b) Displacement Ductility History

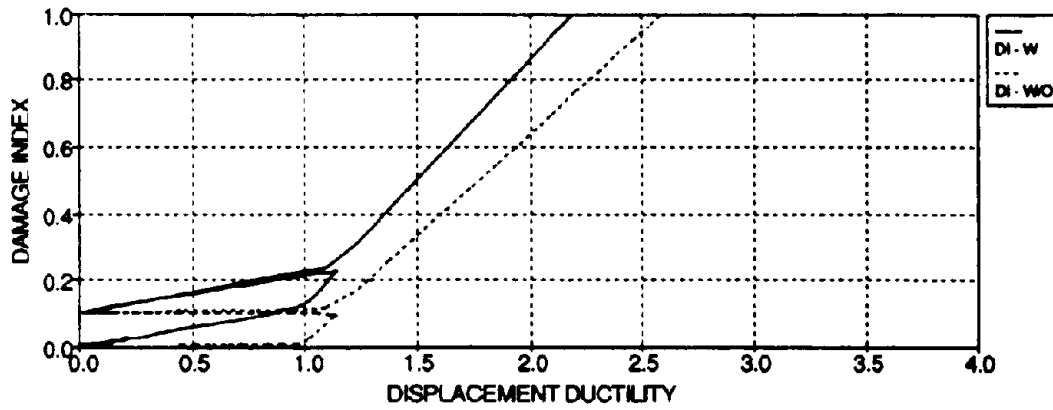


(c) Deformation Damage History

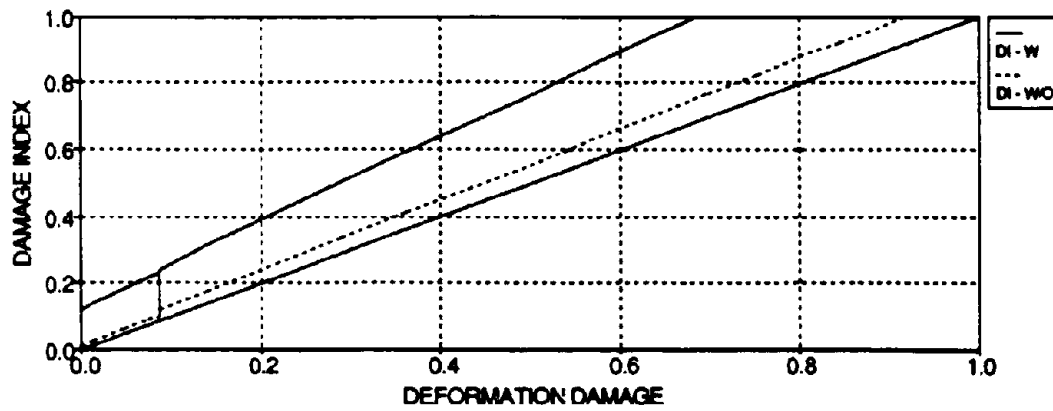
FIG. 3-20 First Story Interior Column Damage Index for 0.35 g with (w) and without (w/o) P- Δ Effect



(a) Time History



(b) Displacement Ductility History



(c) Deformation Damage History

FIG. 3-21 First Story Interior Column Damage Index for 0.40 g with (w) and without (w/o) P-Δ Effect

3.6 Elastic Analysis and Response Reduction Factors

Fig. 3-22 shows a general loading of a base shear versus the story drift for a typical structure and will be referred to in the following discussions.

An elastic analysis is performed on the three story model for the shaking motions with the analytical model developed based on the experimental response fit (see Section 3.2.3) by maintaining the same global stiffness matrix (elastic stiffnesses) throughout the shaking history. Fig. 3-23 shows the predicted elastic base shear histories for the minor, moderate, and severe shaking motions. The peak base shear demands from these elastic analyses were determined as 8.1 kips (10.0% of the total structural weight W), 22.5 kips (27.8% W), and 32.6 kips (40.3% W), respectively. From the inelastic analyses in Section 3.2.3, the analytical base shear demands were calculated as 7.1 kips (8.8% W), 11.9 kips (14.7% W), and 11.8 kips (14.6% W), respectively. This corresponds to force reduction factors (reduction from the elastic demand to the inelastic demand) of 1.15, 1.89, and 2.77, respectively and shown in Fig. 3-22. This force reduction factor is compared to the ductility reduction factor (R_{μ}) in the discussions below. Note it was previously shown that the measured base shears for the moderate and severe shaking approach the capacity obtained from a shakedown analysis (ultimate strength level).

Since a structure can provide a certain amount of ductility (inelastic deformation), UBC (1991) specifies a total strength capacity reduction factor (R_w) of the elastic design force level (C_{ew}) based on allowable stress design. The elastic design force level (C_{ew}) is reduced by R_w to the inelastic design force level (C_w), which allows for more economical design of structures. UBC (1991) specifies only one design earthquake level for the determination of the ultimate limit state capacity. Therefore, the total force reduction factor is related to the inelastic design spectra for the ultimate limit state and is not related to a serviceability limit state from service or moderate design earthquakes. Uang and Bertero (1991) assumed a service design earthquake for steel structures by specifying a drift limit that was inversely proportional to the R_w factor. That study showed that the allowable seismic stress was too high for ductile structures and too low for non-ductile structure.

Uang (1991) suggested that the formulation of the total force reduction factor (R_w) from UBC (1988) includes overstrength, stress factors as well as a ductility based strength reduction as follows:

$$R_w = R_\mu \Omega Y \quad (3.10)$$

where $R_\mu =$ *Ductility Reduction Factor*. Since a structure has the capability of dissipating energy as a result of ductility, the elastic design force level (C_{eu}) is reduced to a level of inelastic ultimate strength (C_y).

$\Omega =$ *Overstrength Reduction Factor*. The structural reserve strength that exists between the inelastic ultimate strength level (C_y) and the first plastic hinge occurrence level (C_s).

$Y =$ *Allowable Stress Factor*. The strength that exists between the first plastic hinge occurrence level (C_s) and the allowable stress level (C_w).

According to the provisions in UBC (1991) for an ordinary moment resisting R/C frame, the total force reduction factor (R_w) is 5 for the three story model in this study. However, this is not the factor to compare with the demand response reduction factor discussed previously. The response reduction factor is equivalent to the required ductility based strength reduction factor, R_μ . For the model building, a dynamic amplification factor (overstrength reduction factor, Ω) of 1.3 is used to adequately represent a projected dynamic ultimate surface for considering strain hardening of the rebars and dynamic strain rate effects (typically shown in Figs. 2-10 and 2-11). The allowable stress factor (Y) typically ranges between 1.4 and 1.5 according to various codes, (Uang, 1991). Therefore the corresponding ductility reduction factor (R_μ) according to UBC (1991) from Eq. (3.10) is 2.75.

Table 3-3 summarizes the response (demand) reduction factors and the ductility based capacity reduction factors for the model, along with the structural damage index, displacement ductility ratio, and the base shear demand and capacity computed analytically. It was observed that the ductility reduction factor and the response demand reduction factor are almost equal when the base shear approaches the ultimate load for the severe shaking.

It should be noted that for response (capacity) reduction factors of 2.75 the associated damage index is high (0.49) with a ductility demand of 1.96 (fairly low). If the structure is to be maintained without damage (index of 0.04), capacity reduction may not be recommended at all for these types of structures or, the ductility of its details must be substantially improved. The

strength demand reduction factors and ductility (displacement) demand ratios can be adequately determined using the calibrated analytical model, for the current study, in association with an allowable target damage index.

TABLE 3-3 Response Reduction Comparison

			Minor (0.05 g)	Moderate (0.20 g)	Severe (0.30 g)
Analytical	Elastic Base Shear (% of structural Weight)	Demand	10.0%	27.8%	40.3%
(Original Bldg.)	Inelastic Base Shear (% of Structural Weight)	Demand (Capacity)	8.8% (15.0%)	14.7% (15.0%)	14.6% (15.0%)
	Damage Index		0.04	0.23	0.49
	Displacement Ductility Demand		1.00	1.38	1.96
	¹ Response Reduction Factor,		1.15	1.89	2.77
Code	² UBC (1991) - Ductility Reduction Factor, R_u		2.75	2.75	2.75

¹ (Demand) Response Strength reduction factor computed from the base shear ratio of the elastic and inelastic analyses based on the experimental response fit model.

² Strength reduction factor for an ordinary moment resisting concrete frame with $R_w = 5$, $\Omega = 1.3$, and $Y = 1.4$.

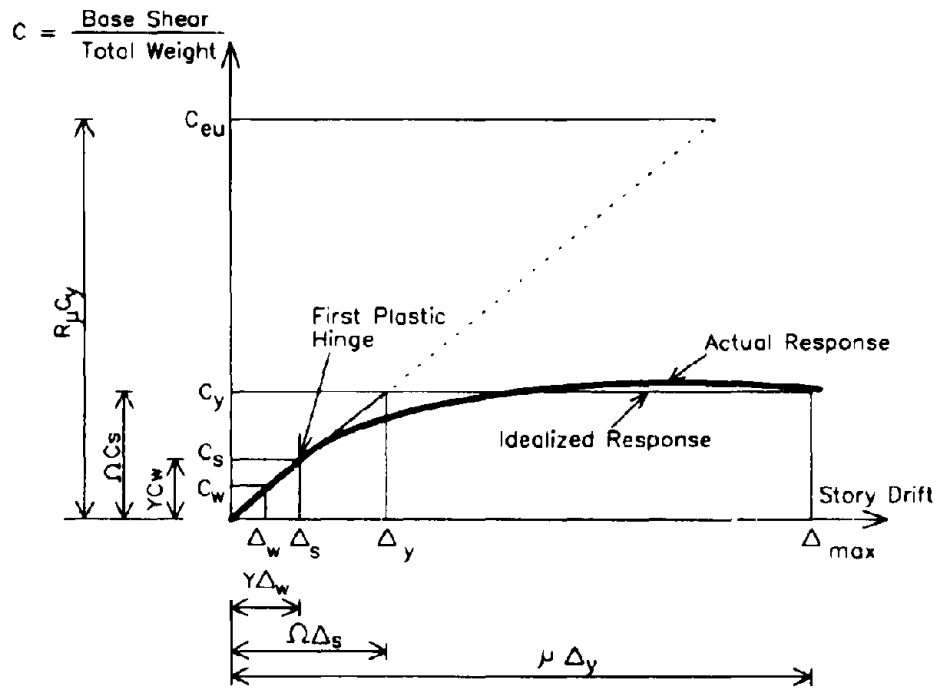
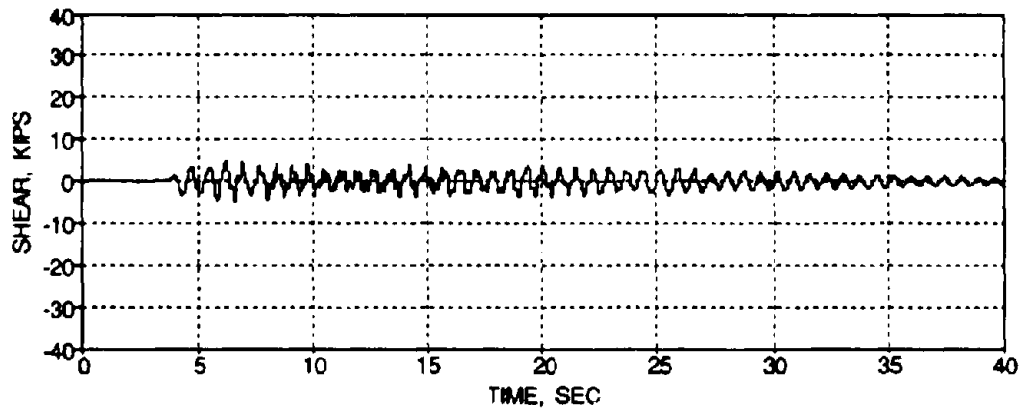
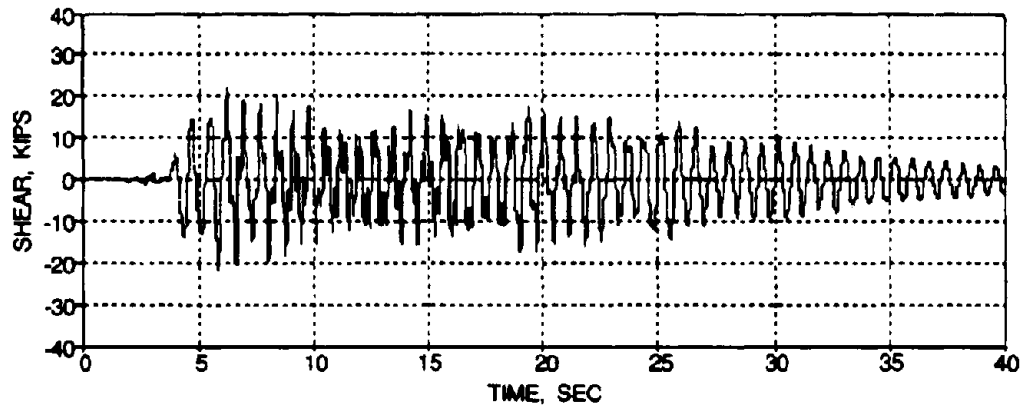


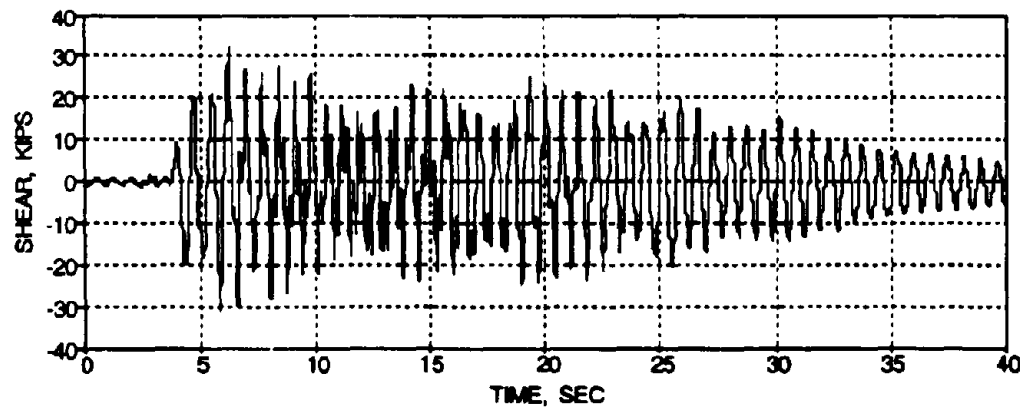
FIG. 3-22 Typical Structural Response



(a) Minor Shaking



(b) Moderate Shaking



(c) Severe Shaking

FIG. 3-23 Elastic Base Shear Response

3.7 Summary Discussions

Three sets of properties were used in an analytical model to simulate the seismic response of the structural scaled model based on: (i) engineering approximations; (ii) component tests; and (iii) an experimental response fit. It was shown that the first two models provide adequate agreement with the experimental response with only slight underpredictions of response in parts of the history. The experimental response fit required slightly varying initial and post-cracking column stiffnesses at different stories to better simulate the experimental response. It was shown that the damage states analytically estimated from the experimental fit model and experimentally observed damage states are similar. However for practicing engineers, analytical modeling can only be carried out using approximations of member property or possibly using component tests. This study shows that analytical, modeling, based on engineering approximations or component tests, can provide adequate prediction of response of structures from earthquakes. It was shown that good correlation was obtained using reduced stiffnesses of 60% and 25% of the calculated gross stiffness properties of columns and beams, respectively. Note that the beam gross stiffness was derived including full slab width contributions. These initial member stiffnesses were comparable with recently suggested values by Paulay and Priestley (1992).

A damage evaluation of the building was also performed by quantifying the induced member damages (through damage indices) from the earthquakes. It was shown that *severe* damage results to the interior columns and *moderate* damage to the exterior columns of the first and second floors of the model after the severe shaking. Little reserve strength remained in the column members for resisting any future lateral loads. The interior beams remained in a "*serviceable*" damage state with *moderate* damage resulting in the first story exterior beams in the pull-out direction. The analytical damage evaluation complements the experimental measured damage state during the test (which alone is not sufficient to assess the damage state of the structure). Also, correlations exist between the damage indices computed from the analytical evaluation and from the measured experimental response. The incipient failure mechanism for the model, derived from the damage evaluation, was identified to be a column-sidesway or soft-story type, which was also observed experimentally. El-Attar et al. (1991) observed collapse of the 1:8 scale model from an identical mechanism that was obtained both analytically and incipiently during experiments in this study.

The critical peak ground acceleration of the Taft N21E motion to cause collapse of the original undamaged model is determined to be about 0.35 g. The critical variables used for this determination were the inter-story drifts, base shear force demand and capacity, critical member damage indices from modified Park's Model (without consideration of P-delta damage), and overall structural damage index.

A modified damage index was proposed to incorporate the strength damage associated with the P-delta effect in columns. This advanced damage index was particularly useful for the critical columns of the model to obtain a critical peak ground acceleration for the Taft N21E motion and compare the influence of P-delta effect on damage. It was shown that the corresponding member damages were increased by about 33% with the additional P-delta effect for the 0.30 g shaking. However, this amplification in the damage index only occurred at large story displacements. With the more appropriate damage index, collapse would occur at a critical peak ground acceleration between 0.30 g and 0.35 g (in comparison to about 0.35 g without the P-delta effect).

With elastic and inelastic analyses of the model, the base shear demand reduction factors from the elastic force level to the inelastic strength level were determined as 1.15, 1.89, and 2.77, respectively for the minor, moderate, and severe earthquakes. In comparison with UBC (1991) for the inelastic design force level, the recommended ductility reduction factor, R_u , is 2.75 for an ordinary moment resisting R/C frame with a total force reduction factor (R_w) of 5, an overstrength reduction factor (Ω) of 1.3, and an allowable stress factor (Y) of 1.4. Therefore, for the severe shaking near ultimate force capacity, the ductility reduction factors are similar. However, for the minor and moderate design earthquakes. The response demand reduction factors do not correlate to the ductility based strength capacity reduction factors specified by UBC (1991). If the design of LRC frames is based on minor earthquakes the strength capacity reduction factors of UBC 1991 might not be adequate. If the design of LRC frames is based on minor earthquakes, the strength capacity reduction factors of UBC 1991 might not be adequate.

SECTION 4

SUMMARY, CONCLUSIONS, AND RECOMMENDATIONS FOR FUTURE WORK

4.1 Summary of LRC Frame Model Testing

4.1.1 Design

A typical three-story moment resisting R/C frame structure was designed primarily to carry only gravity loads ($U = 1.4 D + 1.7 L$). No consideration was made for seismic resistance and the general non-seismic detailing provisions of ACI-318-89 were used. The structure is considered to be representative of low-rise building typically constructed in the Eastern and Central United States, where seismic codes have not been, or are still not, enforced. The structure is probably weaker than the ordinary moment resisting frames designed according to newer codes, which have minimum joint reinforcement and bar continuing in critical regions.

A one-third scale three story R/C model was designed and constructed in the State University of New York at Buffalo Earthquake Simulation Laboratory. The model was one-bay by three-bays with two overhanging sides of one-third bay width and represented the critical interior bay of the prototype structure. The total weight on the shaking table including the model, the base foundation, and the connecting concrete block was about 110 kips, which was the near maximum capacity of the vertical actuators.

4.1.2 Experimental Study

The model was tested on the shaking table using the scaled Taft N21E component to simulate minor (PGA 0.05 g), moderate (PGA 0.20 g), and severe (PGA 0.30 g) earthquakes. The behavior of the model from the *minor earthquake* can be summarized:

1. Response was governed by elastic deformations with only slight cracking in some column members.
2. Response was dominated by the first mode of vibration.

5. Slab steel from the full slab width had a dramatic contribution to the flexural strength of the beams. For a typical beam-column-slab component, the nominal moment capacity of the beams with full slab steel contributions exceeded the capacity of the columns by about 66% (nominal column to beam strength ratio of about 0.60).
6. Large reductions in story stiffness (approximately a total of 40% and 60% for the first and second stories, respectively) and natural frequency (total of 33% in the first mode) were observed after the earthquakes.
7. The measured base shear force demands for the moderate and severe shaking were 15.2% and 15.3% of the total structural weight, respectively. The base strength capacity from a shakedown analysis at a 2% drift limit had been reached during both earthquakes.
8. The equivalent viscous damping factors were determined to have more than tripled in comparison with the undamaged model, due to contributions from hysteretic damping.

4.1.3 Analytical Studies

Three analytical models were developed to simulate the seismic response of the model based on: (i) engineering approximations; (ii) component tests; and (iii) an experimental response fit. The identified structural parameters for each analytical model were: (1) the initial, post-cracking, and post-yielding stiffnesses; (2) the cracking and yielding moments; (3) the damping characteristics; and (iv) the hysteretic properties.

It can be concluded that:

1. The analytical models based on engineering approximations and component tests provided adequate correlation with the experimental response. The peak response was captured and the response trends were similar. However, slight magnitude variations were observed in the latter part of the motion.

2. The fitted model to the experimental response required slightly varying initial stiffnesses and post-cracking stiffnesses in each member to better simulate this experimental response. For the minor shaking, the initial stiffness of the columns and beams were about $0.60 \cdot (EI_{col})_g$ and about $0.25 \cdot (EI_{bm})_g$, respectively. The post-cracking stiffness was $EI/2$ for all members. For the moderate and severe shaking (consecutive runs), the initial stiffness of the columns were $0.39 \cdot (EI_{col})_g$, $0.33 \cdot (EI_{col})_g$, and $0.44 \cdot (EI_{col})_g$, respectively for the first, second and third floors. The initial stiffness of the beams were $0.25 \cdot (EI_{bm})_g$ (same as minor shaking). The post-cracking stiffness was $EI/1.25$ to model stiffer behavior after cracking (similar to a bilinear model). The analytically predicted damage state was similar to the experimentally measured and observed.
3. The damage evaluation indicated *severe* - "irreparable" damage to the interior columns and *moderate* - "repairable" damage to the exterior columns of the first and second floors after the severe shaking. The interior beams remained within the *minor* - "serviceable" damage state with a *moderate* - "repairable" damage state to the first story exterior beams from the pull-out moments. The overall damage indices were 0.04, 0.23, and 0.49, that the structure will suffer only minor damage during minor earthquakes, minor to moderate during moderate earthquakes, and moderate to severe during severe earthquakes.
4. The critical peak ground acceleration of the Taft N21E component to cause collapse of the original undamaged model was determined to be about 0.35 g.
5. A modified damage index was proposed to incorporate the associated damage from the P-delta effect in columns. It was shown that the corresponding member damage indices were increased about 33% with the additional P-delta effect damage for a 0.30 g shaking.
6. The response demand reduction factors from inelastic response were comparable to those of UBC (1991) for the severe shaking. The expected damage, based on such reduction factor, will be irreparable (indicated by the damage index in Table 3.2). However, if smaller damage is the target of the design, **no reduction should be recommended or the ductility of current details should be substantially improved.**

4.2 Conclusions on LRC Frame Structures during Earthquakes

Based on the experimental and analytical study of a one-third scale three story model, the following conclusions can be made about the behavior of lightly reinforced concrete (LRC) structures during earthquakes:

1. For minor earthquakes, the inherent resistance and flexibility of such structures are adequate to resist the seismic forces and avoid major damage.
2. For moderate and severe earthquakes, the structures may withstand the earthquake at the expense of large inter-story drifts, which may be in excess of 2%. Non-structural elements (windows, plumbing, etc.) and internal furnishings would be expected to develop severe damage. Although such deformations are excessively large, the structure does not collapse, therefore life safety can be assured.
3. Under dynamic excitation, the full slab width participates and contributes to the moment capacity of the beams. This places high demands on the columns.
4. Structures are dominated by weak column - strong beam behavior. Under ultimate load, a column-sidesway or soft-story collapse mechanism will be the mode of failure.
5. Dynamic amplifications in material strengths of about 30% are expected from strain hardening of the reinforcement and dynamic strain rate effects.
6. Significant contributions from higher mode effects can develop in typical structures from earthquakes.
7. For undamaged buildings, initial stiffnesses of $0.60 (EI_{col})_i$ and $0.25 (EI_{bm})_i$ are good initial approximations for the columns and beams, respectively, which are similar to the stiffnesses recently suggested by Paulay and Priestley (1992). However, after a damaging earthquake, the columns are expected to develop severe damage and the initial stiffnesses can deteriorate to as low as about $0.25 (EI_{col})_i$. A post-cracking stiffness of $EI/2$ can be used for an undamaged structure. However, if member cracking exists from strong lateral loads, a post-cracking stiffness similar to the initial stiffness (bilinear representation) can be used in those members.

- 8 The strength reduction factors from UBC 1991 are adequate for capacity design using severe earthquakes. The response demand reduction factors match the strength capacity reduction factors by UBC for maximum credible earthquakes in low seismicity areas.
9. Natural period computations from UBC (1991) greatly differ from the observed in such flexible buildings. Possibly a new formulation for predicting the natural period of buildings needs to be developed for lightly reinforced frames based on field testing.
10. Retrofit of such low-rise structures in low seismicity zones may not be necessary because: (i) LRC structures have some inherent resistance to earthquakes; (ii) the high degree of flexibility provides only little amplifications for most earthquakes (Mexico City earthquake is an example of an exception); and (iii) the probability of a severe earthquake striking in a low seismicity zone is small as compared to cost of retrofit. However for important low-rise structures or for medium-rise structures that may require more than preservation of life safety, a minimum retrofit may be necessary to avoid a soft-story collapse mechanism and reconfigure to a more desirable beam-sidesway mechanism.

4.3 Recommendations for Future Research on the Design and Evaluation of LRC Frame Structures

The behavior of lightly reinforced concrete member components and low-rise frame structures has been thoroughly studied in this research program. However, the experimental and analytical studies on frame structures in this work have only considered the Taft N21E ground motion. It is considered of interest to investigate how such typical frame structures would respond to different earthquakes, particular those with ground motion and soil conditions similar to the Eastern United States. It is speculated that the response of such structures would be similar to that presented in this study (weak column - strong beam behavior with large inter-story drifts).

It was shown that analytical models developed from replica component tests provided adequate correlation with the seismic response of the one-third scale model building. For the time being, this analytical model is considered suitable for predicting seismic response behavior of a pro-

totype structure. However, further verification is necessary to consider any variations that may occur due to the scaling involved in this study. One particular variation may be related to strain rate effects which can influence the pull-out of the discontinuous beam reinforcement.

Other types of non-seismically detailed structures also need further experimental verification such as: flat slab buildings; buildings with walls; masonry buildings; and medium to high rise structures.

Another area of research can focus on the non-structural elements of LRC structures. It was shown in this study that such buildings are governed by large story drifts during seismic activity. It is expected that large non-structural damage will develop during moderate and severe type earthquakes.

A sensitivity parametric study can be carried out on the hysteretic properties for analytical modeling based on the experimental results presented in this study. The objective of this work can be focused on establishing default initial values for the hysteretic parameters of gravity load design members.

Further verification of the proposed damage model, which incorporates the damage associated with the P-delta effect, is needed. A multiplicity of indices associated with importance factors might be necessary to characterize damage in structures. More experimental and analytical studies should be carried out for calibrations of the ultimate monotonic displacements and curvatures of individual components.

Finally the retrofit of inadequate structures should be a major concern. A subsequent study on selected seismic retrofit techniques for the R/C frame studied in this report was already completed and is the subject of the Retrofit Report Series (Choudhury et al, 1992, and Bracci et al. 1992b).

SECTION 5 REFERENCES

- Aycardi, L.E., Mander, J.B., and Reinhorn, A.M. (1992). "Seismic Resistance of Reinforced Concrete Frame Structures Designed only for Gravity Loads in Low Seismicity Zones: Part II - Experimental Performance of Subassemblages", Technical Report NCEER-92-0028, National Center for Earthquake Engineering Research, SUNY/Buffalo.
- Bracci, J.M., Reinhorn, A.M., Mander, J.B., and Kunnath, S.K. (1989). "Deterministic Model for Seismic Damage Evaluation of Reinforced Concrete Structure," National Center for Earthquake Engineering Research, Report NCEER-89-0033, State University of New York at Buffalo.
- Bracci, J.M., Reinhorn, A.M., and Mander, J.B. (1992a). "Seismic Resistance of Reinforced Concrete Frame Structures Designed only for Gravity Loads in Low Seismicity Zones: Part I - Shaking Table Study of One-Third Scale Model Structure", Technical Report NCEER-92-0027, National Center for Earthquake Engineering Research, SUNY/Buffalo.
- Bracci, J.M., Reinhorn, A.M., and Mander, J.B. (1992b). "Evaluation of Seismic Retrofit of Reinforced Concrete Frame Structures: Part II - Analytical and Experimental Performance of Retrofitted Model Structure", Technical Report NCEER-92-0031, National Center for Earthquake Engineering Research, SUNY/Buffalo.
- Choudhuri, D., Mander, J.B., and Reinhorn, A.M. (1992). "Evaluation of Seismic Retrofit of Reinforced Concrete Frame Structures: Part I - Experimental Performance of Retrofitted Subassemblages", Technical Report NCEER-92-0030, National Center for Earthquake Engineering Research, SUNY/Buffalo.
- Chung, Y.S., Meyer, C., and Shinozuka, M. (1987). "Seismic Damage Assessment of Reinforced Concrete Members", National Center for Earthquake Engineering Research, Report NCEER-87-0022, State University of New York at Buffalo.
- El-Attar, A.G., White, R.N., and Gergely, P. (1991). "Shaking Table Test of a 1/8 Scale Three-Story Lightly Reinforced Concrete Building", Technical Report NCEER-91-0018, National Center for Earthquake Engineering Research, SUNY/Buffalo.
- Kunnath, S.K., Reinhorn, A.M., and Park, Y.J. (1990). "Analytical Modeling of Inelastic Seismic Response of R/C Structures", *Journal of Structural Engineering*, ASCE, Vol. 116, No. 4, April, 996-1017.
- Lao, Larry F. (1990). "The Effect of Detailing on the Seismic Performance of Gravity Load Dominated Reinforced Concrete Frames", MS Thesis, State University of New York at Buffalo.
- Moehle, J.P. and Mahin, S.A. (1991). "Observations on the Behavior of Reinforced Concrete Buildings During Earthquakes", *Earthquake-Resistance Concrete Structures Inelastic Response and Design*, ACI SP-127, 67-89.
- Park, Y.J., Ang, A. H-S., and Wen, Y.K. (1985). "Mechanistic Seismic Damage Model for Reinforced Concrete", *Journal of Structural Engineering*, ASCE, Vol. 111, No. 4, 722-739.
- Paulay, T. and Priestley, M.J.N. (1992). *Seismic Design of Reinforced Concrete and Masonry Buildings*, John Wiley and Sons, Inc., New York.
- Powell, G.H. and Allahabadi, R. (1988). "Seismic Damage Prediction by Deterministic Methods: Concepts and Procedures", *Earthquake Engineering and Structural Dynamics*, Vol. 16, 719-734.
- Recommended Provisions for the Development of Seismic Regulations for New Buildings, NEHRP 1991 Edition, FEMA 222/January 1992, Washington D.C.*

Shahrooz, B.M. and Moehle, J.P. (1987). "Experimental Study of Seismic Response of R.C. Setback Buildings", Earthquake Engineering Research Center, University of California/Berkeley, California, Report No. UCB/EERC-87/16.

STAADTM (1989). *Integrated Structural Design System*, Research Engineers, Inc., New Jersey.

Uang, C.-M. (1991). "Establishing R (or R_w) and C_d Factors for Building Seismic Provisions", *Journal of Structural Engineering*, Vol. 117, No. 1, January, 19-28.

Uang, C.-M. and Bertero, V.V. (1991). "UBC Seismic Serviceability Regulations: Critical Review", *Journal of Structural Engineering*, Vol. 117, No. 7, July, 2055-2068.

Uniform Building Code (UBC) (1991). International Conference of Building Officials, Whittier, California.

**NATIONAL CENTER FOR EARTHQUAKE ENGINEERING RESEARCH
LIST OF TECHNICAL REPORTS**

The National Center for Earthquake Engineering Research (NCEER) publishes technical reports on a variety of subjects related to earthquake engineering written by authors funded through NCEER. These reports are available from both NCEER's Publications Department and the National Technical Information Service (NTIS). Requests for reports should be directed to the Publications Department, National Center for Earthquake Engineering Research, State University of New York at Buffalo, Red Jacket Quadrangle, Buffalo, New York 14261. Reports can also be requested through NTIS, 5285 Port Royal Road, Springfield, Virginia 22161. NTIS accession numbers are shown in parenthesis, if available.

- NCEER-87-0001 "First-Year Program in Research, Education and Technology Transfer," 3/5/87, (PB88-134275/AS).
- NCEER-87-0002 "Experimental Evaluation of Instantaneous Optimal Algorithms for Structural Control," by R.C. Lin, T.T. Soong and A.M. Reinhorn, 4/20/87, (PB88-134341/AS).
- NCEER-87-0003 "Experimentation Using the Earthquake Simulation Facilities at University at Buffalo," by A.M. Reinhorn and R.L. Ketter, to be published.
- NCEER-87-0004 "The System Characteristics and Performance of a Shaking Table," by J.S. Hwang, K.C. Chang and G.C. Lee, 6/1/87, (PB88-134259/AS). This report is available only through NTIS (see address given above).
- NCEER-87-0005 "A Finite Element Formulation for Nonlinear Viscoplastic Material Using a Q Model," by O. Gyebi and G. Dasgupta, 11/2/87, (PB88-213764/AS).
- NCEER-87-0006 "Symbolic Manipulation Program (SMP) - Algebraic Codes for Two and Three Dimensional Finite Element Formulations," by X. Lee and G. Dasgupta, 11/9/87, (PB88-219522/AS).
- NCEER-87-0007 "Instantaneous Optimal Control Laws for Tall Buildings Under Seismic Excitations," by J.N. Yang, A. Akbarpour and P. Ghaemmaghami, 6/10/87, (PB88-134333/AS).
- NCEER-87-0008 "IDARC: Inelastic Damage Analysis of Reinforced Concrete Frame - Shear-Wall Structures," by Y.J. Park, A.M. Reinhorn and S.K. Kunnath, 7/20/87, (PB88-134325/AS).
- NCEER-87-0009 "Liquefaction Potential for New York State: A Preliminary Report on Sites in Manhattan and Buffalo," by M. Budhu, V. Vijayakumar, R.F. Giese and L. Baumgras, 8/31/87, (PB88-163704/AS). This report is available only through NTIS (see address given above).
- NCEER-87-0010 "Vertical and Torsional Vibration of Foundations in Inhomogeneous Media," by A.S. Veletsos and K.W. Doison, 6/1/87, (PB88-134291/AS).
- NCEER-87-0011 "Seismic Probabilistic Risk Assessment and Seismic Margins Studies for Nuclear Power Plants," by Howard H.M. Hwang, 6/15/87, (PB88-134267/AS).
- NCEER-87-0012 "Parametric Studies of Frequency Response of Secondary Systems Under Ground-Acceleration Excitations," by Y. Yong and Y.K. Lin, 6/10/87, (PB88-134309/AS).
- NCEER-87-0013 "Frequency Response of Secondary Systems Under Seismic Excitation," by J.A. HoLung, J. Cai and Y.K. Lin, 7/31/87, (PB88-134317/AS).
- NCEER-87-0014 "Modelling Earthquake Ground Motions in Seismically Active Regions Using Parametric Time Series Methods," by G.W. Ellis and A.S. Cakmak, 8/25/87, (PB88-134283/AS).
- NCEER-87-0015 "Detection and Assessment of Seismic Structural Damage," by E. DiPasquale and A.S. Cakmak, 8/25/87, (PB88-163712/AS).

- NCEER-87-0016 "Pipeline Experiment at Parkfield, California," by J. Isenberg and E. Richardson, 9/15/87, (PB88-163720/AS). This report is available only through NTIS (see address given above).
- NCEER-87-0017 "Digital Simulation of Seismic Ground Motion," by M. Shinozuka, G. Deodatis and T. Harada, 8/31/87, (PB88-155197/AS). This report is available only through NTIS (see address given above).
- NCEER-87-0018 "Practical Considerations for Structural Control: System Uncertainty, System Time Delay and Truncation of Small Control Forces," J.N. Yang and A. Akbarpour, 8/10/87, (PB88-163738/AS).
- NCEER-87-0019 "Modal Analysis of Nonclassically Damped Structural Systems Using Canonical Transformation," by J.N. Yang, S. Sarkani and F.X. Long, 9/27/87, (PB88-187851/AS).
- NCEER-87-0020 "A Nonstationary Solution in Random Vibration Theory," by J.R. Red-Horse and P.D. Spanos, 11/3/87, (PB88-163746/AS).
- NCEER-87-0021 "Horizontal Impedances for Radially Inhomogeneous Viscoelastic Soil Layers," by A.S. Veletsos and K.W. Dotson, 10/15/87, (PB88-150859/AS).
- NCEER-87-0022 "Seismic Damage Assessment of Reinforced Concrete Members," by Y.S. Chung, C. Meyer and M. Shinozuka, 10/9/87, (PB88-150867/AS). This report is available only through NTIS (see address given above).
- NCEER-87-0023 "Active Structural Control in Civil Engineering," by T.T. Soong, 11/11/87, (PB88-187778/AS).
- NCEER-87-0024 "Vertical and Torsional Impedances for Radially Inhomogeneous Viscoelastic Soil Layers," by K.W. Dotson and A.S. Veletsos, 12/87, (PB88-187786/AS).
- NCEER-87-0025 "Proceedings from the Symposium on Seismic Hazards, Ground Motions, Soil-Liquefaction and Engineering Practice in Eastern North America," October 20-22, 1987, edited by K.H. Jacob, 12/87, (PB88-188115/AS).
- NCEER-87-0026 "Report on the Whittier-Narrows, California, Earthquake of October 1, 1987," by J. Pantelic and A. Reinhorn, 11/87, (PB88-187752/AS). This report is available only through NTIS (see address given above).
- NCEER-87-0027 "Design of a Modular Program for Transient Nonlinear Analysis of Large 3-D Building Structures," by S. Srivastav and J.F. Abel, 12/30/87, (PB88-187950/AS).
- NCEER-87-0028 "Second-Year Program in Research, Education and Technology Transfer," 3/8/88, (PB88-219480/AS).
- NCEER-88-0001 "Workshop on Seismic Computer Analysis and Design of Buildings With Interactive Graphics," by W. McGuire, J.F. Abel and C.H. Conley, 1/18/88, (PB88-187760/AS).
- NCEER-88-0002 "Optimal Control of Nonlinear Flexible Structures," by J.N. Yang, F.X. Long and D. Wong, 1/22/88, (PB88-213772/AS).
- NCEER-88-0003 "Substructuring Techniques in the Time Domain for Primary-Secondary Structural Systems," by G.D. Manolis and G. Juhn, 2/10/88, (PB88-213780/AS).
- NCEER-88-0004 "Iterative Seismic Analysis of Primary-Secondary Systems," by A. Singhal, L.D. Lutes and P.D. Spanos, 2/23/88, (PB88-213798/AS).
- NCEER-88-0005 "Stochastic Finite Element Expansion for Random Media," by P.D. Spanos and R. Ghanem, 3/14/88, (PB88-213806/AS).

- NCEER-88-0006 "Combining Structural Optimization and Structural Control," by F.Y. Cheng and C.P. Pantelides, 1/10/88, (PB88-213814/AS).
- NCEER-88-0007 "Seismic Performance Assessment of Code-Designed Structures," by H.H.-M. Hwang, J.-W. Jaw and H.-J. Shau, 3/20/88, (PB88-219423/AS).
- NCEER-88-0008 "Reliability Analysis of Code-Designed Structures Under Natural Hazards," by H.H.-M. Hwang, H. Ushuba and M. Shinozuka, 2/29/88, (PB88-229471/AS).
- NCEER-88-0009 "Seismic Fragility Analysis of Shear Wall Structures," by J.-W. Jaw and H.H.-M. Hwang, 4/30/88, (PB89-102867/AS).
- NCEER-88-0010 "Base Isolation of a Multi-Story Building Under a Harmonic Ground Motion - A Comparison of Performances of Various Systems," by F.-G. Fan, G. Ahmadi and I.G. Tadjbakhsh, 5/18/88, (PB89-122238/AS).
- NCEER-88-0011 "Seismic Floor Response Spectra for a Combined System by Green's Functions," by F.M. Lavelle, L.A. Bergman and P.D. Spanos, 5/1/88, (PB89-102875/AS).
- NCEER-88-0012 "A New Solution Technique for Randomly Excited Hysteretic Structures," by G.Q. Cai and Y.K. Lin, 5/16/88, (PB89-102883/AS).
- NCEER-88-0013 "A Study of Radiation Damping and Soil-Structure Interaction Effects in the Centrifuge," by K. Weissman, supervised by J.H. Prevost, 5/24/88, (PB89-144703/AS).
- NCEER-88-0014 "Parameter Identification and Implementation of a Kinematic Plasticity Model for Frictional Soils," by J.H. Prevost and D.V. Griffiths, to be published.
- NCEER-88-0015 "Two- and Three- Dimensional Dynamic Finite Element Analyses of the Long Valley Dam," by D.V. Griffiths and J.H. Prevost, 6/17/88, (PB89-144711/AS).
- NCEER-88-0016 "Damage Assessment of Reinforced Concrete Structures in Eastern United States," by A.M. Reinhorn, M.J. Seidel, S.K. Kunnath and Y.J. Park, 6/15/88, (PB89-122220/AS).
- NCEER-88-0017 "Dynamic Compliance of Vertically Loaded Strip Foundations in Multilayered Viscoelastic Soils," by S. Ahmad and A.S.M. Israil, 6/17/88, (PB89-102891/AS).
- NCEER-88-0018 "An Experimental Study of Seismic Structural Response With Added Viscoelastic Dampers," by R.C. Lin, Z. Liang, T.T. Soong and R.H. Zhang, 6/30/88, (PB89-122212/AS). This report is available only through NTIS (see address given above).
- NCEER-88-0019 "Experimental Investigation of Primary - Secondary System Interaction," by G.D. Manolis, G. Juhn and A.M. Reinhorn, 5/27/88, (PB89-122204/AS).
- NCEER-88-0020 "A Response Spectrum Approach For Analysis of Nonclassically Damped Structures," by J.N. Yang, S. Sarkani and F.X. Long, 4/22/88, (PB89-102909/AS).
- NCEER-88-0021 "Seismic Interaction of Structures and Soils: Stochastic Approach," by A.S. Veletsos and A.M. Prasad, 7/21/88, (PB89-122196/AS).
- NCEER-88-0022 "Identification of the Serviceability Limit State and Detection of Seismic Structural Damage," by E. DiPasquale and A.S. Cakmak, 6/15/88, (PB89-122188/AS). This report is available only through NTIS (see address given above).
- NCEER-88-0023 "Multi-Hazard Risk Analysis: Case of a Simple Offshore Structure," by B.K. Bhartia and E.H. Vanmarcke, 7/21/88, (PB89-145213/AS).

- NCEER-88-0024 "Automated Seismic Design of Reinforced Concrete Buildings," by Y.S. Chung, C. Meyer and M. Shinozuka, 7/5/88, (PB89-122170/AS). This report is available only through NTIS (see address given above).
- NCEER-88-0025 "Experimental Study of Active Control of MDOF Structures Under Seismic Excitations," by L.L. Chung, R.C. Lin, T.T. Soong and A.M. Reinhorn, 7/10/88, (PB89-122600/AS).
- NCEER-88-0026 "Earthquake Simulation Tests of a Low-Rise Metal Structure," by J.S. Hwang, K.C. Chang, G.C. Lee and R.L. Ketter, 8/1/88, (PB89-102917/AS).
- NCEER-88-0027 "Systems Study of Urban Response and Reconstruction Due to Catastrophic Earthquakes," by F. Kozin and H.K. Zhou, 9/22/88, (PB90-162348/AS).
- NCEER-88-0028 "Seismic Fragility Analysis of Plane Frame Structures," by H.H.-M. Hwang and Y.K. Low, 7/31/88, (PB89-131445/AS).
- NCEER-88-0029 "Response Analysis of Stochastic Structures," by A. Kardara, C. Bucher and M. Shinozuka, 9/22/88, (PB89-174429/AS).
- NCEER-88-0030 "Nonnormal Accelerations Due to Yielding in a Primary Structure," by D.C.K. Chen and L.D. Lutes, 9/19/88, (PB89-131437/AS).
- NCEER-88-0031 "Design Approaches for Soil-Structure Interaction," by A.S. Veletsos, A.M. Prasad and Y. Tang, 12/30/88, (PB89-174437/AS). This report is available only through NTIS (see address given above).
- NCEER-88-0032 "A Re-evaluation of Design Spectra for Seismic Damage Control," by C.J. Turkstra and A.G. Tallin, 11/7/88, (PB89-145221/AS).
- NCEER-88-0033 "The Behavior and Design of Noncontact Lap Splices Subjected to Repeated Inelastic Tensile Loading," by V.E. Sagan, P. Gergely and R.N. White, 12/8/88, (PB89-163737/AS).
- NCEER-88-0034 "Seismic Response of Pile Foundations," by S.M. Mamoon, P.K. Banerjee and S. Ahmad, 11/1/88, (PB89-145239/AS).
- NCEER-88-0035 "Modeling of R/C Building Structures With Flexible Floor Diaphragms (IDARC2)," by A.M. Reinhorn, S.K. Kunnath and N. Panahshahi, 9/7/88, (PB89-207153/AS).
- NCEER-88-0036 "Solution of the Dam-Reservoir Interaction Problem Using a Combination of FEM, BEM with Particular Integrals, Modal Analysis, and Substructuring," by C-S. Tsai, G.C. Lee and R.L. Ketter, 12/31/88, (PB89-207146/AS).
- NCEER-88-0037 "Optimal Placement of Actuators for Structural Control," by F.Y. Cheng and C.P. Pantelides, 8/15/88, (PB89-162846/AS).
- NCEER-88-0038 "Teflon Bearings in Aseismic Base Isolation: Experimental Studies and Mathematical Modeling," by A. Mokha, M.C. Constantinou and A.M. Reinhorn, 12/5/88, (PB89-218457/AS). This report is available only through NTIS (see address given above).
- NCEER-88-0039 "Seismic Behavior of Flat Slab High-Rise Buildings in the New York City Area," by P. Weidlinger and M. Ettouney, 10/15/88, (PB90-145681/AS).
- NCEER-88-0040 "Evaluation of the Earthquake Resistance of Existing Buildings in New York City," by P. Weidlinger and M. Ettouney, 10/15/88, to be published.
- NCEER-88-0041 "Small-Scale Modeling Techniques for Reinforced Concrete Structures Subjected to Seismic Loads," by W. Kim, A. El-Attar and R.N. White, 11/22/88, (PB89-189625/AS).

- NCEER-88-0042 "Modeling Strong Ground Motion from Multiple Event Earthquakes," by G.W. Ellis and A.S. Cakmak, 10/15/88, (PB89-174445/AS).
- NCEER-88-0043 "Nonstationary Models of Seismic Ground Acceleration," by M. Gngoriu, S.E. Ruiz and E. Rosenblueth, 7/15/88, (PB89-189617/AS).
- NCEER-88-0044 "SARCF User's Guide: Seismic Analysis of Reinforced Concrete Frames," by Y.S. Chung, C. Meyer and M. Shinozuka, 11/9/88, (PB89-174452/AS).
- NCEER-88-0045 "First Expert Panel Meeting on Disaster Research and Planning," edited by J. Pantelic and J. Stoyke, 9/15/88, (PB89-174460/AS).
- NCEER-88-0046 "Preliminary Studies of the Effect of Degrading Infill Walls on the Nonlinear Seismic Response of Steel Frames," by C.Z. Chrysostomou, P. Gergely and J.F. Abel, 12/19/88, (PB89-208383/AS).
- NCEER-88-0047 "Reinforced Concrete Frame Component Testing Facility - Design, Construction, Instrumentation and Operation," by S.P. Pessiki, C. Conley, T. Bond, P. Gergely and R.N. White, 12/16/88, (PB89-174478/AS).
- NCEER-89-0001 "Effects of Protective Cushion and Soil Compliancy on the Response of Equipment Within a Seismically Excited Building," by J.A. HoLung, 2/16/89, (PB89-207179/AS).
- NCEER-89-0002 "Statistical Evaluation of Response Modification Factors for Reinforced Concrete Structures," by H.H.M. Hwang and J.W. Jaw, 2/17/89, (PB89-207187/AS).
- NCEER-89-0003 "Hysteretic Columns Under Random Excitation," by G-Q. Cai and Y.K. Lin, 1/9/89, (PB89-196513/AS).
- NCEER-89-0004 "Experimental Study of 'Elephant Foot Bulge' Instability of Thin-Walled Metal Tanks," by Z-H. Jia and R.L. Ketter, 2/22/89, (PB89-207195/AS).
- NCEER-89-0005 "Experiment on Performance of Buried Pipelines Across San Andreas Fault," by J. Isenberg, E. Richardson and T.D. O'Rourke, 3/10/89, (PB89-218440/AS).
- NCEER-89-0006 "A Knowledge-Based Approach to Structural Design of Earthquake-Resistant Buildings," by M. Subramani, P. Gergely, C.H. Conley, J.F. Abel and A.H. Zaghw, 1/15/89, (PB89-218465/AS).
- NCEER-89-0007 "Liquefaction Hazards and Their Effects on Buried Pipelines," by T.D. O'Rourke and P.A. Lane, 2/1/89, (PB89-218481).
- NCEER-89-0008 "Fundamentals of System Identification in Structural Dynamics," by H. Imai, C-B. Yun, O. Maruyama and M. Shinozuka, 1/26/89, (PB89-207211/AS).
- NCEER-89-0009 "Effects of the 1985 Michoacan Earthquake on Water Systems and Other Buried Lifelines in Mexico," by A.G. Ayala and M.J. O'Rourke, 3/8/89, (PB89-207229/AS).
- NCEER-89-R010 "NCEER Bibliography of Earthquake Education Materials," by K.E.K. Ross, Second Revision, 9/1/89, (PB90-125352/AS).
- NCEER-89-0011 "Inelastic Three-Dimensional Response Analysis of Reinforced Concrete Building Structures (IDARC-3D), Part I - Modeling," by S.K. Kunnath and A.M. Reinhorn, 4/17/89, (PB90-114612/AS).
- NCEER-89-0012 "Recommended Modifications to ATC-14," by C.D. Poland and J.O. Malley, 4/12/89, (PB90-108648/AS).
- NCEER-89-0013 "Repair and Strengthening of Beam-to-Column Connections Subjected to Earthquake Loading," by M. Corazao and A.J. Durrani, 2/28/89, (PB90-109885/AS).

- NCEER-89-0014 "Program EXKAL2 for Identification of Structural Dynamic Systems," by O. Maruyama, C-B. Yun, M. Hoshiya and M. Shinozuka, 5/19/89, (PB90-109877/AS).
- NCEER-89-0015 "Response of Frames With Bolted Semi-Rigid Connections. Part I - Experimental Study and Analytical Predictions," by P.J. DiCorso, A.M. Reinhorn, J.R. Dickerson, J.B. Radzinski and W.L. Harper, 6/1/89, to be published.
- NCEER-89-0016 "ARMA Monte Carlo Simulation in Probabilistic Structural Analysis," by P.D. Spanos and M.P. Mignolet, 7/10/89, (PB90-109893/AS).
- NCEER-89-P017 "Preliminary Proceedings from the Conference on Disaster Preparedness - The Place of Earthquake Education in Our Schools," Edited by K.E.K. Ross, 6/23/89.
- NCEER-89-0017 "Proceedings from the Conference on Disaster Preparedness - The Place of Earthquake Education in Our Schools," Edited by K.E.K. Ross, 12/31/89, (PB90-207895). This report is available only through NTIS (see address given above).
- NCEER-89-0018 "Multidimensional Models of Hysteretic Material Behavior for Vibration Analysis of Shape Memory Energy Absorbing Devices, by E.I. Graesser and F.A. Cozzarelli, 6/7/89, (PB90-164146/AS).
- NCEER-89-0019 "Nonlinear Dynamic Analysis of Three-Dimensional Base Isolated Structures (3D-BASIS)," by S. Nagarajah, A.M. Reinhorn and M.C. Constantinou, 8/3/89, (PB90-161936/AS). This report is available only through NTIS (see address given above).
- NCEER-89-0020 "Structural Control Considering Time-Rate of Control Forces and Control Rate Constraints," by F.Y. Cheng and C.P. Pantelides, 8/3/89, (PB90-120445/AS).
- NCEER-89-0021 "Subsurface Conditions of Memphis and Shelby County," by K.W. Ng, T-S. Chang and H-H.M. Hwang, 7/26/89, (PB90-120437/AS).
- NCEER-89-0022 "Seismic Wave Propagation Effects on Straight Jointed Buried Pipelines," by K. Elhadi and M.J. O'Rourke, 8/24/89, (PB90-162322/AS).
- NCEER-89-0023 "Workshop on Serviceability Analysis of Water Delivery Systems," edited by M. Grigoriu, 3/6/89, (PB90-127424/AS).
- NCEER-89-0024 "Shaking Table Study of a 1/5 Scale Steel Frame Composed of Tapered Members," by K.C. Chang, J.S. Hwang and G.C. Lee, 9/18/89, (PB90-160169/AS).
- NCEER-89-0025 "DYNA1D: A Computer Program for Nonlinear Seismic Site Response Analysis - Technical Documentation," by Jean H. Prevost, 9/14/89, (PB90-161944/AS). This report is available only through NTIS (see address given above).
- NCEER-89-0026 "1:4 Scale Model Studies of Active Tendon Systems and Active Mass Dampers for Aseismic Protection," by A.M. Reinhorn, T.T. Soong, R.C. Lin, Y.P. Yang, Y. Fukao, H. Abe and M. Nakai, 9/15/89, (PB90-173246/AS).
- NCEER-89-0027 "Scattering of Waves by Inclusions in a Nonhomogeneous Elastic Half Space Solved by Boundary Element Methods," by P.K. Hadley, A. Askar and A.S. Cakmak, 6/15/89, (PB90-145699/AS).
- NCEER-89-0028 "Statistical Evaluation of Deflection Amplification Factors for Reinforced Concrete Structures," by H.H.M. Hwang, J-W. Jaw and A.L. Ch'ng, 8/31/89, (PB90-164633/AS).
- NCEER-89-0029 "Bedrock Accelerations in Memphis Area Due to Large New Madrid Earthquakes," by H.H.M. Hwang, C.H.S. Chen and G. Yu, 11/7/89, (PB90-162330/AS).

- NCEER-89-0030 "Seismic Behavior and Response Sensitivity of Secondary Structural Systems," by Y.Q. Chen and T.T. Soong, 10/23/89, (PB90-164658/AS)
- NCEER-89-0031 "Random Vibration and Reliability Analysis of Primary-Secondary Structural Systems," by Y. Ibrahim, M. Grigoriu and T.T. Soong, 11/10/89, (PB90-161951/AS)
- NCEER-89-0032 "Proceedings from the Second U.S. - Japan Workshop on Liquefaction, Large Ground Deformation and Their Effects on Lifelines, September 26-29, 1989," Edited by T.D. O'Rourke and M. Hamada, 12/1/89, (PB90-209388/AS).
- NCEER-89-0033 "Deterministic Model for Seismic Damage Evaluation of Reinforced Concrete Structures," by J.M. Bracci, A.M. Reinhorn, J.B. Mander and S.K. Kunnath, 9/27/89.
- NCEER-89-0034 "On the Relation Between Local and Global Damage Indices," by E. DiPasquale and A.S. Cakmak, 8/15/89, (PB90-173865).
- NCEER-89-0035 "Cyclic Undrained Behavior of Nonplastic and Low Plasticity Silts," by A.J. Walker and H.E. Stewart, 7/26/89, (PB90-183518/AS).
- NCEER-89-0036 "Liquefaction Potential of Surficial Deposits in the City of Buffalo, New York," by M. Budhu, R. Giese and L. Baumgrass, 1/17/89, (PB90-208455/AS).
- NCEER-89-0037 "A Deterministic Assessment of Effects of Ground Motion Incoherence," by A.S. Veletsos and Y. Tang, 7/15/89, (PB90-164294/AS)
- NCEER-89-0038 "Workshop on Ground Motion Parameters for Seismic Hazard Mapping," July 17-18, 1989, edited by R.V. Whitman, 12/1/89, (PB90-173923/AS).
- NCEER-89-0039 "Seismic Effects on Elevated Transit Lines of the New York City Transit Authority," by C.J. Costantino, C.A. Miller and E. Heymsfield, 12/26/89, (PB90-207887/AS).
- NCEER-89-0040 "Centrifugal Modeling of Dynamic Soil-Structure Interaction," by K. Weissman, Supervised by J.H. Prevost, 5/10/89, (PB90-207879/AS)
- NCEER-89-0041 "Linearized Identification of Buildings With Cores for Seismic Vulnerability Assessment," by I.K. Ho and A.E. Aktan, 11/1/89, (PB90-251943/AS).
- NCEER-90-0001 "Geotechnical and Lifeline Aspects of the October 17, 1989 Loma Prieta Earthquake in San Francisco," by T.D. O'Rourke, H.E. Stewart, F.T. Blackburn and T.S. Dickerman, 1/90, (PB90-208596/AS).
- NCEER-90-0002 "Nonnormal Secondary Response Due to Yielding in a Primary Structure," by D.C.K. Chen and L.D. Lutes, 2/28/90, (PB90-251976/AS).
- NCEER-90-0003 "Earthquake Education Materials for Grades K-12," by K.E.K. Ross, 4/16/90, (PB91-113415/AS).
- NCEER-90-0004 "Catalog of Strong Motion Stations in Eastern North America," by R.W. Busby, 4/3/90, (PB90-251984/AS).
- NCEER-90-0005 "NCEER Strong-Motion Data Base: A User Manual for the GeoBase Release (Version 1.0 for the Sun3)," by P. Friberg and K. Jacob, 3/31/90 (PB90-258062/AS).
- NCEER-90-0006 "Seismic Hazard Along a Crude Oil Pipeline in the Event of an 1811-1812 Type New Madrid Earthquake," by H.H.M. Hwang and C.H.S. Chen, 4/16/90 (PB90-258054).
- NCEER-90-0007 "Site-Specific Response Spectra for Memphis Sheahan Pumping Station," by H.H.M. Hwang and C.S. Lee, 5/15/90, (PB91-108811/AS).

- NCEER-90-0008 "Pilot Study on Seismic Vulnerability of Crude Oil Transmission Systems," by T. Arman, R. Dobry, M. Grigoriu, F. Kozin, M. O'Rourke, T. O'Rourke and M. Shinozuka, 5/25/90, (PB91-108837/AS).
- NCEER-90-0009 "A Program to Generate Site Dependent Time Histories: EQGEN," by G.W. Ellis, M. Srinivasan and A.S. Cakmak, 1/30/90, (PB91-108829/AS).
- NCEER-90-0010 "Active Isolation for Seismic Protection of Operating Rooms," by M.E. Talbott, Supervised by M. Shinozuka, 6/8/9, (PB91-110205/AS).
- NCEER-90-0011 "Program LINEARID for Identification of Linear Structural Dynamic Systems," by C.B. Yun and M. Shinozuka, 6/25/90, (PB91-110312/AS).
- NCEER-90-0012 "Two-Dimensional Two-Phase Elasto-Plastic Seismic Response of Earth Dams," by A.N. Yiagos, Supervised by J.H. Prevost, 6/20/90, (PB91-110197/AS).
- NCEER-90-0013 "Secondary Systems in Base-Isolated Structures: Experimental Investigation, Stochastic Response and Stochastic Sensitivity," by G.D. Manolis, G. Juhn, M.C. Constantinou and A.M. Reinhorn, 7/1/90, (PB91-110320/AS).
- NCEER-90-0014 "Seismic Behavior of Lightly-Reinforced Concrete Column and Beam-Column Joint Details," by S.P. Pessiki, C.H. Conley, P. Gergely and R.N. White, 8/22/90, (PB91-108795/AS).
- NCEER-90-0015 "Two Hybrid Control Systems for Building Structures Under Strong Earthquakes," by J.N. Yang and A. Danielians, 6/29/90, (PB91-125393/AS).
- NCEER-90-0016 "Instantaneous Optimal Control with Acceleration and Velocity Feedback," by J.N. Yang and Z. Li, 6/29/90, (PB91-125401/AS).
- NCEER-90-0017 "Reconnaissance Report on the Northern Iran Earthquake of June 21, 1990," by M. Mehraein, 10/4/90, (PB91-125377/AS).
- NCEER-90-0018 "Evaluation of Liquefaction Potential in Memphis and Shelby County," by T.S. Chang, P.S. Tang, C.S. Lee and H. Hwang, 8/10/90, (PB91-125427/AS).
- NCEER-90-0019 "Experimental and Analytical Study of a Combined Sliding Disc Bearing and Helical Steel Spring Isolation System," by M.C. Constantinou, A.S. Mokha and A.M. Reinhorn, 10/4/90, (PB91-125385/AS).
- NCEER-90-0020 "Experimental Study and Analytical Prediction of Earthquake Response of a Sliding Isolation System with a Spherical Surface," by A.S. Mokha, M.C. Constantinou and A.M. Reinhorn, 10/11/90, (PB91-125419/AS).
- NCEER-90-0021 "Dynamic Interaction Factors for Floating Pile Groups," by G. Gazetas, K. Fan, A. Kaynia and E. Kausel, 9/10/90, (PB91-170381/AS).
- NCEER-90-0022 "Evaluation of Seismic Damage Indices for Reinforced Concrete Structures," by S. Rodriguez-Gomez and A.S. Cakmak, 9/30/90, PB91-171322/AS).
- NCEER-90-0023 "Study of Site Response at a Selected Memphis Site," by H. Desai, S. Ahmad, E.S. Gazetas and M.R. Oh, 10/11/90, (PB91-196857/AS).
- NCEER-90-0024 "A User's Guide to Strongmo: Version 1.0 of NCEER's Strong-Motion Data Access Tool for PCs and Terminals," by P.A. Friberg and C.A.T. Susch, 11/15/90, (PB91-171272/AS).
- NCEER-90-0025 "A Three-Dimensional Analytical Study of Spatial Variability of Seismic Ground Motions," by L-L. Hong and A.H.-S. Ang, 10/30/90, (PB91-170399/AS).

- NCEER-90-0026 "MUMOID User's Guide - A Program for the Identification of Modal Parameters," by S. Rodriguez-Gomez and E. DiPasquale, 9/30/90, (PB91-171298/AS).
- NCEER-90-0027 "SARCF-II User's Guide - Seismic Analysis of Reinforced Concrete Frames," by S. Rodriguez-Gomez, Y.S. Chung and C. Meyer, 9/30/90, (PB91-171280/AS).
- NCEER-90-0028 "Viscous Dampers: Testing, Modeling and Application in Vibration and Seismic Isolation," by N. Makris and M.C. Constantinou, 12/20/90 (PB91-190561/AS).
- NCEER-90-0029 "Soil Effects on Earthquake Ground Motions in the Memphis Area," by H. Hwang, C.S. Lee, K.W. Ng and T.S. Chang, 8/2/90, (PB91-190751/AS).
- NCEER-91-0001 "Proceedings from the Third Japan-U.S. Workshop on Earthquake Resistant Design of Lifeline Facilities and Countermeasures for Soil Liquefaction, December 17-19, 1990," edited by T.D. O'Rourke and M. Hamada, 2/1/91, (PB91-179259/AS).
- NCEER-91-0002 "Physical Space Solutions of Non-Proportionally Damped Systems," by M. Tong, Z. Liang and G.C. Lee, 1/15/91, (PB91-179242/AS).
- NCEER-91-0003 "Seismic Response of Single Piles and Pile Groups," by K. Fan and G. Gazetas, 1/10/91, (PB92-174994/AS).
- NCEER-91-0004 "Damping of Structures: Part 1 - Theory of Complex Damping," by Z. Liang and G. Lee, 10/10/91, (PB92-197235/AS).
- NCEER-91-0005 "3D-BASIS - Nonlinear Dynamic Analysis of Three Dimensional Base Isolated Structures: Part II," by S. Nagarajaiah, A.M. Reinhorn and M.C. Constantinou, 2/28/91, (PB91-190553/AS).
- NCEER-91-0006 "A Multidimensional Hysteretic Model for Plasticity Deforming Metals in Energy Absorbing Devices," by E.J. Gracasser and F.A. Cozzarelli, 4/9/91, (PB92-108364/AS).
- NCEER-91-0007 "A Framework for Customizable Knowledge-Based Expert Systems with an Application to a KBES for Evaluating the Seismic Resistance of Existing Buildings," by E.G. Ibarra-Anaya and S.J. Fenves, 4/9/91, (PB91-210930/AS).
- NCEER-91-0008 "Nonlinear Analysis of Steel Frames with Semi-Rigid Connections Using the Capacity Spectrum Method," by G.G. Deierlein, S-H. Hsieh, Y-J. Shen and J.F. Abel, 7/2/91, (PB92-113828/AS).
- NCEER-91-0009 "Earthquake Education Materials for Grades K-12," by K.E.K. Ross, 4/30/91, (PB91-212142/AS).
- NCEER-91-0010 "Phase Wave Velocities and Displacement Phase Differences in a Harmonically Oscillating Pile," by N. Makris and G. Gazetas, 7/8/91, (PB92-108356/AS).
- NCEER-91-0011 "Dynamic Characteristics of a Full-Size Five-Story Steel Structure and a 2/5 Scale Model," by K.C. Chang, G.C. Yao, G.C. Lee, D.S. Hao and Y.C. Yeh, 7/2/91.
- NCEER-91-0012 "Seismic Response of a 2/5 Scale Steel Structure with Added Viscoelastic Dampers," by K.C. Chang, T.T. Soong, S-T. Oh and M.L. Lai, 5/17/91 (PB92-110816/AS).
- NCEER-91-0013 "Earthquake Response of Retaining Walls; Full-Scale Testing and Computational Modeling," by S. Alampalli and A.W.M. Elgamal, 6/20/91, to be published.
- NCEER-91-0014 "3D-BASIS-M: Nonlinear Dynamic Analysis of Multiple Building Base Isolated Structures," by P.C. Tsopelas, S. Nagarajaiah, M.C. Constantinou and A.M. Reinhorn, 5/28/91, (PB92-113885/AS).

- NCEER-91-0015 "Evaluation of SEAOC Design Requirements for Sliding Isolated Structures," by D. Theodossiou and M.C. Constantinou, 6/10/91, (PB92-114602/AS).
- NCEER-91-0016 "Closed-Loop Modal Testing of a 27-Story Reinforced Concrete Flat Plate-Core Building," by H.R. Somaprasad, T. Toksoy, H. Yoshiyuki and A.E. Aktan, 7/15/91, (PB92-129980/AS).
- NCEER-91-0017 "Shake Table Test of a 1/6 Scale Two-Story Lightly Reinforced Concrete Building," by A.G. El-Attar, R.N. White and P. Gergely, 2/28/91, (PB92-222447/AS).
- NCEER-91-0018 "Shake Table Test of a 1/8 Scale Three-Story Lightly Reinforced Concrete Building," by A.G. El-Attar, R.N. White and P. Gergely, 2/28/91.
- NCEER-91-0019 "Transfer Functions for Rigid Rectangular Foundations," by A.S. Veletsos, A.M. Prasad and W.H. Wu, 7/31/91.
- NCEER-91-0020 "Hybrid Control of Seismic-Excited Nonlinear and Inelastic Structural Systems," by J.N. Yang, Z. Li and A. Daniellians, 8/1/91, (PB92-143171/AS).
- NCEER-91-0021 "The NCEER-91 Earthquake Catalog: Improved Intensity-Based Magnitudes and Recurrence Relations for U.S. Earthquakes East of New Madrid," by L. Seeber and J.G. Armbruster, 8/28/91, (PB92-176742/AS).
- NCEER-91-0022 "Proceedings from the Implementation of Earthquake Planning and Education in Schools: The Need for Change - The Roles of the Changemakers," by K.E.K. Ross and F. Winslow, 7/23/91, (PB92-129998/AS).
- NCEER-91-0023 "A Study of Reliability-Based Criteria for Seismic Design of Reinforced Concrete Frame Buildings," by H.H.M. Hwang and H.M. Hsu, 8/10/91, (PB92-140235/AS).
- NCEER-91-0024 "Experimental Verification of a Number of Structural System Identification Algorithms," by R.G. Ghanem, H. Gavin and M. Shinozuka, 9/18/91, (PB92-176577/AS).
- NCEER-91-0025 "Probabilistic Evaluation of Liquefaction Potential," by H.H.M. Hwang and C.S. Lee, 11/25/91, (PB92-143429/AS).
- NCEER-91-0026 "Instantaneous Optimal Control for Linear, Nonlinear and Hysteretic Structures - Stable Controllers," by J.N. Yang and Z. Li, 11/15/91, (PB92-163807/AS).
- NCEER-91-0027 "Experimental and Theoretical Study of a Sliding Isolation System for Bridges," by M.C. Constantinou, A. Kartoun, A.M. Reinhorn and P. Bradford, 11/15/91, (PB92-176973/AS).
- NCEER-92-0001 "Case Studies of Liquefaction and Lifeline Performance During Past Earthquakes, Volume 1: Japanese Case Studies," Edited by M. Hamada and T. O'Rourke, 2/17/92, (PB92-197243/AS).
- NCEER-92-0002 "Case Studies of Liquefaction and Lifeline Performance During Past Earthquakes, Volume 2: United States Case Studies," Edited by T. O'Rourke and M. Hamada, 2/17/92, (PB92-197250/AS).
- NCEER-92-0003 "Issues in Earthquake Education," Edited by K. Ross, 2/3/92, (PB92-222389/AS).
- NCEER-92-0004 "Proceedings from the First U.S. - Japan Workshop on Earthquake Protective Systems for Bridges," 2/4/92, to be published.
- NCEER-92-0005 "Seismic Ground Motion from a Haskell-Type Source in a Multiple-Layered Half-Space," A.P. Theoharis, G. Deodatis and M. Shinozuka, 1/2/92, to be published.
- NCEER-92-0006 "Proceedings from the Site Effects Workshop," Edited by R. Whitman, 2/29/92, (PB92-197201/AS).

- NCEER-92-0007 "Engineering Evaluation of Permanent Ground Deformations Due to Seismically-Induced Liquefaction," by M.H. Baziar, R. Dobry and A.W.M. Elgarnal, 3/24/92, (PB92-222421/AS).
- NCEER-92-0008 "A Procedure for the Seismic Evaluation of Buildings in the Central and Eastern United States," by C.D. Poland and J.O. Mailey, 4/2/92, (PB92-222439/AS).
- NCEER-92-0009 "Experimental and Analytical Study of a Hybrid Isolation System Using Friction Controllable Sliding Bearings," by M.Q. Feng, S. Fujii and M. Shinozuka, 5/15/92, (PB93-150282/AS).
- NCEER-92-0010 "Seismic Resistance of Slab-Column Connections in Existing Non-Ductile Flat-Plate Buildings," by A.J. Durrani and Y. Du, 5/18/92.
- NCEER-92-0011 "The Hysteretic and Dynamic Behavior of Brick Masonry Walls Upgraded by Ferrocement Coatings Under Cyclic Loading and Strong Simulated Ground Motion," by H. Lee and S.P. Prawel, 5/11/92, to be published.
- NCEER-92-0012 "Study of Wire Rope Systems for Seismic Protection of Equipment in Buildings," by G.F. Demetriades, M.C. Constantinou and A.M. Reinhorn, 5/20/92.
- NCEER-92-0013 "Shape Memory Structural Dampers: Material Properties, Design and Seismic Testing," by P.R. Witting and F.A. Cozzarelli, 5/26/92.
- NCEER-92-0014 "Longitudinal Permanent Ground Deformation Effects on Buried Continuous Pipelines," by M.J. O'Rourke, and C. Nordberg, 6/15/92.
- NCEER-92-0015 "A Simulation Method for Stationary Gaussian Random Functions Based on the Sampling Theorem," by M. Grigoriu and S. Balopoulou, 6/11/92, (PB93-127496/AS).
- NCEER-92-0016 "Gravity-Load-Designed Reinforced Concrete Buildings: Seismic Evaluation of Existing Construction and Detailing Strategies for Improved Seismic Resistance," by G.W. Hoffmann, S.K. Kunnath, J.B. Mander and A.M. Reinhorn, 7/15/92, to be published.
- NCEER-92-0017 "Observations on Water System and Pipeline Performance in the Limón Area of Costa Rica Due to the April 22, 1991 Earthquake," by M. O'Rourke and D. Ballantyne, 6/30/92, (PB93-126811/AS).
- NCEER-92-0018 "Fourth Edition of Earthquake Education Materials for Grades K-12," Edited by K.E.K. Ross, 8/10/92.
- NCEER-92-0019 "Proceedings from the Fourth Japan-U.S. Workshop on Earthquake Resistant Design of Lifeline Facilities and Countermeasures for Soil Liquefaction," Edited by M. Hamada and T.D. O'Rourke, 8/12/92, (PB93-163939/AS).
- NCEER-92-0020 "Active Bracing System: A Full Scale Implementation of Active Control," by A.M. Reinhorn, T.T. Soong, R.C. Lin, M.A. Riley, Y.P. Wang, S. Aizawa and M. Higashino, 8/14/92, (PB93-127512/AS).
- NCEER-92-0021 "Empirical Analysis of Horizontal Ground Displacement Generated by Liquefaction-Induced Lateral Spreads," by S.F. Bartlett and T.L. Youd, 8/17/92.
- NCEER-92-0022 "IDARC Version 3.0: Inelastic Damage Analysis of Reinforced Concrete Structures," by S.K. Kunnath, A.M. Reinhorn and R.F. Lobo, 8/31/92, to be published.
- NCEER-92-0023 "A Semi-Empirical Analysis of Strong-Motion Peaks in Terms of Seismic Source, Propagation Path and Local Site Conditions," by M. Kamiyama, M.J. O'Rourke and R. Flores-Berrones, 9/9/92, (PB93-150266/AS).
- NCEER-92-0024 "Seismic Behavior of Reinforced Concrete Frame Structures with Nonductile Details, Part I: Summary of Experimental Findings of Full Scale Beam-Column Joint Tests," by A. Beres, R.N. White and P. Gergely, 9/30/92, to be published.
- NCEER-92-0025 "Experimental Results of Repaired and Retrofitted Beam-Column Joint Tests in Lightly Reinforced Concrete Frame Buildings," by A. Beres, S. El-Borgi, R.N. White and P. Gergely, 10/29/92, to be published.

- NCEER-92-0026 "A Generalization of Optimal Control Theory: Linear and Nonlinear Structures," by J.N. Yang, Z. Li and S. Vongchavalitkul, 11/2/92.
- NCEER-92-0027 "Seismic Resistance of Reinforced Concrete Frame Structures Designed Only for Gravity Loads: Part I - Design and Properties of a One-Third Scale Model Structure," by J.M. Bracci, A.M. Reinhorn and J.B. Mander, 12/1/92.
- NCEER-92-0028 "Seismic Resistance of Reinforced Concrete Frame Structures Designed Only for Gravity Loads: Part II - Experimental Performance of Subassemblages," by L.E. Aycardi, J.B. Mander and A.M. Reinhorn, 12/1/92.
- NCEER-92-0029 "Seismic Resistance of Reinforced Concrete Frame Structures Designed Only for Gravity Loads: Part III - Experimental Performance and Analytical Study of a Structural Model," by J.M. Bracci, A.M. Reinhorn and J.B. Mander, 12/1/92.